UNIVERSITY OF OKLAHOMA

GRADUATE COLLEGE

DEVELOPMENT OF NOVEL HPLC-MASS SPECTROMETRY METHODS FOR THE ANALYSIS OF NEUROCHEMICALS IN RAT BRAIN STRIATAL MICRODIALYSATES IN RESPONSE TO THE PARKINSONIAN NEUROTOXIN 1-METHYL-4-PHENYL-1,2,3,6-TETRAHYDROPYRIDINE

A DISSERTATION

SUBMITTED TO THE GRADUATE FACULTY

in partial fulfillment of the requirements for the

degree of

Doctor of Philosophy

By

GE ZU

Norman, Oklahoma

2007

DEVELOPMENT OF NOVEL HPLC-MASS SPECTROMETRY METHODS FOR THE ANALYSIS OF NEUROCHEMICALS IN RAT BRAIN STRIATAL MICRODIALYSATES IN RESPONSE TO THE PARKINSONIAN NEUROTOXIN 1-METHYL-4-PHENYL-1,2,3,6-TETRAHYDROPYRIDINE

A DISSERTATION APPROVED FOR THE
DEPARTMENT OF CHEMISTRY AND BIOCHEMISTRY

BY

_____
Glenn Dryhurst, Committee Chair

_____
LeRoy Blank

_____
Richard Taylor

_____
Robert White

_____
George Richter-Addo

_____
Lance Lobban

Acknowledgements

I thank my wife and daughter. My family provided the ultimate motivation, strength and care I needed to go through the strenuous study in the University of Oklahoma. I would be in nowhere without them.

Thank you, Dr. Monika Wrona. Thank you for trusting me and showing me the way and encouraging me when I was in the darkness of research. My appreciation for you is beyond any words.

And, Dr. Glenn Dryhurst, under your mentoring, I finally finished all my studies. I could not have done so without your understanding, tolerance and generous support. With your support, I had the privilege to use a personal state-of-the-art mass spectrometer for my research; this is extremely rare for a graduate student. You are a model for me to follow both in academic research and philosophy of life.

Dr. Li Zhang, thank you for your selfless support and guidance. For so many times, your professional suggestions enlightened the way leading to completion of my studies. I will never forget the legendary San Antonio trip we had. I will always appreciate you as colleague and as a mentor.

Many thanks to Dr. Steven Foster, as the research associate in our group, you hand-by-hand taught me how to perform animal surgery and setup the delicate experiment for *in vivo* microdialysis.

Also I want to thank my Graduate Committee: Professors C. LeRoy Blank, Robert L. White, George B. Richter-Addo, Richard Taylor and Lance Lobban. Thank you for the kindly recommendation so I had the chance to work in the departmental Mass Spectrometry facility which turned out to be the beginning of a series of amazing opportunities. Thank you for the many occasions I heard the words: “You are different, you can do it.” It was these words that made a difference for me.

Thank you, Dean, John and Carl in the electronics shop, you made my life much easier by providing the service in repairing all kinds of instruments. I would also like to thank Scott Zerger for taking care of the animals.

Many thanks to the Department of Chemistry and Biochemistry Staff: Teresa Hackney, Laura Cornell, Susan Lauterbach.

Thank God for letting all these things happen.

Table of Contents

Chapter One

Introduction.

Chapter Two

A Fully Automated System

Chapter Three

On-line Ion-pair Reversed Phase Solid Phase Extraction (IP-RP-SPE)

Chapter Four

Fully Automated On-line Sample Cleanup and HPLC-MS/MS Determination of Catecholamines and Related Compounds in Rat Brain Striatum: An *In Vivo* Microdialysis Study

Chapter Five

Fully Automated On-line Sample Cleanup and HPLC-MS/MS Determination of GSH and CySH in Rat Brain Striatum: An *In Vivo* Microdialysis Study.

Chapter Seven

List of Tables

List of Figures

Chapter One

Introduction

A. Parkinson's Disease.

Human history is accompanied by people combating disease. However, developments in the biological sciences, particularly recent breakthroughs in molecular and genetic biology, have led to significant advances in knowledge concerning the human body and its diseases.[1,2] Nevertheless, there are numerous diseases, notably those afflicting the brain and central nervous system, about which their mechanism or origin are largely unknown, and for which there are no cures. Parkinson's disease (PD) is one such disorder.[3]

PD is a degenerative brain disorder that has been known from ancient times. Nonetheless, it was first formally documented in 1817 by the British physician James Parkinson in his book: *An Essay on the Shaking Palsy* in which he described PD as having the following physical manifestations: tremor, muscular rigidity, bradykinesia and simian posture.[4] Currently, PD affects millions of people worldwide afflicting about 1% of people older than 60 years of age.[5]

It took more than another century for biomedical scientists to obtain any insights into the pathogenesis of PD. In the 1950s, a critical breakthrough was obtained by a Swedish scientist, Arvid Carlsson, who discovered key biochemical change in the brains of PD patients. In his discovery, Carlsson noted that dopamine, which prior to that time was believed to be of importance solely as the precursor of norepinephrine, was in fact itself probably a key neurotransmitter in the nigrostriatal

pathway. Furthermore, Carlsson also discovered that a profound decrease of dopamine content in the substantia nigra pars compacta (SN_{pc}) was characteristic in the brains of PD patients.[6] Carlsson's contributions led to the award of the 2000 Nobel Price in Physiology or Medicine. They also led to the discovery and use of 3,4-dihydroxy-L-phenylalanine (L-DOPA, the precursor of dopamine) as the only truly effective PD therapy.[7,8]

Despite extensive investigations over the past fifty years or more, the cause(s) of PD remain unknown and hence most forms of the disorder are referred to as idiopathic (*i.e.*, of no known cause). However, a small number of PD cases have been linked to exposure to certain toxic substances, drugs, genetic mutations, and head trauma.[3,9-16] Aging is considered to be the most robust risk factor for PD.[17] However, the reasons for the more rapid dropout of dopaminergic neurons in the SN_{pc} of PD patients than for age-matched controls remains a mystery.[18]

There is no definitive diagnosis for PD; its earliest symptoms are non-specific including weakness, tiredness, and fatigue. When the characteristic symptoms of PD become clearly evident approximately 70-80% of striatal dopamine (DA) has been irreversibly lost.[19]

Neurosurgery was employed to treat the symptoms PD patients for many decades before L-DOPA therapy was introduced in the1960s but has now been nearly totally abandoned because of unexpected and, often, deadly side-effects.[20,21] While still in its infancy, stem cell implantation has attracted considerable attention, although this enthusiasm has been severely dampened by unsuccessful attempts at implantation of DA neurons from fetal tisue.[22-24,25]

For many decades, L-DOPA was considered the only effective, although only symptomatic, therapy for PD. Administration of L-DOPA increases DA levels in the patient's brain thus relieving the

symptom of PD. However, L-DOPA does not halt further deterioration of nigrostriatal dopaminergic neurons. Furthermore, after long term use the therapeutic effects of L-DOPA decline and debilitating side-effects develop such as aberrant movement, nausea, blood pressure changes, and psychiatric complications. These side effects eventually make L-DOPA therapy of limited value.[7,8,20,26]

Figure 1-1 outlines the biosynthetic pathway for catecholamines. DA, norepinephrine (NE), and epinephrine (EPI) are all catecholaminergic neurotransmitters and the DA and to a lesser extent NE pathways are affected in PD. In this dissertation research, all of these neurotransmitters were targeted for *in vivo* monitoring by the system developed.

B. An Animal Modal of PD

A series of tragic events that occurred in late 1970s and early 1980s led to, arguably, the best animal model of PD.[27] It all began with a 23-year old Maryland chemistry graduate student, Barry Kidston, who developed symptoms of advanced PD a few days after injecting himself with a home-synthesized synthetic heroin. Kidston had been attempting to synthesize MPPP (1-methyl-4-phenyl-4-propionoxypiperidine). However the synthetic route he employed accidentally created an unexpected byproduct – 1-methyl-4-phenyl-1,2,3,6-tetrahydropyridine (MPTP). This event attracted little notice at that time. However, in July 1982 there was a further outbreak when six young addicts also simultaneously developed PD in Santa Clara County, California. MPTP was readily identified as the probable culprit for this outbreak of PD.

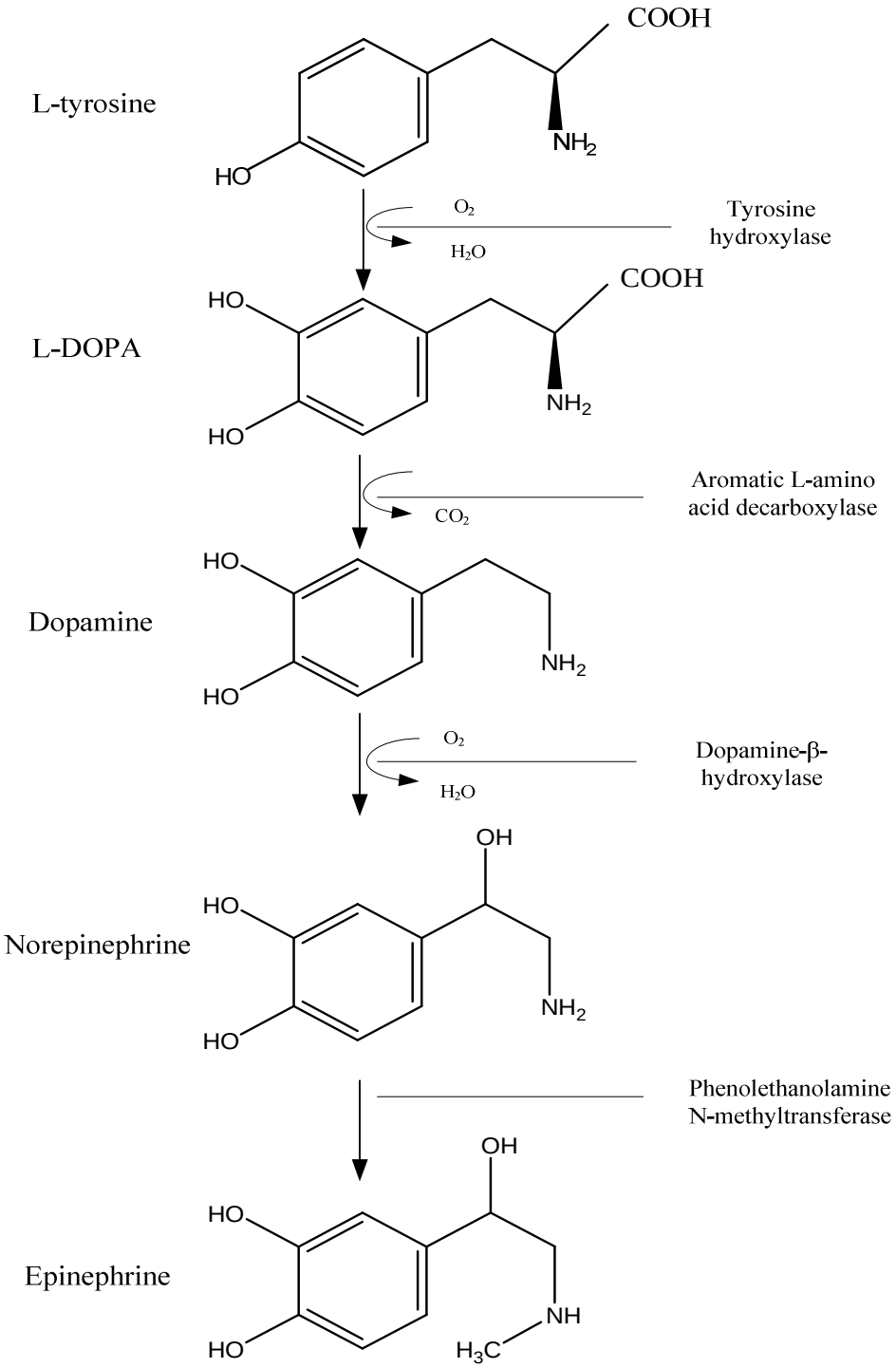

Figure 1- 1. Biosynthetic pathway for catecholamines.

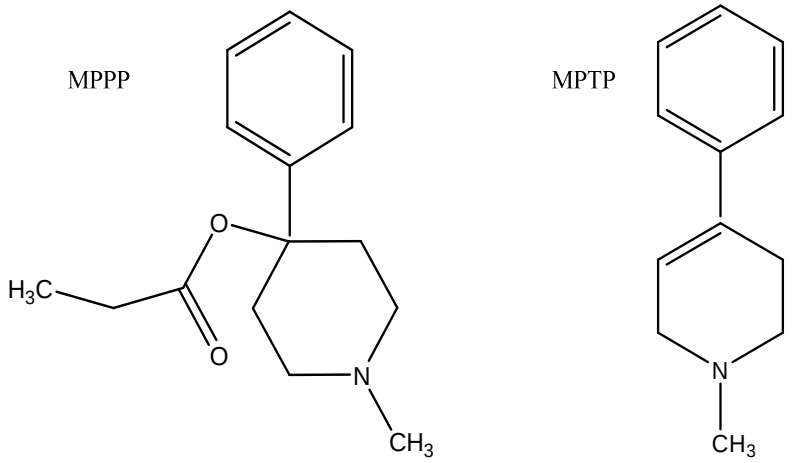

Figrure 1- 2. Chemical structures of MPPP and MPTP.

The mechanism of action of MPTP is widely believed to hold the key to an understanding and treatment of PD.[28,29] Thus, research has shown that MPTP evokes PD symptoms when administered to non-human primates and rodents such as mice. However, rats seem have a particularly strong resistance to MPTP toxicity apparently related the difficulty of systemically administered MPTP crossing the blood-brain barrier.[30,31] However, direct perfusion of MPTP or its active metabolite MPP^+ into the striatum or SN_{pc} of rats causes the same biochemical, pathological and immunohistochemical changes as other animal models systemically administered MPTP.[32,33]

Figure 1-3 shows the putative metabolism of MPTP. The upper part of Figure 1-3 shows the metabolism of MPTP to 4-phenyl-1,2,3,6-tetrahydropyridine (PTP) catalyzed by cytochrome P-450 oxidase and to MPTP-N-oxide via flavin monooxygenase. These two pathways, which occur primarily in the liver, are considered to be detoxication pathways. The lower pathway is believed to be the metabolic activation of MPTP to its highly toxic metabolite 1-methyl-4-phenylpyridinium (MPP^+). The first step in this pathway is the transformation (oxidation) of MPTP to 1-methyl-4-phenyl-2,3-dihydropyridinium ($MPDP^+$) catalyzed by monoamine oxidase B (MAO-B), a process that has

considerable experimental support. However, the biochemical details of the oxidation of $MPDP^+$ to MPP^+ is still the subject of investigation.[34-36] As part of the dissertation research, these molecules were targeted for *in vivo* monitoring.

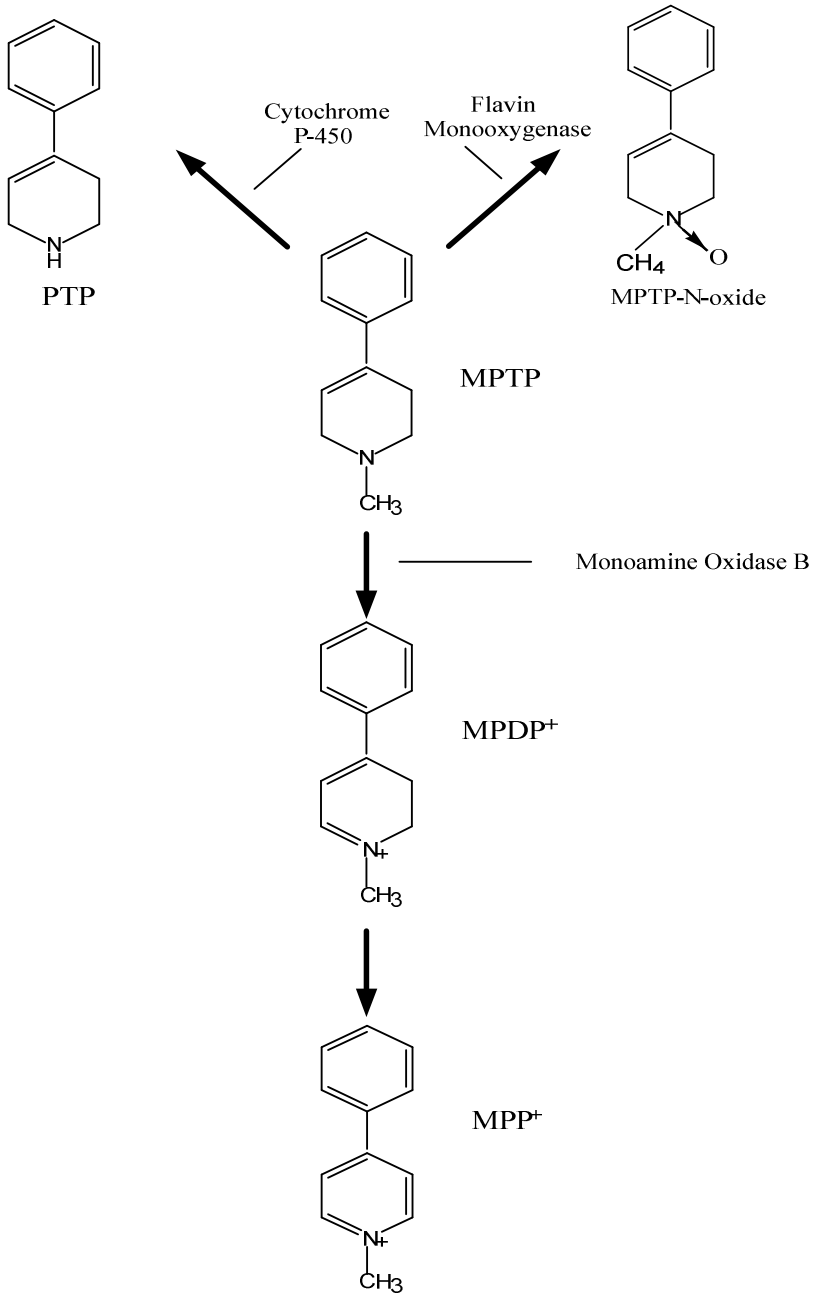

Figrure 1- 3. Putative metabolism of MPTP.

C. Systems Biology, Metabolomics and HPLC-MS Methods – the Future for PD.

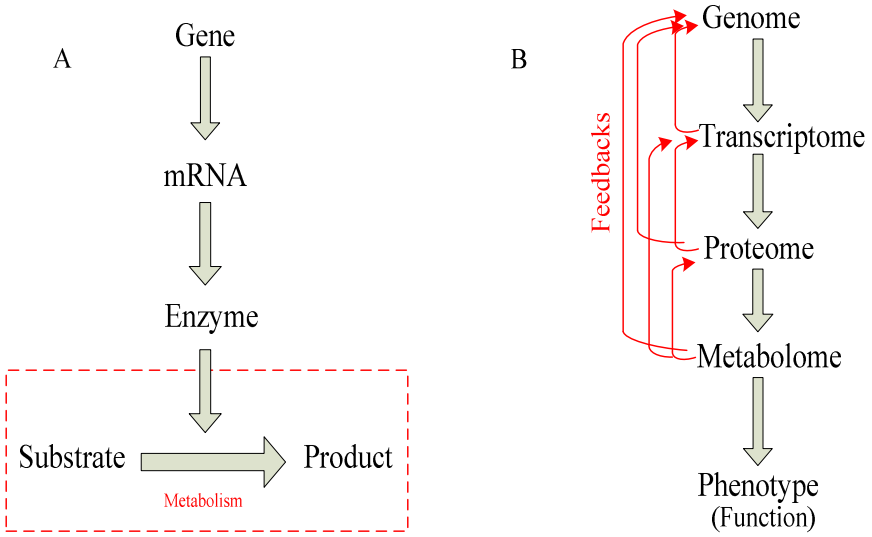

Figrure 1- 4 Traditional view (A) and –omics view (B) of biology systems

Currently, many scientists believe systems biology holds the key to understanding and finding cures for disorders such as PD.[2,37-43] This is because systems biology aims to integrate genomic, proteomic, transcriptomic, and metabolomic information to give a more complete picture of living organisms.[44] Figure 1-4 compares the traditional and current '–omics' view of biological systems.

Systems biology has existed as a concept for at least fifity years. However, it was the critical development of new experimental devices and novel analytical methods that made it a realistic concept.[40, 45-47] Although completion of the human genome project greatly boosted systems biology, it is still considered to be in its infancy mainly because the crucial techniques for proteomics and

metabolomics still need to be fully developed and implemented.[48,49] These future techniques have to be as effective as the polymerase chain reaction (PCR) and high-throughput fully automated gene sequencing machines have been to the development of genomics.

Metabolomics, which occupies the end position of the -omics cascade, measures all of the small molecules (metabolome) in an organism.[44] The metabolome is the end product of cellular functions and its study holds the key to an understanding of fundamental questions bearing on the activity of proteins, physiological mechanisms for the response of an organism to environmental stressors, and factors that regulate changes of the proteome, transcriptome, and genome.[44,49-52] In the history of PD research, targeted or focused metabolitic studies have been one of the areas of major focus. Nonetheless, systems biology emphasizes investigating multi-class metabolites at the same time.

The difficulties associated with metabolomics studies include:

1) The metabolome changes continuously and almost instantaneously in response to various biological challenges.
2) Metabolites are a highly heterogeneous group of compounds, and exist over wide dynamic concentration ranges and have highly variable chemical and physical properties.
3) The number of all metabolites (the metabolome) is probably much larger than other –omes. For example, while there are about 25,000 genes in the human genome, the metabolites in the human metabolome are expected to exceed 200,000.[52]

Numerous techniques have been developed for measuring different types of metabolites in PD and other disorders. Traditional targeted metabolite analyses are generally labor-intensive and

time-consuming processes. The trend for PD or any other metabolite studies is to simultaneously measure as many metabolites as possible in a fast and automated fashion.

Existing techniques that permit large numbers of metabolites to be measured simultaneously include nuclear magnetic resonance (NMR) spectroscopy, and tandem analytical techniques such as gas chromatography-mass spectrometry, *i.e.*, GC-MS and high performance liquid chromatography (HPLC)-MS. These are rational tools for modern metabolomics studies. The main drawback for NMR spectroscopy is its low sensitivity, which is inadequate for low abundance metabolite detection.[53-56] GC-MS, prominent because of its superior resolving power and sensitivity, has the problem of its limited application only to those metabolites that have sufficient volatility and thermal stability.[57-61] HPLC-MS approaches, based on the revolutionary development of atmospheric soft-ionization techniques, capillary/nano-HPLC and ultra-performance LC (UPLC) techniques, are becoming the approaches of choice for modern metabolomic studies.[55,62-68]

D. Challenges and Critical Techniques in Metabolite Studies in Animal Models of PD.

"Progress in science depends on new techniques, new discoveries and new ideas, probably in that order." Sydney Brenner , Nobel Prize for Physiology or Medicine 2002.[69]

Any successful analysis depends on a complete analytical system (illustrated in Figure 1-5) in which every part of the whole system is of equal importance.

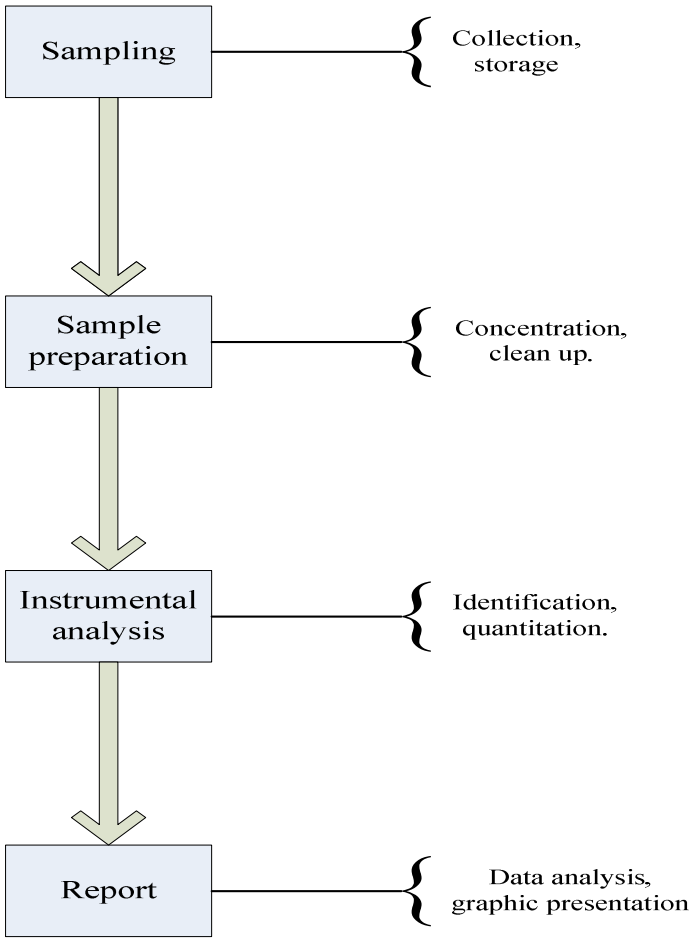

Figrure 1- 5. Complete analytical system

For the sampling step, animal brain tissue biopsy has been employed from the very beginning of PD research and is still widely used. Microdialysis, a newer technique which emerged about two decades ago, has shown tremendous advantages over tissue biopsy for metabolite analysis and has become accepted as the preferred sampling technique for studies of animal models of PD and other disorders where *in vivo* monitoring of chemicals are performed.[70-73] Microdialysis is a minimally invasive sampling technique, and its application in clinical human research has been increasingly reported.[74-81]

Microdialysate samples are generally considered to be much cleaner in the sense that they are

free from macromolecules such as proteins which, in turn, eliminates additional tedious sample preparation step needed for tissue analysis. More importantly, continuous *in vivo* monitoring of metabolites in almost real time is possible.

Nevertheless, being derived from a biological system, microdialysis samples are still very complicated containing abundant low molecular weight compounds that pose significant challenges to scientists to develop analytical techniques for their identification and quantitation.

As discussed previously, HPLC-MS is generally considered to be the method of choice for identifying and quantitating metabolites. Nevertheless, there are several challenges associated with HPLC-MS analyses of microdialysate samples. For example, microdialysate samples normally contain high concentrations of inorganic salts (NaCl, KCl, $MgCl_2$, *etc*.) that are included in the perfusion solution (perfusate) in order to mimic the concentrations of these salts in biological fluids such as plasma and cerebrospinal fluid (CSF). Such salts are innocuous for most conventional assays utilizing UV-vis, electrochemical, and florescence detectors. In contrast, these salts must be completely removed in the case of HPLC-MS in order to protect the mass spectrometer from contamination with resultant loss of sensitivity or worse.[82,83] The only practical method for removal of inorganic salts in an automated HPLC-MS analysis system is apparently on-line solid phase extraction (SPE).[82,84-88]

The targeted analytes in *in vivo* microdialysis experiments are often present in very low concentrations (μM or lower), and many are unstable in the presence of oxygen or light. Typically, microdialysis is employed to monitor time-dependent changes in analyte concentrations in response to some biochemical, chemical or behavioral insult. In order to achieve this goal, sample throughput and handling become of ultimate concern.

All the above challenges and requirements demand the development of an analytical system which has the following capabilities:

a) Fully automated, with minimal sample handling and very restricted or no exposure of samples to the external environment in order to achieve the greatest possible analytical accuracy and precision.

b) High sample throughput. The system should be fast enough to monitor time-dependent concentration changes of target compounds *in vivo*.

c) High detection power. The system should have low detection limits and the largest possible linear dynamic range for multi-classes of analytes.

d) High adaptability. The system should have the ability to analyze various compounds having very different chemical/physical properties with minimal modification.

e) Highly robust and reliable permitting extended periods of use.

Besides important requirements such as full automation, microdialysis sampling, on-line SPE sample preparation and HPLC-MS instrumental analysis, ion-pairing (IP) is another critical technique for metabolite analysis in animal models of PD. Its application to on-line SPE and HPLC is the key to the success of the whole system.

One of the fundamental challenges for HPLC-MS applications in metabolomic studies in biological samples is that metabolites exist in a wide polarity range. Traditionally, pre-column derivatization or ion-exchange chromatography has been required to measure highly polar or ionic molecules.[89-91] But these techniques are difficult to integrate into a high throughput fully automated

system which is built for multi-class metabolite monitoring. IP-reversed phase HPLC-MS might be the answer for highly polar or ionic molecules.

IP reagents have long been known for their capability to increase the retention times of highly polar to ionic molecules while leaving less polar or non-polar molecules unaffected in reversed phase (RP) HPLC.[92] This makes it possible to analyze the whole spectrum of molecules using a single RP-HPLC column.

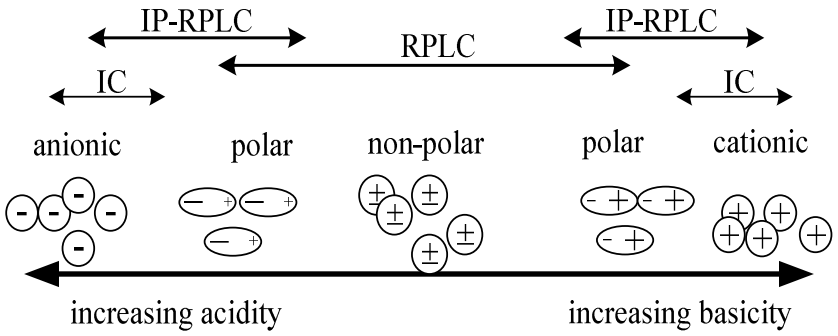

Figrure 1- 6. Analyte properties and HPLC methods.

Traditional IP reagents, principally alkylsulfonates with different alkyl chain lengths, are non-volatile and therefore are unsuitable for HPLC-MS. Volatile IP reagents have been studied intensively to cope with the rapid development of HPLC-MS techniques in recent years.[24,92-98] Typically, the volatile IP reagents for cationic analytes are perfluorinated carboxylic acids, *e.g.,* trifluoroacetic acid (TFA), heptafluorobutyric acid (HFBA), nonafluoropentanoic acid (NOFPA), tridecafluoroheptanoic acid (TDFHA) and pentadecafluorooctanoic acid (PDFOA). For acidic analytes typical IP reagents are trialkylamines such as triethylamine and tributylamine.

IP reversed-phase SPE (IP-RP-SPE) is a relatively new and less well-known technique compared to conventional reversed-phase or ion-exchange SPE. Nevertheless, it has the same mechanism as IP-RP-HPLC and has advantages over conventional SPE that include selectivity, compatibility with multi-class analysis, and direct coupling to reversed-phase HPLC analytical columns.[99-103]

E. Dissertation Purpose

The initial goals of the dissertation research was to monitor *in vivo* arachidonic acid metabolites (eicosanoids) utilizing HPLC-MS techniques. We initially focused on the instrumentation development and established a very specific and sensitive method which combined the techniques of normal phase HPLC with electron capture atmospheric pressure chemical ionization (EC-APCI). In these preliminary studies the impact of sample preparation and system automation was disregarded. However, when the HPLC-EC-APCI technique developed was applied to *in vivo* experiments, the project was severely impaired by necessary tedious manual sample pre-treatment, which involved labor intensive and time consuming sample collection, liquid-liquid extraction, off-line derivatization and multiple desolvation steps. Thus, this project yielded only limited results. Both the results and the method development are summarized in Chapter 7. More meaningful than the results was the lesson learned that automation and on-line sample preparation were as important as instrumental analysis part to the complete system, especially for experiments aimed at *in vivo* monitoring of metabolites.

The second stage of the research was aimed at monitoring neurochemicals and related low molecular weight compounds of relevance to the pathogenesis of PD in the striatum of awake rats. In

general, the HPLC-MS was the technique of choice for the instrumental analysis. A fully automated, labor free system which combined microdialysis sampling, on-line IP-RP-SPE sample preparation, IP-RP-HPLC separation and tandem MS/MS detection techniques was established.

The system developed was shown to be very effective for a project aimed at monitoring catecholamines and metabolites in microdialysate samples collected from the striatum of awake rats. In the second project, where the important antioxidants glutathione (GSH) and (highly ionic) cysteine (CySH) were targeted, an on-line derivitization step was added before on-line SPE. With this modification, both GSH and CySH could be successfully profiled *in vivo* in the animal model of PD. Another *in vivo* project was focused on MPTP and MPP^+. Thus, MPTP and MPP^+ could be successfully monitored in rat striatal microdialysates without modification of the initial fully automated system. There is no doubt that this system is capable of profiling a wide range of metabolites simultaneously in a highly sensitive and expeditious way.

F. Project Description

The following work was conducted as presented in the following chapters.

Chapter Two. A fully automated system.

A. Schematic overview diagram of the fully automated system is presented.

B. Individual components of the system, their function, operating conditions and the system alignment are illustrated using a control chart and an events chart.

C. The stability, repeatability of the fully automated system was evaluated by 9-h continuous measuring of different model compounds.

D. Time arrangement for complete *in vivo* animal experiments is presented and their importance discussed.

Chapter Three. On-line ion-pair reversed phase SPE

A. Solvent front elution profile for the RP-SPE column was obtained by loop injection of methanol onto the SPE column the eluent being monitored by full scan MS.

B. Theoretical consideration of SPE is discussed. Theoretical SPE breakthrough curves for unretained substances (salts) were calculated.

C. Different concentrations and pH of the IP agent HFBA was applied to the SPE mobile phase, and their influence on IP-RP-SPE efficiency for DA is discussed.

D. The IP agent TDFHA was tested and compared with HFBA for IP-RP-SPE efficiency on catecholamines and serotonin (5-hydroxytryptamine, 5-HT) and 3-methoxytyramine (3-MT).

E. Utilizing the automated system described in Chapter Two, experiments were carried out to obtain breakthrough curves for the catecholamines, 5-HT, 3-MT, GSH, CySH, GSH-MPB, CySH-MPB, MPTP, and MPP^+**.** SPE optimization for these compounds are discussed.

Chapter Four. *In vivo* catecholamines and related compounds analysis.

A. Off line (loop injection) mass spectrometry experiments were performed to obtain parent and daughter ion mass spectra and to optimize selected reaction monitoring (SRM) conditions for the catecholamines (DA, NE and EPI), 5-HT and the metabolite 3-MT.

B. Calibration curves were obtained utilizing the fully automated system described in Chapter Two.

C. *In vitro* microdialysis experiments were performed for catecholamine mixtures with different concentrations to determine probe recoveries.

D. Surgical procedures were conducted to implant guide cannula in the rat striatum.

E. Employing microdialysis, 10 mM MPTP was perfused for 30 min into the striatum of freely-moving rats and microdialysate samples were analyzed using the fully automated system described in Chapter Two.

Chapter Five. *In vivo* GSH/CySH analysis

A. Off-line mass spectrometry experiments were performed to obtain parent and daughter ion mass spectra and to optimize SRM conditions for GSH and CySH.

B. The fully automated system described in Chapter Two was applied for GSH/CySH standard solutions; the necessity for on-line derivatization is discussed.

C. An on-line derivatization step, which utilized a home made on-line mixer, was added before on-line SPE. A modified schematic diagram is presented.

D. The chemistry of the derivatization reaction is presented.

E. HPLC-MS and HPLC-MS/MS experiments were performed to obtain parent and daughter ion mass spectra, and to optimize SRM conditions for GSH-MPB and CySH-MPB.

F. Calibration curves for GSH and CySH were measured utilizing the modified fully automated system.

G. *In vitro* microdialysis experiments were performed for standard solutions of GSH and CySH to obtain probe recoveries.

H. Surgical procedures were conducted to implant guide cannula into the rat striatum.

I. Employing microdialysis, solutions of 10 mM MPTP, 2.5 mM MPP^+, and 5 mM MPP^+ were perfused for 30 min into the striatum of freely-moving rats and microdialysate samples were analyzed using the modified fully automated system described in this chapter.

Chapter Six. *In vivo* MPTP and related metabolites analysis

A. Off-line mass spectrometry experiments were performed to obtain parent and daughter ion mass spectra, and to optimize SRM conditions for MPTP and MPP^+.

B. Calibration curves were determined utilizing the fully automated system described in Chapter Two.

C. *In vitro* microdialysis experiments were performed for standard solutions of MPTP and MPP^+ to obtain probe recoveries.

D. Surgical procedures were conducted to implant guide cannula into the rat striatum.

E. Employing microdialysis, solutions of 10 mM MPTP were perfused for 30 min into the striatum of freely-moving rats and MPTP, PTP, $MPDP^+$, MPTP-N-Oxide and MPP^+ levels in mocrodialysate were monitored using the fully automated system described in Chapter Two.

Chapter Seven. Arachidonic acid metabolites analysis by HPLC-ECAPCI-MS/MS

A. Introduction to the arachidonic acid (AA) metabolites (eicosanoids) cascade, the metabolic scheme and putative relationship to PD are presented.

B. Instrumental analysis method developed for arachidonic and its metabolites.

C. Off-line mass spectrometry experiments were performed to obtain parent and daughter ion mass spectra, and to optimize SRM conditions for AA, prostaglandin E_2 (PGE_2), prostaglandin D_2 (PGD_2), and prostaglandin $F_{2\alpha}$ ($PGF_{2\alpha}$)

D. Surgical procedures were conducted to implant guide cannula into the rat striatum.

E. Employing microdialysis, microdialysate samples were collected and the basal levels of PGE_2, PGD_2 and $PGF_{2\alpha}$ were measured using the method developed in this chapter.

Chapter Two

A Fully Automated System

A. Introduction

Recently, fully automated systems utilizing HPLC-MS to study metabolites in biological samples have become more and more popular. Such systems usually employ an on-line SPE directly coupled to the HPLC-MS system. Sample collection and storage is still required isolated from the automated system.[104-107]

On-line microdialysis, *i.e.*, microdialysis directly coupled to an HPLC or capillary electrophoresis (CE) system, is also a frequently used technique. The major advantages of on-line microdialysis include simple sample preparation, automated analysis, and reduced exposure of microdialysate samples to air and light. In on-line microdialysis, the detection techniques coupled to HPLC or CE[108-111] include UV-vis,[112-117] atomic absorption spectroscopy,[118,119] electrochemical,[120-125] fluorescence,[126-128] laser-induced fluorescence[129,130] and enzyme-based biosensing.[131-137] However MS, as the leading detection technique for metabolites, has rarely been employed as a detection/analytical tool in connection with on-line microdialysis.[138] The reason for this, as discussed in the previous chapter, is that electrospray ionization-MS (ESI-MS) is highly susceptible to the presence of salts and other low molecular weight impurities that are always present in biological samples.[139] Integrating an on-line SPE procedure into the on-line microdialysis system to provide a clean sample for MS detection represents a potential solution to this difficulty. In this chapter, a fully automated system

consisting of on-line microdialysis sampling, on-line SPE and HPLC-MS is described.

B. Experimental

1. Chemicals.

Milli-Q (Continental Water System; El Paso, TX) deionized water (18 MΩ) was used. HPLC grade methanol (MeOH) was obtained from Fisher Scientific (Fairlawn, NJ, USA). Heptafluorobutanoic acid (HFBA, 99%), was purchased from Sigma-Aldrich (St. Louis, MO, USA). HFBA is a liquid at room temperature and was used as received from the supplier without further purification. Tridecafluoroheptanoic acid (TDFHA, 99%), was purchased from Aldrich. TDFHA is a solid at room temperature (melting point 30°C). Before use, the glass bottle containing TDFHA was placed in an oven at ~40°C for 15 minutes to liquefy the solid. Artificial cerebrospinal fluid (aCSF) was water containing: 147.0 mM NaCl, 2.7 mM KCl, 1.2 mM $CaCl_2$ and 0.85 mM $MgCl_2$, pH adjusted to 7.40 by a phosphate buffer.

Ammonium hydroxide (NH_4OH) (28% in H_2O, 99.99+%) was purchased from Sigma-Aldrich (St. Louis, MO, USA), it was diluted to ~7% with deionized water for further use. Formic acid (FA) (ACS grade, 88% in water) was purchased from Sigma-Aldrich. Dopamine (DA), epinephrine (EPI), norepinephrine (NE), serotonin (5-HT), and 3-methoxytyramine (3-MT) were also obtained from Sigma-Aldrich.

2. Stock and Working Standard Solutions.

Stock standard solutions (1.0 mM) of the three individual catecholamines (DA, NE. EPI), 5-HT, and 3-MT were prepared in water containing 0.1% FA and stored at -80^{o}C. The working solutions were prepared by diluting the stock standard solution with aCSF. Thus, a 0.2 μM standard solution containing two catecholamines (DA and EPI; NE was not studied), 5-HT and 3-MT was prepared as follows: 10 μL of each of the four stock solutions was added to 960 μL of aCSF to obtain 10 μM solution; 20 μL of the resulting solution was then added into 980 μL of aCSF to obtain 0.2 μM standard solution. All resulting solutions were stored in plastic vials and were passed through 0.2 μm centrifuge filter (NanoSEP™; VWR, USA) before use.

3. Instrumentations Overview.

An overview diagram of the automated system is shown in Figures 2-1 and 2-2. Note that the BAS rat housing/containment system (Raturn®; BAS, IN, USA) shown in Figure 2-1 is not included in Figure 2-2 because it was not an integral part of the analytical system.

4. On-line Microdialysis Sampling

Immediately prior to microdialysis experiments, the aCSF solution was filtered through a 0.2 μm NanoSEP™ centrifuge filter and thoroughly degassed with ultra pure helium gas. A gas tight 1000 μL syringe (BAS Bee Stinger®, model MD-0100) was then filled with this aCSF solution. A microinjection syringe pump (CMA 100®; CMA, Stockholm, Sweden) was used to deliver the aCSF at a flow rate of 1.5 μL/min. The syringe was connected to the inlet of a CMA 12® microdialysis probe (4 mm membrane, MW cutoff 20,000 Da) using 0.12 mm ID × 0.65 mm OD PEEK capillary tubing

(BAS), with dead volume of 1.2 µL/100 mm. CMA capillary tube adapters were used to provide tight, close to zero internal volume, connections. Such tubing adapters were easy to use because they swell in 70 % alcohol and shrink in air. The outlet of the probe was connected to a microbore 10 port valve (Cheminert®; Valco Instruments, Houston, TX, USA) through CMA PEEK capillary tubing. The microdialysate from the probe was introduced into one of the two sample loops of the 10 port valve. The sample loops were made of 0.20 in ID × 1/16 in OD orange PEEK tubing (Upchurch, WA, USA). The two loops had identical length of 17.2 cm and, hence, their volume was 35.0 µL. The 10 port valve was controlled by a BAS Pollen-8® on-line injector controller through a Valco microelectric actuator.

5. Chromatographic System and MS detection.

The on-line SPE was coupled to the HPLC by a column-switch technique shown in Figure 2-2. A BAS PM-80® solvent delivery system was used to deliver mobile phase F to the SPE column at the flow-rate of 200 µL/min. A second HPLC pump, Thermal Finnigan Surveyor® MS pump (Thermal Corp., San Jose, CA, USA) was used to deliver mobile phases A and B (gradient) to the analytical column at a flow-rate of 80 µL/min. The column switch employed a 6-port valve Cheminert® (Valco) equipped with a microelectric actuator (Valco). This valve was controlled by the data acquisition program of the TSQ 7000 mass spectrometer. All connections for chromatography employed red PEEK tubing – 0.005 in ID × 1/16 in OD.

Chromatograms were recorded by the Thermal Finnigan TSQ® 7000 triple quadrupole mass spectrometer operated in the ESI positive mode. The scan mode was selected reactions monitoring

(SRM). The details of the MS method development are presented in Chapter Four. The mass spectrometer conditions were as follows: ion source temperature 250^{o}C; manifold temperature 70^{o}C; ionization voltage 5000V; desolvation gas pressure 50 psi; a nebulization gas was not used.

Figure 2- 1. Photograph of the fully automated system.

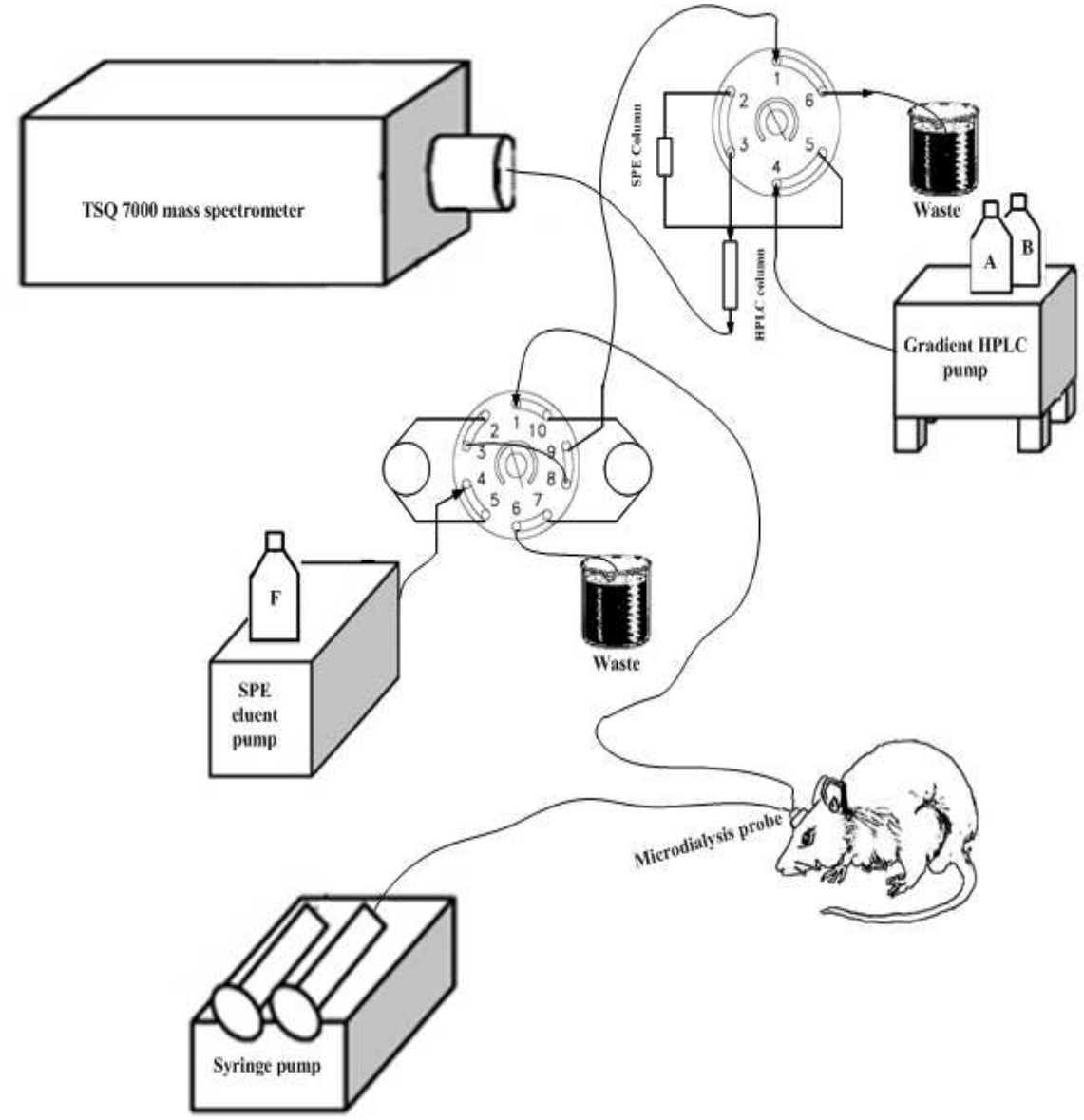

Figure 2- 2. Overall schematic of the instrument connections for the fully automated system.

6. Columns and Mobile Phases

The analytical column was an ODS microbore 150 × 1.0 mm ID – 4 µm Hydro-RP® (Phenomenex, CA USA), with a Phenomenex 20 × 3.0 mm ID C_{18} guard column in an integrated guard column housing. The SPE column was an ODS microbore 14 × 1 mm ID – 3 µm, 80 Å BAS UniJet® guard column. The SPE column was mounted directly on the 6 port valve using a BAS

UniNut® male-female union to minimize dead volume as shown in Figure 2-3.

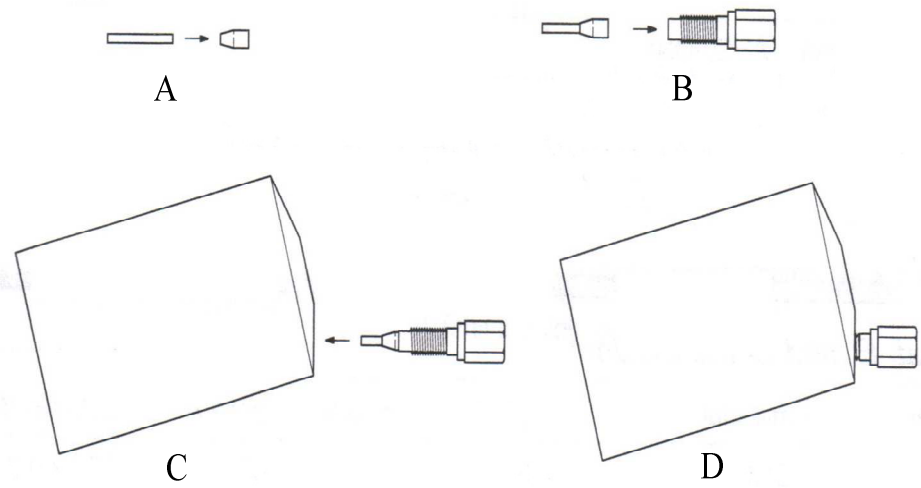

Figure 2- 3. SPE column directly mounted on the 6 port valve. A: SPE column with a PEEK ferrule, B: male-female union. C: mounting to valve port, D: finished.

Mobile phase F1 consisted of 5 mM TDFHA in water with the pH adjusted to 6.5-7.5 with NH_4OH prepared as follows: 508.5 µL TDFHA was added to 500 mL of deionized water; then NH_4OH was slowly added while the solution was stirred and the pH measured. The solution was filtered through a 0.45 µm nylon filter (Millipore Corporation, Bedford, MA), then degassed with ultra pure Helium gas before use. Mobile phase F2 consisted of 50 mM HFBA prepared similarly to mobile phase F1, except 3.25 mL of HFBA was added to 500 mL water.

Mobile phase A consisted of 0.1% formic acid in MeOH, prepared as follows: 568 µL formic acid (88%) was added to 500 mL of MeOH. Mobile phase B consisted of 95% water (v/v) and 5% MeOH (v/v) containing 1.0 mM HFBA, prepared as follows: 12.5 mL MeOH was added to 237.5 mL water, and then 32.8 µL HFBA was added. The final pH of this solution was 2.5 (no pH adjustment

was necessary). The solution was filtered through a 0.45 μm nylon filter and then degassed with an embedded vacuum degasser in the Surveyor® MS HPLC system. Gradient: linear increase from 100% solvent B to 100% solvent A over10 min, 100% solvent A for 1 min, decrease to 100% solvent B over 1 min, then 100% solvent B for 8 min. The total HPLC run time was 20 min. The flow rate was 80 μL/min.

7. Evaluation of the Stability of the Fully Automated System.

In experiments aimed at evaluating instrument stability, the microdialysis probe was not used. The syringe was loaded with 1000 μL, 0.2 μM standard solution containing DA, EPI, 5-HT and 3-MT. The solution was pumped directly to the sample loops on the 10 port valve at 1.5 μL/min. The system was allowed to run unattended for 9 h 40 min.

C. Results and Discussion

1. System Control.

For a fully automated system consisting of so many individual components, synchronization of their actions is extremely important. The control relationships of the components are summarized in Figure 2-4 and explained subsequently.

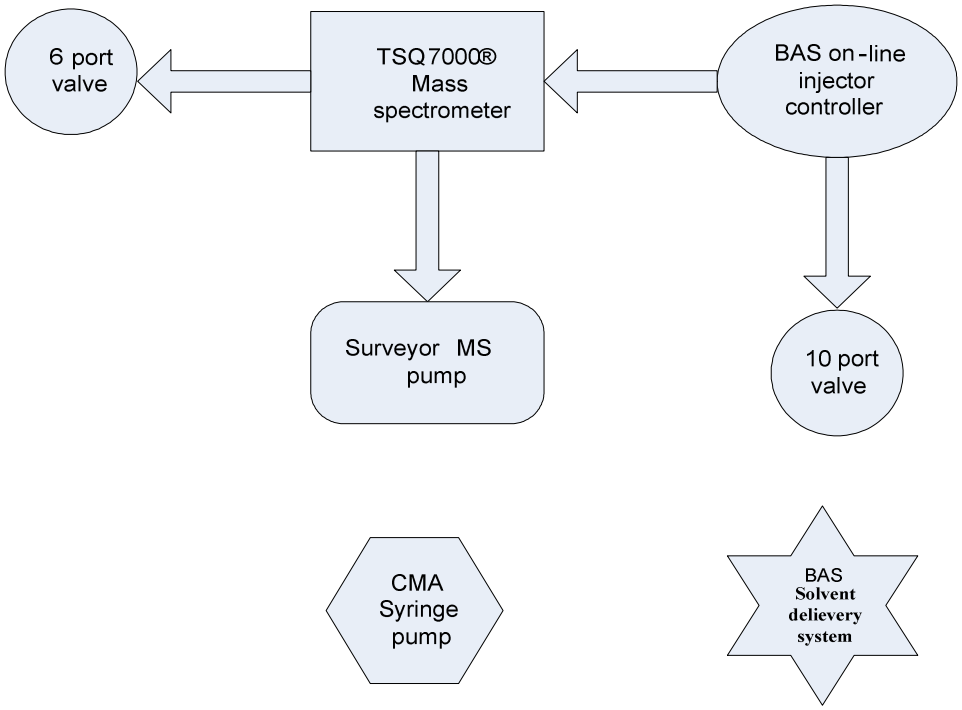

Figure 2- 4. Instrument control chart

1) CMA syringe pump (microdialysis pump) and BAS solvent delivery system (SPE pump) worked as stand-alone instruments. Throughout experiments, the syringe pump pumped the perfusate at a rate of 1.5 µL/min; the SPE pump pumped mobile phase F at 200 µL/min.
2) The BAS on-line injector controller had two controlling functions: 1) to toggle the 10 port valve every 20 minutes; and, 2) to simultaneously start the mass spectrometry data acquisition process.
3) The TSQ 7000 mass spectrometer controlled the 6 port valve and the Surveyor MS pump (HPLC gradient pump)

2. Flow Scheme.

The eluent flow scheme, presented in Figure 2-5, illustrates how the 10 port valve and 6 port valve were coordinated to achieve automated microdialysis sampling and on-line SPE for the system.

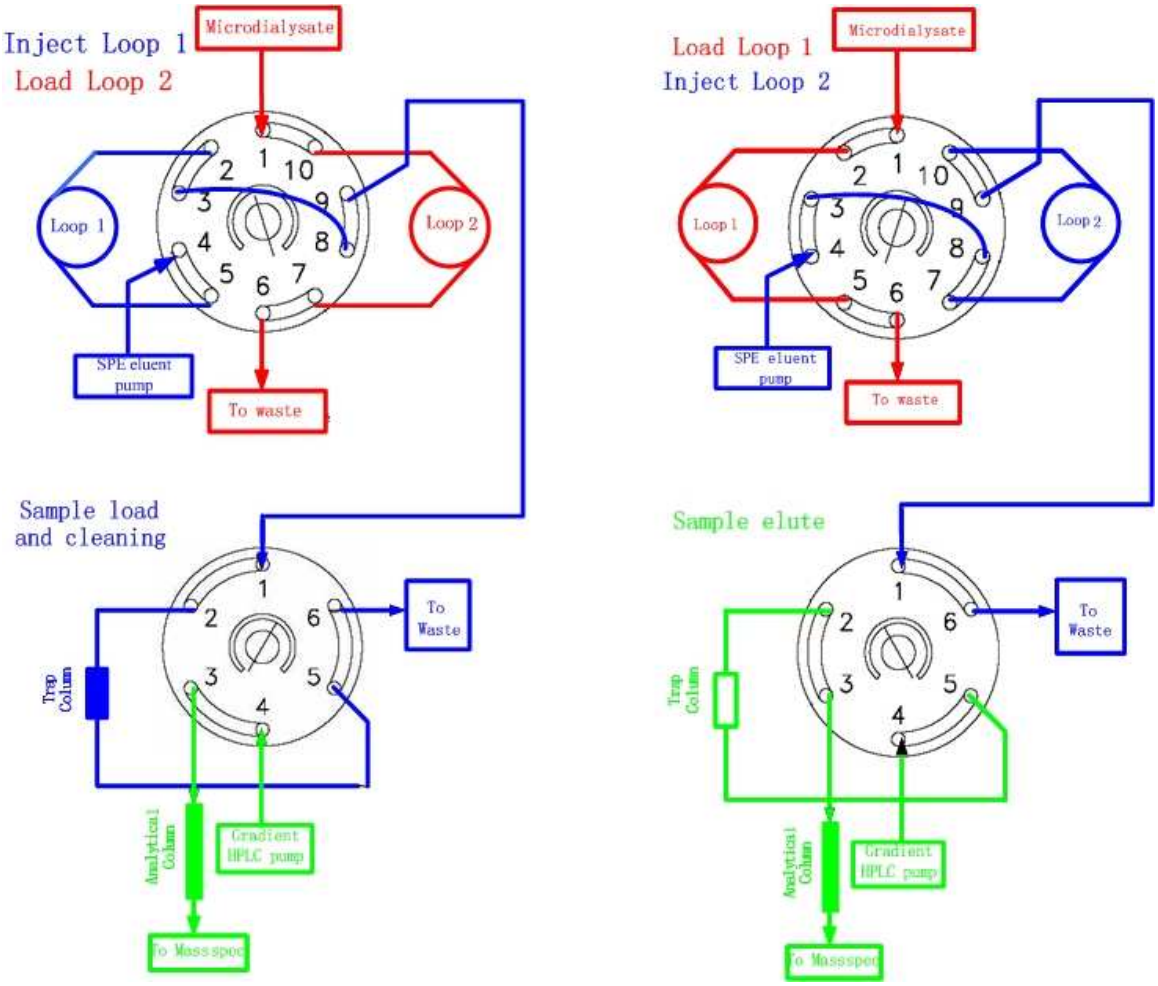

Figure 2- 5. Flow scheme.

During the experiment, the 10 port valve was toggled every 20 min. In each 20 min cycle, one of the loops was filled with the perfusate solution (*i.e.*, aCSF or, in later experiments, aCSF containing the parkinsonian toxicant). The sample stored in the second loop was loaded onto the SPE column

during the first min of the cycle. Then the loop was washed for the remaining 19 min by the SPE mobile phase. The 6 port valve was controlled separately by the MS data acquisition system and independent to the 10 port valve.

During each 20 min cycle, the 6 port valve was toggled twice. In the first event, which was before the first toggle occurred, the SPE column was loaded with sample which was swept out of the loop by the SPE mobile phase. The sample was then continuously washed with the SPE mobile phase. The time of loading and washing was an important factor which decided the efficiency of the on-line SPE, and was optimized according the properties of the target analytes. The detailed optimization procedures for SPE were presented in Chapter Three. Generally, washing time around 1.0 min was employed. During the time for sample loading and washing to the SPE column, the analytical HPLC column was under the initial gradient elution. At the end of SPE washing, the 6 port valve was toggled to another position and the second event initiated. This event lasted for 13 min. During this event, the targeted analytes were back-flushed onto the analytical HPLC column by the gradient and chromatographically separated. Usually it only took a very short time to wash the analyte molecules off the SPE column. The additional time was necessary for the HPLC gradient solvents to clean and regenerate the SPE column. The gradient theoretically reached 100% organic solvent (MeOH) in 10 min. However, the dead volume for the HPLC system had to be considered in the experimental setting. Thus, the dead volume for the Surveyor MS pump itself plus the tubing connecting the pump and HPLC column was about 160 µL, *i.e.*, the dead time was approximately 2 min. Thus, 13 min was employed to make sure that the SPE column was thoroughly washed with 100% MeOH. At 14 min of the cycle, the 6 port valve was toggled again to trigger the third event. In this event, the SPE column

was flushed and equilibrated with the SPE mobile phase and the HPLC column was equilibrated with aqueous mobile phase B prior to the next run.

3. Event Flow Chart.

The events for all instruments are presented more clearly in the Events Flow Chart (Figure 2-6). It is important to track and synchronize all the events according to this chart in order to avoid confusion and mishandling since events from different instruments are intimately related to each other. The details of all events for each instruments is explained and discussed subsequently.

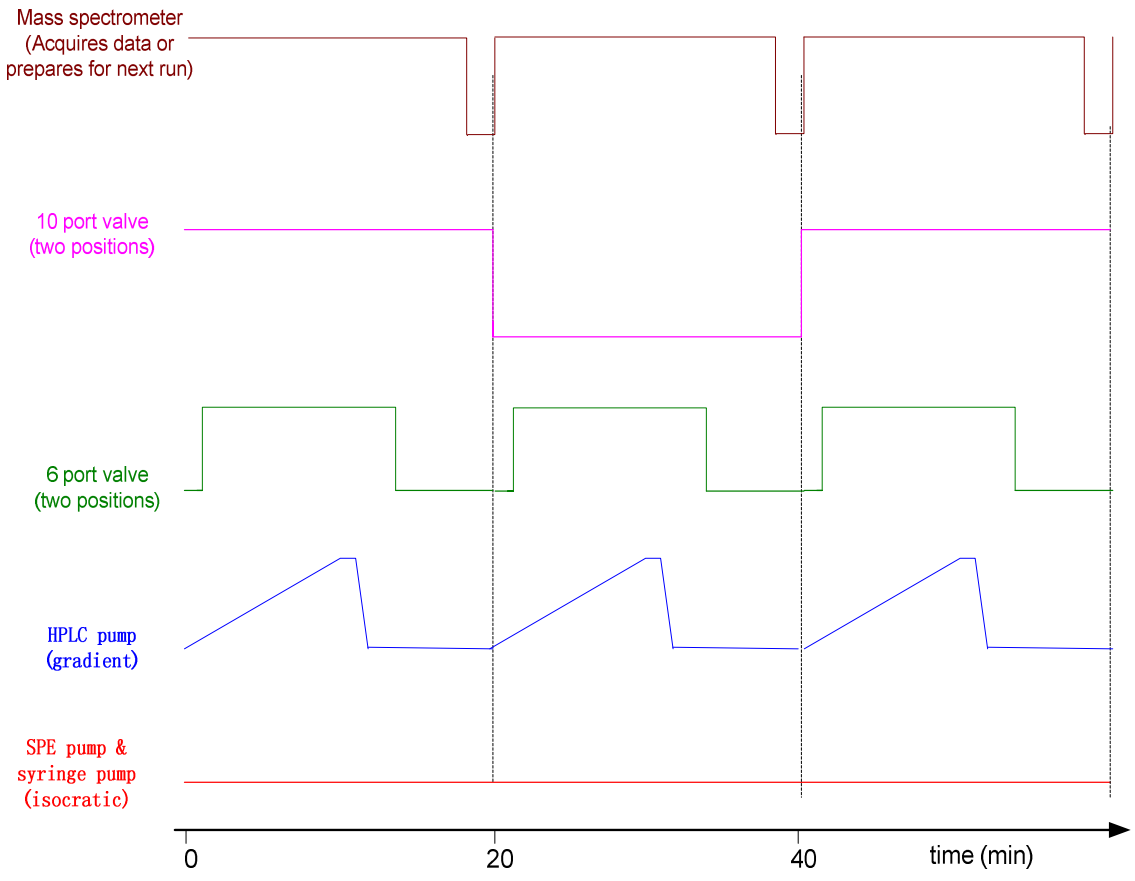

Figure 2- 6. Events flow chart for the fully automated system.

1) The events of all components are strictly aligned, although each is flexible and could be adjusted individually. This is critical in the method development process for the fully automated analytical system.

2) During experiments, each run cycle was fixed at 20 min. This was an arbitrary choice, partially based on previous experience in the development of an *in vivo* eicosanoids assay. Theoretically, the shorter this cycle time, the better the time resolution would be for the monitored analytes. Although a shorter cycle time necessarily requires higher detection power, it is in fact limited by the HPLC separation step, *i.e.*, solvent gradient running time and column re-equilibration time. This is particularly true when the monitored analytes have large differences in chromatographic behavior. Since the concentrations and chromatographic properties of target analytes vary tremendously, the cycle time should be optimized for each type of analysis.

3) The TSQ 7000 mass spectrometer performs two tasks in each cycle, *i.e.*, data acquisition for the first 18 minutes, after which data acquisition is terminated to permit method loading in readiness for the next acquisition.

4) The 10 port valve is toggled every 20 min. During each 20 min interval it permits the filling of one of the two 35 µL loops, and empties and washes the other loop.

5) The 6 port valve performs three events in each cycle as described in detail previously. It should be emphasized that the first event decides how long the sample is to be loaded and washed on the SPE column. SPE breakthrough curves were determined by changing the time

of this event and measuring how much targeted substance remained after the washing step. Breakthrough curves and SPE efficiency are discussed in detail in Chapter Three. In our experiments, 1.0 min SPE washing (or 200 µL SPE solvent) was a general guideline. The second event decides how long the SPE column is backflushed. The last event is reconditioning of the column by the SPE mobile phase. In most experiments, this is 6 min or 1200 µL of SPE mobile phase.

6) The Surveyor HPLC pump is triggered by the mass spectrometer and run the gradient described previously.

7) The syringe pump pumps the perfusate at 1.5 µL/min throughout the experiment. The SPE pump pumps the SPE mobile phase (isocratic) throughout the experiment. Theoretically, the higher the SPE flow rate, the better it is for the whole experiment, since it shortens the SPE process. However, this has to be optimized taking into account the back pressure and the lifespan of SPE columns.

4. System Stability.

The system stability was measured during 9 h 40 min of continuous running, since typical *in vivo* monitoring experiment lasted 6-8 h, subject to the durability of the microdialysis probe.

1) Data Processing Method.

The extracted ion chromatography (EIC) method was applied to all HPLC-MS/MS data in order to obtain accurate chromatography peak parameters for every analyte. EIC is also known as reconstructed ion chromatography (RIC). The difference between total ion chromatography (TIC) and

EIC is that TIC plots the *total* ion current (intensity) vs. time, whereas EIC plots a *single* ion signal intensity vs. time. The mechanism of EIC is similar to selected ion monitoring (SIM), whereas SIM is a MS data acquisition technique, EIC is a MS data processing technique. EIC is a basic function for all MS data processing software. To obtain EIC for a particular ion, simply input the m/z value of the ion and the deviation allowed (usually ± 0.5 m/z). EIC is extremely useful when peaks are overlapped in total ion chromatography (TIC), as shown in Figure 2-7.

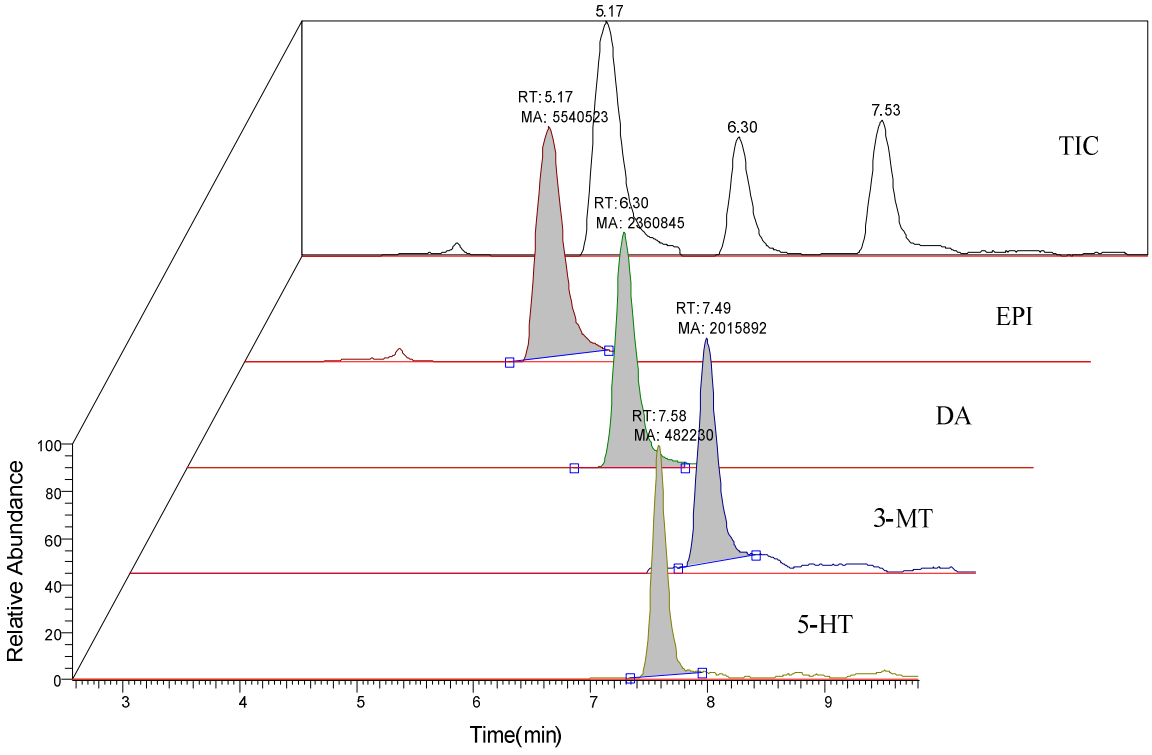

Figure 2- 7. Data processing method. TIC and EICs for four measured analytes.

In TIC chromatography (top trace in Figure 2-7), the chromatography peaks for 3-MT and 5-HT were overlapped, but separated by their EIC (bottom two traces in Figure 2-7).

2) Microdialysis sampling delay effects.

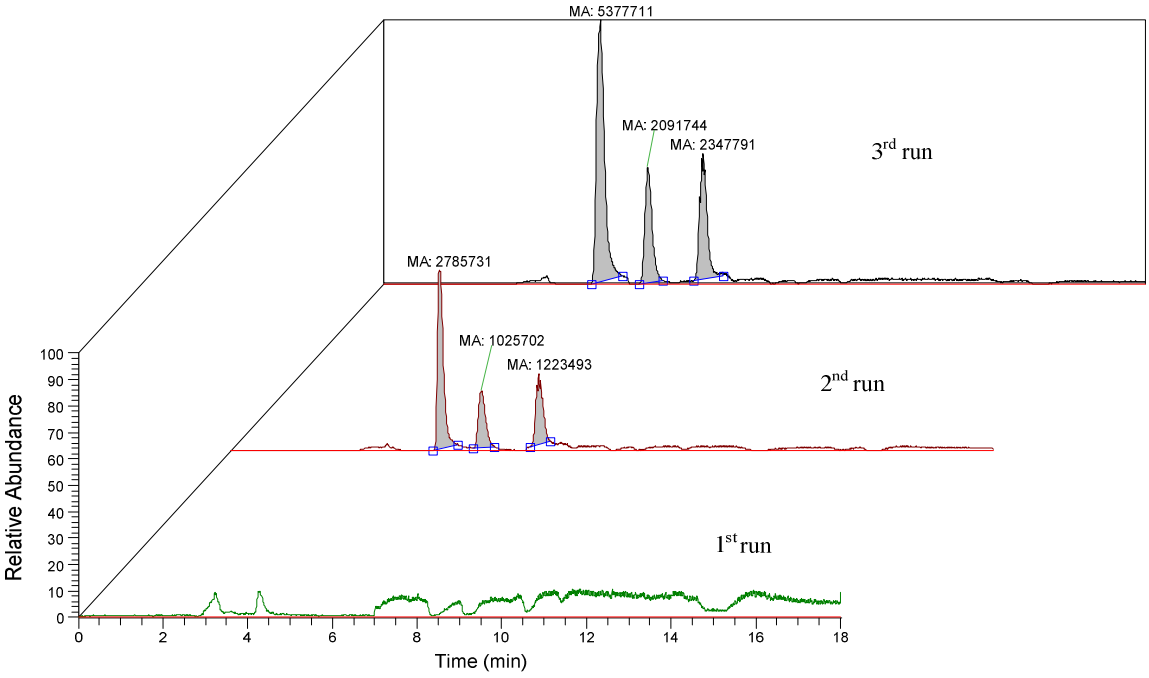

Figure 2- 8 Chromatographies for the first three runs.

Because of the very low perfusion flow rate (1.5 µL/min), the dead time must be carefully considered in on-line microdialysis experiments. For example, in Figure 2-8 the first run shows no signal because when it was started, the syringe pump began pumping the standard solution, hence no sample reached the sampling loop. Nevertheless, the data of the first run was valuable since it provided the mobile phase blank data. In the second run, although the sample loop had been continuously filled with analytes for 20 min, the dead volume between syringe and the sample loop has to be taken into account. For a typical 40 cm length of capillary PEEK tubing for the connection, the dead volume was ~4.8 µL. However, any connections, syringe needle and the pathway inside 10

port valve contributed to the dead volume. Thus, the total dead volume was much larger than 4.8 µL. Accordingly, it was no surprise that the signal intensity (peak area) for the second run was only ~50% of that measured for the third run. From the third run on, the signal intensity became constant. Thus stability was measured by comparing chromatograph peak areas for each analyte sample during the 3rd to the 29th run (totally 9-h).

3) System Stability.

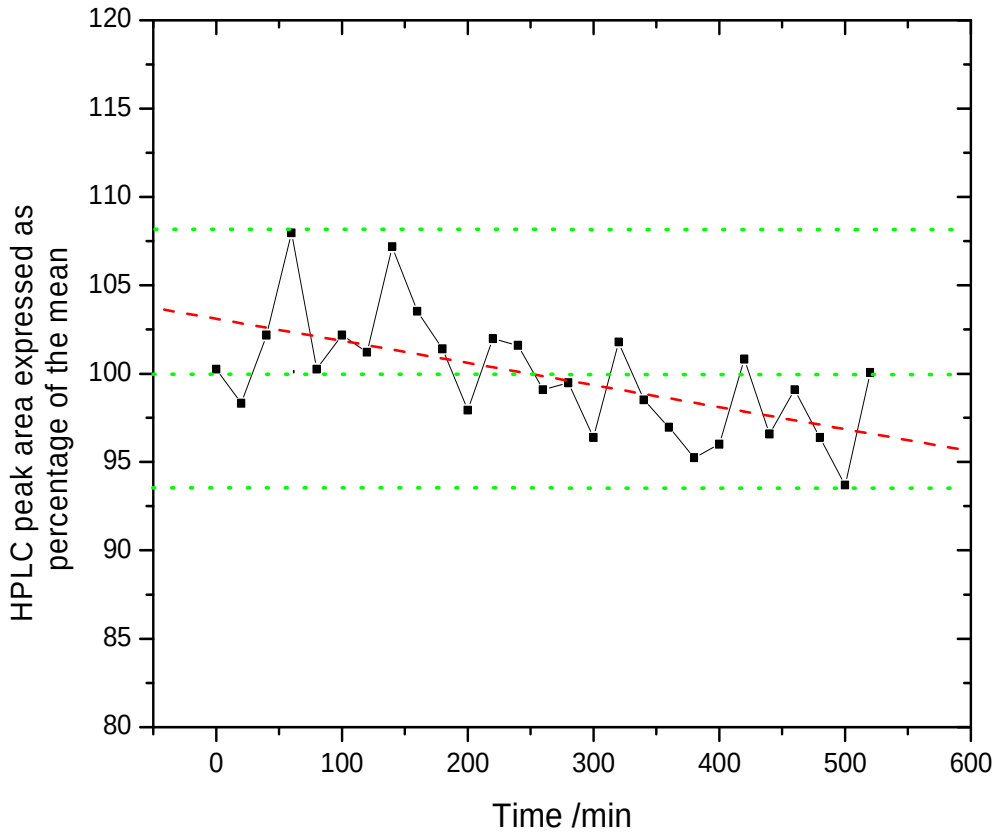

Figure 2- 9. System stability test: EPI. The green dotted lines are the maximum, mean and minimum for all data. The red dotted line is the linear fit for all data.

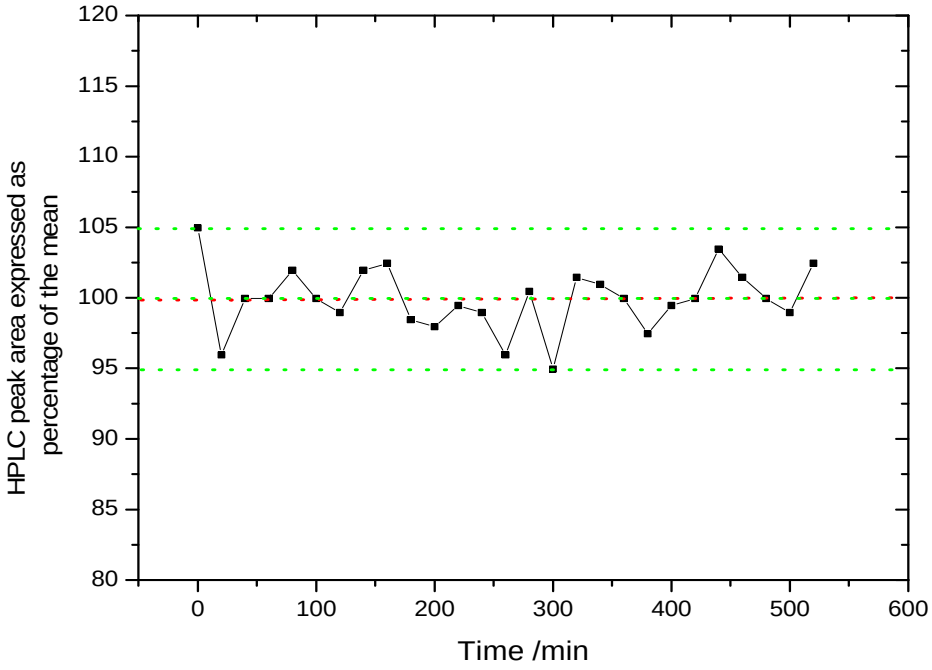

Figure 2- 10. System stability test: DA. The green dotted lines are the maximum, mean and minimum for all data. The red dotted line is the linear fit for all data.

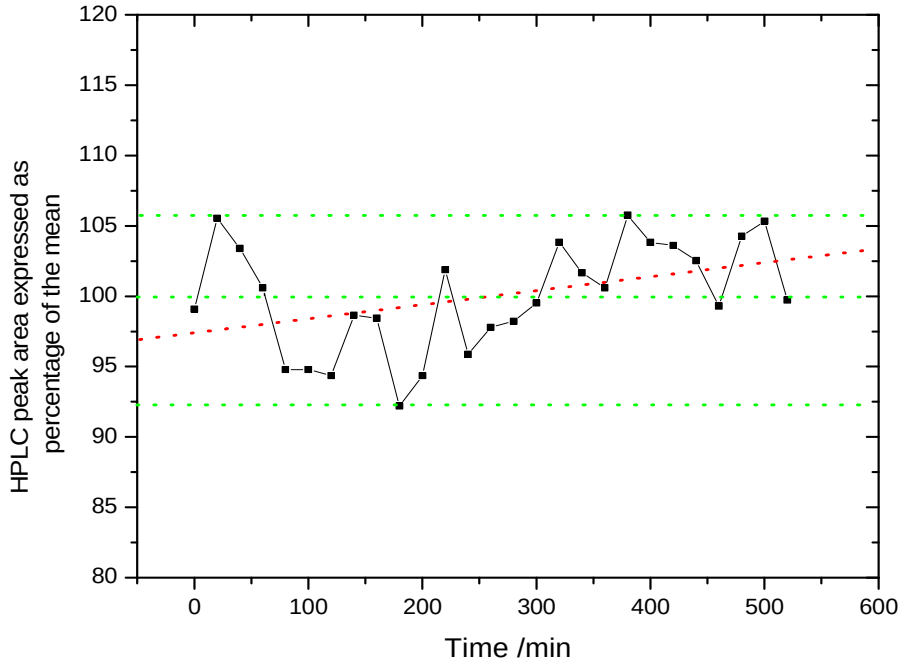

Figure 2- 11. System stability test: 3-MT. The green dotted lines are maximum, mean and minimum for all data. The red dotted line is the linear fit for all data.

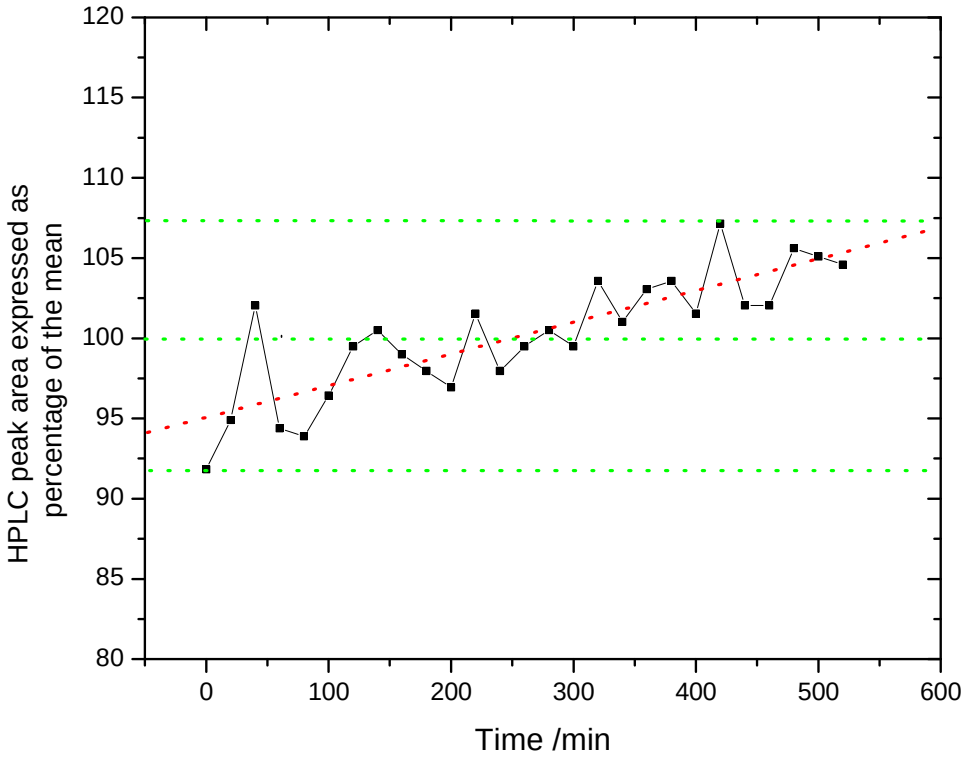

Figure 2- 12. System stability test: 5-HT. The green dotted lines are maximum, mean and minimum for all data. The red dotted line is the linear fit for all data.

Substance	Peak area mean $\times 10^6$	SD $\times 10^6$	SEM $\times 10^6$
EP	5.18	0.177	0.034
DA	2.00	0.051	0.0098
3-MT	1.96	0.075	0.0051
5-HT	0.464	0.018	0.0035

Table 2- 1. System stability statistics data.

Figure 2-9 – 2-12 are plots of HPLC peak area expressed as the percentage of the average of 27 runs against time. The red dotted lines are the linear fit of the data and show the overall trend for the signals. For EPI, the overall trend for the signal was to decrease. For DA, no obvious trend was observed. For 3-MT and 5-HT the trend for the signal was to increase. The mechanisms behind these

trends were subjected to further investigation. Putatively, the declining trend for EPI might be related to its lower stability than the other analytes, meaning the actual EPI concentration in perfusate declined with time. The increasing trend for 3-MT and 5-HT could be caused by their higher affinity to the reversed phase SPE column, since both of them are lower polarity molecules. Thus, they could have a tendency to accumulate on the SPE column and subsequently cause increasing signals for later runs. Nevertheless, the variations observed for all analytes were small (Table 2-1). Thus, it was concluded that the fully automated system was a high precision system with very good stability.

5. Time Arrangement for *In Vivo* Experiments Utilizing the Fully Automated System.

The fully automated system was largely labor free, with high precision and high sample throughput. Nevertheless, careful time arrangement for the whole *in vivo* experiment was necessary in order to maximize the usefulness of the system and to minimize human error. Figure 2-13 describes the experimental schedule from ordering the animal to the end of *in vivo* experiments. Human interactions are shown in the gray boxes; these actions are potentially subject to further automation. Some of the actions, such as drug perfusion, can be automated with an extra electronic controlled device. Some of the actions, including placing the microdialysis probe in a standard solution (*in vitro* examination) and then to an aCSF blank solution (in order to be flushed and cleaned), could be automated with the help of robotic devices. For the remainder of the actions, such as surgery and implanting the microdialysis probe into an awake rat are difficult to automation, at least at the present time.

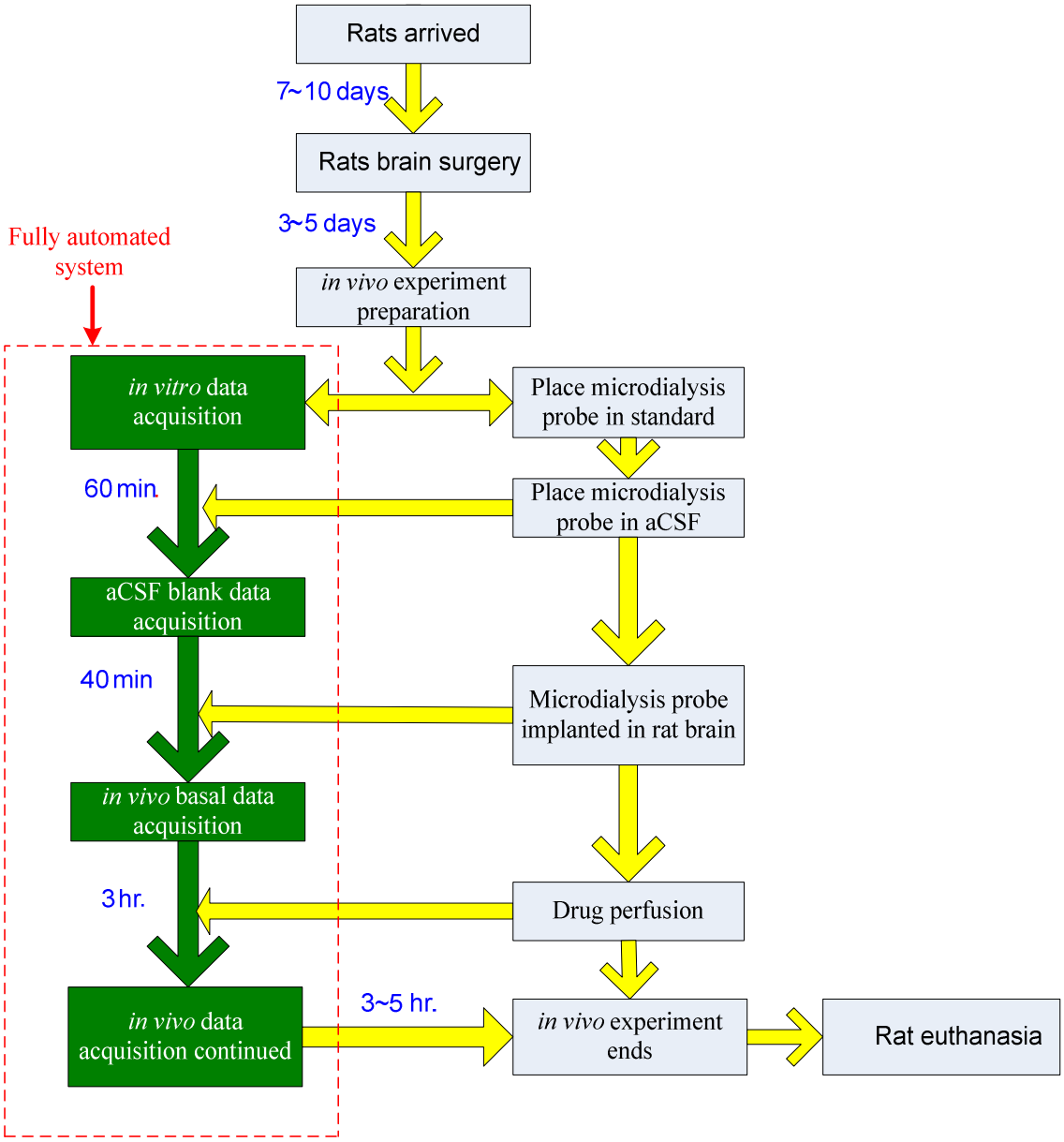

Figure 2- 13. Time arrangement for *in vivo* experiments utilizing the fully automated system.

D. Conclusions

In this chapter, a fully automated system combining on-line microdialysis sampling, on-line SPE and HPLC-MS techniques was constructed. The coordination of the components is illustrated by

the control relation chart, eluent flow chart and event flow chart. The stability of the system was tested by 9 h 40 min of continuous, unattended running. The system was proved to be stable, labor free and had high throughput. The system therefore has the potential to provide an important research tool for *in vivo* monitoring of all kinds of metabolites, which will be demonstrated in later chapters.

Chapter Three

On-line Ion-pair Reversed Phase Solid Phase Extraction (IP-RP-SPE)

A. Introduction

Ion-pair (IP) techniques held the key to the success of the automated *in vivo* monitoring project. In this project, IP was intensively used in RP-SPE to clean up and pre-concentrate analytes in microdialysate samples. IP was also applied to HPLC in order to improve retention for targeted analytes.

The mechanism for ion-pairing is quite straightforward:[140-144] IP reagents contain a nonpolar portion, usually a long chain aliphatic hydrocarbon (perfluorination is employed in order to increase the volatility of the agent), and a polar portion, such as an acid or base. The polar portion of the IP reagent interacts with the analyte counter-ions, forming an ‘‘ion-pair.’’ The nonpolar portion interacts with the nonpolar reversed phase media, usually the C_{18} hydrocarbon chain of the octadecylsiloxane-bonded silica surface. Retention of an analyte may be enhanced by increasing the carbon chain length of the IP reagent and by increasing the concentration of the IP reagent.

In principle, many volatile organic acids, bases, or salts could be used as IP reagents in RP-HPLC-MS techniques.[145] Among them, formic acid (FA), acetic acid (AA), ammonium acetate (NH_4OAC) are widely employed. However, such compounds are more properly considered as pH modifiers or buffer additives than IP reagents. Indeed, their IP functions are weak owing to the very

short nonpolar segment of their structures. Among the IP reagent arsenal, trifluoroaectic acid (TFA) is the most well-known and widely used volatile IP reagent, especially in the field of peptide and protein analysis.[146] Larger analogs of TFA are more useful for small, very polar or ionic substances.[94,147-154] Among them, HFBA and TDFHA are the most popular.[94,155-157]

TFA

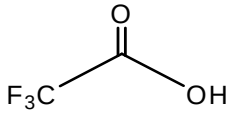

HFBA

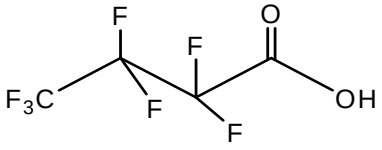

TDFHA

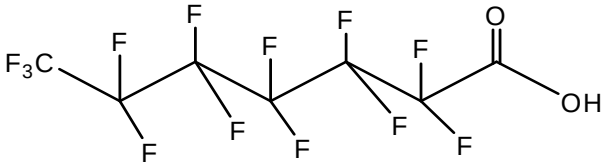

Figure 3- 1. Chemical structures of three IP agents

The major limitations of IP reagents is their propensity for signal suppression in ESI-MS.[158] Nevertheless, many methods to address this problem have been developed including post-column organic solvent or acid addition.[159] In the present study, however, high concentrations of a moderately strong IP reagent such as HFBA or a very strong reagent such as TDFHA at low concentrations were used for the SPE process, while only very low concentrations (1mM) of HFBA were used in HPLC mobile phases. Thus, the amount of IP reagent that entered the mass spectrometer was kept minimal.

This approach benefited from prudent selection of the HPLC column (Phenomenex Synergi Hydro-RP®). The separation properties of this column are based on a mixed mechanism. While the column stationary phase basically consists of a nonpolar C_{18} reversed phase, the unbound silanol groups on the silica are end-capped with a polar functional group. This arrangement results in the column exhibiting good retention for both non-polar and highly polar compounds.[160-164] Nevertheless, for extremely polar and ionic compounds, an IP reagent was still needed in order to obtain reasonable retention of the target analytes, although the minimum amount of IP reagent needed to effect appropriate retention was employed. In our experiments, ESI-MS signal suppression was not prominent and, hence, it was not necessary to devise strategies to address this issue.

B. Experimental

1. Chemicals and Chromatographic Conditions.

Most chemicals and chromatographic conditions were the same as described in detail in Chapter Two. MPTP and MPP^+ were purchased from Research Biochemicals International (RBI; Natick, MA). Reduced glutathione (GSH) and cysteine (CySH) were obtained from Sigma. GSH-MPB and CySH-MPB were produced as described in Chapter Five. Several more SPE mobile phase solutions were prepared and tested. These SPE mobile phases were:

1.) Mobile phase F3, water containing 0.1% FA

2.) Mobile phase F4, water containing 20 mM NH_4OAC.

3.) Mobile phase F5, water containing 25 mM HFBA, pH 2.5.

4.) Mobile phase F6, water containing 50 mM HFBA, pH 2.0.

5.) Mobile phase F7, water containing 50 mM HFBA; pH was adjusted to 4.8 with NH_4OH.

2. Standard Solutions.

Stock standard solutions were prepared and stored as described in Chapter Two. A 1 μM DA standard solution was prepared as follows: 10 μL of 1 mM DA stock standard solution was added to 990 μL of aCSF; 100 μL of this solution was then added to 900 μL aCSF. The 1 μM standard solution containing three catecholamines (DA, NE, EPI), 5-HT and 3-MT was prepared as follows: 10 μL of each of five stock standard solutions (each 1mM) was added to 950 μL aCSF; 100 μL of the resulting solution was added to 900 μL aCSF. All solutions were stored in plastic vials and were passed through 0.2 μm centrifuge filter (NanoSEP™, VWR, USA) before use. The 1 μM standard solutions for MPTP, MPP^+, GSH, and CySH were prepared similarly. All aCSF solutions were degassed with He sparging.

3. Basic Chromatographic Properties of the SPE Column: Dead Volume and Solvent Front Profile.

These experiments focused only on SPE and, hence, the fully automated system was modified as follows:

1) The HPLC pump, HPLC column and microdialysis instrumentation were not used.

2) PEEK tubing (Upchurch), 0.005 in ID × 1/16 in OD, was used to connect the TSQ 7000 MS ion source inlet and port 6 on the 6-port valve; the 6-port valve was set to sample load

and cleaning position at all times so that the SPE column was directly connected to the mass spectrometer during experiments.

3) An injection adapter was installed on port 1 of the 10-port valve so that samples were manually loaded into the sample loop.

4) The injection was controlled by manually pushing the trigger button on the BAS on-line injection controller. After the sample was loaded the button was pushed to toggle the 10-port valve so that the sample was delivered to the SPE column. At the same time the TSQ 7000 MS was triggered to initiate data acquisition. The SPE eluent was continuously monitored by MS.

5) The SPE mobile phase used in this experiment was mobile phase F3.

With the above modification, 35 μL MeOH was injected and the SPE eluent was monitored by MS in the full scan (50-500 m/z) mode.

4. Influence of Different Ion-Pair Agents on the SPE Efficiency.

Using the above instrumental arrangement, SPE mobile phases F3, F4, F5 were tested. The 1 μM DA (as model compound, MW = 153.1) standard solution was manually injected and the SPE eluent monitored by MS in the single ion monitoring (SIM - 154.1) scan mode.

5. Influence of HFBA Concentration and pH on SPE Efficiency.

The instrumentation used in these experiments was the same as above. SPE mobile phases F6, F7 and F1 were tested. The 1 μM DA standard solution was manually injected and the SPE

eluent monitored by MS in the single ion monitoring scan mode.

6. SPE Breakthrough Curves for Catecholamines, 5-HT and 3-MT Using HFBA- and TDHFA- Based Mobile Phases.

The fully automated system described in Chapter Two was employed. The standard solution containing a mixture of 1 μM catecholamines, 5-HT and 3-MT was perfused by a syringe pump. The SPE wash times were programmed between 0.2 and 2.5 minute, using 0.2 or 0.5 min increments for each step. The first experiment employed mobile phase F1. This was then repeated using SPE mobile phase F2. The mass spectrometer was set to the selected reactions monitoring (SRM) scan mode. Detail of SRM settings will be presented in Chapter Four.

7. SPE Breakthrough Curves for MPTP and MPP^+

Using the fully automated system (Chapter Two) and mobile phase F2, the standard mixture solution of MPTP and MPP^+ (each 1 μM) was perfused using a syringe pump. The SPE wash times were programmed between 0.2 and 3.0 min in 0.2 min increment. MS SIM scan was employed where the ion of 174 m/z was monitored for MPTP and 170 m/z for MPP^+.

8. SPE Breakthrough Curves for GSH, CySH, GSH-MPB and CySH-MPB.

Using the fully automated system (Chapter Two) and mobile phase F2, a standard solution of GSH and CySH (1 μM each) was perfused by a syringe pump. The SPE wash times were programmed between 0.3 and 3.0 minute in 0.2 min increments. GSH and CySH in the HPLC eluent were

monitored by MS in the SRM mode. Using the modified fully automated system (Chapter Five), the 10 µM standard solution for GSH, CySH together with the 5mM MPB solution (on-line derivatization) were perfused by a syringe pump. GSH-MPB and CySH-MPB were monitored by MS in the SRM mode.

C. Results and Discussion

1. Solvent Front of the SPE Column and Theoretical Considerations.

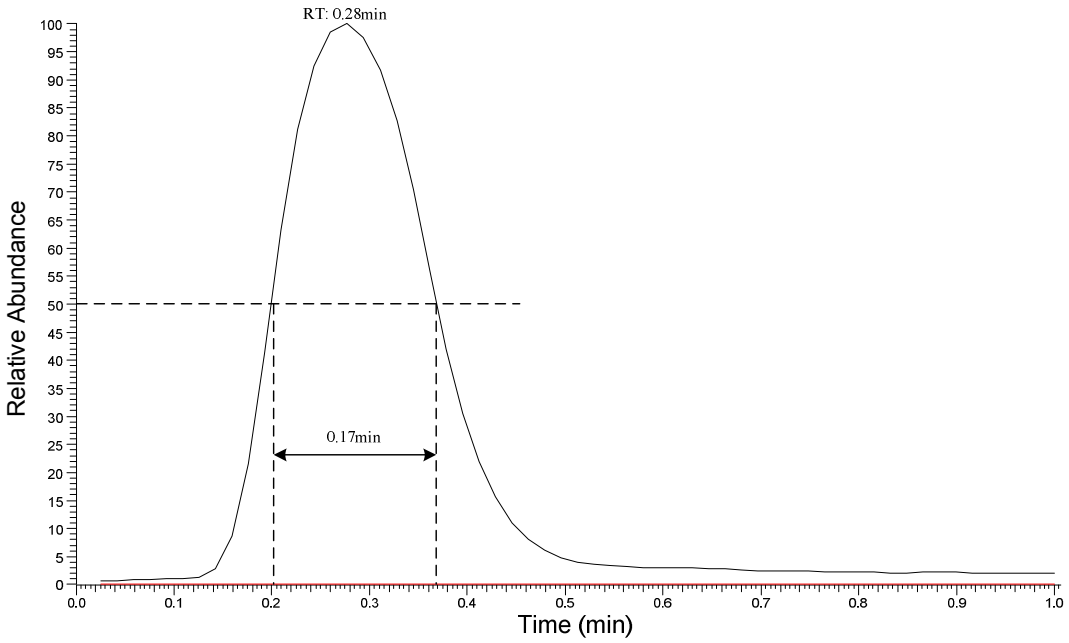

Figure 3- 2. Solvent front profile for the SPE column, showing the retention time (0.28 min) and peak width at half maximum (FWHM) (0.17 min).

The dead time (t_d) for the SPE was 0.28 min at a flow rate (r) of 200 µL/min. Thus, the dead volume (V) was calculated as $V = t_d \times r = 56$ µL. The full width at half maximum (FWHM) of the

peak was 0.17 min. The simplest theoretical simulation was to fit the chromatographic peaks to a normal distribution curve:

$$S = \frac{1}{\sigma\sqrt{2\pi}} \exp\left(-\frac{(t - t_d)^2}{2\sigma^2}\right)$$

where $\sigma = \frac{1}{2\sqrt{2\ln 2}} FWHM \approx 0.425 FWHM$

Using the experimental values of t_d and σ, a normal distribution simulation was carried out and is presented in Figure 3-3.

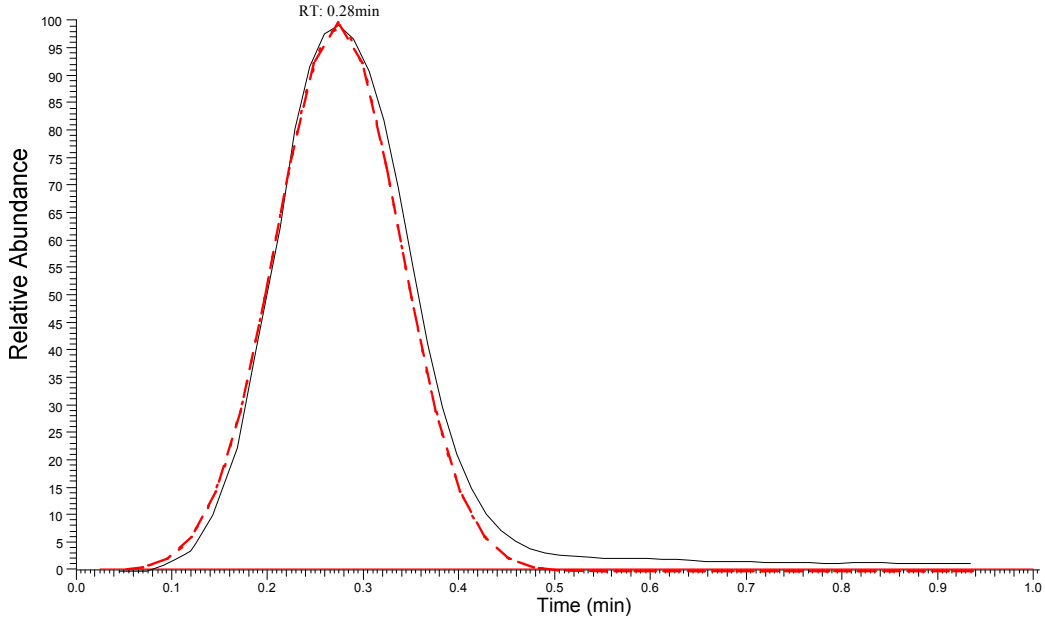

Figure 3- 3. Normal distribution curve (red dashed line) superimposed on the experimental SPE solvent front profile (black curve)

With this simulation it was possible to calculate the theoretical breakthrough curve for the solvent front for salts. A breakthrough curve is a graphic representation of the recovery rate of the

monitored analyte relative to the time employed to wash the SPE column. Measuring and studying the breakthrough curve was important to justify the efficiency and to optimize the SPE. For HPLC-MS techniques, the experimental measurement of breakthrough curves for salts and other unretained small molecules is difficult, if not impossible.

Thus, the theoretical breakthrough curve is a tool to study the behavior of salts in SPE processes. From the normal distribution formulation, the breakthrough curve can be derived as:

$$R = 50 \times [1 - erf(\frac{t - t_d}{\sigma\sqrt{2}})]$$

where R is the SPE recovery, expressed as a percentage; and erf is the Gaussian error function. Using experimental t_d and σ values, the breakthrough curve is presented in Figure 3-4.

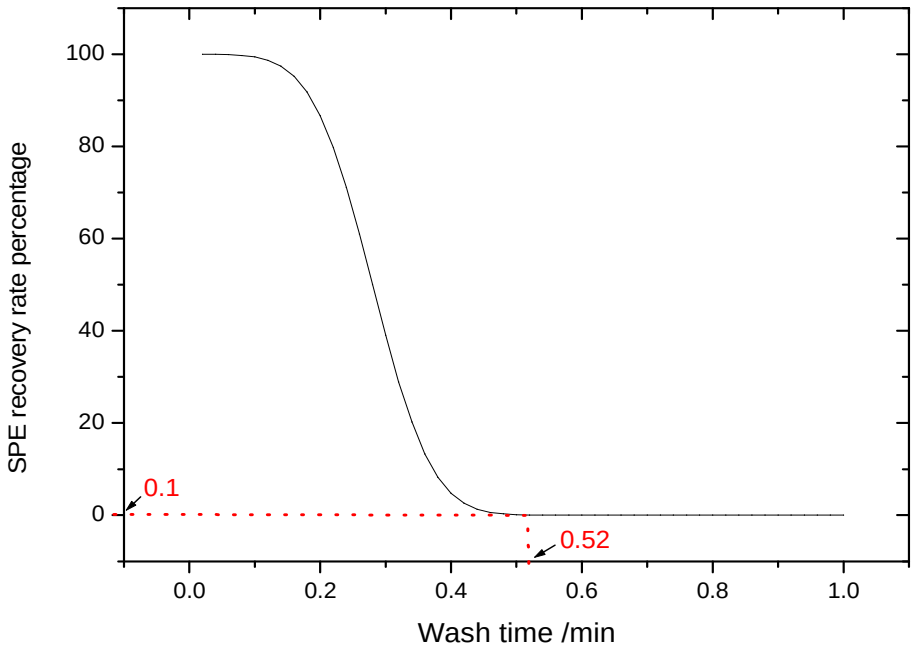

Figure 3- 4. Theoretical breakthrough curve for solvent front (salts). The wash time required to remove 99.9% of salts was 0.52 min.

From the simulation data sheet (not shown), a 0.52 min wash time was necessary to wash

out 99.9% of salts. It should be noted, however, that 0.52 min is the theoretical minimal time. In reality, longer washing times are always necessary. One consideration is that there are endogenous matrix compounds which are not totally unretained and, therefore, longer wash times are required to remove these substances.

If a recovery of 99.9% is assigned for a compound with a maximum of 0.1% of the salts remain left on the SPE column, and it can be calculated from theoretical simulations (process not shown) that a minimum retention time of 0.75 min is required for that compound, which corresponds the retention factor K:

$$K = \frac{t_r - t_d}{t_d} = 1.68$$

2. **Influence of Different Ion-Pair Reagents on SPE efficiency**.

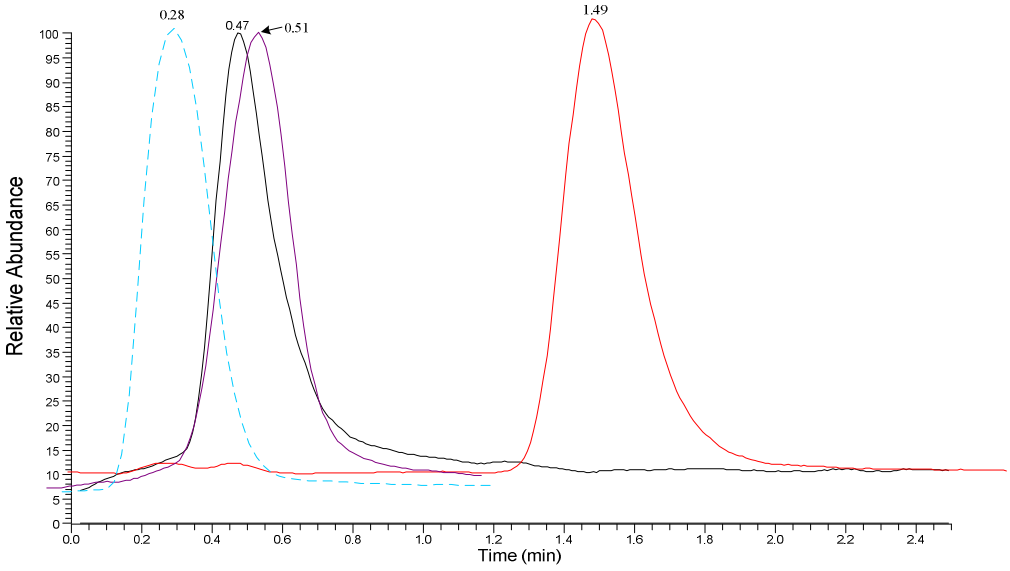

Figure 3- 5. DA SPE eluent profiles for different IP reagent-modified SPE mobile phases. From left to right: solvent front (blue dotted line); mobile phase F4 (solid black line); mobile phase F3 (solid violet line) and mobile phase F5 (solid red line).

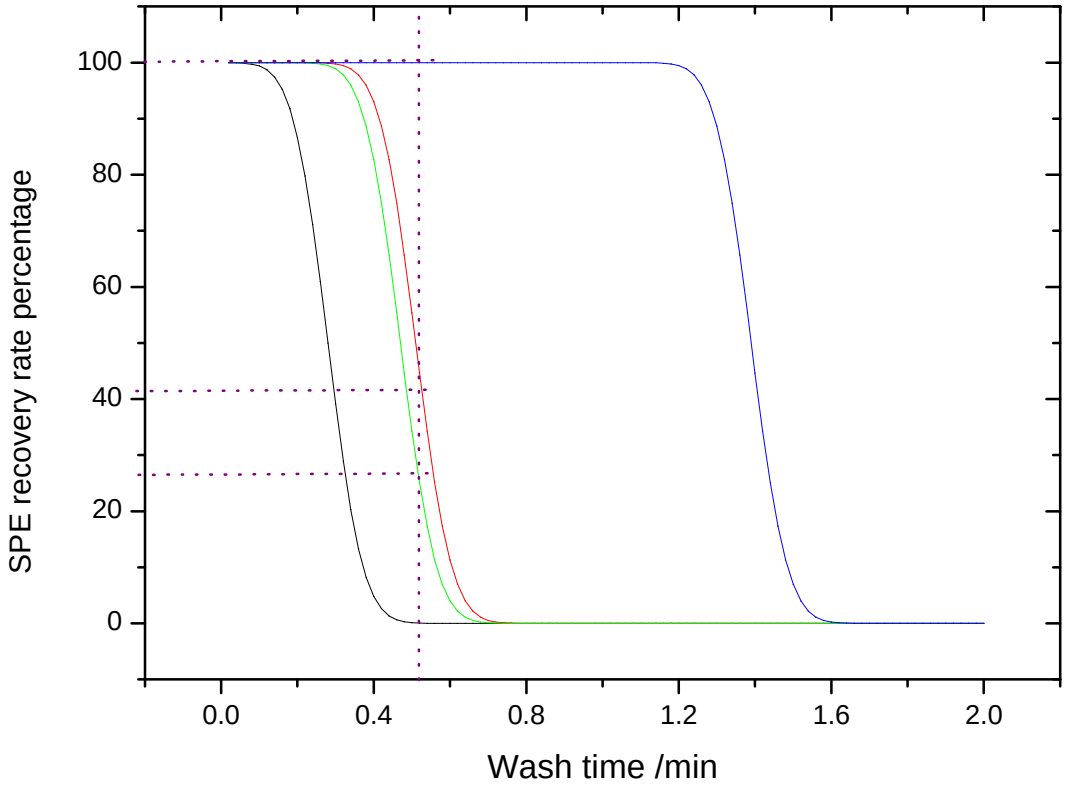

Figure 3- 6. Theoretical breakthrough curve for solvent front (salts) and DA in different mobile phases. From left to right: solvent front, mobile phase F4 (NH_4OAC), mobile phase F3 (FA) and mobile phase F5 (HFBA).

The dotted line in Figure 3-6 indicates the situation when the theoretical minimal wash time (0.52 min) is applied. Under these conditions, only mobile phase F5 met the requirement for a DA recovery of 99.9+%. NH_4OAC and formic acid were not adequate IP reagents to extract DA. HFBA was a good IP reagent for DA in IP-RP-SPE.

3. HFBA Concentration and pH Influence on SPE Efficiency for DA.

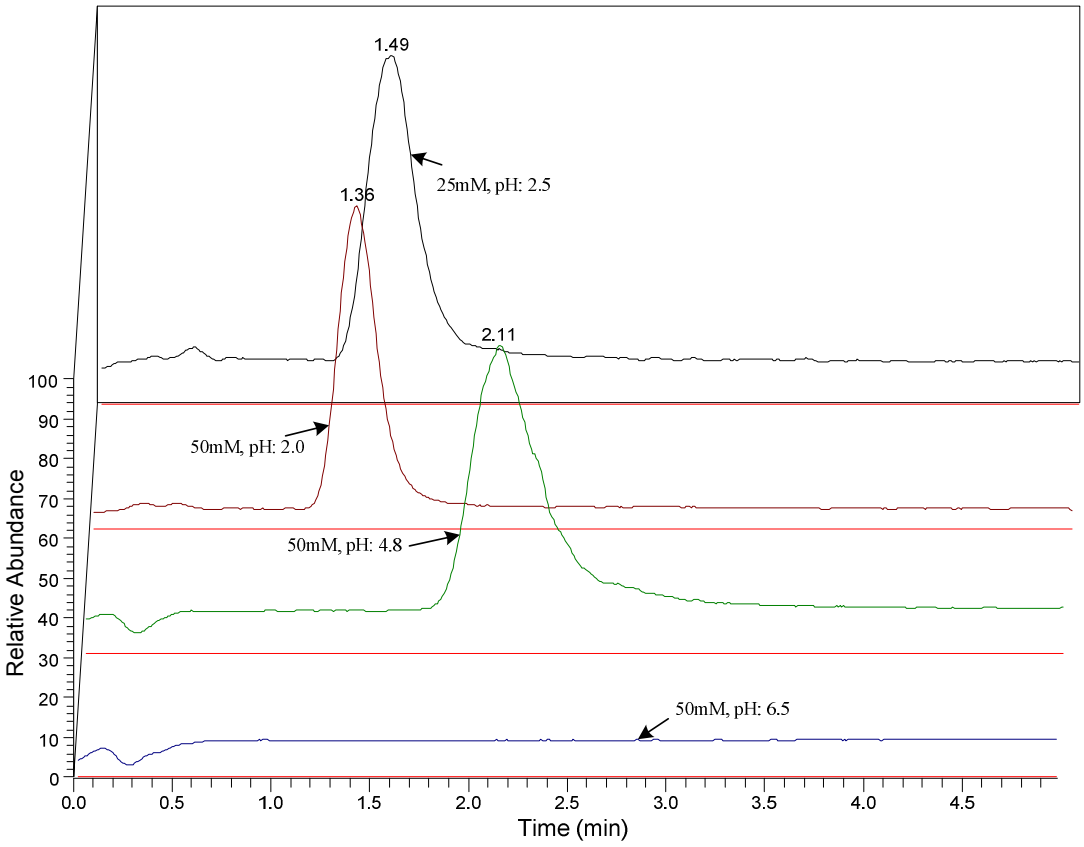

Figure 3- 7. HFBA concentration and pH influence on DA extraction. The numbers represent HPBA concentrations and pH.

The experimental results displayed in Figure 3-7 show that increasing the HFBA concentration from 25 mM to 50 mM decreases the retention time for DA from 1.49 to 1.36 min. Increasing pH greatly increased retention time. When the pH was increased to 6.5, no detectable DA was washed out from the SPE column in 5 min. The conclusion, therefore, is that the concentration of the IP reagent has a limited influence on SPE efficiency, while pH has a tremendous influence. This is reasonable because: 1) the concentration of IP was always several orders of magnitude greater than that of the analytes; and, 2) in order to have the ability to form an ion-pair the IP reagent must be in its ionic form, meaning it has to be deprotonated. Deprotonation is always facilitated by higher pH.

4. Experimental Breakthrough Curves for Catecholamines, 5-HT and 3-MT.

Previous experiments showed that direct measurement of SPE eluent profiles for the analytes was a useful technique to evaluate SPE efficiency. However, when the analytes were 'truly' retained on the SPE column, *e.g.,* DA in mobile phase F1, an elution profile cannot be obtained. Nevertheless, experimental measurement of the breakthrough curve was feasible thus providing a better way to optimize SPE conditions. In experiments measuring breakthrough curves, assigned wash times were applied to the targeted compound, then it was backflashed out of the SPE column and subsequently analyzed by HPLC-MS. The advantages of direct breakthrough curve measurements include:

1) A breakthrough curve can be measured for most compounds. The experimental set-up is straightforward and easy to perform with the fully automated system. During the experimental design, a sample acquisition queue was designed such that all acquisitions in the queue were identical except the SPE wash times were programmed to increase (or decrease) in a stepwise fashion. The details of how to change the wash time is described in Chapter Two. Once the acquisition queue was started, the whole experiment was fully automated and unattended.

2) The system setting used to measure breakthrough curves was the same as the *in vivo* experiments. Thus, SPE condition optimization directly related to *in vivo* experimental results.

3) When measuring breakthrough curves, salts were washed from the sample before further analysis thus protecting the MS detector

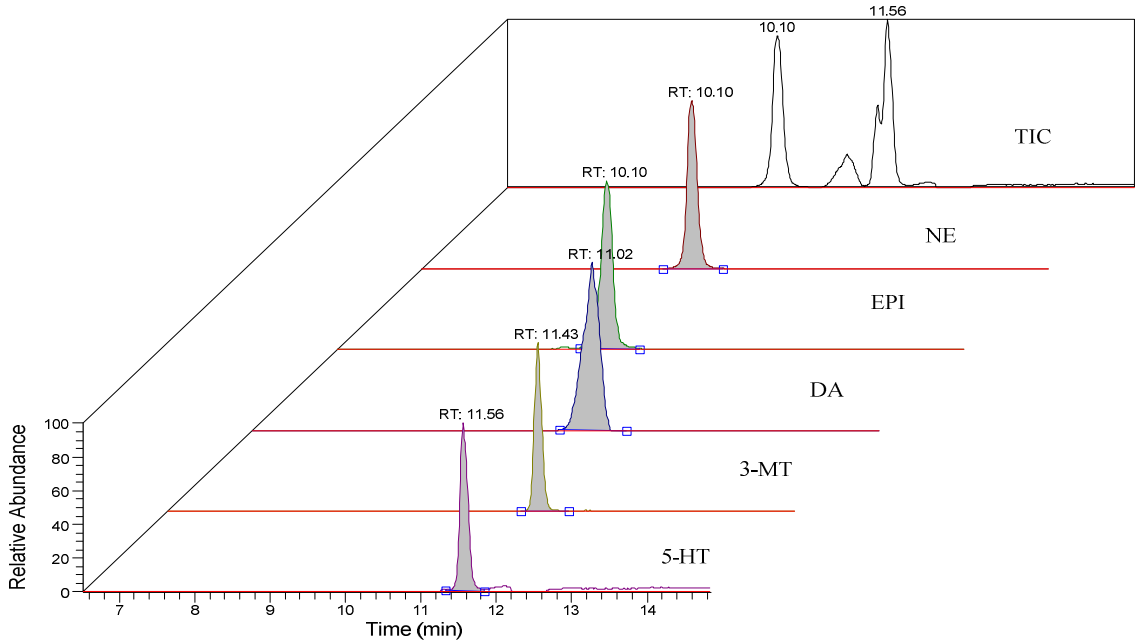

Figure 3- 8. A typical data in the breakthrough curve measurements for catecholamines, 5-HT and 3-MT. Extracted ion chromatography (EIC) was applied for all 5 analytes.

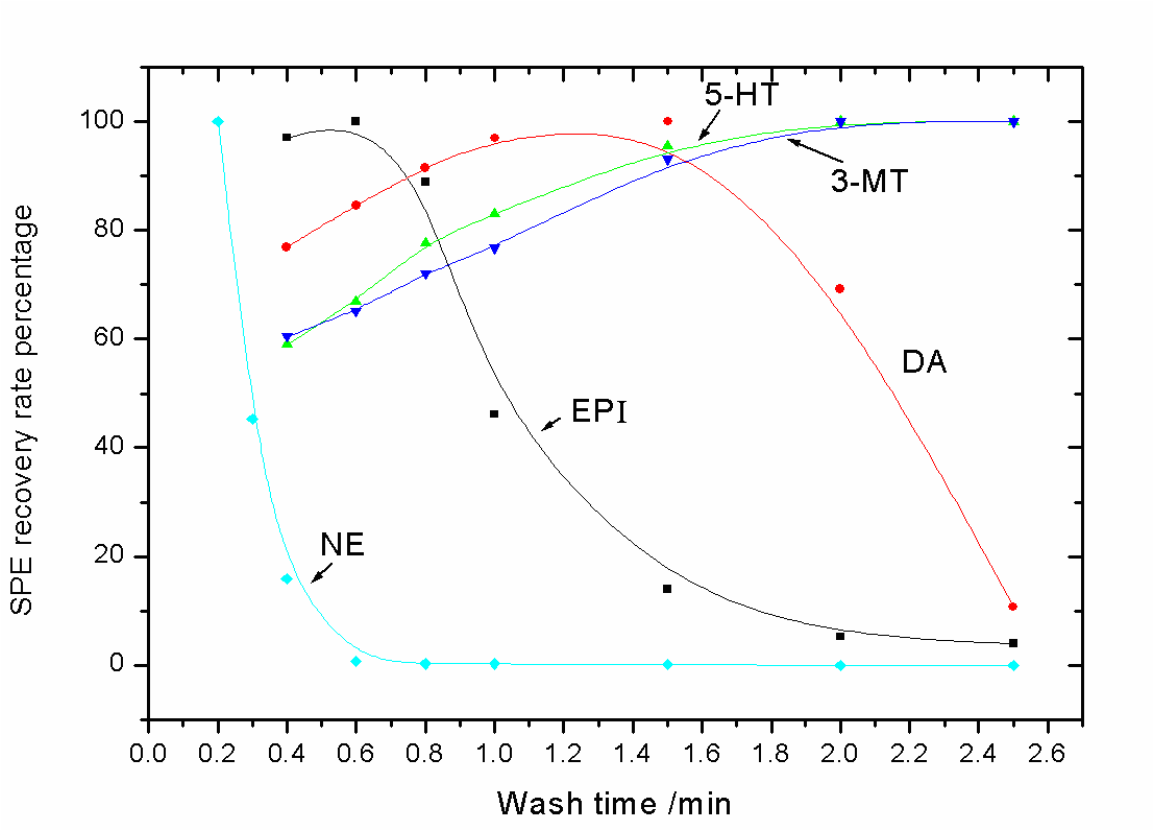

Figure 3- 9. Breakthrough curves for catecholamines, 5-HT and 3-MT in mobile phase F1.

The above graphs show breakthrough curves for the three catecholamines, 5-HT and 3-MT using SPE mobile phase F1. Clearly, NE was not retained very well, meaning that most NE actually co-eluted with the solvent front or salts. EPI had a much better (longer) retention time than NE although a shorter wash time (~0.7 min) was required to achieve a high recovery. The optimal wash time for DA was around 1.2 min. For 3-MT and 5-HT, wash times longer than 2 min were preferable.

Theoretically, the recovery rate always decreases with wash time. However, it was commonly noted in SPE experiments that the recovery rate increased in the early stages of washing, as shown on the graph for DA, 3-MT and 5-HT (Figure 3-9). The explanation for this relies on the fact that the detection of many compounds is affected by the matrices that co-elute. Prolonged wash times help to remove these matrices.

From the above experiment, NE could not be analyzed using mobile phase F1. Accordingly, another experiment was carried out using mobile phase F2, where a much stronger IP reagent, TDFHA, was employed.

The following graphs show the breakthrough curves for five targeted analytes – three catecholamines (DA, EPI and NE), 5-HT and 3-MT. They were analyzed by the fully automated system (Chapter Two) using SPE mobile phase F2 (TDFHA). All of the targeted analytes were recovered to a satisfactory extent. From the graph, a wash time of 1.0 to 1.2 min was an optimized practical choice for the analysis of these compounds.

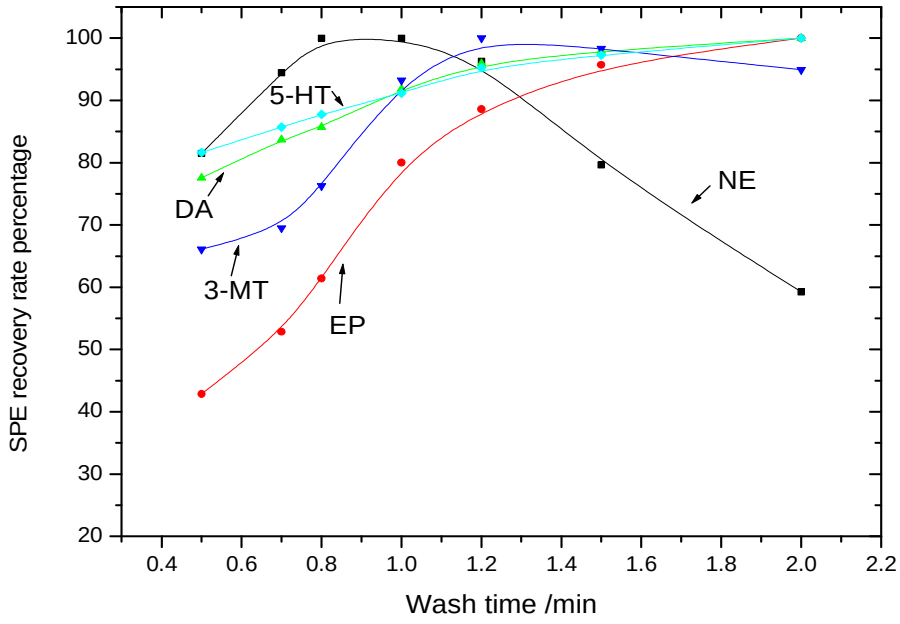

Figure 3- 10. Breakthrough curve for catecholamines, 5-HT and 3-MT in mobile phase F2.

5. Breakthrough Curves for MPTP and MPP^+

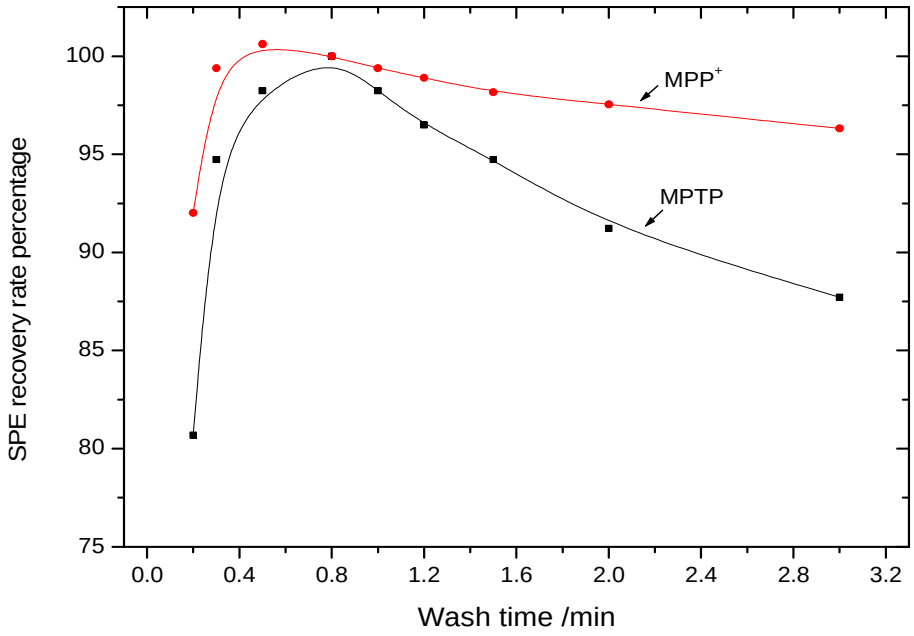

Figure 3- 11. Breakthrough curves for MPTP and MPP^+ using mobile phase F2.

The above graph (Figure 3-11) show MPTP and MPP^+ breakthrough curves in mobile phase F2. An SPE wash time of 0.8 –1.0 min was a practical choice.

6. Breakthrough Curves for GSH, CySH, GSH-MPB and CySH-MPB

Sometimes even a very strong IP reagent such as TDFHA is unable to permit the SPE column to retain strongly ionic molecules. This effect was observed when analyzing GSH and CySH (Figure 3-12). Accordingly, it was necessary to derivatize GSH and CySH with MPB in order to enable the SPE extraction. A full description of the derivatization process is presented in Chapter Five. The breakthrough curves for GSH, CySH, GSH-MPB and CySH-MPB are summarized in Figure 3-12.

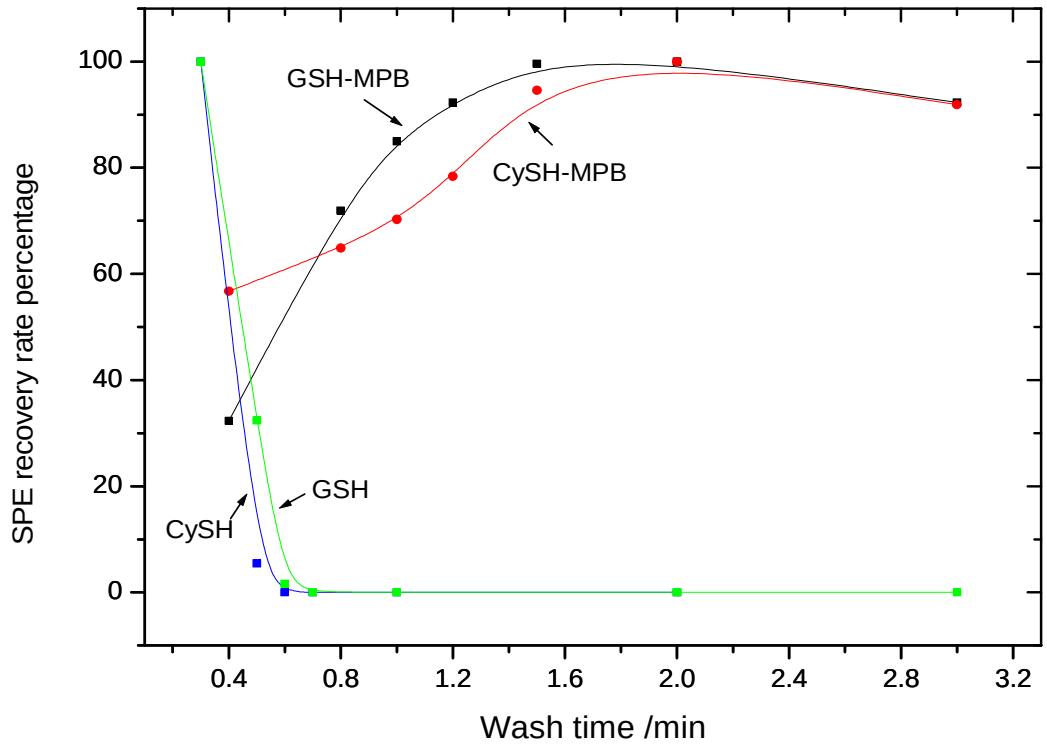

Figure 3- 12. Breakthrough curves for GSH, CySH, GSH-MPB and CySH-MPB using mobile phase F2.

As illustrated in Figure 3-12, GSH and CySH were co-eluted with the solvent front in mobile phase F2 and, consequently, could not be analyzed. However, following derivatization, GSH-MPB and CySH-MPB were extracted very well by SPE. A wash time from 1.8 to 2.0 min was a practical choice.

D. Conclusions

The use of IP reagents in SPE and HPLC was the key to the successes of fully automated system. Optimization of the SPE process for any analyte is the most important step for the whole experiment. In order to determine the optimum SPE conditions, different IP agents were tested. Experiments showed that pH was the most important factor relating to IP efficiency. HFBA exhibited a very good ability to increase SPE efficiency for most catecholamines, 5-HT and 3-MT. However, HFBA was inadequate for NE. TDFHA is the reagent of choice for IP-RP-HPLC. However, TDFHA was inadequate for very ionic molecules such as GSH and CySH. Thus, other approaches such as pre-SPE derivatization were necessary in order to analyze GSH and CySH. During SPE optimization, breakthrough curve measurement was a powerful tool.

Chapter Four

Fully Automated On-line Sample Cleanup and HPLC-MS/MS Determination of Catecholamines and Related Compounds in Rat Brain Striatum: An *In Vivo* Microdialysis Study.

A. Introduction

Catecholamines such as dopamine (DA), norepinephrine (NE) and epinephrine (EPI), are naturally occurring molecules that act as neurotransmitters and hormones regulating multiple physiological processes in organisms.[165] In animal brain, abnormal physiological concentrations of these compounds are often related to neuroendocrine disorders.[166-169] Massive release of DA is one of the characteristic effects observed in response to the administration of certain widely used neurotoxicants that mimic, in experimental animals, the selective neurodegeneration that occurs in Parkinson's disease (PD).[170,171] Catecholamine metabolism is also believed to provide an important source of free radicals.[172] For example, during the monoamine oxidase-B (MAO-B)-mediated degradation of DA a byproduct is H_2O_2 that can serve as a source of the highly cytotoxic hydoxyl radical ($HO^{\cdot}$) by transition metal catalyzed Fenton or Haber-Weiss chemistry.[173-175] Accordingly, accurate, selective *in vivo* measurement of catecholamine and related metabolite levels in biological systems could be important in pathological studies of many diseases. In our laboratory, catecholamines and related metabolites in animal models of PD have been routinely analyzed. Historically, the methods for catecholamine and related metabolites analyses in biological fluids have

primarily utilized HPLC with electrochemical[176-179] or fluorimetric[180-182] detection. However, such methods are unable to provide unequivocal identification of analytes and require considerable analytical skills. More recently, mass spectrometry (MS)-based methods, particularly HPLC-MS, have begun to be employed for analysis of catecholamines and related metabolites in biological samples[183-189] In this chapter, a fully automated system combining microdialysis sampling, on-line IP-RP-SPE sample preparation, IP-RP-HPLC separation and tandem MS/MS detection techniques has been developed and employed to monitor *in vivo* three catecholamines (NE, DA and EPI), 5-HT and 3-MT.

B. Experimental

1. Chemicals and Chromatographic Conditions.

Chemicals and chromatographic conditions were the same as described in Chapters Two and Three. One extra HPLC mobile phase was tested: mobile phase B2 which was water containing 0.1% FA.

2. Standard Solutions.

Stock standard solutions for NE, DA, EPI, 5-HT and 3-MT (1 mM) were prepared and stored as described in Chapter Two.

Five 1 μM standard solutions for individual analytes were prepared as follows: 10 μL of each 1 mM individual stock solution was added to 990 μL aCSF to obtain 10 μM solution of all compounds;

100 μL of this solution was added into 900 μL aCSF to obtain a solution containing 1 μM of each compound.

A series of calibration standard mixture solutions (1000 nM, 500 nM, 100 nM, 50 nM, 20 nM, 5 nM, 2 nM, 1 nM and 0.5 nM) was prepared as follows: a 1 μM standard solution containing NE, DA, EPI, 5-HT and 3-MT was prepared the same way described above. 500 μL of this solution was added to 500 μL aCSF to obtain a 500nM solution; 100 μL of 500 nM solution was added into 400 μL aCSF to obtain a 100nM solution; 500 μL of 100 nM solution was added into 500 μL aCSF to obtain a 50 nM solution; 400 μL of 50 nM solution was added into 600 μL aCSF to obtain a 20 nM solution; 200 μL of 20 nM solution was added into 600 μL aCSF to obtain a 5 nM solution; 400 μL of 5 nM solution was added into 600 μL aCSF to obtain a 2 nM solution; 500 μL of 2 nM solution was added into 500 μL aCSF to obtain a 1 nM solution; 500 μL of 1 nM solution was added into 500 μL aCSF to obtain a 0.5 nM solution. All solutions were stored in plastic vials placed on ice in a covered container, and were passed through 0.2 μm centrifuge filter before use.

The standard mixture solutions for in vitro experiments (500 nM, 100 nM and 50 nM, 1000 μL each) were prepared in the same manner described above.

3. Selected Reaction Monitoring (SRM) Optimization.

In SRM optimization experiments, off-line loop injections were performed and the fully automated system was not employed. The 6 port valve was modified as a loop injector as follows: a 10 μL PEEK sample loop (Upchurch) was installed on ports No. 2 and 5; a injection adapter was installed on port No. 4; port No. 1 was connected to the HPLC eluent; port No. 6 was connected to the mass

spectrometer; port No. 3 led to waste. Mobile phase A (100%) at a flow rate of 100 μL/min was employed.

MS full scan: 10 μL of 1 μM individual standard solutions were injected, while MS scan range of m/z = 50 to 500 was employed in order to obtain parent ion information. Other MS conditions were the same as described in Chapter Two.

MS/MS scan conditions: 10 μL of 1 μM individual standard solutions were injected. The collision gas was ultra high purity argon; the pressure of argon in the collision cell chamber was 2.7 mTorr. Other MS conditions were the same as described in Chapter Two. In each experiment, a data acquisition sequence was established in which the collision induced dissociation (CID) energy was programmed to increase in a stepwise fashion from 10 eV to 50 eV in 5 eV steps, with each step lasting 2.5 min. The total experiment lasted 22.5 min. For each step, one injection of the standard solution was manually performed. MS/MS mass spectra and chromatograms were collected continuously. This type of scheme was called CID energy-step-increase experiment.

4. Influence of Different MS Scan Modes on the HPLC-MS Signal/Noise Ratio.

In these experiments the instrumentation was the same as described above except that: a) a Phenomenex Synergi™ Hydro-RP column was installed between port No. 4 and the MS ion source inlet, and, b) the HPLC eluent was 100% mobile phase B2 in isocratic condition. Three MS scan modes were employed: a) full scan, 50 to 500 m/z; b) SIM scan, m/z =154.1 and, c) SRM scan, 154.1→137.1@16eV. For each experiment, 10 μL of the 1 μM DA standard solution was injected.

5. Calibration Curves

The fully automated system (Chapter Two) was employed for calibration curve determinations. However, the microdialysis probe was not used and the BAS gastight syringe was loaded with the standard mixture solution. The solution was perfused directly to the sample loop on the 10-port valve at a rate of 1.5 µL/min. Experiments were performed starting from the lowest concentration (0.5 nM) to the next higher concentration and so on. For each concentration, at least six runs were performed with the first two runs being considered as equilibration processes.

6. *In Vitro* Microdialysis Experiments

Utilizing the fully automated system (Chapter Two), the syringe was loaded with aCSF. The tip of the microdialysis probe was immersed into standard mixture solutions stored in plastic vials. The recovery was expressed as the percentage ratio of the measured dialysate concentration compared to the known concentration of the *in vitro* standard solutions. Experiments were performed starting from the lowest *in vitro* concentration (50 nM) to the next higher concentration and so on. For each concentration, at least six runs were performed, the first two runs being considered equilibration processes.

7. Animals and Surgical Procedures

All animal experiments were performed in strict accordance with the protocols approved by the Institutional Animal Care and Use Committee at the University of Oklahoma. Adult male albino Sprague-Dawley rats (Harlan Sprague-Dawley, Madison, WI) weighing 320-350 g were used. Upon

arrival they were allowed 5–7 days to become equilibrated with their new environment. Animals were housed individually in cages with bedding (Sani Chips®; P.J. Murphy Forest Products, Montville, NJ) and free access to food (Lab Diet® #5008 Formulab Diet; PMI® Nutrition International, LLC; Brentwood, MO) and water. The room that housed the rats had a 12 hour light-dark cycle. During the equilibration period, rats were brought into the laboratory for 4 –6 h each day prior to surgery. The purpose of this was to allow the rats to become accustomed to the smell, noises and handling of the researcher prior to surgery.

On the day of surgery, all rats were weighed, and the heaviest in the group was selected for the first surgical procedure. The rat was pre-anesthetized with diethyl ether (in a desiccator) prior to injection of the anesthetic (ketamine, 85.72 mg/kg; *ca.* 0.3 mL) and analgesic (xylazine, 5.72 mg/kg; *ca.* 0.2 mL). Ten minutes after the initial anesthesic/analgesic, animals were tested for limb reflex by pinching the muscles in its hind legs with tweezers. If the animal was not completely unconscious, an additional dose of anesthesic/analgesic at 67% of the original dose, *i.e.*, ~0.2 mL of ketamine and ~0.15 mL of xylazine was administered. During surgery, the animal's consciousness was checked periodically and additional doses of ~0.2 mL ketamine and ~0.15 mL xylazine were administered if limb reflex was exhibited. Animals were placed in a stereotaxic instrument (Lab Standard™, Stoelting, Wood Dale, IL) with the nose bar positioned 3.3 mm below the interaural line. Sterile eye lubricant (Moisture Eyes™ PM; Bausch and Lomb, Rochester, NY) was applied to the animal's eyes for protection. The scalp was trimmed of excess hair and sterilized with 70% ethanol. A midsagital incision was made with a surgical scalpel and the skull was exposed. With the help of the stereotaxic instrument, an initial hole was made above the right striatum (8 mm lateral and 0.5 mm anterior to

bregma). The hole was made with an electric drill handpiece system (XL-30W; Osada Electric Co., LTD, Tokyo, Japan) using a surgical trephine drill bit (BAS). Three smaller trapenizations were made in the area surrounding the initial holes and cranial screws (Plastics One, Roanoke, VA) were secured (1 mm depth below the surface of skull) in these locations. The microdialysis probe guide/dummy cannula (CMA-12) was implanted into the initial hole location, with the tip positioned 3.4 mm below dura. The probe guide/dummy cannula was secured to the skull by means of the three screws and cranioplastic cement (Plastics One).

At the end of surgery, the incision was closed with two sutures using monofilament polyglyconate synthetic absorbable sterile surgical suture (Maxon 5-0, 17 mm; Davis + Geck, Danbury, CT). A collar (Bar-Lok® Cable Ties; Avery Dennison, Framingham, MA) was fastened around the animal's neck. The animal was then transferred to its own cage and left undisturbed for 1–2 days to recover with food and water provided. Two days before microdialysis experiments, animals were placed in a bedding-lined 40 cm diameter Plexiglas bowl seated on a BAS Raturn during the daytime to become accustomed to the surrounding in preparation for *in vivo* microdialysis studies. The animal's collar was attached to a tether (with the ability to move freely) and it had access to food and water *ad libitum* through the study.

8. *In Vivo* Microdialysis.

The *in vivo* microdialysis experiment utilized the fully automated system and generally followed the protocol described in Chapter Two. The following presents the detailed step-by-step procedure:

1) *In vivo* experiment preparation.

A new microdialysis probe was prepared for use according to the manufacture's (CMA) recommendations (not shown). The aCSF solution was filtered, degassed (He sparging) and then transferred to the BAS 1000 μL syringe. A 100 nM standard mixture solution (for *in vitro* examination) was prepared as described previously. A TSQ 7000 MS data acquisition queue was established. The queue contained all the data acquisition sequences needed for *in vitro* examination, the aCSF blank wash, and *in vivo* microdialysis experiments. For a typical (*ca.* 9-h) experiment, a total of 27 data acquisition sequences were contained in the queue. The first 3 sequences were assigned for *in vitro* studies (probe recovery measurements), followed by 3 acquisitions assigned for aCSF blank washes. Basal neurochemical level monitoring usually required 6–9 acquisitions (*ca.* 2–3 h). Drug perfusion began at the same time that the last basal acquisition was started. The remaining 12–15 acquisitions (4 –5 h) were for the *in vivo* microdialysis experiments.

If necessary, individual data acquisition sequences could be added to or deleted from the queue even after the acquisition had begun. The instrumentation method, which defined the SPE loading and wash time, HPLC gradient and all MS parameters *etc*., was embedded in the individual sequences and could be modified during the experiment. This feature of flexibility was extremely useful for real-time monitoring experiments. Because experimental settings could be modified in real time according to the newest data acquired, it was not necessary to halt the whole experiment.

2) *In vitro* examination.

Approximately 20 min after the syringe pump began perfusion of aCSF, the acquisition queue was started and the microdialysis probe was dipped into the standard mixture (DA, NE, EPI, 5-HT,

3-MT) solution. This step was designed to determine both the microdialysis probe recovery and to establish that the entire system was operating correctly.

3) aCSF blank wash

When the probe recovery was in a satisfactory range, the microdialysis probe was taken out from the *in vitro* standard mixture solution, rinsed briefly with deionized water and placed into fresh aCSF. During this period, aCSF continued to be pumped through the probe in order to flush out any trace standards.

4) *In vivo* basal neurochemical level monitoring.

Once the signal (*i.e.*, HPLC peaks) for standards disappeared from the aCSF wash solution the dummy probe was removed from the guide cannula (in the animal) and replaced by the microdialysis probe with the tip being positioned 7.4 mm below dura. Throughout microdialysis experiments, the rat was attached to a tether in a bedding-lined BAS Raturn and, therefore, was able to move freely, and had access to food and water *ad libitum*.

5) Drug perfusion.

Once the basal neurochemical levels (*i.e.*, HPLC peaks) became constant, a BAS Uniswitch® Syringe Selector switched the perfusion solution to aCSF containing 10.0 mM MPTP for 30 min, after which the perfusate was switched back to aCSF. Microdialysate samples were then monitored for the next 4 to 5 h.

9. Calculations and Statistics

Analyte concentrations measured in *in vivo* microdialysis samples were expressed as nM ±

SEM (or percentage of basal level ± SEM) based on at least three replicate experiments. The effects of MPTP on neurochemical levels compared concentrations measured before, during and after perfusion using one-way ANOVA. A p-value < 0.05 was taken as significant. Origin™ (version 6.0, Microcal Software Inc.; Northampton, MA) was used for plots and statistical calculations.

C. Results and Discussion

1. Parent Ions, Daughter Ions and CID Optimization for All Analytes.

Parent ions information was obtained from MS full scan spectra. Daughter ions and CID optimization were achieved by CID with energy-step-increase experiments.

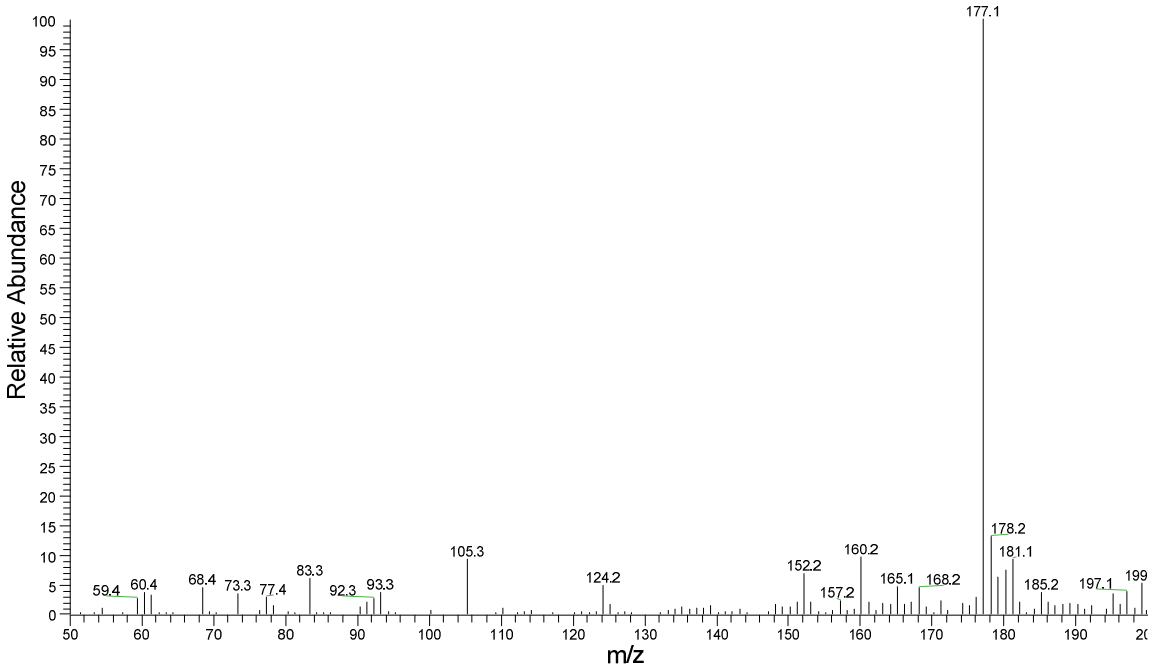

Figure 4- 1. Mass spectrum of 5-HT.

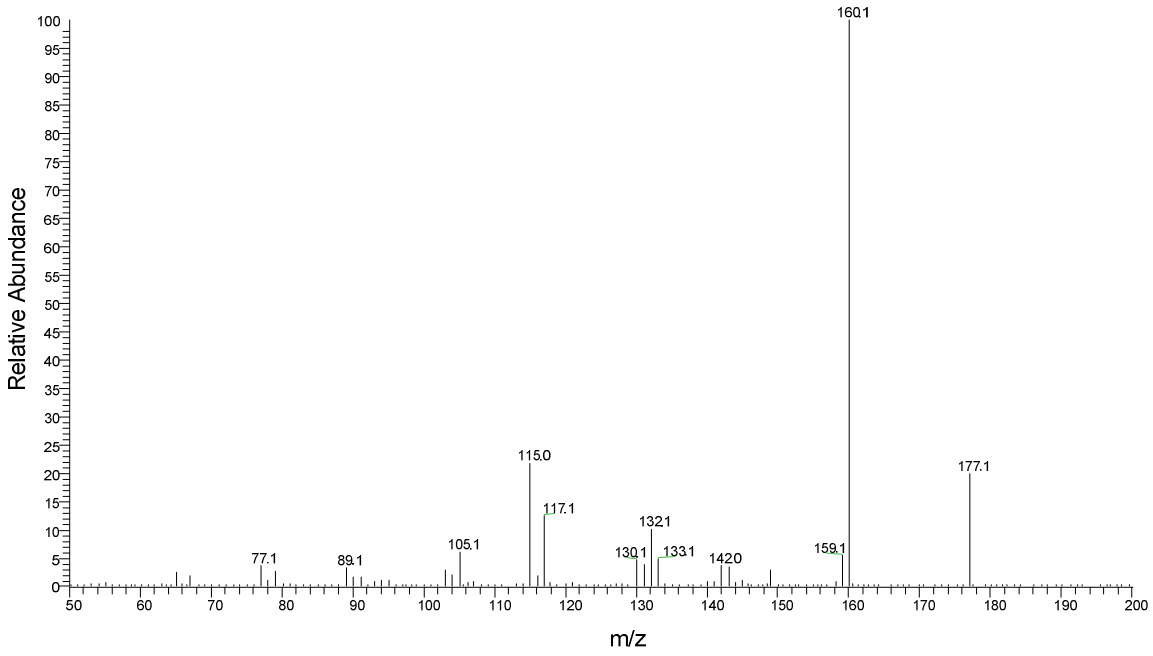

Figure 4- 2. MS/MS spectrum of 5-HT (177.1).

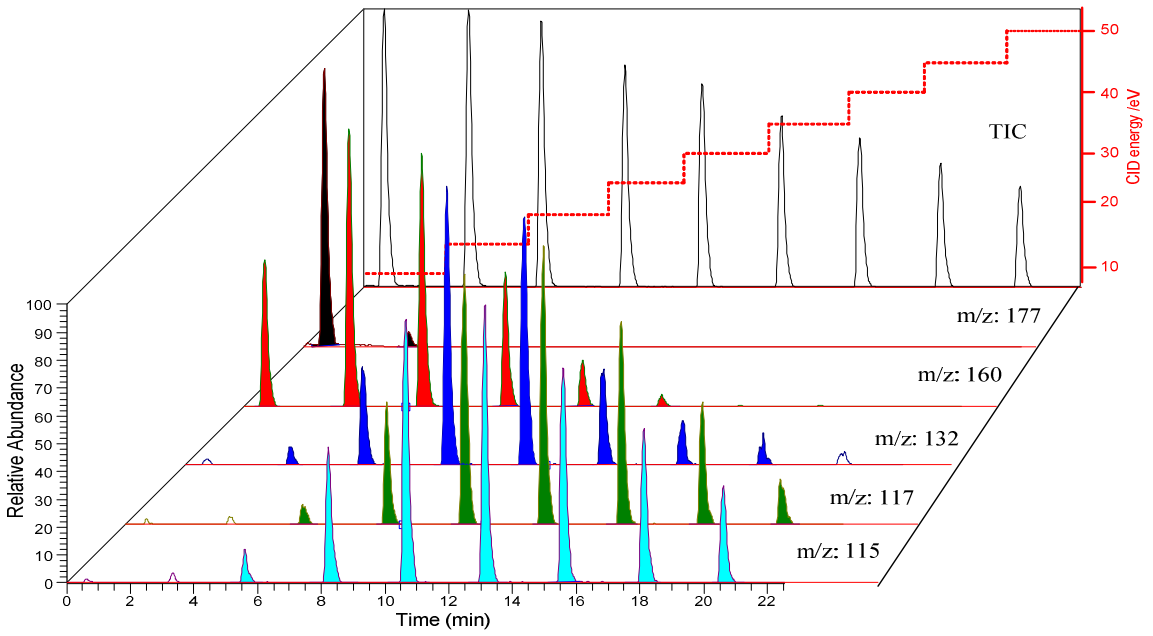

Figure 4- 3. CID optimization data processing for 5-HT.

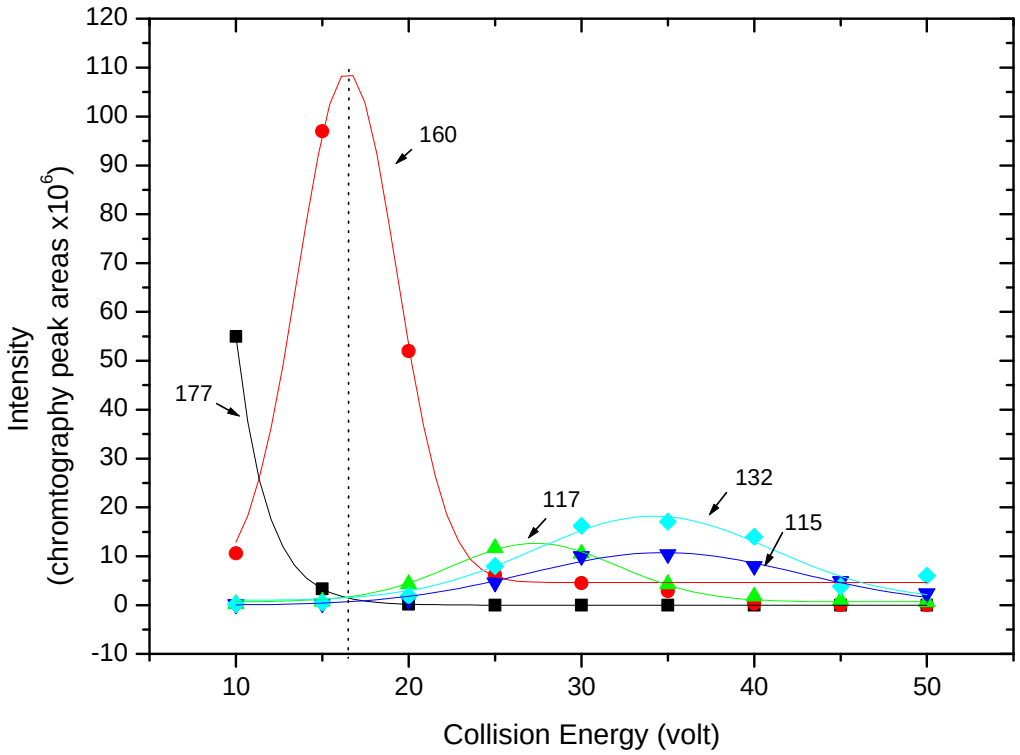

Figure 4- 4. CID breakdown curve for 5-HT.

Figures 4-1 through 4-4 illustrate how CID optimization was performed for 5-HT. Parent ion (177 m/z) and major daughter ions (160, 132, 117, 115 m/z) information was obtained from the MS full scan and MS/MS spectra, respectively. Extracted Ion Chromatography (EIC) for the parent ion and major daughter ions were established and are presented in Figure 4-3. A plot of their peak areas versus collision energy is shown in Figure 4-4; this is also known as the CID breakdown curve. Thus, from this curve it is clear that the best CID condition was ~16 eV for the daughter ion of 160 m/z. Thus the optimized SRM condition for 5-HT is 177.1→160.1@16eV.

Figures 4-5 – 4-16 show spectra and CID breakdown curves for each of the other four analytes. The optimized SRM conditions are summarized in Table 4-1.

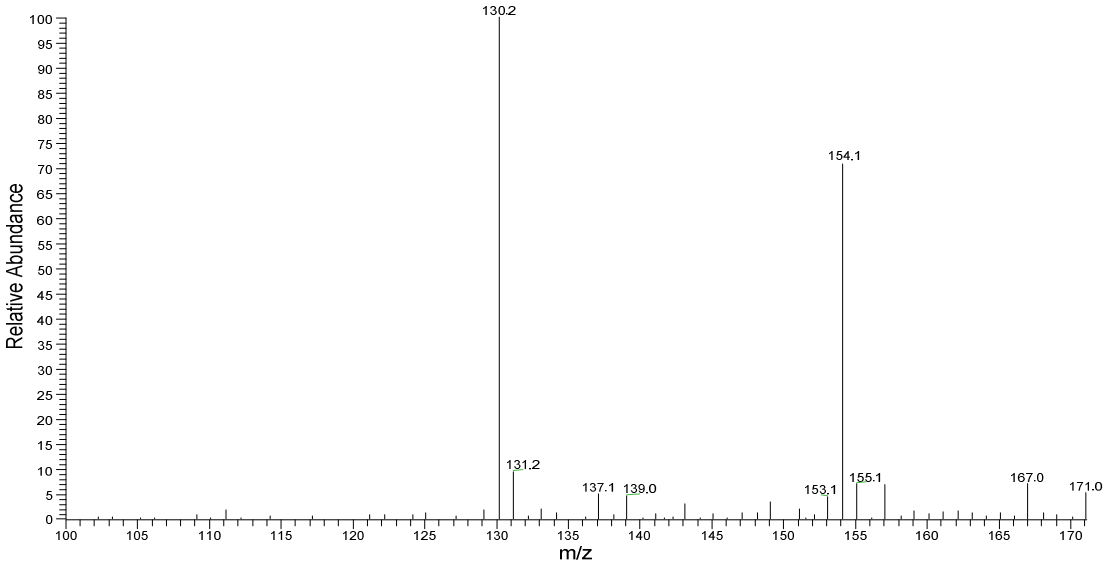

Figure 4- 5. Mass spectrum of DA

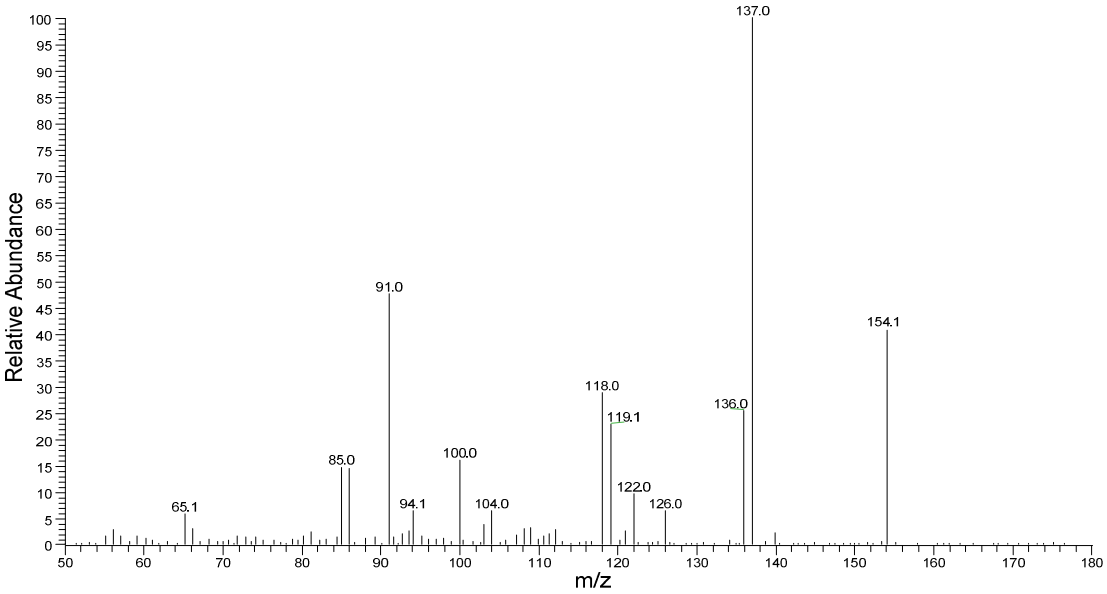

Figure 4- 6. MS/MS spectrum of DA

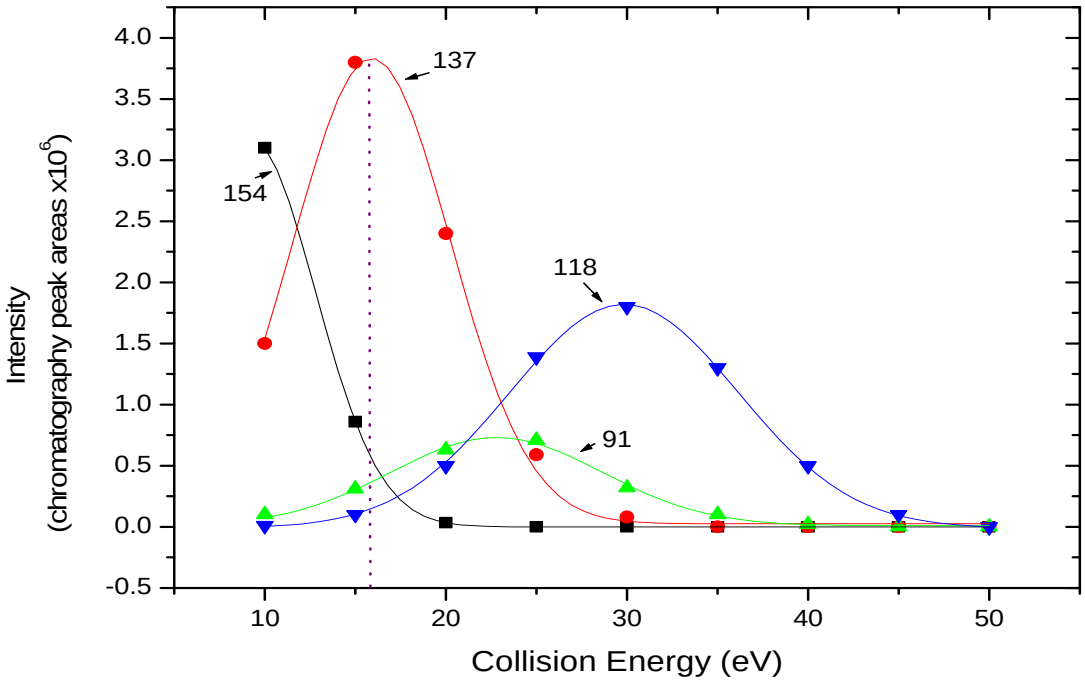

Figure 4- 7. CID breakdown curve for DA

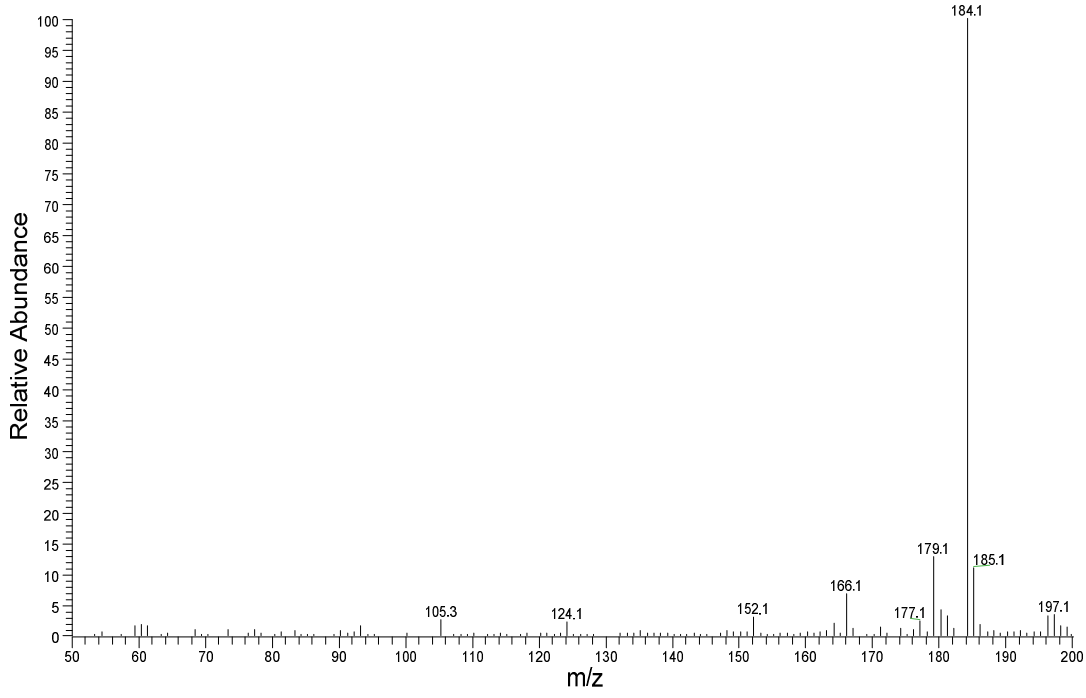

Figure 4- 8. Mass spectrum of EPI.

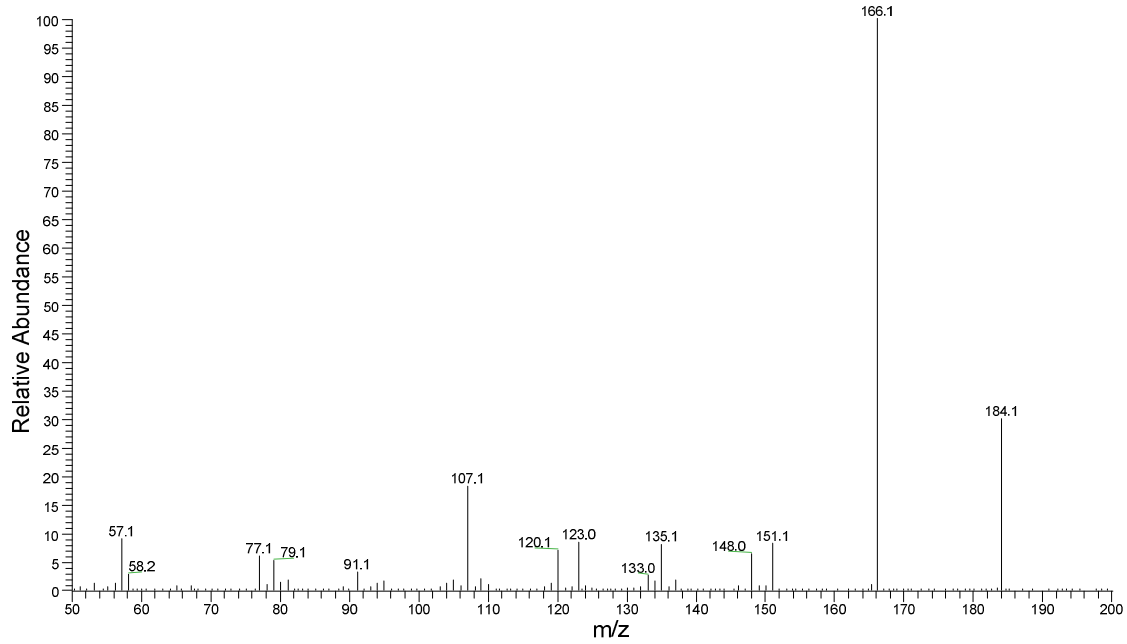

Figure 4- 9. MS/MS spectrum of EPI.

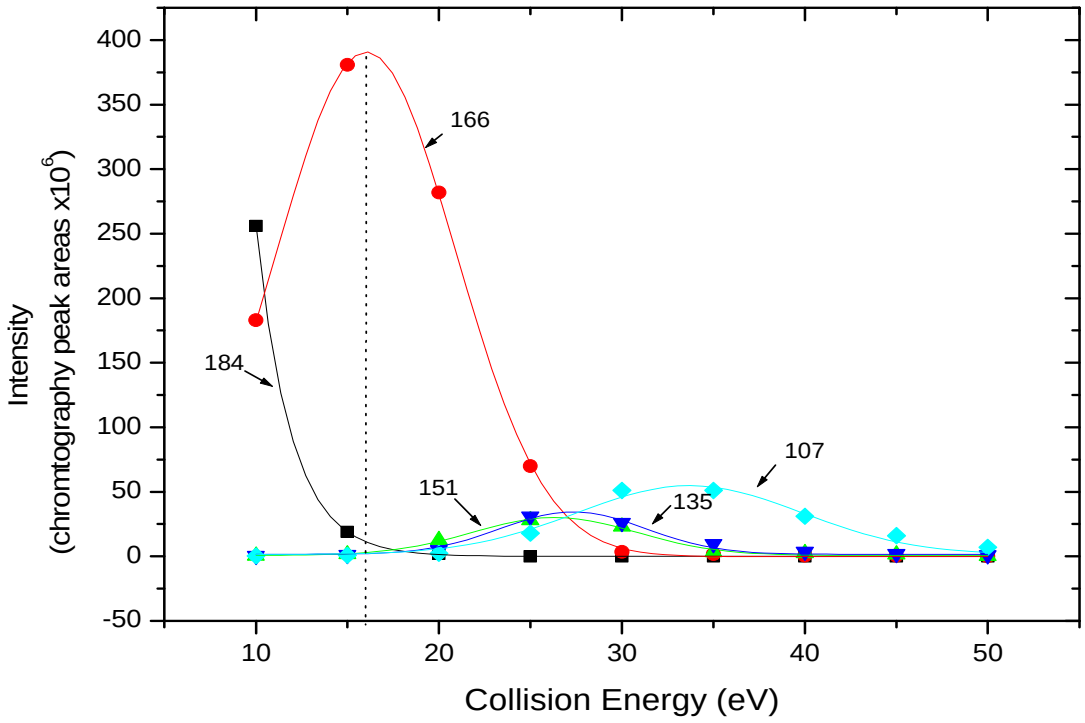

Figure 4- 10. CID breakdown curve for EPI.

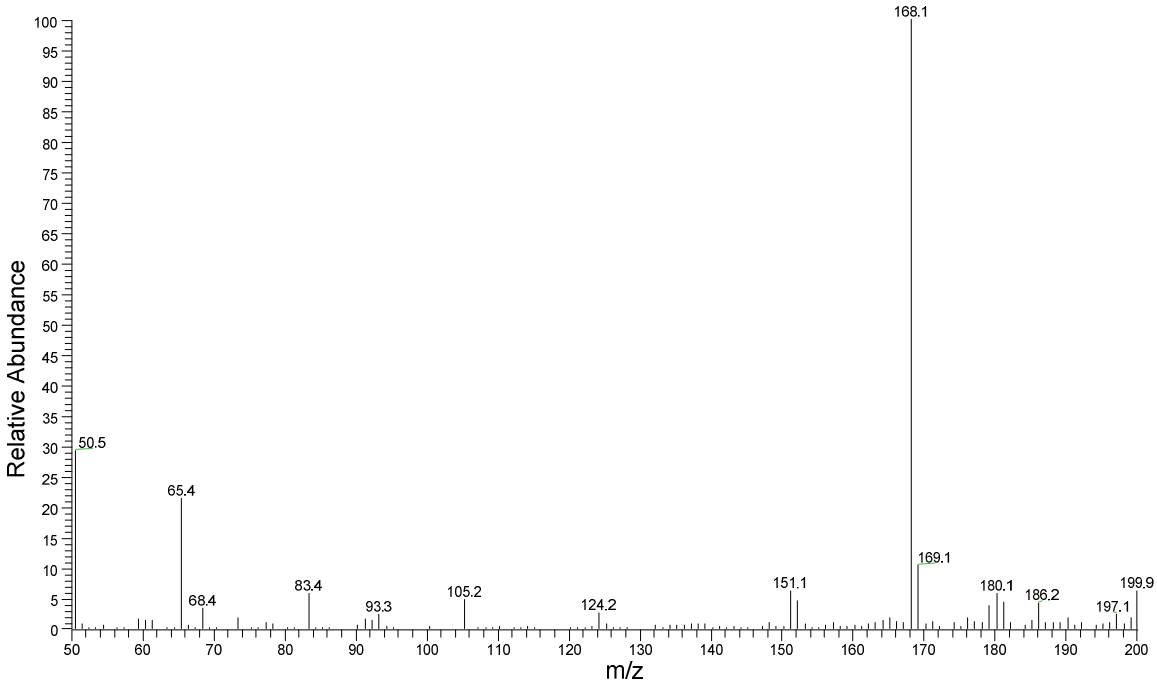

Figure 4- 11. Mass spectrum of 3-MT.

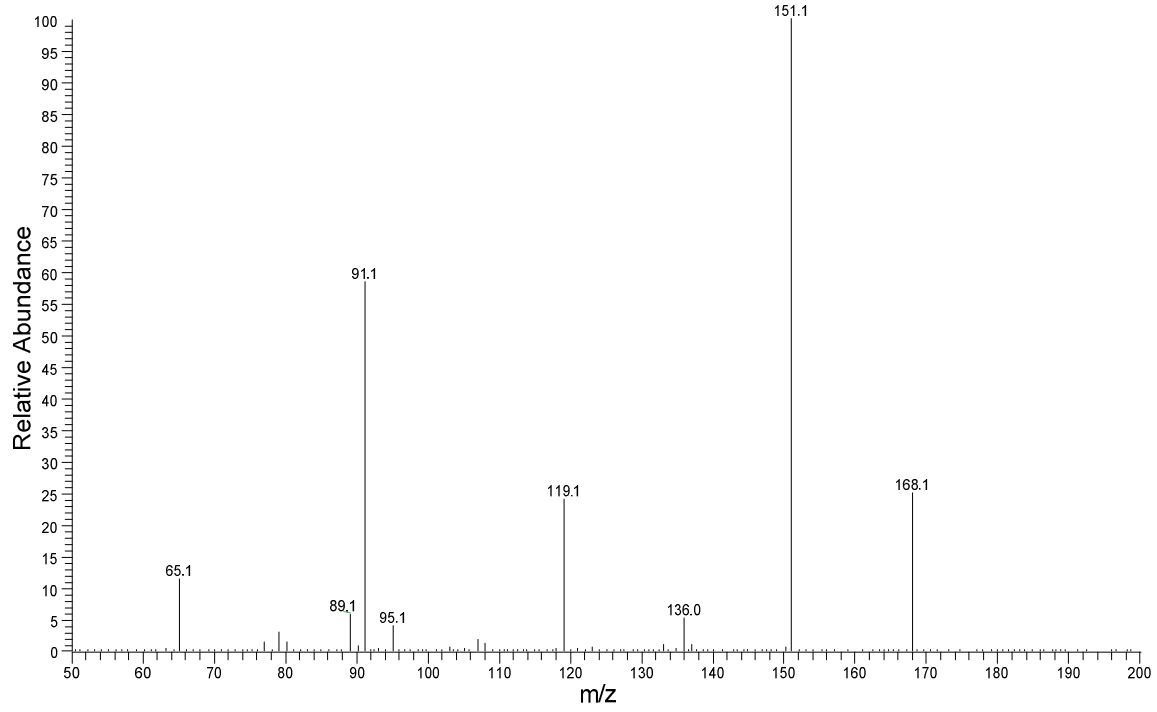

Figure 4- 12. MS/MS spectrum of 3-MT.

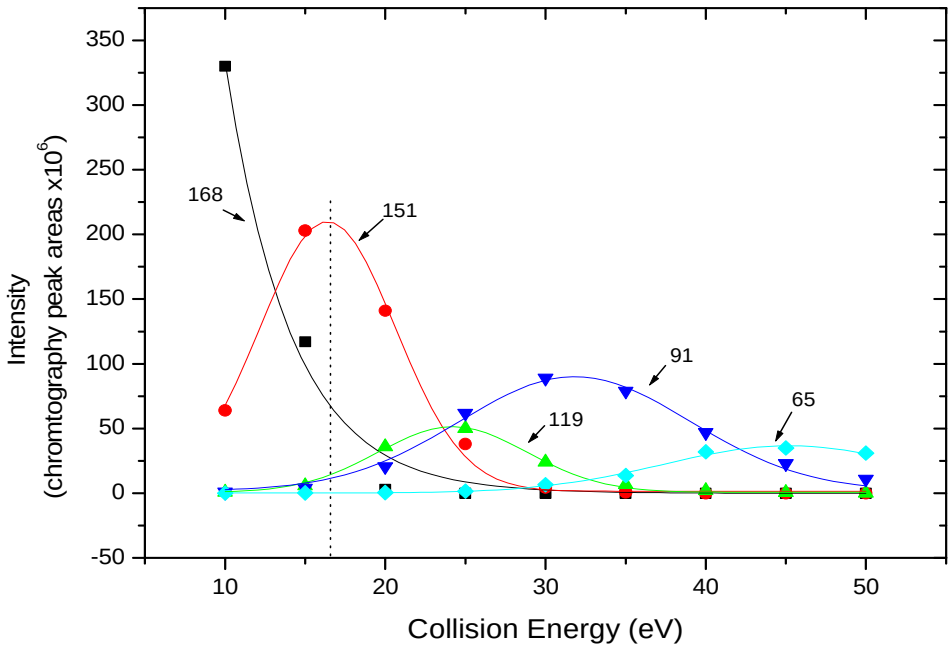

Figure 4- 13. CID breakdown curve for 3-MT.

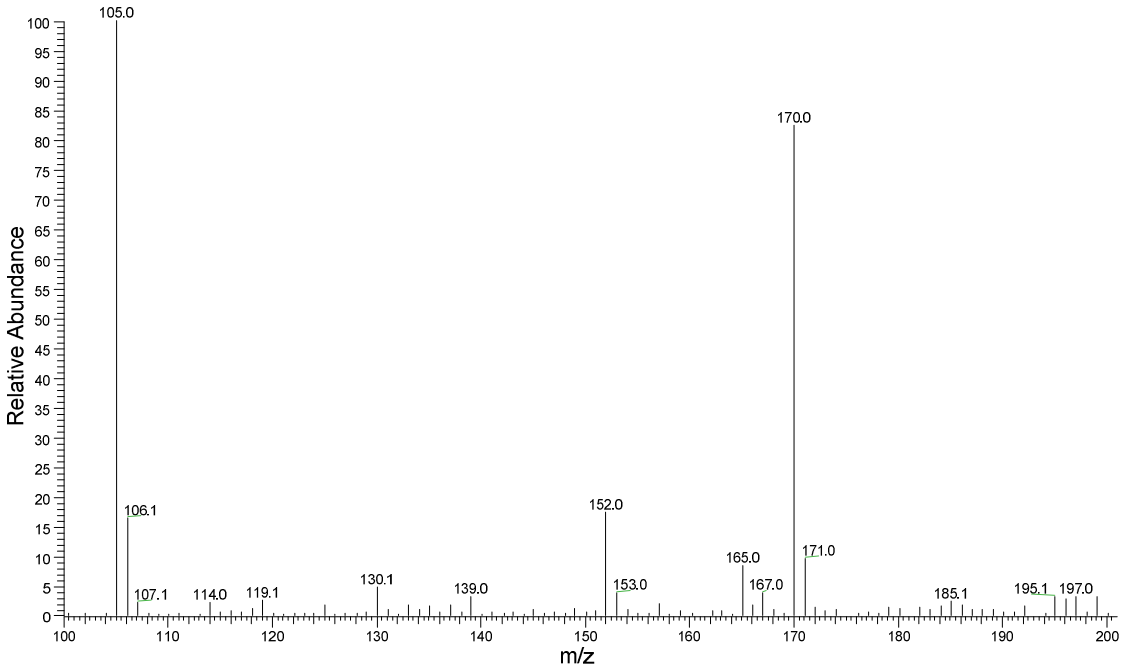

Figure 4- 14. Mass spectrum of NE

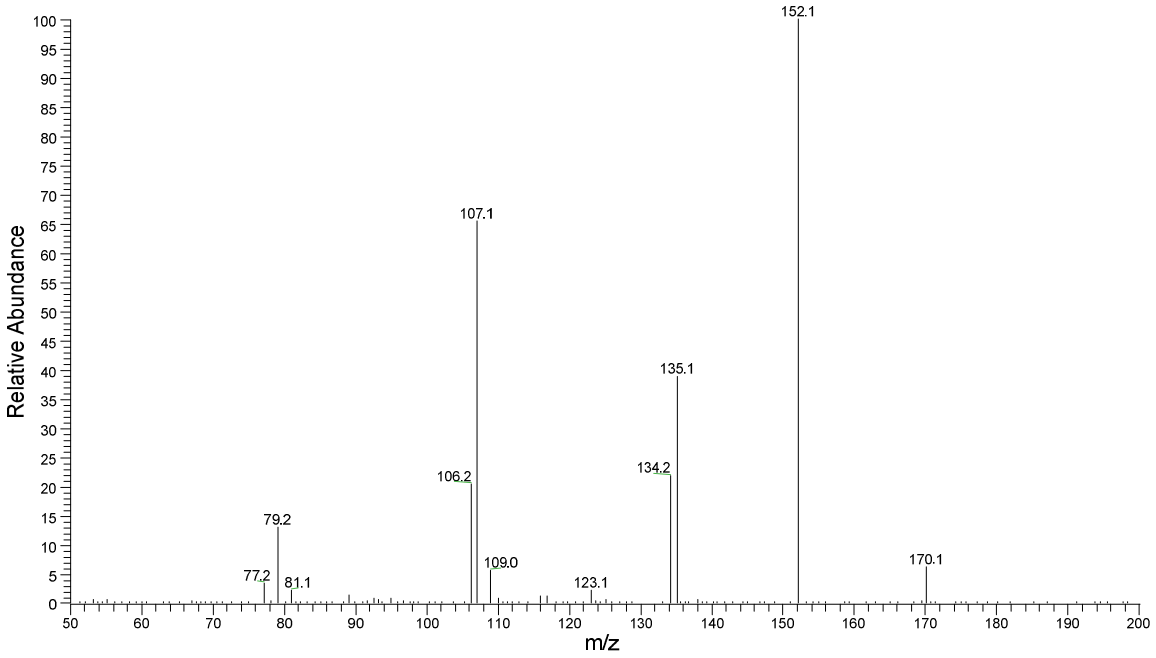

Figure 4- 15. MS/MS spectrum of NE

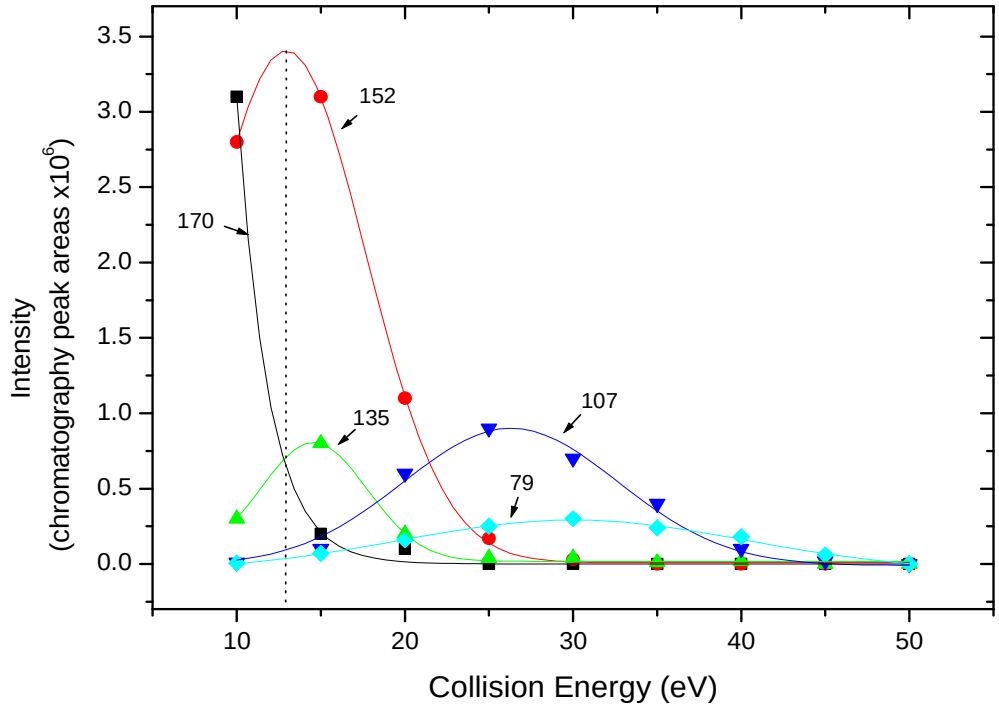

Figure 4- 16. CID breakdown curve for NE.

Substance	SRM optimized conditions
3-MT	168.1→151.1@16eV.
5-HT	177.1→160.1@16eV.
DA	154.1→137.1@16eV.
EPI	184.1→166.1@16eV.
NE	170.1→152.1@13eV.

Table 4- 1. Optimized SRM conditions for all analytes

2. Influence of Different MS Scan Modes on the HPLC-MS S/N.

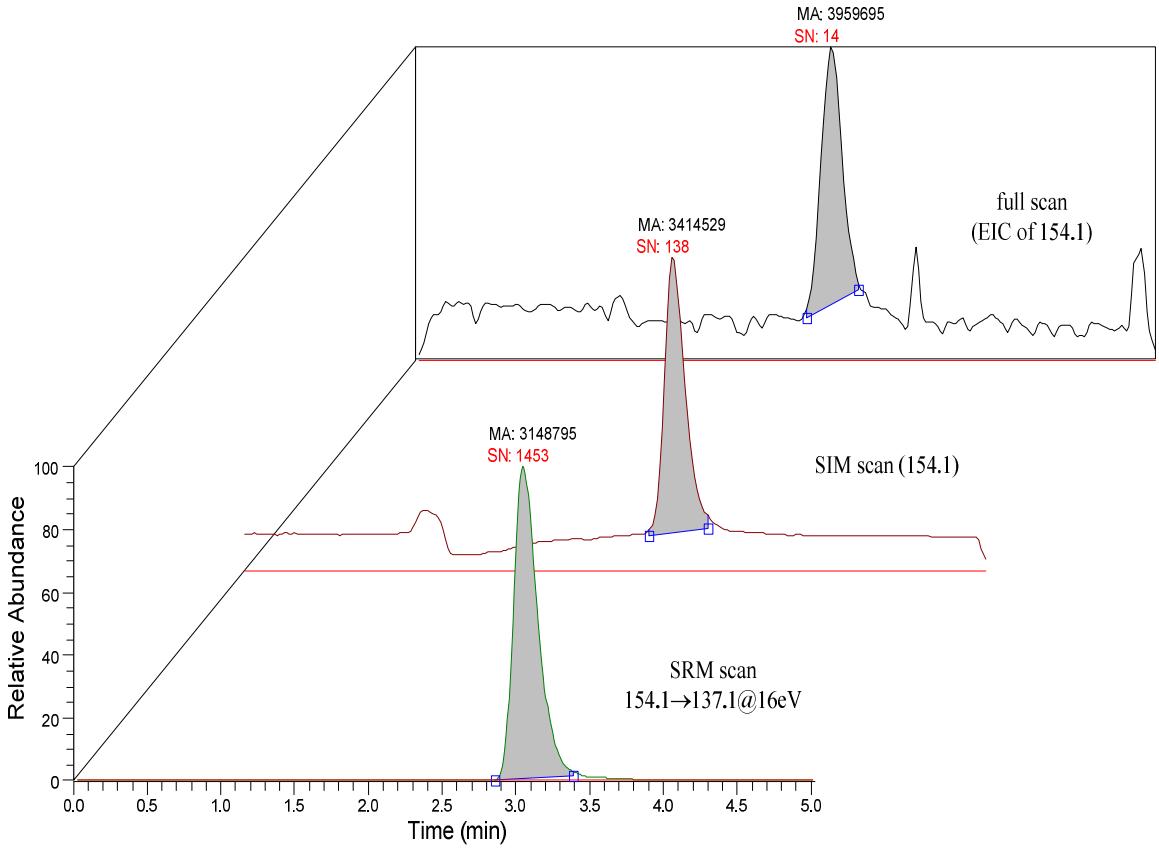

Figure 4- 17. MS scan mode influence on S/N ratio in HPLC-MS.

In Figure 4-17, the signal to noise (SN) ratio increased one order of magnitude when the SIM scan mode was compared to the full scan mode, and another order of magnitude enhancement was achieved when the SRM scan mode was employed. This illustrates the reason that the SRM approach is more and more popular and becomes the method of choice for HPLC-MS analysis of biological samples.

Still in Figure 4-17, a comparison of the DA HPLC peak areas (noted as MA) for three different scan modes reveals that they are opposite to the trend for the S/N ratio. The increase of the S/N ratio is due totally to decreasing noise. This reveals a fundamental mechanism to enhance the S/N ratio by employing a different scan mode: SIM or SRM did not increase the signal intensity, but selectively decreased the noise intensity. This unique capability is a huge advantage for MS compared to other commonly used detection techniques.

3. Standard Curves and Sensitivity.

Analyte	Equation	Correlation coefficient	Liner range (nM)	LOD (nM)
3-MT	$y = 29547 + 23278 \cdot X$	0.9993	2.0-500	1.0
5-HT	$y = -3816 + 9178 \cdot X$	0.9996	1.0-500	0.5
EPI	$y = 13183 + 19048 \cdot X$	0.9999	1.0-1000	0.5
DA	$y = -22428 + 7594 \cdot X$	0.9999	2.0-1000	0.5
NE	$y = -2330 + 7906 \cdot X$	0.9995	2.0-500	1.0

Table 4- 2. Calibration curves, limit of detection (LOD) and linear dynamic range.

Calibration information is summarized in Table 4-2. SRM is a very specific detection technique and matrix interference with the analyte signal is minimized. Thus, not only were better LOD values (compared to full scan or SIM scan MS) achieved, but also better correlation coefficients and wider linear dynamic ranges were obtained routinely.

4. *In Vitro* Experiments

Microdialysis probe recovery values obtained from in vitro experiments are summarized in Table 4-3.

	Recovery rate (mean±S.E.M., n=4) /%				
Substance / *in vitro* conc.	**NE**	**EPI**	**DA**	**5-HT**	**3-MT**
50nM	21.9± 1.6	17.1± 1.7	21.4± 1.9	21.1±1.8	18.7±1.5
100nM	25.3± 0.8	26.3± 0.3	27.1± 0.7	23.5±0.9	24.3±1.3
500nM	16.9± 0.2	27.5± 0.3	30.5± 0.4	26.0±1.1	22.1±0.4

Table 4- 3. *In vitro* microdialysis probe recoveries for all analytes at different concentrations.

5. *In Vivo* Experiments.

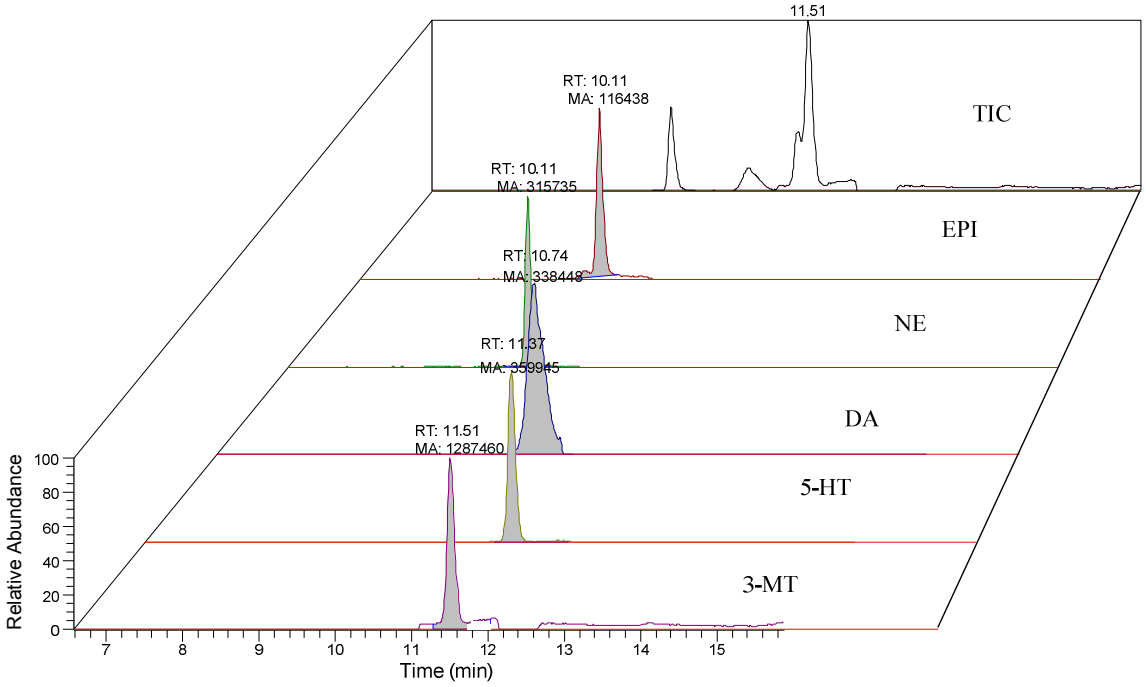

Figure 4- 18. Typical data for *in vitro* examination.

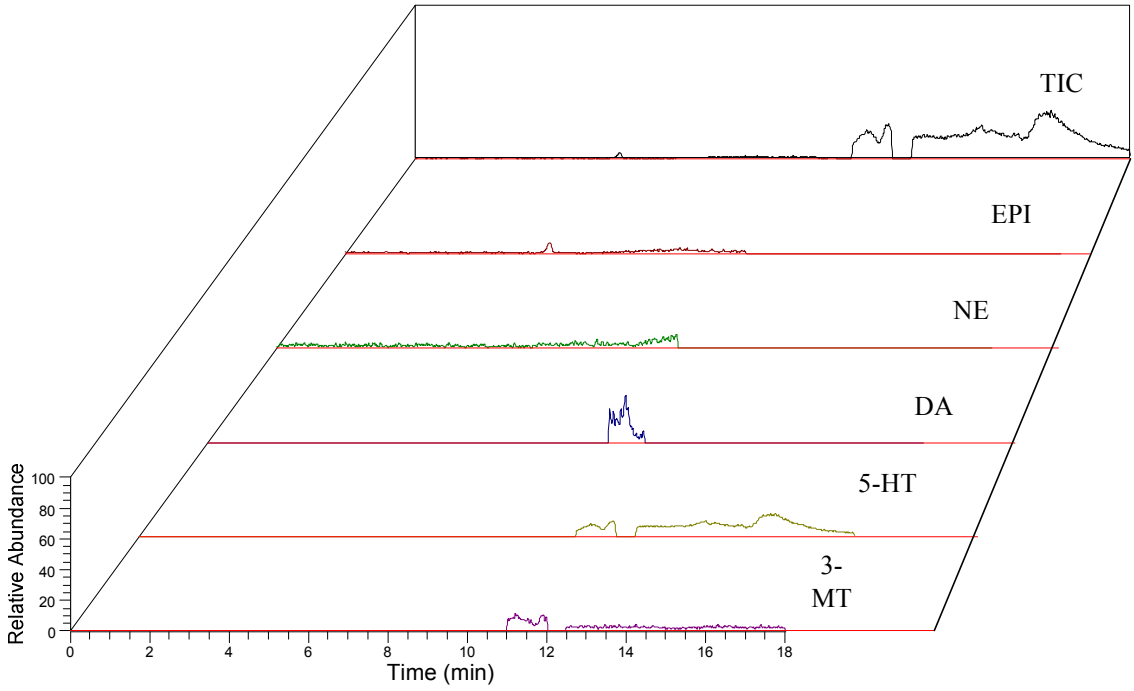

Figure 4- 19. Typical data after aCSF wash and before probe implantation.

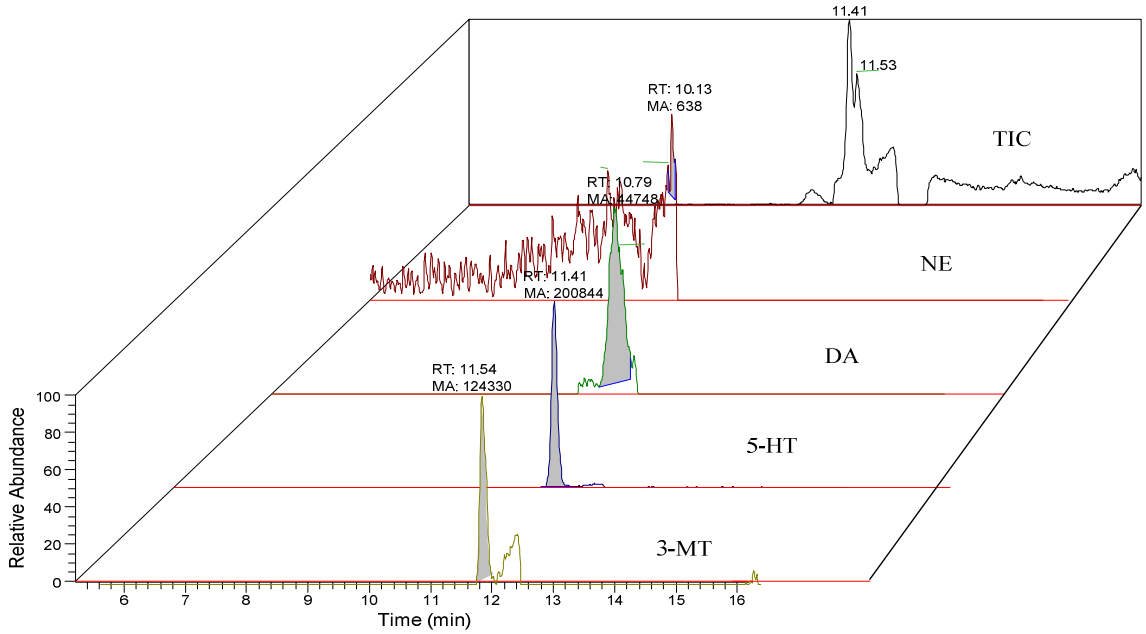

Figure 4- 20. Typical data for microdialysate basal neurochemical levels (EPI not detected).

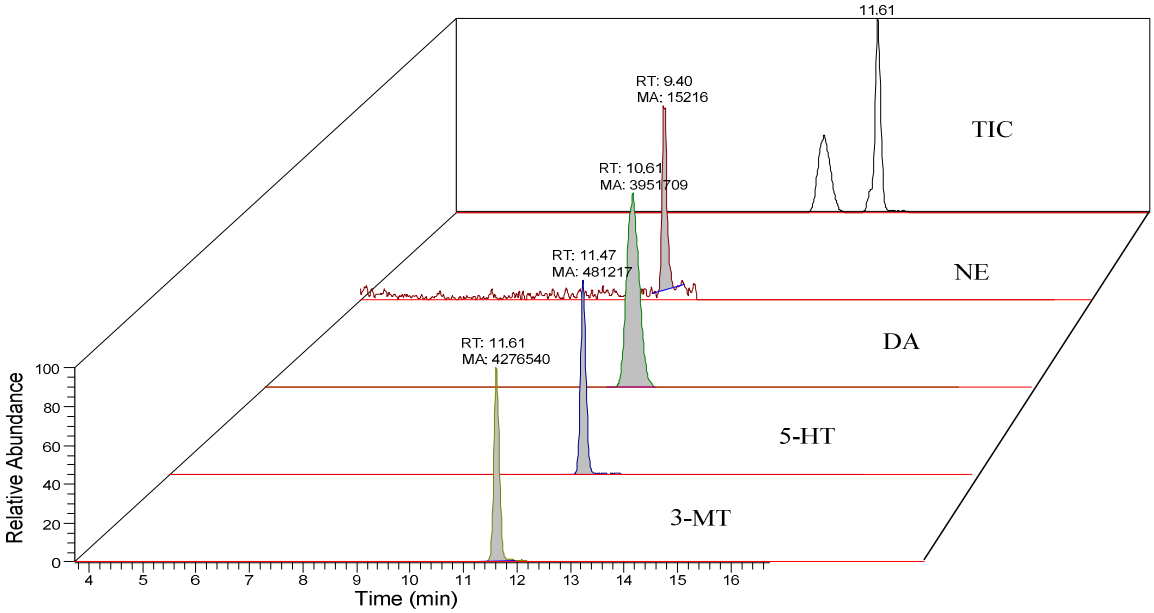

Figure 4- 21. Typical data for microdialysate neurochemical levels after drug perfusion (EPI not detected).

Figures 4-18 to 4-21 show representative neurochemical levels observed in *in vitro* experiments, aCSF wash solutions, *in vivo* basal, and *in vivo* post-drug measurement.

The following table lists basal microdialysate levels of the targeted neurochemicals measured *in vivo*.

Substance	Basal level in dialysate (mean ± SEM, n=3) /nM
3-MT	**3.5±0.4**
5-HT	**4.3±2.1**
DA	**6.4±0.7**
EPI	**Not detected**
NE	**0.8±0.2**

Table 4- 4. Basal microdialysate levels of targeted neurochemicals.

The following figures present microdialysate concentration-time profiles for NE, DA, 3-MT and 5-HT detected in *in vivo* experiments.

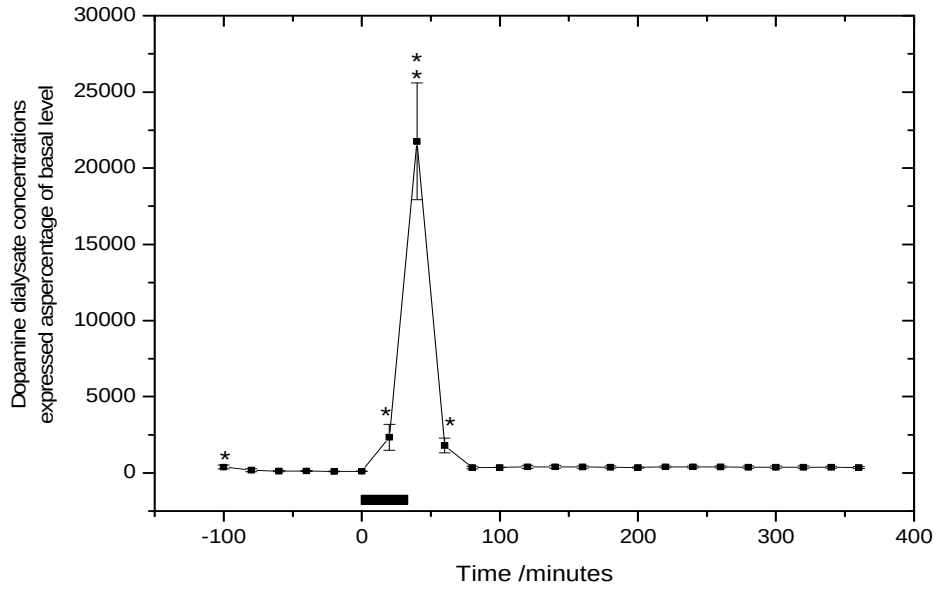

Figure 4- 22. Time-dependent effects of a 30-min perfusion of 10 mM MPTP into the rat striatum on microdialysate levels of DA. The horizontal black bar shows the time during which MPTP was perfused. Data are mean ± SEM (bars) percentages of basal DA levels (n=3). * p < 0.05, ** p < 0.01.

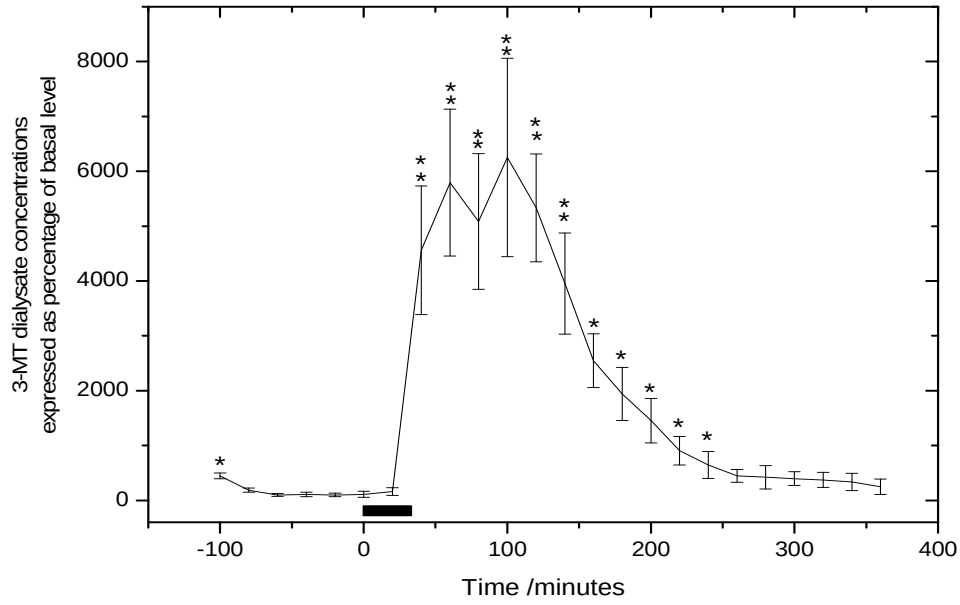

Figure 4- 23. Time-dependent effects of a 30-min perfusion of 10 mM MPTP into rat striatum on microdialysate levels of 3-MT. The horizontal black bar shows the time during which MPTP was perfused. Data are mean ± SEM (bars) percentages of basal 3-MT levels (n=3). * p < 0.05, ** p < 0.01.

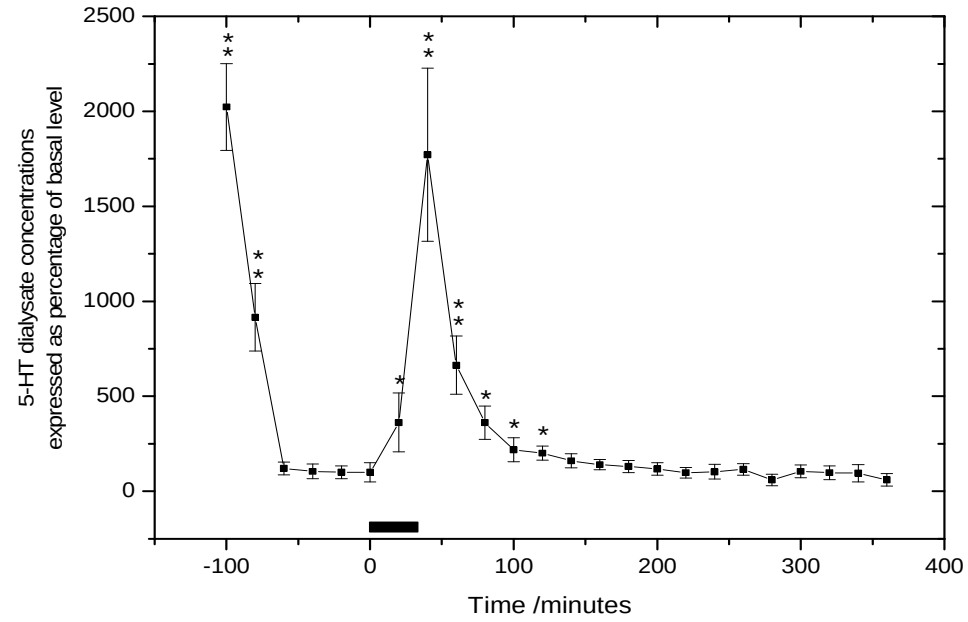

Figure 4- 24. Time-dependent effects of a 30-min perfusion of 10 mM MPTP into rat striatum on microdialysate levels of 5-HT. The horizontal black bar shows the time during which MPTP was perfused. Data are mean±SEM (bars) percentages of basal 5-HT levels (n=3). * p < 0.05, ** p < 0.01.

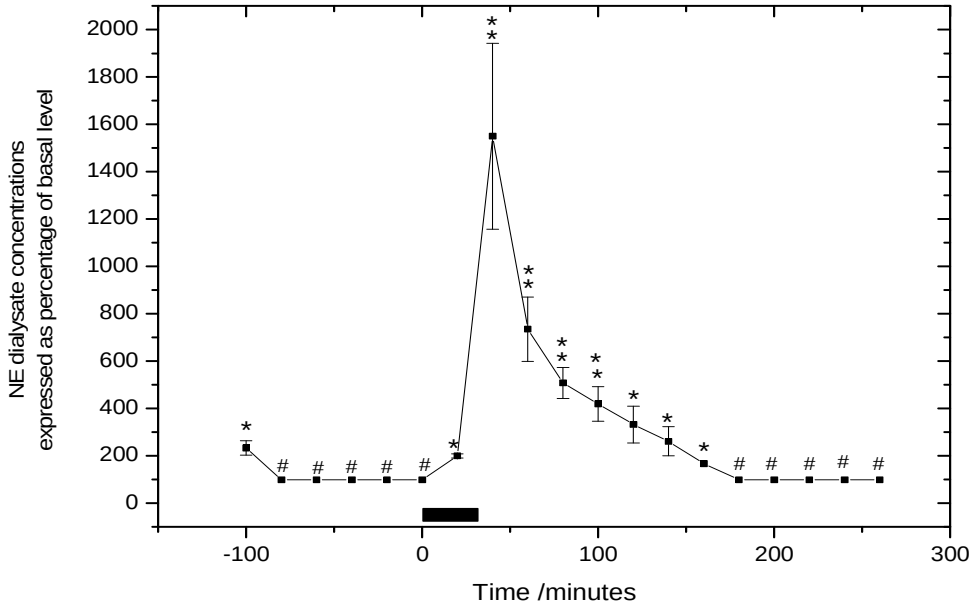

Figure 4- 25. Time-dependent effects of a 30-min perfusion of 10 mM MPTP into rat striatum on microdialysate levels of NE. The horizontal black bar shows the time during which MPTP was perfused. Data are mean ± SEM (bars) percentages of basal NE levels (n=3). (* p<0.05, ** p<0.01, # virtually undetectable).

Probe insertion caused extracellular levels of all four detected analytes to increase significantly. Subsequently, all analytes rapidly declined to basal levels in 30 min. Perfusion of 10 mM MPTP dissolved in aCSF evoked an almost immediate and significant release of DA, 5-HT and NE. The massive release of all three analytes reached peak values at *ca*. 40 min. The peak value for DA was 20,000%, 5-HT was 1,700% and NE was 1,600% above basal levels. After reaching peak levels, extracellular concentrations of DA and 5-HT declined rapidly (100-120 min) to basal levels, whereas the decline of NE was much slower (180 min). The concentration-time profile for 3-MT was different from the other analytes. Thus, there was a 20-min delay before microdialysate levels of 3-MT began to increase upon MPTP perfusion. The massive release of 3-MT reached a peak value of 6,000% above basal level after 60 min, remained at this peak value for another 60 min, and then declined slowly to basal level after 240 min. Compared to the previous studies done in our lab[170,190] and other researchers,[191] where electrochemical detection was employed, the basal dialysate concentrations are very close and the concentration profiles are also similar. However, HPLC-MS has advantages over other detection methods because it usually gives unequivocal evidence for the identity of analytes.

D. Conclusions

In this chapter, the fully automated system was employed to monitor *in vivo* three catecholamines (DA, NE and EPI), 5-HT and 3-MT. The SRM conditions for all analytes were optimized by off-line experiments. The fully automated system was extensively used to prepare calibration curves, determine *in vitro* microdialysis probe recoveries, and in connection with *in vivo* experiments. These studies established that the system was a powerful tool for real-time, highly sensitive and specific measurement of multiple metabolites in a living animal.

Chapter Five

Fully Automated On-line Sample Cleanup and HPLC-MS/MS Determination of GSH and CySH in Rat Brain Striatum: An *In Vivo* Microdialysis Study.

A. Introduction

GSH and CySH are ubiquitous thiol-containing molecules in organisms. GSH and CySH play a central role in cell biology, especially cellular protection against various toxic compounds such as free radicals and hydroperoxides.[192,193] GSH and CySH status is a highly sensitive indicator of cell functionality.[194]

Numerous analytical approaches have been established to determine GSH and CySH in biological samples. Among them, capillary electrophoresis coupled with UV[195-199] or fluorimetric detection,[200] and HPLC coupled with UV[200-204] or electrochemical detection[205-207] have been frequently employed. In addition, NMR spectroscopy has been utilized for analysis of intact cells for GSH and CySH.[208] However, direct GSH and CySH analyses without derivatization are rare. The purposes of derivatization are to prevent autoxidation of GSH and CySH, to improve chromatographic retention, or to enhance sensitivity. HPLC-MS is a highly specific and sensitive technique, and has been applied to the analysis of blood cell and liver GSH content. However, the available methods are time consuming because of sample preparation procedures such as liquid-liquid extraction and off-line derivatization.[151,209-211] Fully automated HPLC-MS analyses of GSH and CySH in microdialysate

samples have not been previously reported.

In this chapter, a fully automated system is described which combines microdialysis sampling, on-line derivatization (Figures 5-1 and 5-2), on-line IP-RP-SPE sample clean-up, IP-RP-HPLC separation and tandem MS/MS detection techniques to monitor GSH and CySH in the striatum of rats in response to perfusion of the parkinsonian toxins MPTP and MPP^+.

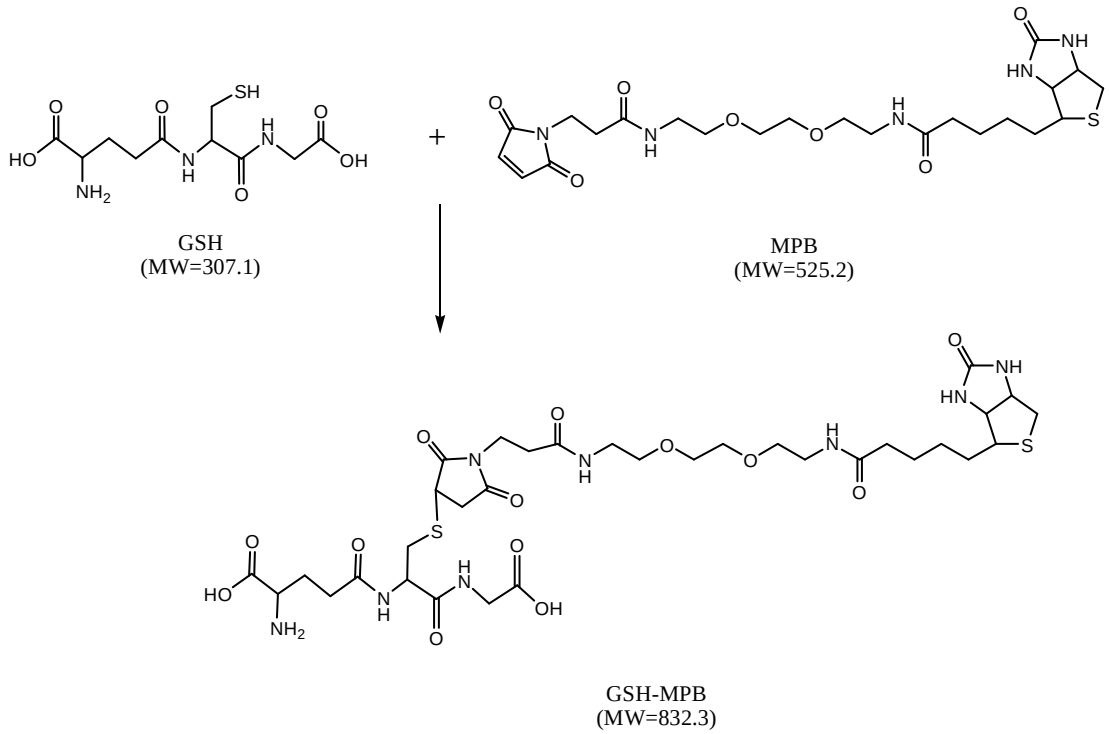

Figure 5- 1. Derivatization reaction for GSH.

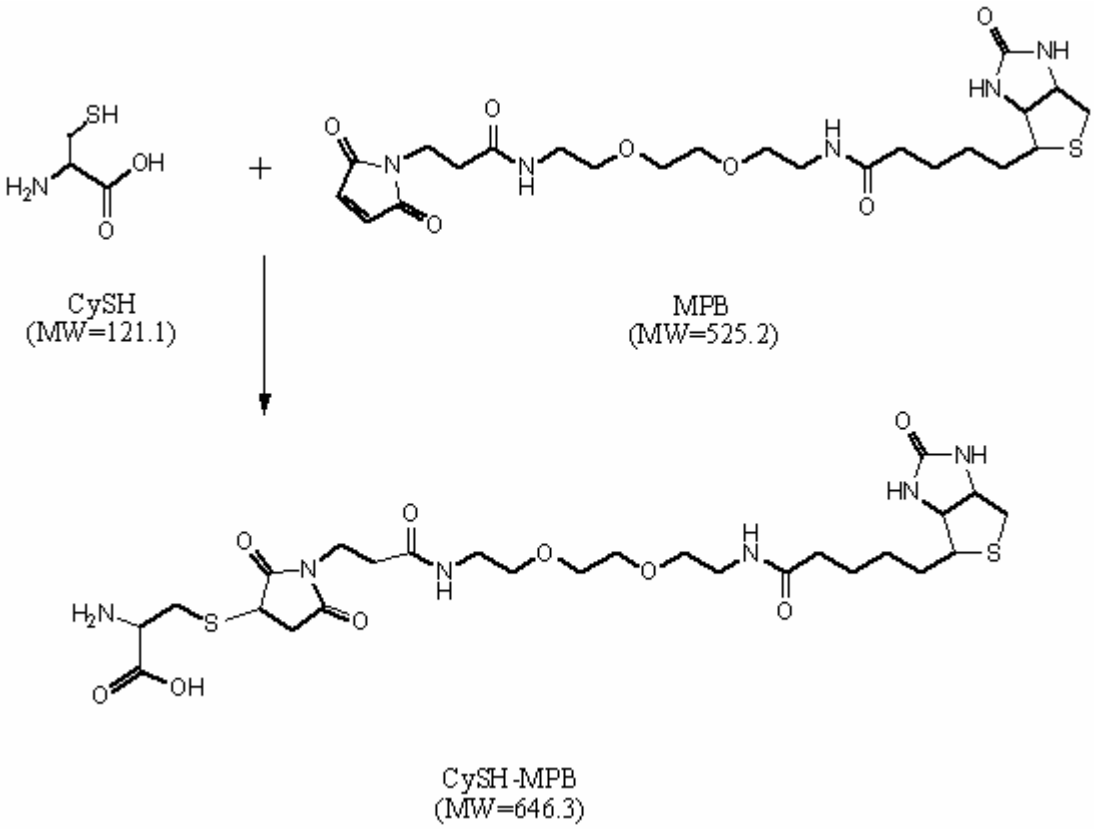

Figure 5- 2. Derivatization reaction for CySH.

B. Experimental

1. Chemicals and Chromatographic Conditions.

Most of the chemicals used and chromatographic conditions were the same as described in Chapters Two and Three. EZ-Link® Maleimide polyethyleneoxide, 2 (PEO_2)-Biotin (MPB; structure shown in Figures 5-1 and 5-2) was purchased from Pierce Inc (Rockford, IL). Upon arrival, the MPB was weighed and distributed into smaller portions (0.6-1.2 mg each) and stored in securely capped plastic vials. The vials were stored in a dessiccator at ~4^{o}C. MPB solution was always freshly prepared before experiment. Upon usage, the calculated amount of water was added to the above vials to obtain MPB at the desired concentrations. All of the above approaches were employed to protect the

moisture-sensitive MPB from hydrolysis and loss of function.

2. Instrumentation.

On-line derivatization was carried out by adding a 3-way micro-mixer to the fully automated system described in Chapter Two. An overview of the modified system is presented in Figure 5-3.

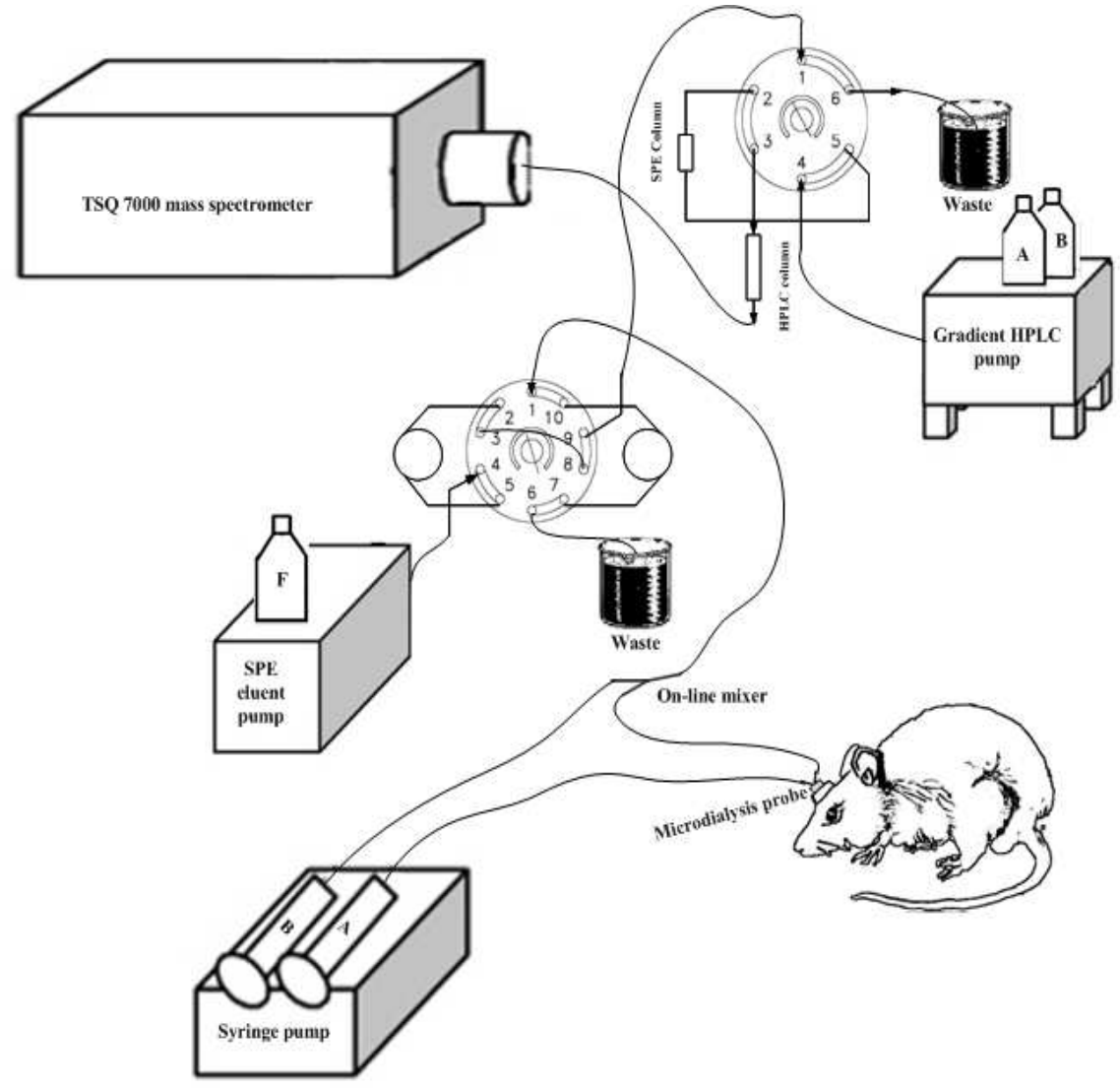

Figure 5- 3. Overview of the modified fully automated system

The additional syringe B was a Hamilton gastight® 250 µL syringe (1700 series; VWR Scientific, West Chester, PA). It had the same effective length (6.0 cm) as syringe A. Thus the actual output flow rate from syringe B was 0.375 µL/min. This syringe was filled with 5.0 mM MPB in water. The solution was thoroughly degassed (He sparging) prior to use. After mixing with dialysate, which was driven by syringe A, the MPB was automatic diluted (1 : 4) to a concentration of 1.0 mM in the perfusate solution.

The on-line micro-mixer was a homemade device using a modified CMA 12® microdialysis probe (Figure 5-4). Thus, the probe membrane was removed and the inlet needle tubing was cut to the level of the end of the shield tubing. During experiments the microdialysate solution coming from the rat brain was connected to the original inlet of the probe. The inlet and the inlet needle has a very small dead volume (<1 µL) so that chromatographic resolution was not compromised. The MPB solution was connected to the original outlet of the probe and flowed out through the shield tubing. The outlet and the shield tubing had a larger dead volume (~3 µL), but it does not matter for the homogenous MPB solution. In such a setting, the MPB solution appears as a sheath solution to the microdialysate. (Figure 5-4) The microdialysate and MPB solutions mix together at the end point of the shield tubing and continue mixing as they are pumped into the sample loop. The derivatization reactions (Figures 5-1 and 5-2) occur in room temperature when these solutions are mixed. The advantages of this on-line mixer include very low dead volume, easy connection using microdialysis tubing and adapters, and low cost.

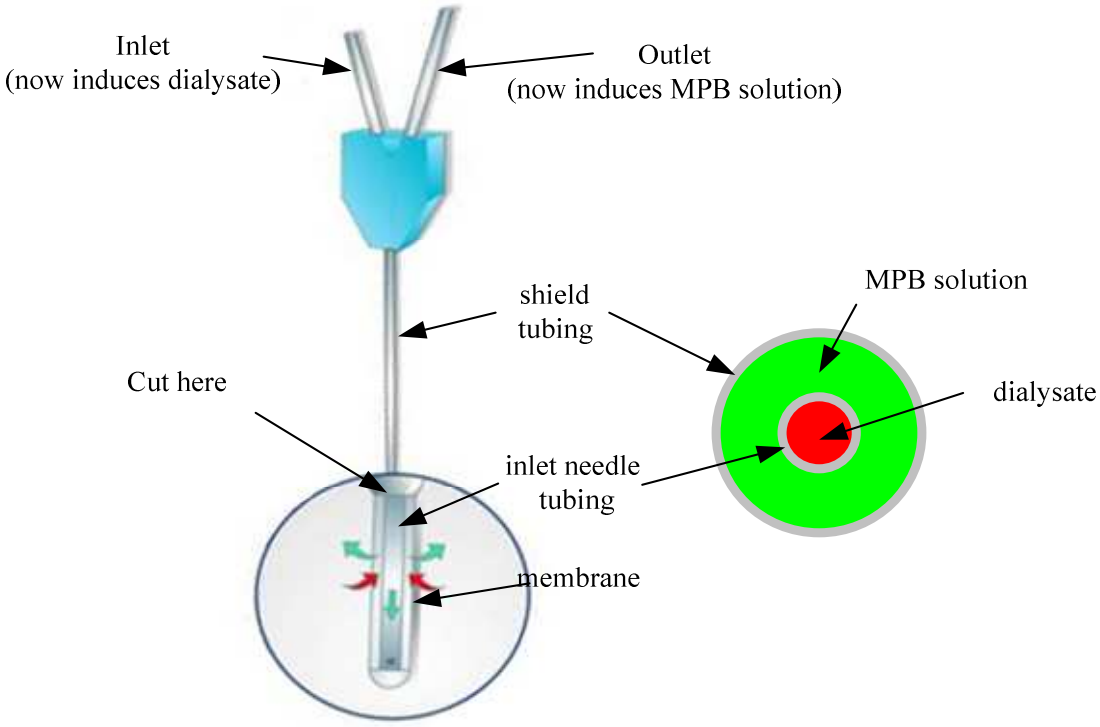

Figure 5- 4. Structure of microdialysis probe and its modification to be as a micro-mixer.

3. Stock and Standard Solutions.

Stock standard solutions of GSH and CySH (10 mM) were prepared and stored as described in Chapter Two. GSH-MPB and CySH-MPB stock standard solutions (1 mM, stoichiometric calculated by assuming a 100% yield for the derivatization reactions) used to optimize SRM conditions were prepared as follows: 25 µL 10 mM GSH/CySH stock standard solution and 25 µL 20 mM MPB solution were added to 200 µL aCSF solution in a plastic vial. The vial was left in room temperature for 1h to complete the reaction, then stored at ~ 4^{o}C for later use.

GSH-MPB/CySH-MPB standard solution (10 µM each) was prepared by adding 10 µL GSH-MPB/CySH-MPB stock standards (1 mM) to 990 µL aCSF.

Standard solution for GSH/CySH (10 μM) was prepared as follows: 10 μL of 10 mM individual stock solutions were added to 990 μL aCSF to obtain a 100 μM solution; 100 μL of such solution was added to 900 μL aCSF to obtain the 10 μM solution.

A series of calibration standard mixture solution (50 μM, 20 μM, 10 μM, 5 μM, 2 μM, 1 μM, 0.5 μM and 0.2 μM) were prepared as follows: 10 μL of 10 mM stock standard solutions of GSH and CySH were added to 980 μL aCSF to obtain a 100 μM mixed standard solution; 500 μL of this solution was added to 500 μL aCSF to obtain a 50 μM solution; 400 μL of the 50 μM solution was added to 600 μL aCSF to obtain a 20 μM solution; 200 μL of 20 μM solution was added to 600 μL aCSF to obtain a 5 μM solution; 400 μL of 5 μM solution was added to 600 μL aCSF to obtain 2 μM solution; 500 μL of 2 μM solution was added to 500 μL aCSF to obtain 1 μM solution; 500 μL of 1 μM solution was added to 500 μL aCSF to obtain 0.5 μM solution; 400 μL of 0.5 μM solution was added to 600 μL aCSF to obtain 0.2 μM solution. All solutions were stored in plastic vials on ice in a covered container and were passed through 0.2 μm centrifuge filter before use.

The standard mixture solutions (40 μM, 10 μM, 5 μM and 2 μM) for *in vitro* experiments were prepared in a similar manner to that described above.

4. Selected Reaction Monitoring (SRM) Optimization.

SRM optimization was carried out in the same way described in Chapter Four except that 10 μM GSH, CySH, GSH-MPB and CySH-MPB standard solutions were used.

5. Calibration Curves

Calibration curves were determined in the same way described in Chapter Four except that a series of GSH and CySH standard mixture solutions were used and the modified fully automated system describe earlier in this chapter was employed.

6. *In Vitro* Microdialysis Experiments

The procedure for *in vitro* microdialysis experiments was the same as described in Chapter Four, except that 2 μM, 5 μM, 10 μM and 40 μM mixed GSH and CySH standard solutions were used and the modified fully automated system describe previously in this chapter was employed.

7. Animals and Surgical Procedures

Animals and surgical procedures were the same as in Chapter Four.

8. *In Vivo* Microdialysis (Probe Recovery Studies).

In vivo microdialysis followed the same protocols described in Chapter Four but with the following differences: 1) the modified fully automated system described in this chapter was employed: 2) a 5 mM MPB in water solution was prepared in the preparation step; 3) a 10 μM GSH and CySH standard mixture solution was employed for the *in vitro* studies (probe recoveries); and, 4) 10 mM MPTP, 2.5 mM MPP^+ and 5 mM MPP^+ were perfused into the rat striatum.

9. Calculations and Statistics

Data calculations and statistics were the same as described in Chapter Four.

C. Results and Discussion

1. Parent Ions, Daughter Ions and CID Optimization for GSH, CySH, GSH-MPB and CySH-MPB.

Parent ion information was obtained by means of MS full scan spectra; daughter ion information and CID optimization were achieved using CID energy-step-increase experiments. The data processing technique for CID breakdown curve establishment was described in Chapter Four.

Figures 5-5 – 5-16 present spectra and CID breakdown curves for each of the four analytes. The optimized SRM conditions are summarized in Table 5-1.

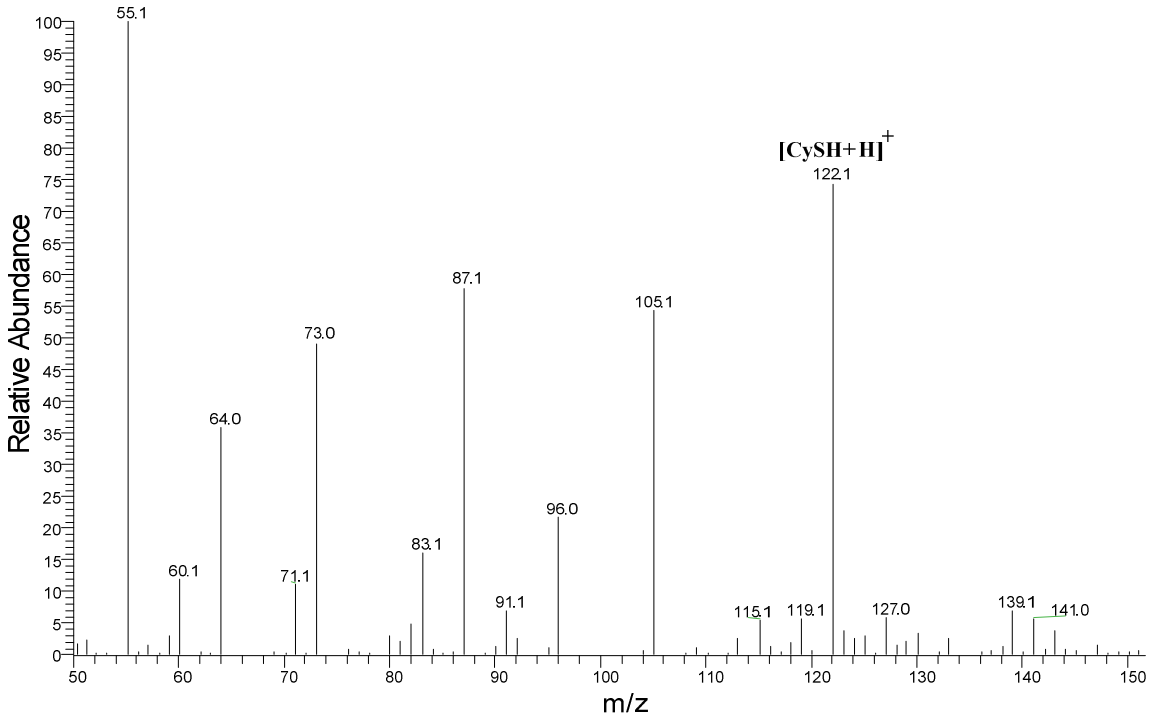

Figure 5- 5. Mass spectrum of CySH.

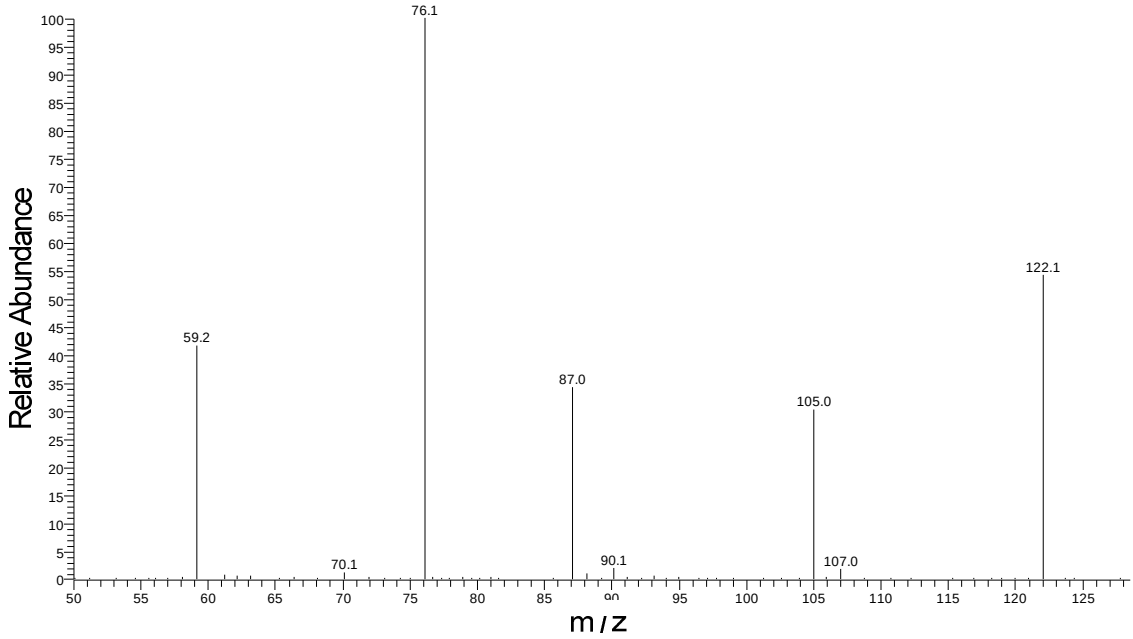

Figure 5- 6. MS/MS spectrum for CySH.

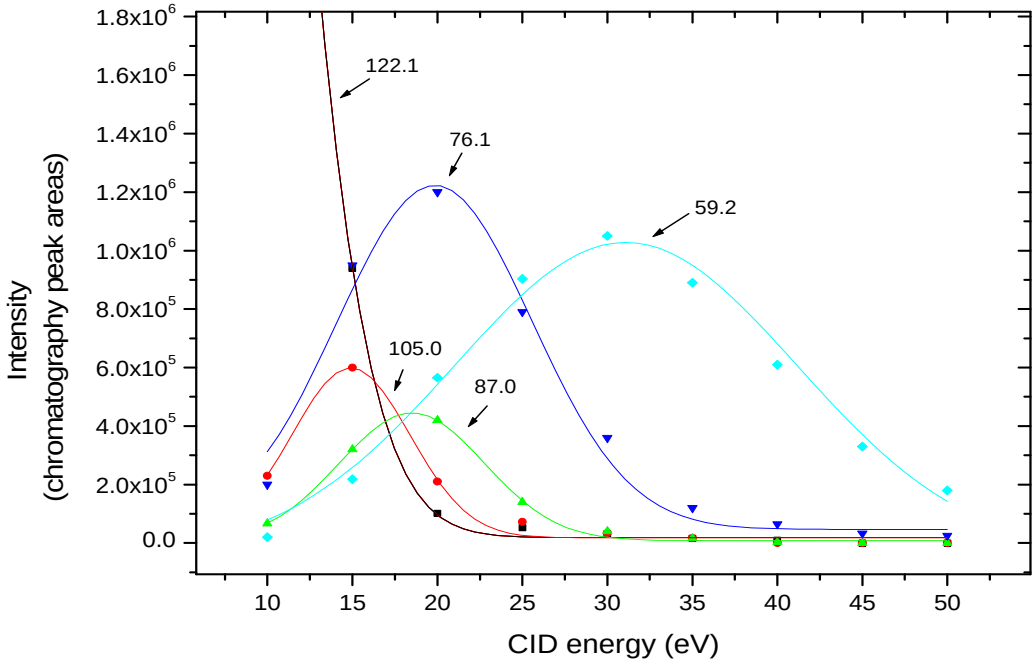

Figure 5- 7. CID breakdown curve for CySH

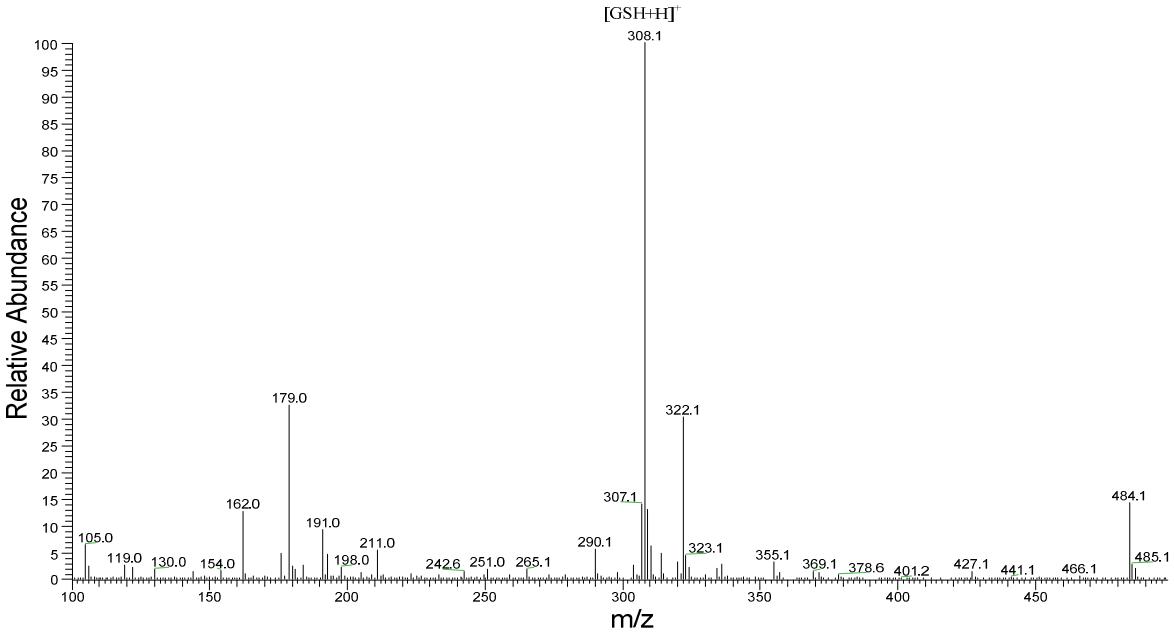

Figure 5- 8. Mass spectrum of GSH.

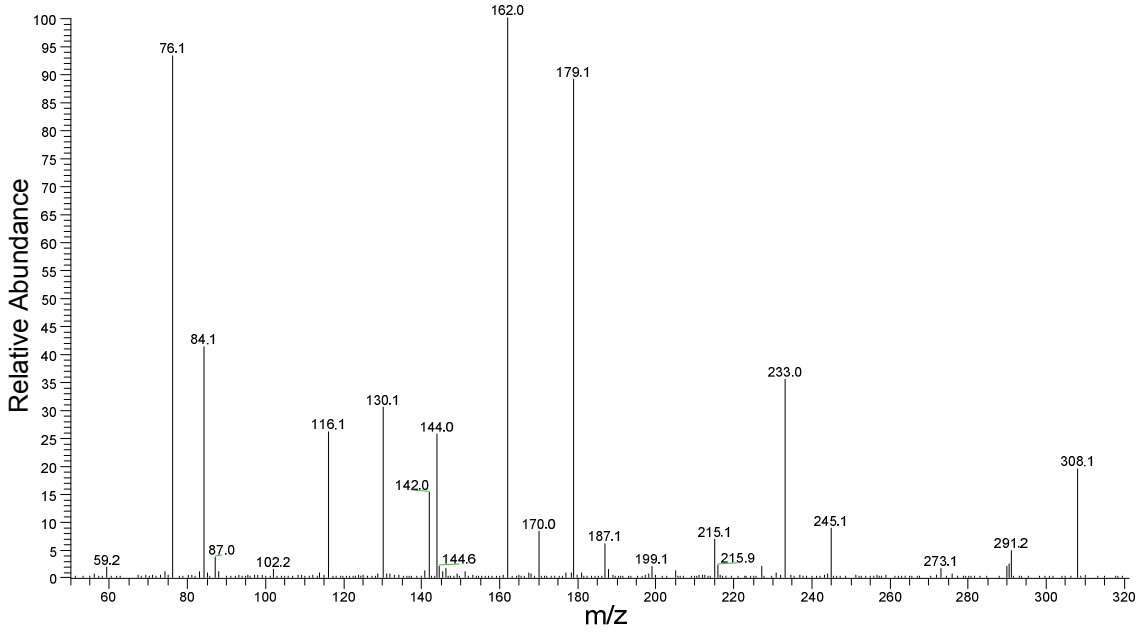

Figure 5- 9. MS/MS spectrum for GSH.

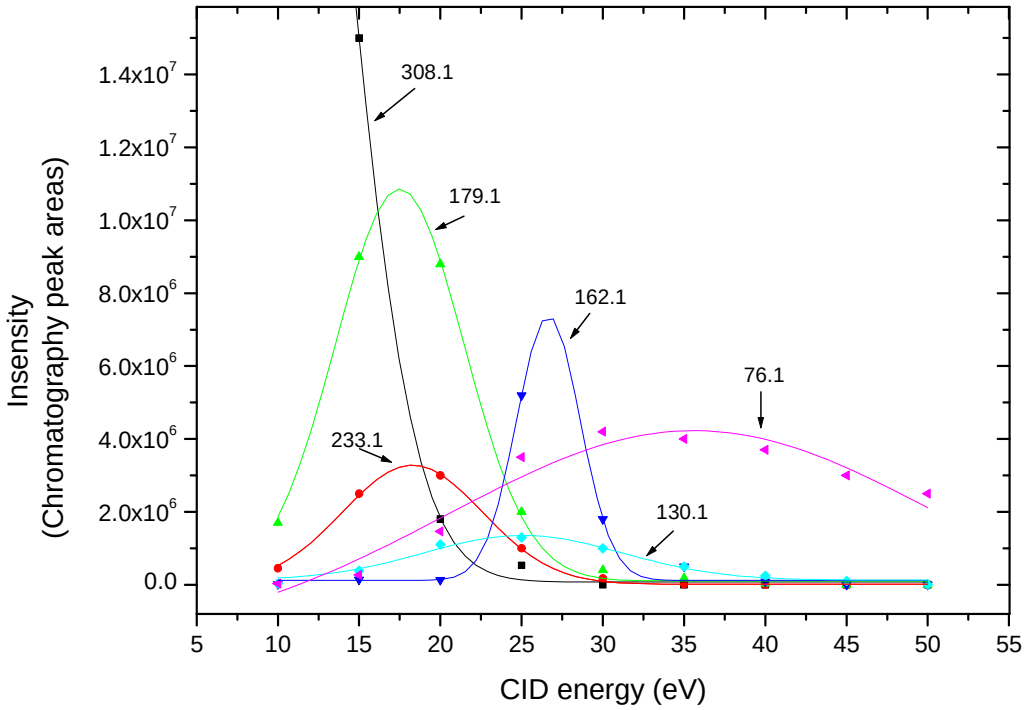

Figure 5- 10. CID breakdown curves for GSH.

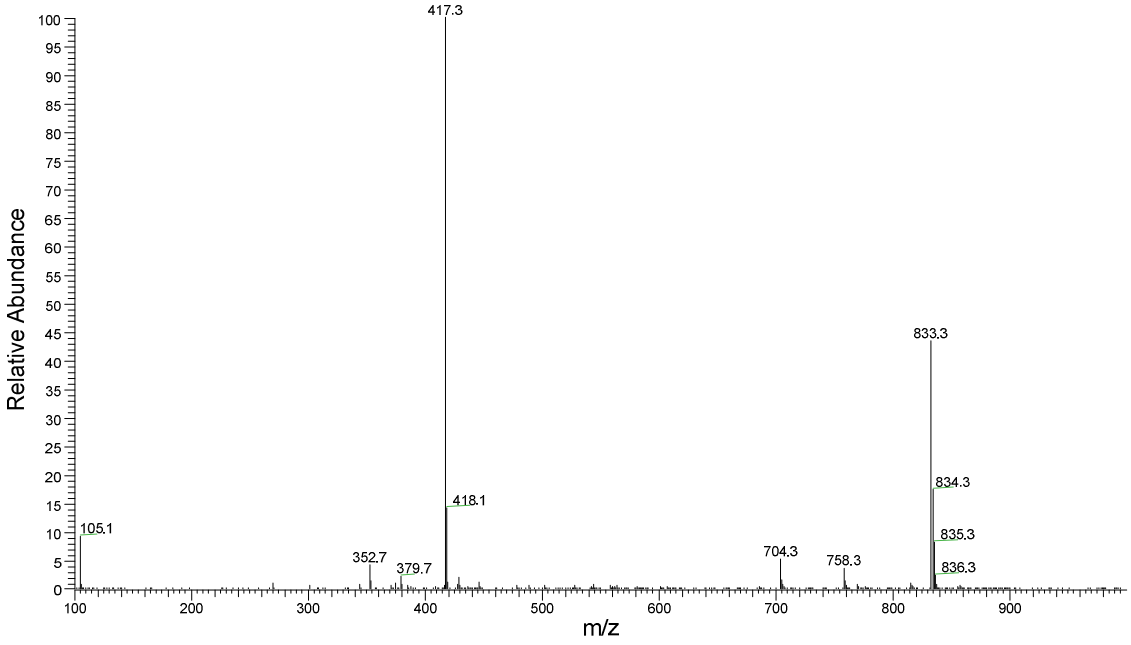

Figure 5- 11. Mass spectrum of GSH-MPB.

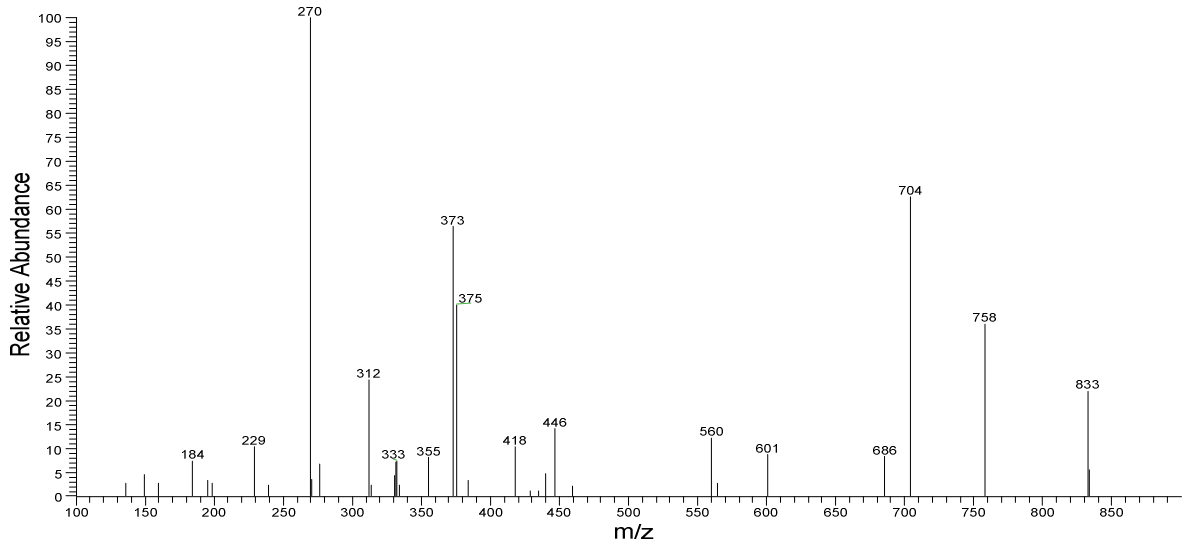

Figure 5- 12. MS/MS spectrum for GSH-MPB.

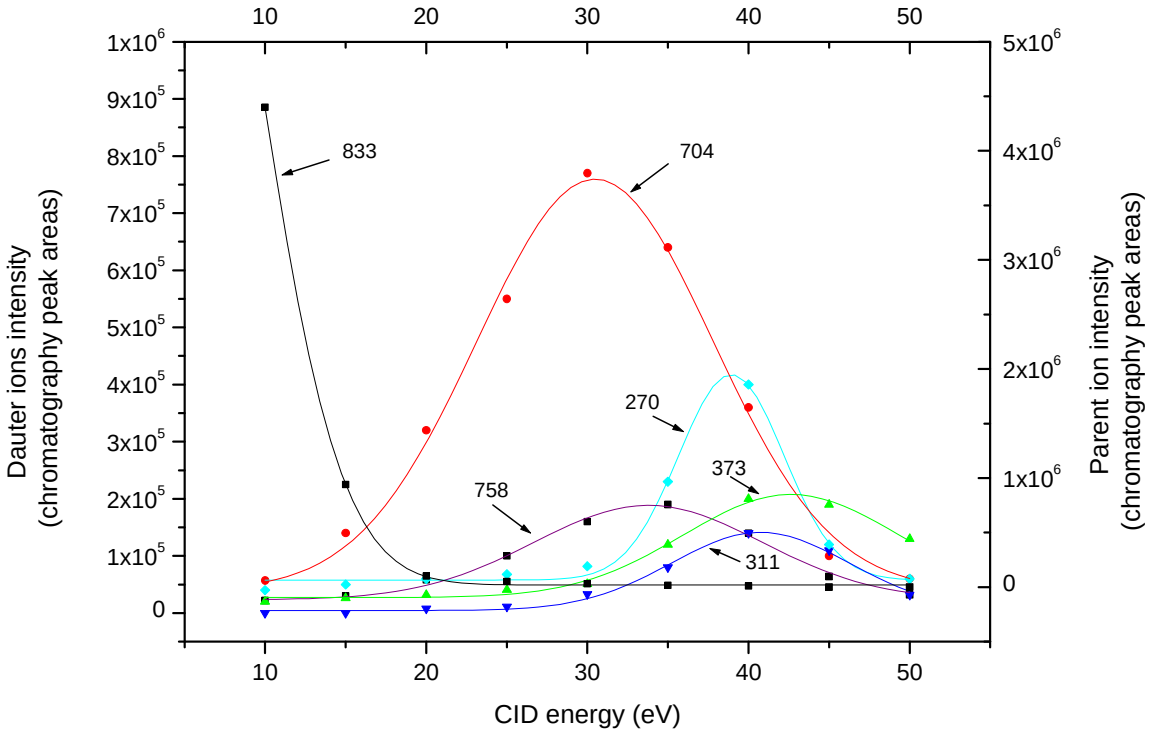

Figure 5- 13. CID breakdown curves for GSH-MPB.

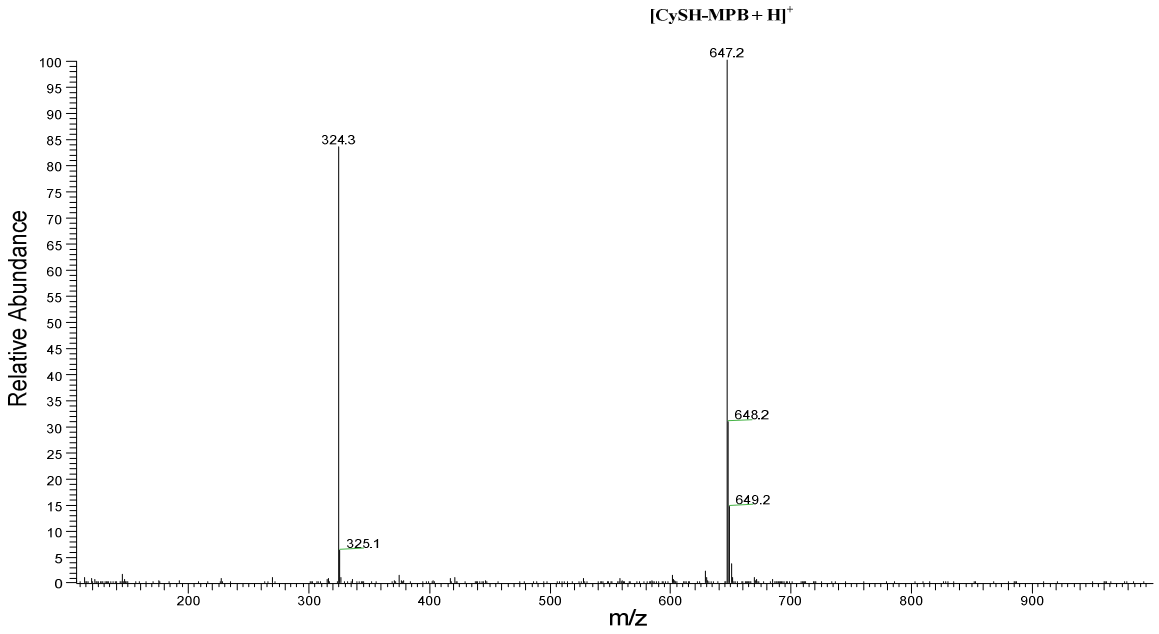

Figure 5- 14. Mass spectrum of CySH-MPB.

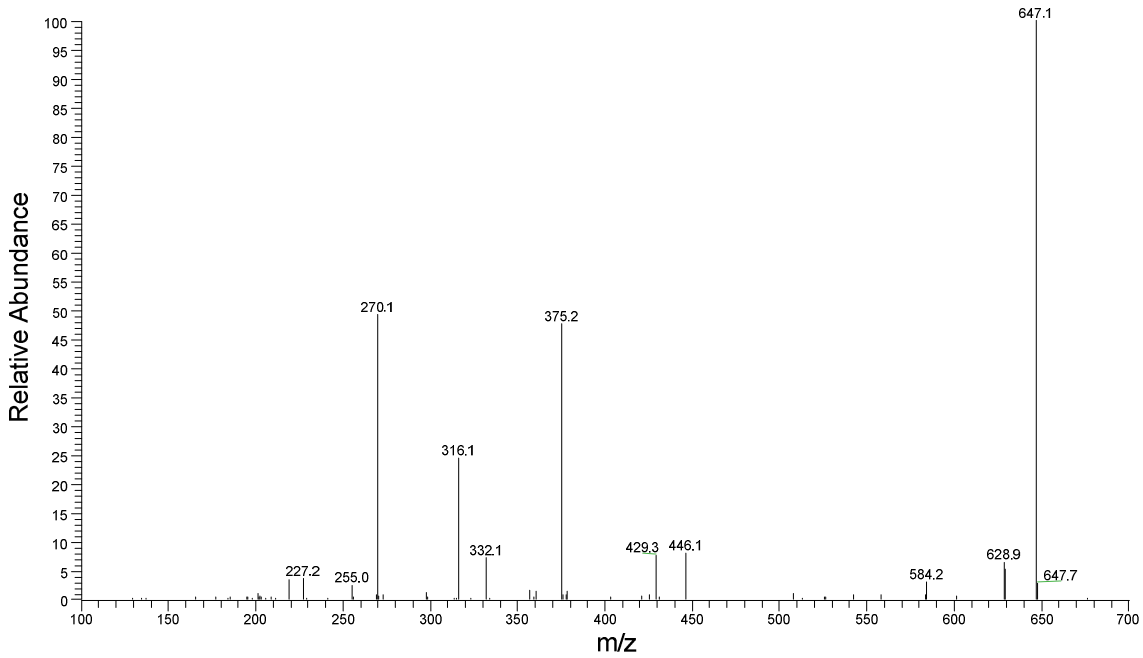

Figure 5- 15. MS/MS spectrum for CySH-MPB.

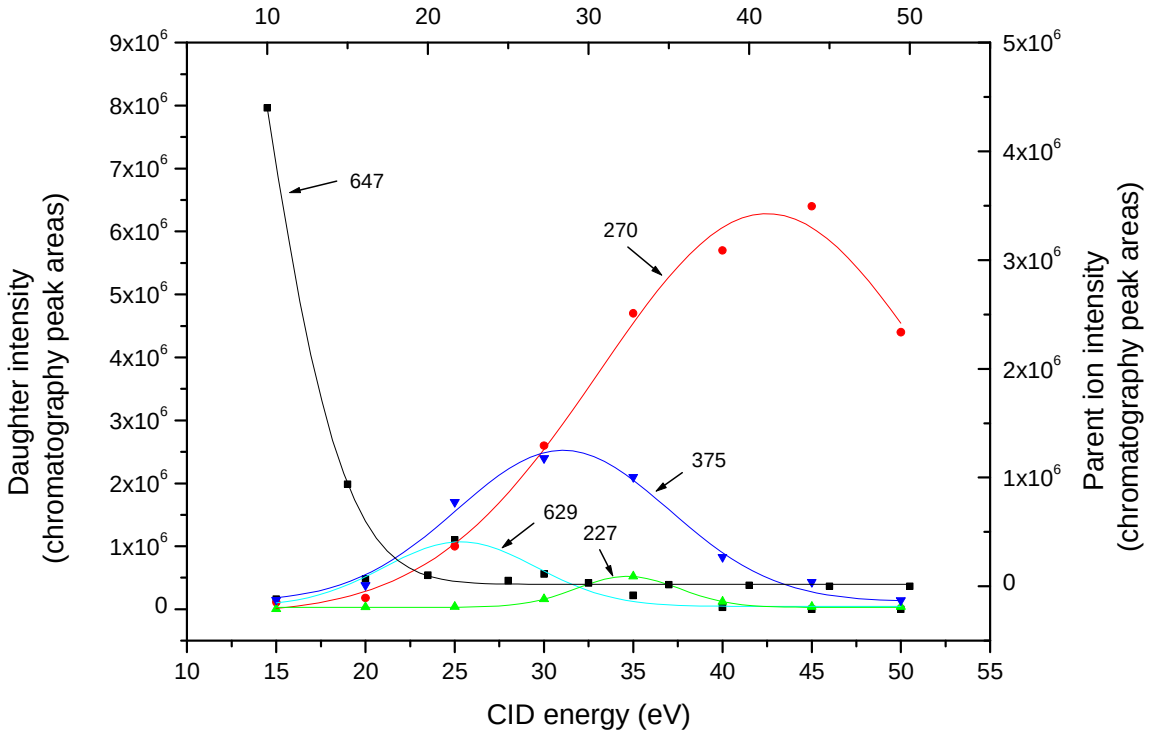

Figure 5- 16. CID breakdown curves for CySH-MPB.

Substance	SRM optimized conditions
GSH	308.1 → 179.1 @ 17 eV
CySH	122.1 →76.1 @ 19 eV
GSH-MPB	833.3 → 704.3 @ 30 eV
CySH-MPB	647.2 → 629.2 @ 25 eV*

Table 5- 1. SRM optimized conditions for all analytes.
*** Not obtained from graph; discussed further later in this chapter.**

2. Pre-Column Derivatization: Why It Was Necessary?

As discussed in Chapter Three, the primary reason for pre-column derivatization was that GSH and CySH were literally not retained on the SPE column. Another reason was that CySH displayed very poor chromatographic behavior on the HPLC column we used. The following Figure compares the chromatographic behavior of CySH and GSH.

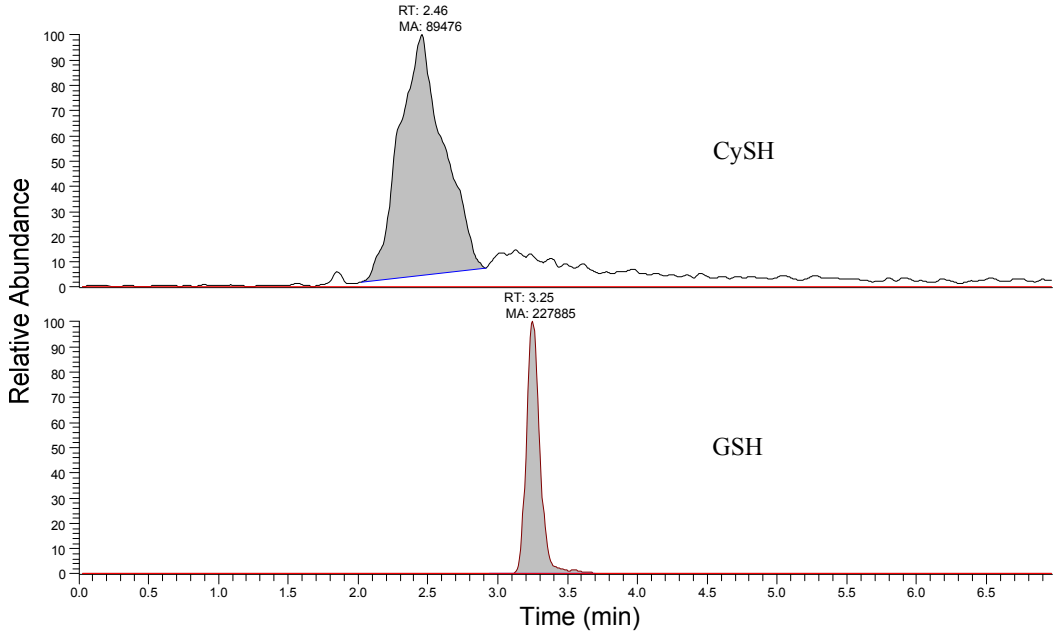

Figure 5- 17. GSH and CySH standard, SPE wash time: 0.2 min.

As illustrated in Figure 5-17, GSH exhibited much better chromatographic behavior. Thus, the retention time was longer (3.25 min vs. 2.48 min for CySH.), and the peak shape was much better (FWHM: 0.08 min *vs.* 0.4 min). It is worth noting that a very short SPE wash time (0.2 min) was employed for the above experiment in order to obtain any signals for GSH and CySH. Such a short SPE wash time was deemed unacceptable because they actually co-eluted from SPE column with salts in aCSF.

However, when the sample pH was decreased (by adding formic acid), the detection of GSH drastically improved, as illustrated in Figure 5-18. Also note that for this experiment a longer SPE wash time (0.5 min) SPE was used.

Thus, no signal was detected for GSH at pH 6 (Figure 5-18, lower trace). A weak peak appeared when the pH was decreased to 3 and the signal intensified further as the pH was decreased

further. Lower pH values than 1 were not studied because under such conditions the SPE column can be damaged or destroyed. Nonetheless, acidification did not improve CySH detection (data not shown).

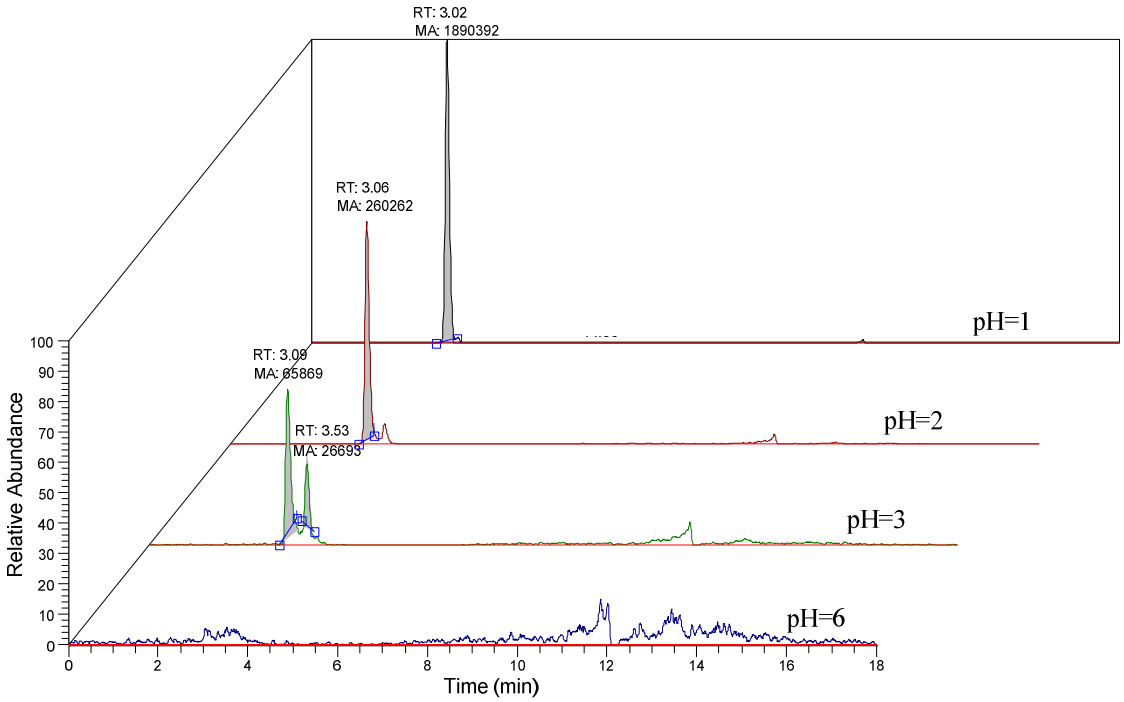

Figure 5- 18. 1μM GSH standard at different pH values; the SPE wash time was 0.5 min.

The conclusion from the preceding experiments was that GSH can be analyzed without on-line derivatization although on-line acidification was necessary. On the other hand, for CySH analysis, on-line derivatization seemed inevitable for utilizing the fully automated system. Following on-line derivatization, the derivatization products, GSH-MPB and CySH-MPB, exhibited very good chromatographic behaviors (Figure 5-19).

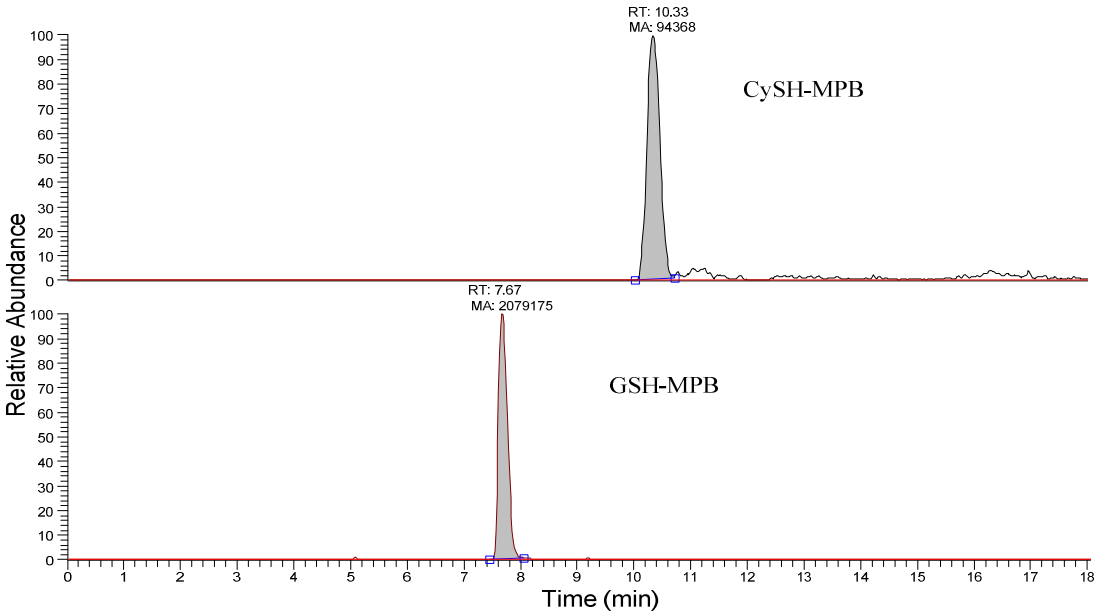

Figure 5- 19. 10 μM GSH and CySH mixture in aCSF solution with on-line derivatization (resulted in GSH-MPB and CySH-MPB) and a SPE wash time of 1.0 min.

3. Standard Curves and Limits of Detection (LOD).

Analyte	Equation	Correlation coefficient	Liner range (μM)	LOD (μM)
GSH	y= –79670+192945·X	0.9996	0.2-20	0.1
CySH	y= –28123+13323·X	0.9984	2.0-50	1.0

Table 5- 2. Calibration, LOD and linear dynamic range for GSH and CySH.

4. Derivatization – "to be or not to be, that is the question".

The main purpose for derivatization was to improve GSH and CySH retention on the SPE column such that interfering substances like salts were washed away in the SPE step. The dilemma was that the derivatization process necessarily introduces a new interferent, unreacted MPB. A huge excess of MPB (concentration ~3 orders of magnitude higher than the analytes) was employed to facilitate the

derivatization reaction. Unfortunately, the on-line SPE process was unable to eliminate unreacted MPB, as illustrated in Figures 5-20 and 5-21.

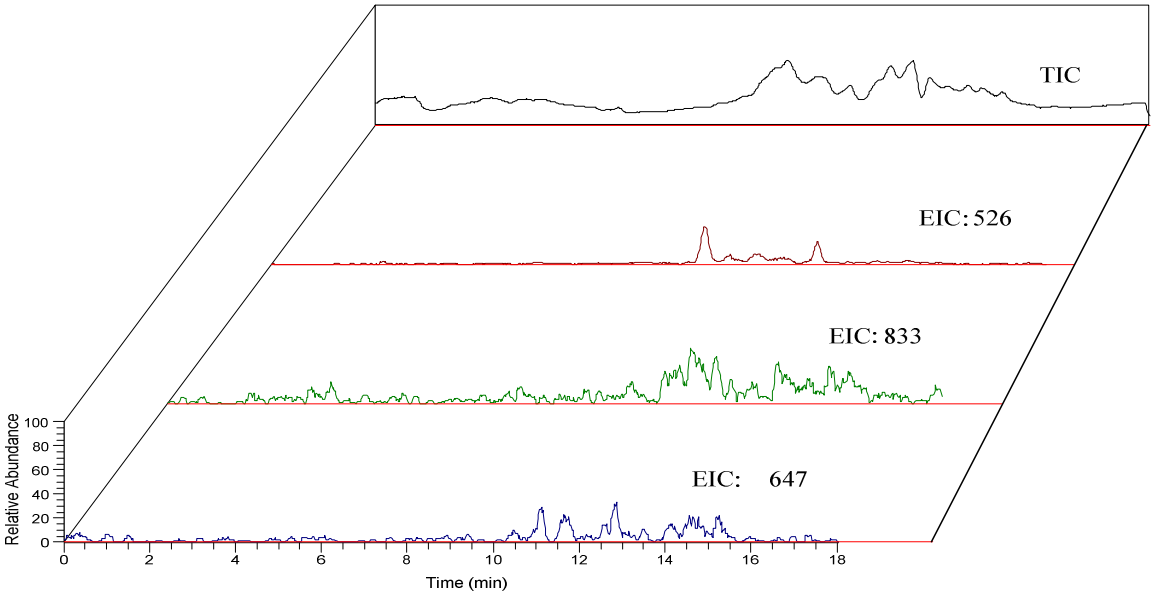

Figure 5- 20. aCSF blank solution, on-line-SPE-HPLC-MS in full scan mode.

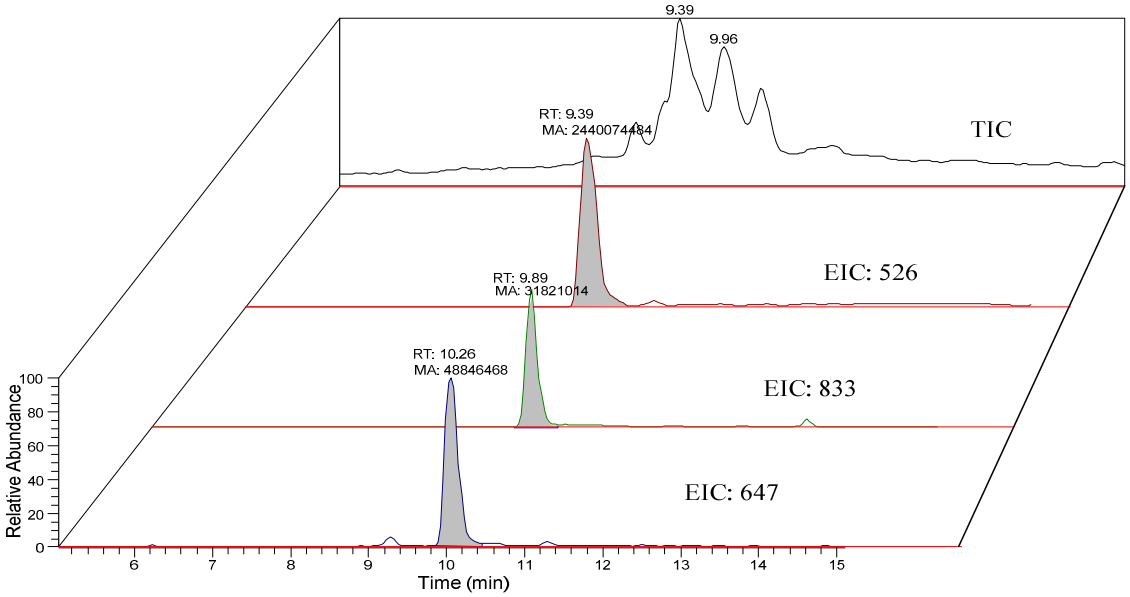

Figure 5- 21. MPB in aCSF, on-line-SPE-HPLC-MS in full scan mode.

Comparing Figures 5-20 and 5-21, the use of MPB caused tremendous contamination. In the TIC chromatogram in Figure 5-21, many pollutant peaks appeared between 9–11 min. The chemical identity of these contaminants, except unreacted MPB, was hard to determine. The EIC chromatogram of MPB (526 m/z) itself indicated a giant peak (huge peak area) with a retention time of 9.39 min, which appeared distinct from the peaks for both GSH-MPB (~7.5 min) and CySH-MPB (~10.3 min). Thus, unreacted MPB itself does not directly affect the analysis of GSH and CySH. However, the unknown impurities of MPB could caused significant interference. EICs with the same m/z values as the parent ions for GSH-MPB (833) and CySH-MPB(647) are displayed in Figure 5-21, lower two traces. The 833 m/z interfering peak (~9.9 min) appears far away from the GSH-MPB peak at ~7.5 min, meaning GSH analysis should not be affected. Unfortunately, there was a significant 647 m/z HPLC peak close to the CySH-MPB retention time (10.3-10.5 min).

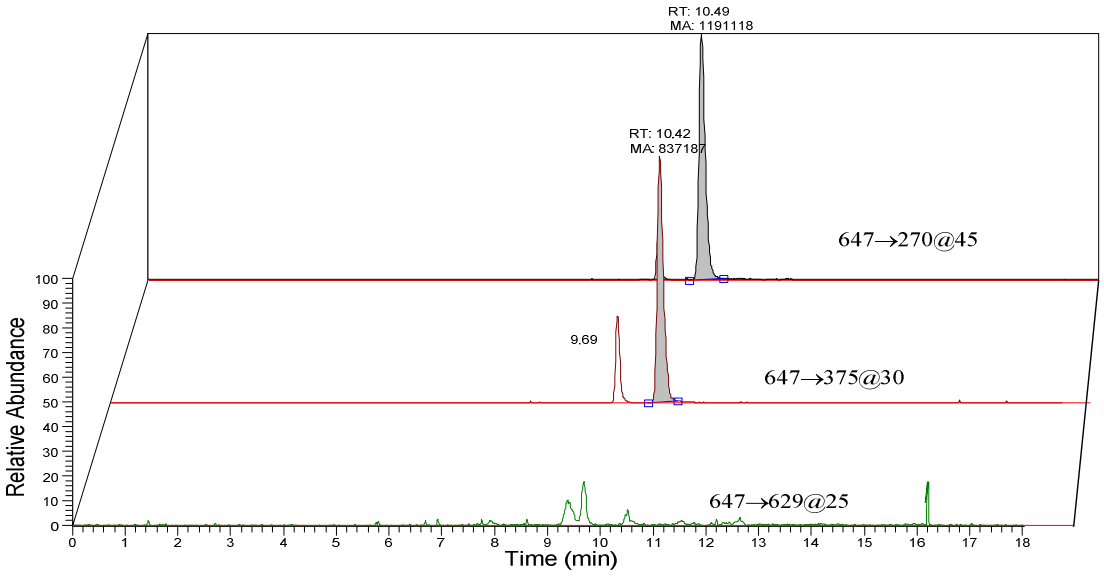

Figure 5- 22. MPB in aCSF, on-line-SPE-HPLC-MS in SRM scan mode.

If the daughter ion pattern for the interferent at 647 m/z are different from those of CySH-MPB, they would not interfere with the determination of the latter derivative using the SRM technique. However, Figure 5-22 illustrates how the 647 m/z ion from MPB solution in fact interfered the analysis of CySH-MPB. In this experiment, MPB in aCSF solution was used, three reactions were monitored simultaneously: 647→270@42eV, 647→375@32eV, 647→629@25eV. These reactions were three best reactions for SRM analysis of CySH-MPB derived in Figure 5-16. In Figure 5-22, the first two reactions have significant HPLC peaks close to the CySH-MPB peak (not shown), which would severely affect the analysis of CySH. However, the third reaction appeared free from interference. Thus, the reaction 647→629@25eV became the optimized SRM condition for CySH analysis (Table 5-1). It should be pointed out that this reaction had a much lower sensitivity compared to the other two reactions, especially to 647→270@42eV (peak intensity: 1.0×10^6 *vs.* 6.8×10^6, Figure 5-16). Thus, the interference accompanied with derivatization procedure causes lower sensitivity for CySH detection. That was a price paid for derivatization analysis.

As stated previously, determination of the chemical structure of the interferent (647 m/z) in the MPB solution is virtually impossible. However, MS technique provided an opportunity to investigate the interferent which has the same parent ion (647 m/z), the same daughter ions (270 and 375) and the same retention time (~10.4 min) as CySH-MPB. Figure 5-23 is full scan (100-900 m/z) mass spectrum of all the compounds in the MPB/aCSF solution that eluted at retention times ranging from 10.3 to 10.5 min in Figure 5-21.

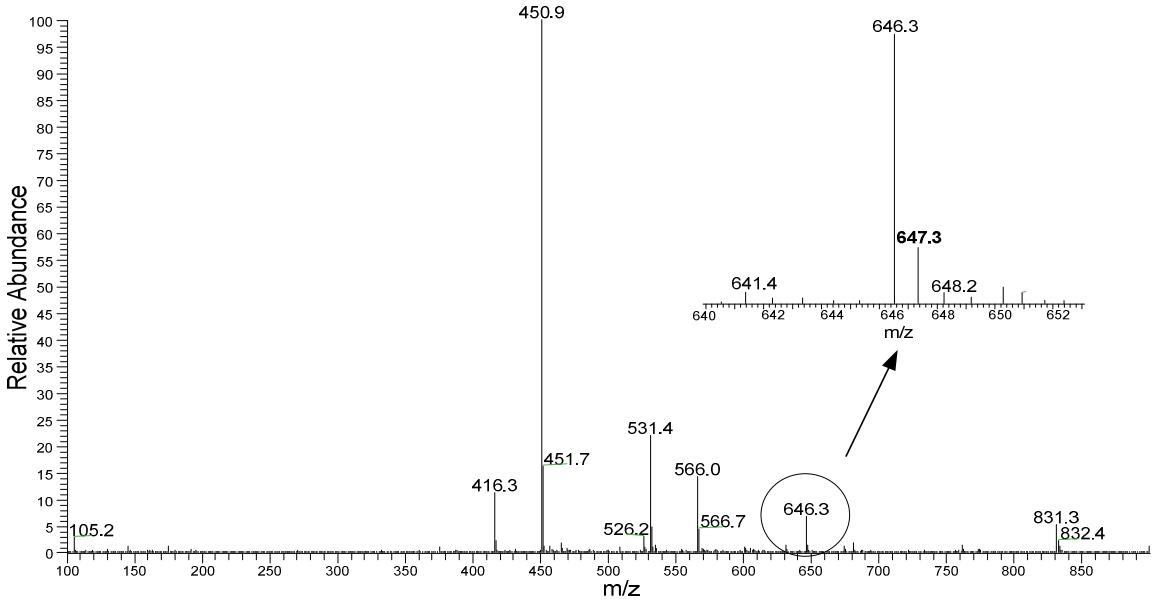

Figure 5- 23. Full scan mass spectrum between retention times 10.3 to 10.5 min of MPB in aCSF solution.

All of the ions shown in Figure 5-23 co-eluted with CySH-MPB, for they have identical retention times. Nonetheless, for SRM analysis only one ion survived after the first quadrupole filtering, which is the ion of 647.3 m/z (parent ion for CySH-MPB). The actual procedure to do this was to set up a small window which has a width of 1.0 m/z centered at 647.3 m/z. Then this small window was applied to the first quadrupole, so only this ion was passed through. The embedded spectrum in Figure 5-23 shows the detailed mass spectrum of the ions (647.3 m/z) and surrounding ions. The series 646.3, 647.3 and 648.3 peaks apparently fit an isotopic pattern for a typical organic molecule. Thus, the ion of 647.3 m/z, which originated from MPB aCSF solution, is actually the isotopic ion of 646.3 m/z. This ion was resulted from the less abundant naturally occurred isotopes ^{13}C, ^{2}H, ^{15}N *etc*. in the 646.3 compound. The chemical structure of the interferent ion, at 646.3 m/z, could be further elucidated by measuring its accurate m/z value, the relative abundances of all isotopic peaks and MS/MS spectrum. Nonetheless this was beyond the scope of this research project.

This is an example of how MS, as sensitive as it is, is vulnerable to minute impurities in the sample. It also raised the question of whether derivatization should be employed, since the impairments caused by a huge excess of the derivatization reagent with all kinds of unknown impurities might be much greater than endogenous matrix compounds in microdialysates like salts. Indeed, it is a widely-held opinion that derivatization should always be treated as a last resort in HPLC-MS method development. When derivatization must be employed, great caution should be taken concerning the reagent purity and possible side reactions. In this research project, it was concluded that CySH has to be derivatized, although at the expense of decreased sensitivity and much more frequent mass spectrometer maintenance, *i.e.*, from every 3 month to every 2 weeks, in order to maintain sensitivity.

5. *In Vitro* Microdialysis (Probe Recovery Studies).

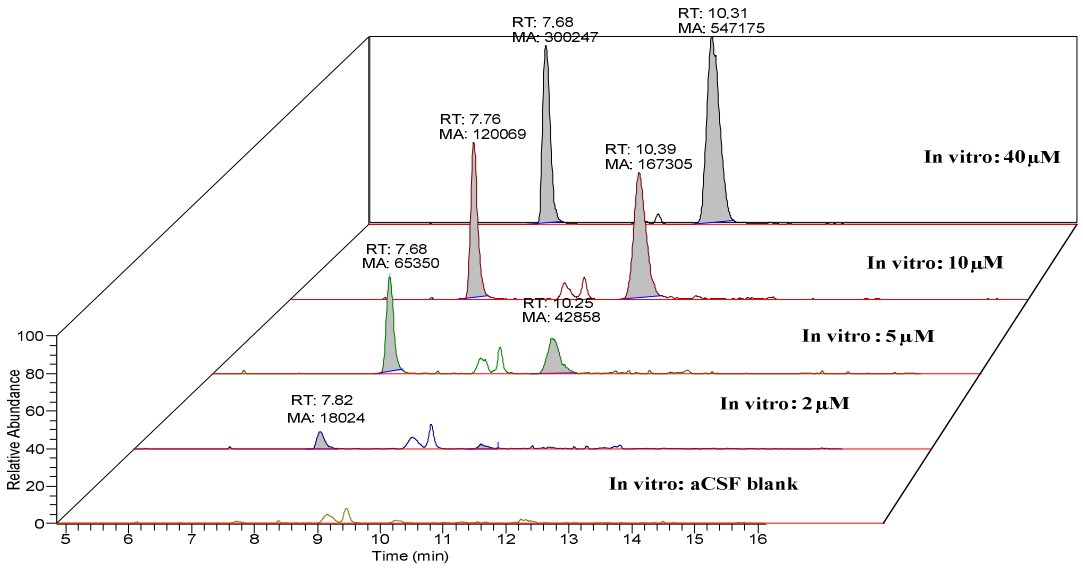

Figure 5- 24. Typical data for *in vitro* experiments.

Recovery rate (Mean ± S.E.M., n=4) /%		
Substance / *in vitro* conc.	**GSH**	**CySH**
2μM	24.8±1.6	
5μM	15.7±1.0	59.7±2.0
10μM	11.0±0.8	64.6±2.1
40μM	5.1±0.6	41.1±1.2

Table 5- 3. Probe recoveries for GSH and CySH.

6. *In Vivo* Experiments.

The following are the results obtained from *in vivo* experiments.

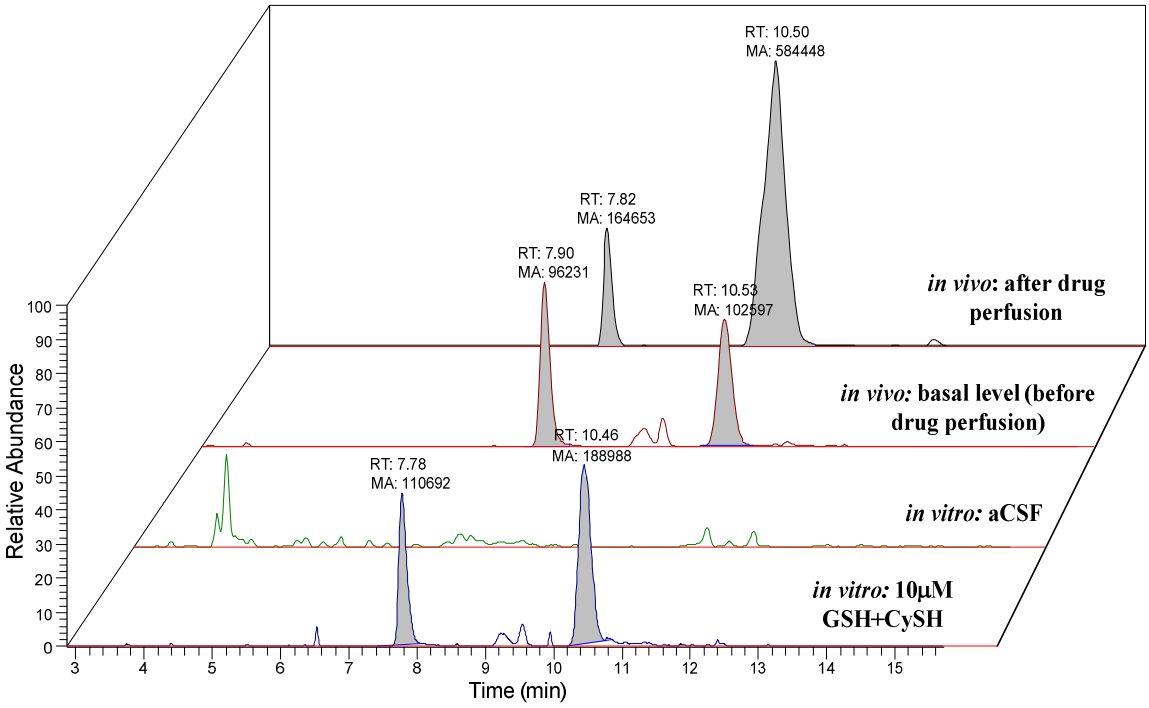

Figure 5- 25. Typical data for *in vivo* experiments, including necessary *in vitro* checkup

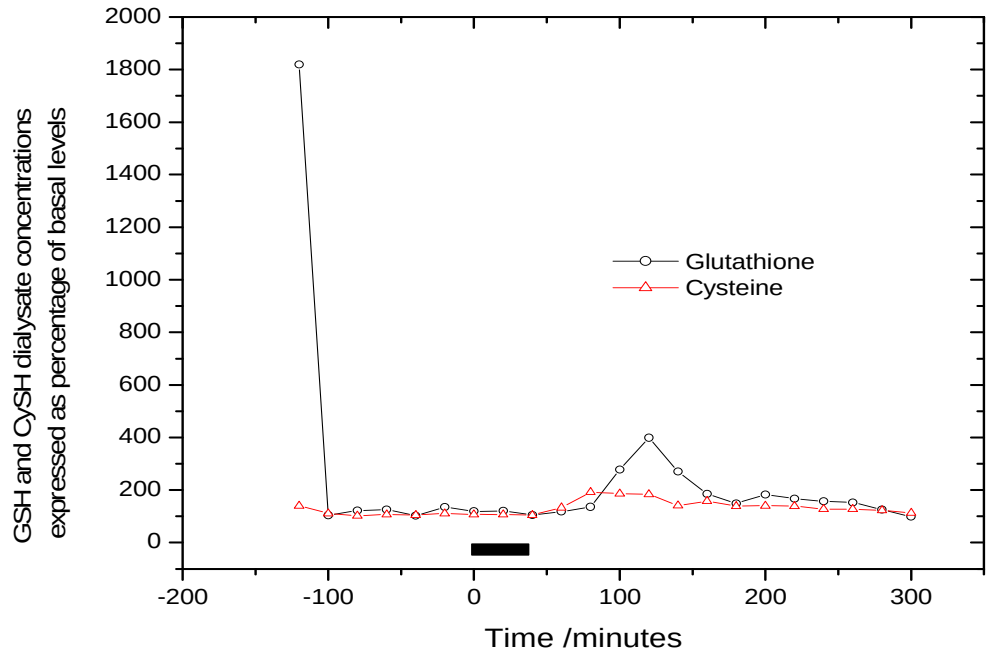

Figure 5- 26. Time-dependent effects of a 30-min perfusion of 2.5 mM MPP+ into rat striatum on microdialysate levels of GSH and CySH. The horizontal black bar shows the time during which MPP+ (dissolved in aCSF) was perfused. Data are percentages of basal GSH and CySH levels

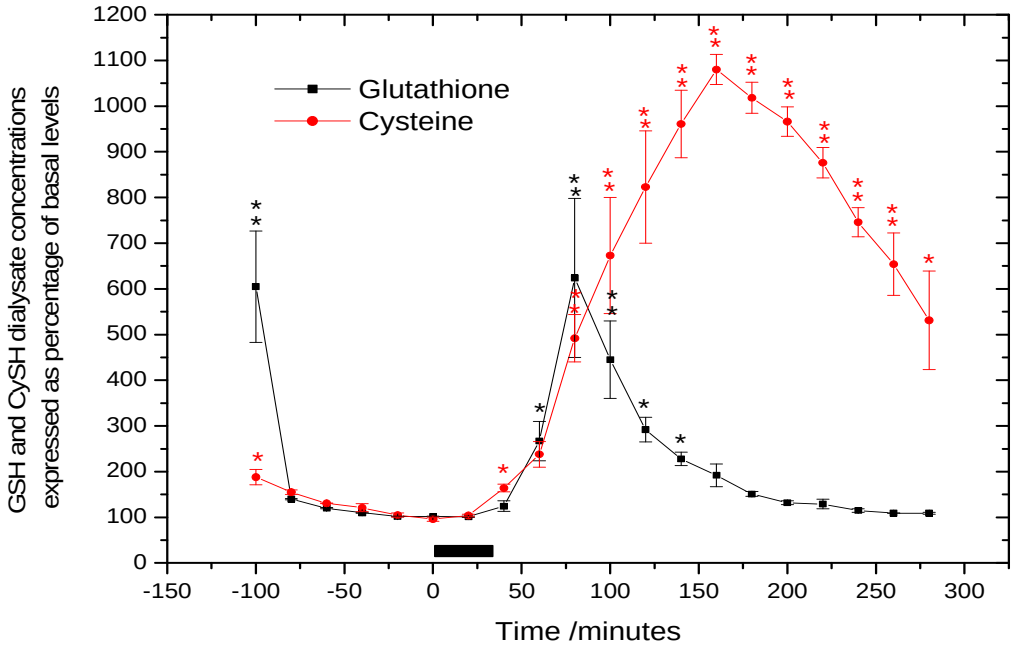

Figure 5- 27. Time-dependent effects of a 30-min perfusion of 5mM MPP^+ into rat striatum on microdialysate levels of GSH and CySH. The horizontal black bar shows the time during which MPP^+ (dissolved in aCSF) was perfused. Data are mean ± SEM bars) percentages of basal GSH and CySH levels (n = 3). * p < 0.05, ** p < 0.01.

The basal concentration for GSH was 0.6 ± 0.1 μM (mean ± SEM, n=3) in microdialysate samples and for CySH was 6.2 ± 0.4 μM (mean ± SEM, n=3). The probe insertion caused extracellular (microdialysate) concentrations of both GSH and CySH to increase significantly (Figure 5-27), and then both declined rapidly to basal levels. In preliminary experiments, perfusions of 10 mM MPTP in aCSF solution failed to evoke any increase in microdialysate levels of GSH or CySH (data not shown). Accordingly, the effects of its metabolite MPP^+ were studied. In preliminary experiment, the concentration of MPP^+ employed was 2.5 mM and the effect of MPP^+ on GSH and CySH was so small that it was decided not to waste additional animals. Accordingly, in subsequent experiments, a MPP^+ concentration of 5 mM was employed. In experiments using 5 mM MPP^+ (Figure 5-27), during perfusions extracellular concentrations of GSH and CySH were not significantly different from basal levels. However, when MPP+ perfusions were discontinued, extracellular GSH increased massively, reaching 650% (60 min) of basal levels, and then declined to basal level in about 90 min. After discontinuing MPP^+ perfusion, CySH continued to increase but more slowly and peaked later than that GSH at 1,100% (180 min) above basal level. Subsequently, extracellular CySH slowly declined, although remaining significantly above basal level until the end of the experiment (270 min).

The extracellular GSH and CySH profiles reported above are in approximate agreement with previously results from our laboratory when HPLC-EC was employed to monitor levels of these thiols in microdialysate samples.[207] However, the maximum increase of GSH was much higher previously (5,000% vs. 650%), whereas the CySH peak values were very similar (1,540% vs. 1,100%). It is worth pointing out that HPLC-MS/MS (SRM) is a much more specific technique than HPLC-EC.

D. Conclusions

In this chapter, the highly specific and sensitive fully automated system combining microdialysis sampling, on-line derivatization, on-line IP-RP-SPE sample preparation, IP-RP-HPLC separation, and tandem MS/MS detection techniques were applied to monitor GSH and CySH in rat striatal microdialysates in response to MPTP or MPP^+ perfusion. The conditions for SRM of all analytes were optimized using off-line experiments. The fully automated system was extensively used in calibration curve, *in vitro* microdialysis probe recovery, and *in vivo* experiments. All these experiments showed this system to be a powerful tool for real-time, highly specific and sensitive monitoring of targeted metabolites in biological systems.

Chapter Six

Fully Automated On-line Sample Cleanup and HPLC-MS Determination of MPTP Metabolites in Rat Brain Striatum: An *In Vivo* Microdialysis Study.

A. Introduction

1-methyl-4-phenyl-1,2,3,6- tetrahydropyridine (MPTP) is considered by many neuroscientists to hold the key to understanding the pathogenesis of idiopathic PD. The history of MPTP as an animal model for PD was described previously. However, the detailed mechanism of MPTP–mediated dopaminergic nerotoxicity has yet to be fully established.[212,213] Nevertheless, it has been well established that MPTP exerts its selective neurotoxic effects through its active metabolite MPP^+.[214-218] Direct measurement of MPTP and its metabolites in the brains of animal models of PD should be an effective way to help contribute to an understanding of the biological pathway for its selective toxicity towards dopaminenergic neurons. The results of such studies, in turn, might thus contribute to an understanding of the mechanisms underlying PD.

Historically, MPTP and its metabolites have been analyzed principally by HPLC-UV[215,219-222] and GC-MS.[215,223-225] There have been very few reports of the use of HPLC-MS techniques for such analyses although they should, in principal, have great potential.[226] The limitations of HPLC-UV analyses include its low specificity, since it mainly depends on retention time measurement, and susceptibility to many interferences present in biological samples. In the case of GC-MS, the major

drawback it that it requires the analytes to be volatile and thermally stable, which was not the case for MPTP and its metabolites.

In this chapter a fully automated system which combines microdialysis sampling, on-line IP-RP-SPE sample clean-up, IP-RP-HPLC separation, and selected ions monitoring (SIM) detection techniques was employed to monitor MPTP and its metabolites 4-phenyl-1,2,3,6-tetrahydropyridine (PTP), 1-methyl-4-phenyl-2,3-dihydropyridinium ($MPDP^+$), 1-methyl-4-phenyl-1,2,3,6-tetrahydropyridine- N-Oxide (MPTP-*N*-Oxide) and (1-methyl-4-phenylpyridinium) MPP^+ in rat striatal microdialysates in response to perfusion of MPTP.

B. Experimental

1. Chemicals and Chromatographic Conditions.

Chemicals and chromatographic conditions were the same as in Chapters Two and Three.

2. Instrumentation.

The fully automated system used was described in Chapter Two

3. Stock and Standard Solutions.

Stock standard solutions for MPTP (10 mM) and MPP^+ (5 mM) were prepared and stored as described in Chapter Two.

Standard solutions for MPTP/MPP^+ (10 μM) was prepared as follows: 10 μL of 10 mM individual stock solutions were added to 990 μL aCSF to obtain 100 μM solutions; 100 μL of such solution was added to 900 μL aCSF to obtain 10 μM solutions.

A series of calibration standard mixture solutions (2 μM, 500 nM, 100 nM, 20 nM, 5 nM, 2 nM, 1 nM and 0.5 nM) was prepared as follows: 10 μL 10 mM stock standard solution of MTPT and MPP^+ was added to 980 μL aCSF to obtain 100 μM mixed standard solution; 20 μL of this solution was added to 980 μL aCSF to obtain 2 μM solution; 400 μL of 2 μM solution was added to 600 μL aCSF to obtain 500 nM solution; 200 μL of 500 nM solution was added to 800 μL aCSF to obtain 100 nM solution; 200 μL of 100 nM solution was added to 800 μL aCSF to obtain 20 nM solution; 400 μL of 20 nM solution was added to 600 μL aCSF to obtain 5 nM solution; 400 μL of 5 nM solution was added into 600 μL aCSF to obtain 2 nM solution; 500 μL of 2 nM solution was added into 500 μL aCSF to obtain 1 nM solution; 500 μL of 1 nM solution was added into 500 μL aCSF to obtain 0.5 nM solution; All solutions were stored in plastic vials placed on ice in a covered igloo, and were passed through 0.2 μm centrifuge filter before use.

The standard mixture solutions for *in vitro* (1 μM and 5 μM) experiments were prepared in the same manner described above.

4. Selected Reaction Monitoring (SRM) Optimization.

SRM optimization was carried out in the same way described in Chapter Four except that10 μM MPTP and MPP^+ individual standard solutions were injected.

5. Calibration Curves

The fully automated system describe in Chapter Two was employed to determine calibration curves. Detailed procedures are described in Chapter Four except that a series of MPTP and MPP^+ standard mixture solutions were used. In addition, MS in the SIM scan mode for MPTP (174 m/z) and MPP^+ (170 m/z) was employed.

6. *In Vitro* Microdialysis Experiments

The fully automated system was employed to perform *in vitro* microdialysis experiments (probe recoveries), the procedures being the same as in Chapter Four except that 1 μM and 5 μM mixed MPTP and MPP^+ standard solutions were used and the MS SIM scan mode was employed.

7. Animals and Surgical Procedures

Animals and surgical procedures were the same as described in Chapter Four.

8. *In Vivo* Microdialysis.

In vivo microdialysis followed the same protocols described in Chapter Four with the following modifications: a) a 1 μM MPTP and MPP^+ standard mixture solution was employed in the *in vitro* studies (probe recovery check); and, b) the MS SIM scan mode was performed at 160 m/z (PTP), 170 m/z (MPP^+), 172 m/z ($MPDP^+$), 174 m/z (MPTP) and 190 m/z (MPTP-N-Oxide).

9. Calculations and Statistics

Data calculations and statistics were the same as described in Chapter Four.

C. Results and Discussion

1. Parent Ions, Daughter Ions and CID Optimization for MPTP and MPP^+.

Parent ion information was obtained by means of MS full scan spectra. Daughter ion information and CID optimization were achieved by CID energy-step-increase experiments. Data processing for CID breakdown curve establishment was described in Chapter Four.

Figure 6-1 and 6-2 present spectra and CID breakdown curves for MPTP and MPP^+. The optimized SRM conditions are summarized in Table 6-1.

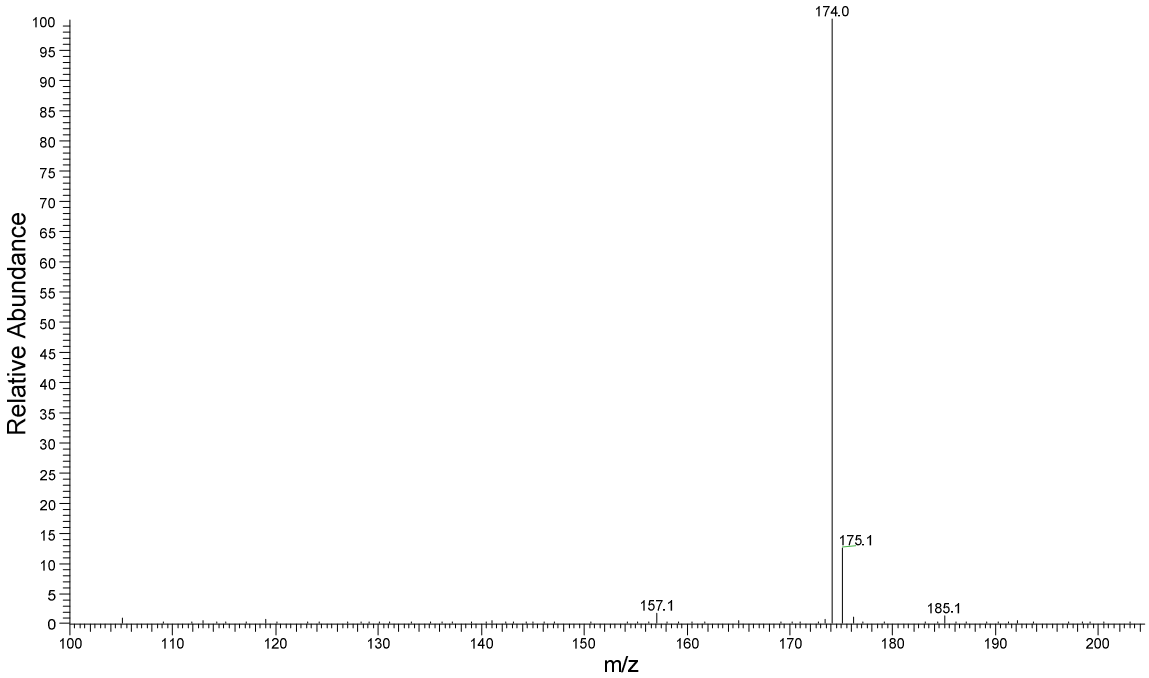

Figure 6- 1. Mass spectrum of MPTP.

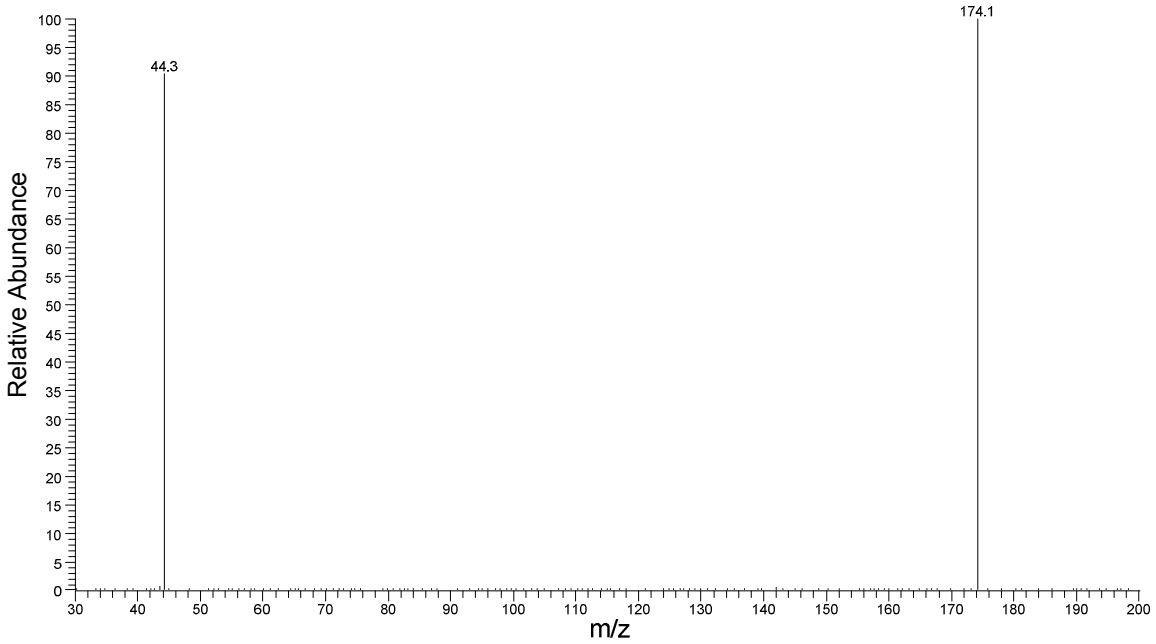

Figure 6- 2. MS/MS spectrum of MPTP.

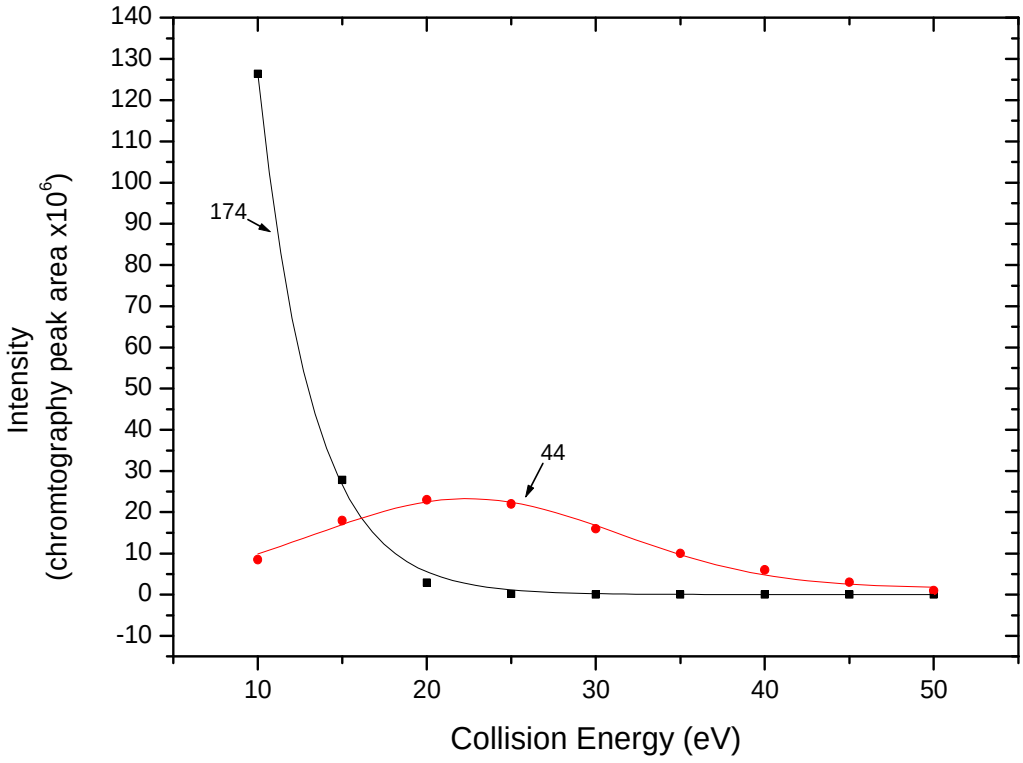

Figure 6- 3. CID breakdown curves for MPTP.

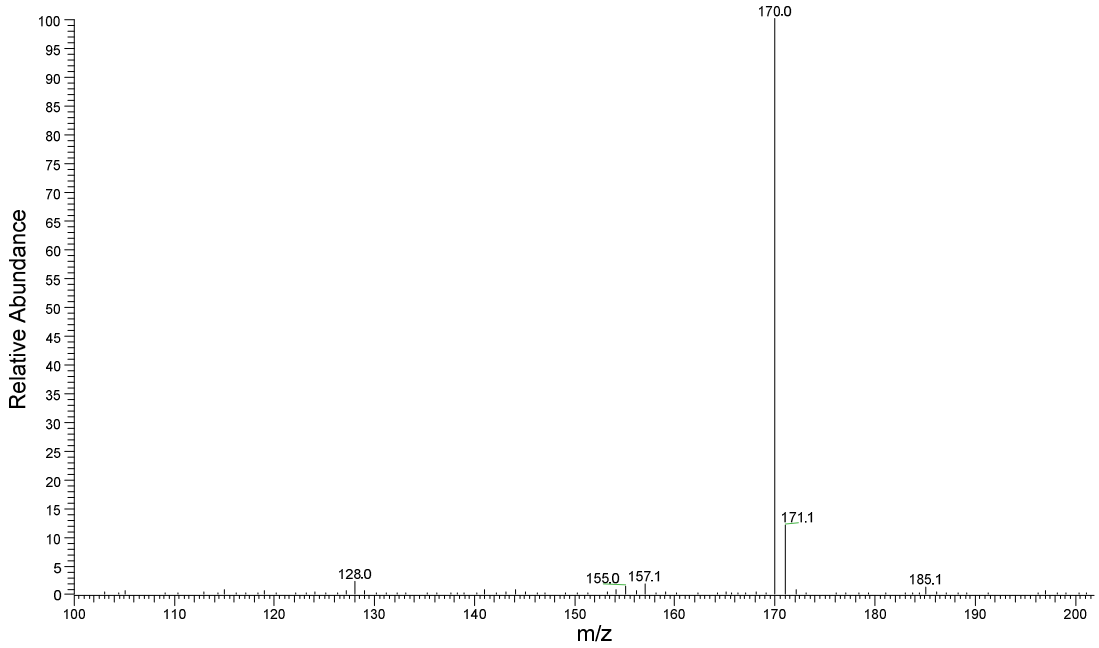

Figure 6- 4. Mass spectrum of MPP^+.

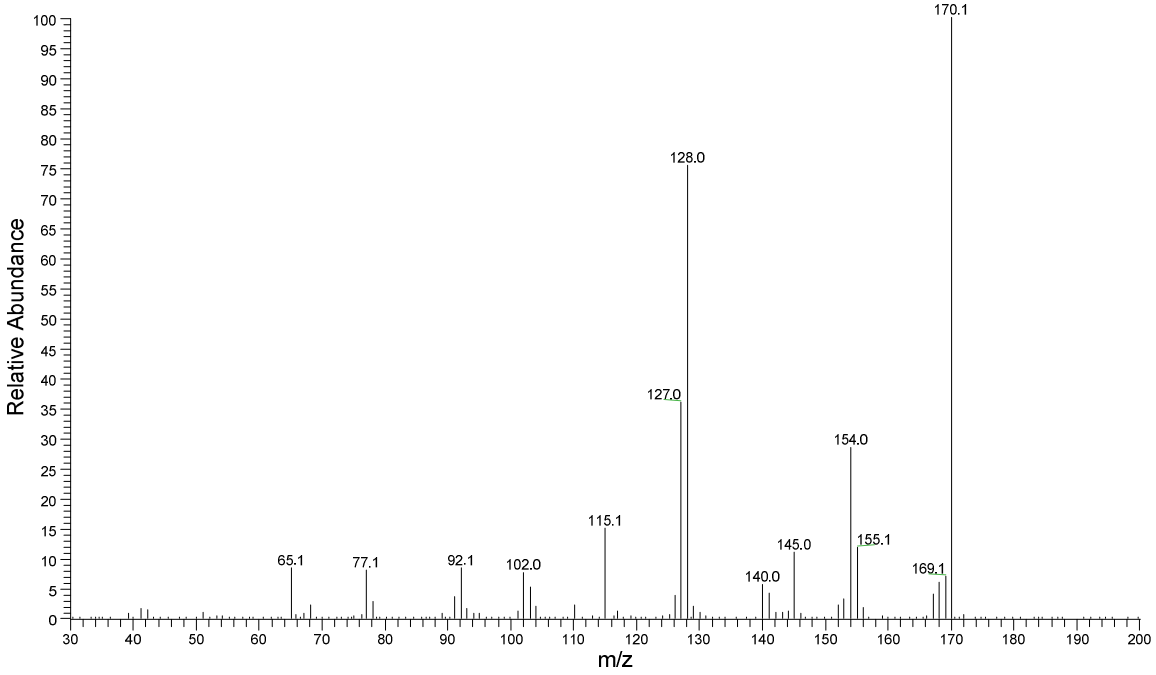

Figure 6- 5. MS/MS spectrum of MPP^+.

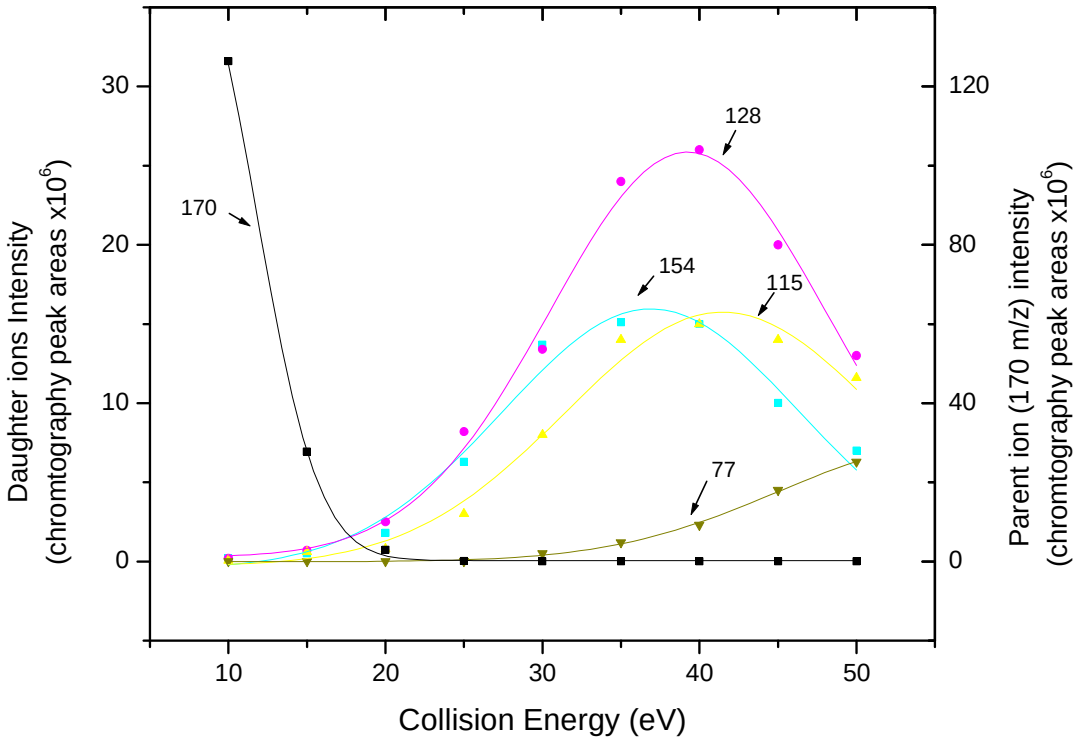

Figure 6- 6. CID breakdown curves for MPP^+

Substance	SRM optimized conditions
MPTP	174.1 → 44.1 @ 30 eV
MPP^+	170.0 →128.0 @ 40 eV

Table 6- 1. SRM optimized conditions for MPTP and MPP^+.

Although SRM is the preferred MS technique on most occasions for biological samples, selected ion monitoring (SIM) was employed for the remainder of the experiments described in this chapter, including calibration curves, *in vitro* and *in vivo* experiments. The reasons were: 1) it was not possible to obtain the standards for three targeted MPTP metabolites, *i.e.* PTP, $MPDP^+$, MPTP-*N*-Oxide; 2) only parent ion information was available in literature sources for the above three

metabolites, which could be used for the SIM experiment setup but inadequate for SRM experiments; and, 3) the fragmentation pattern for MPTP was not very suitable for SRM, *i.e.* MPTP has only one detectable daughter ion, and its intensity was low (< 20% of the parent ion signal intensity as shown in Figure 6-3). The principle disadvantage of the SIM approach is its relatively low specificity compared to SRM. Thus it may not appropriate when server interference happens. However, in our experiment, the interference was not significant.

2. Standard Curves and Sensitivity.

Calibration information for MPTP and MPP^+ is summarized in the Table 6-2.

Analyte	Equation	Correlation coefficient	Liner range (nM)	LOD (nM)
MPTP	y=5285800 + 95755 • x	0.9997	5.0 - 2000	1.0
MPP^+	y=721590 + 224460 • x	0.9998	2.0 - 2000	0.5

Table 6- 2. Calibration parameters, LOD and linear dynamic range for MPTP and MPP^+.

3. *In Vitro* Microdialysis and Probe Recovery Measurements.

Figure 6-7 presents typical data obtained from *in vitro* experiments. The *in vitro* standard mixture solution used contained 1 μM concentrations of both MPTP and MPP^+. Also shown are results for aCSF solution (blank). Compared to SRM data reported in previous chapters, SIM was less specific, thus there were some interfering peaks at retention times of 1.0 min and 4.8 min for both MPTP and MPP^+. Nonetheless, no significant interference appeared at the retention time of ~12.5 min

where both MPTP and MPP^+ eluted. The peaks for MPTP and MPP^+ were almost overlapped in TIC (not shown), however they were separated in EIC chromatograms. Table 6-3 summarizes microdialysis probe recovery data.

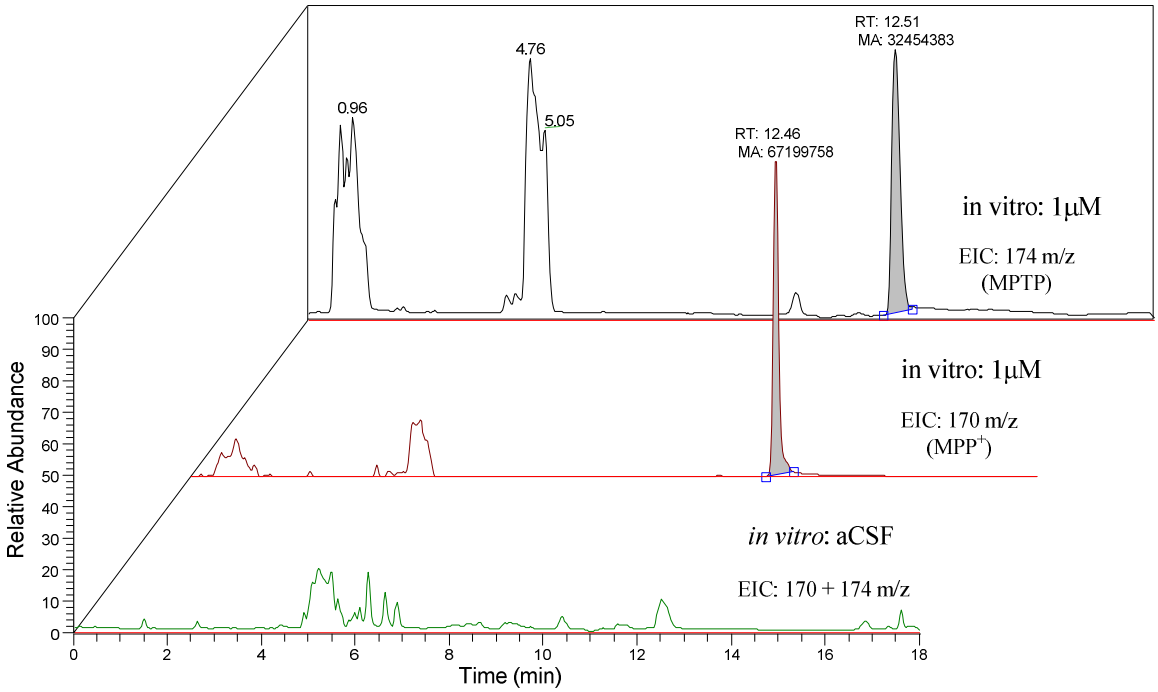

Figure 6- 7. Typical data from *in vitro* (probe recovery) experiments.

	Recovery rate (Mean ± S.E.M. ,n=4) /%	
Substance / *in vitro* conc.	**MPTP**	**MPP^+**
1 μM	28.9 ± 1.1	30.5 ± 1.1
5 μM	19.1 ± 0.9	24.1 ± 1.3

Table 6- 3. Probe recoveries for MPTP and MPP^+

4. *In Vivo* Experiments.

During *in vivo* experiments, five ions were monitored at m/z = 160 (PTP), 170 (MPP^+), 172 ($MPDP^+$), 174 (MPTP), and 190 (MPTP-N-Oxide). In order to protect the MS detector, MPTP was not monitored until 30 min after the perfusion finished. The following figures present the results obtained from *in vivo* experiments.

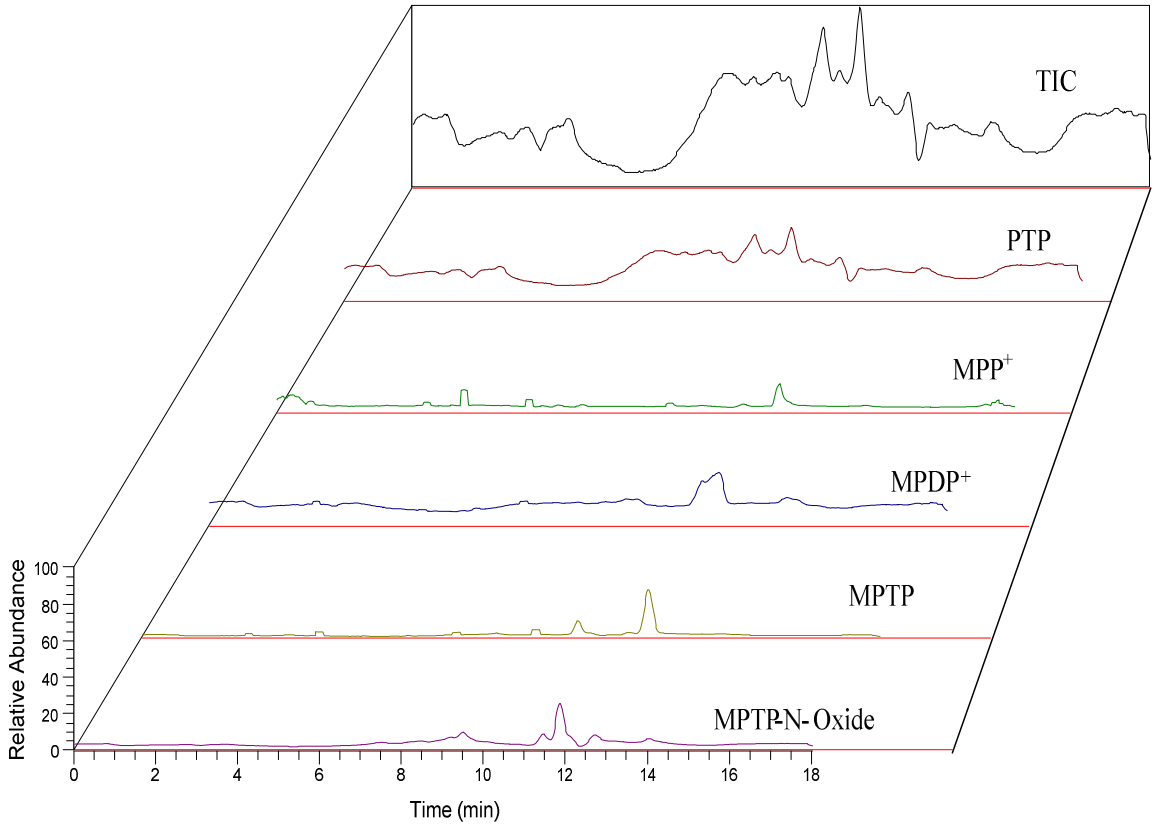

Figure 6- 8. Typical aCSF blank data (before probe implanted in rat brain).

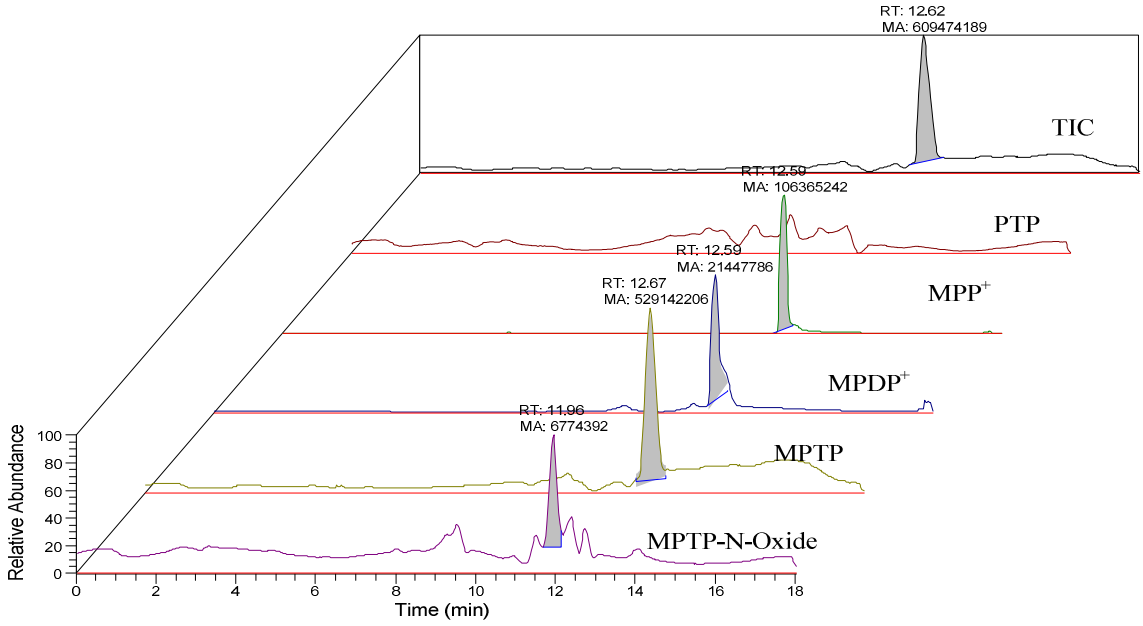

Figure 6- 9. Typical data from *in vivo* experiments: 100 min after MPTP perfusion was terminated.

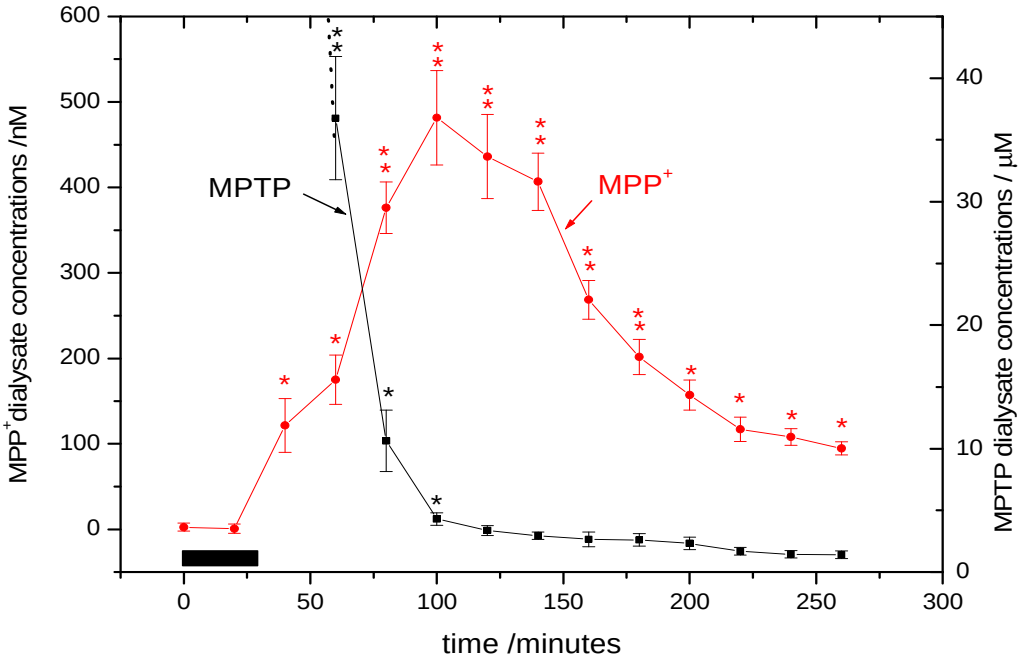

Figure 6- 10. Time-dependent effects of a 30-min perfusion of 10mM MPTP into rat striatum on microdialysate levels of MPTP and MPP^+. The horizontal black bar shows the time during which MPTP was perfused. Data are mean ± SEM (n = 3). * $p < 0.05$, ** $p < 0.01$.

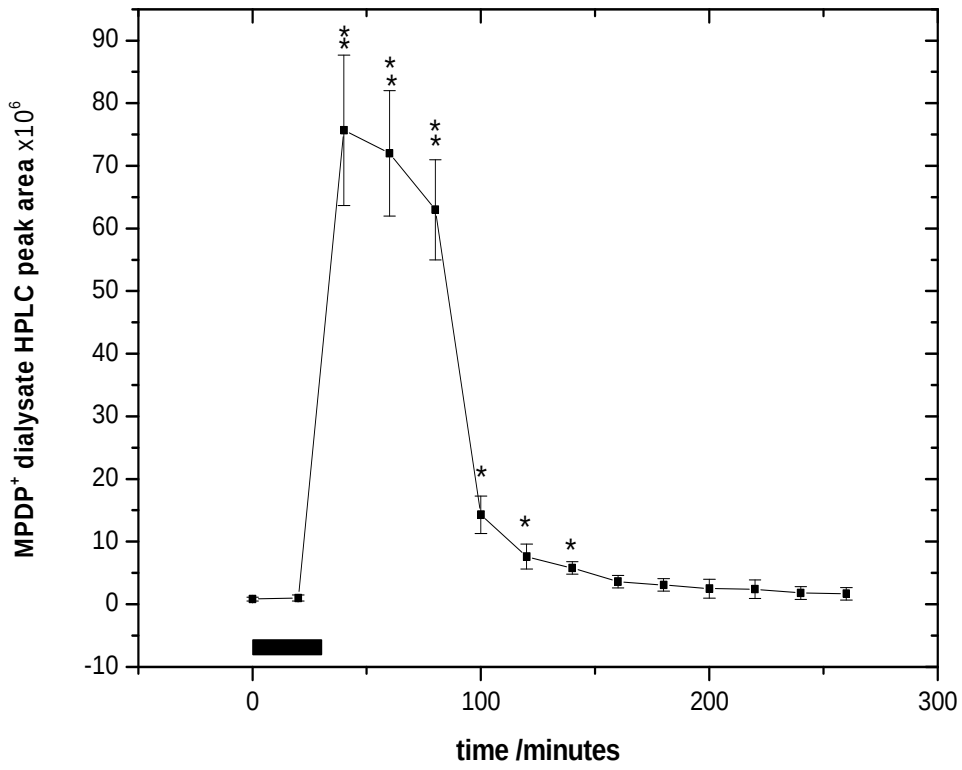

Figure 6- 11. Time-dependent effects of a 30-min perfusion of 10mM MPTP into rat striatum on microdialysate levels of putative $MPDP^+$. The horizontal black bar shows the time during which MPTP was perfused. Data are mean ± SEM (n = 3). * p < 0.05, ** p < 0.01.

In *in vivo* experiments, PTP chromatograms did not show any significant peaks throughout the experiment (data not shown). MPTP-N-Oxide chromatography peaks did not change significantly throughout the experiment. During 10 mM MPTP perfusion, extracellular concentrations of MPP^+ and MPDP remained very low. However, when MPTP perfusions were discontinued, extracellular MPP^+ and $MPDP^+$ increased significantly, $MPDP^+$ rapidly reaching a peak value at 60 min and remained at this peak value for about 40 min, then declined rapidly over the next 90 min. MPP^+ increased less rapidly than $MPDP^+$ by reaching the peak concentrations of 500 nM at 100 min, then slowly declined.

D. Conclusions

In this chapter, a highly specific and sensitive fully automated system combining microdialysis sampling, on-line derivatization, on-line IP-RP-SPE sample clean-up, IP-RP-HPLC separation, and tandem MS/MS detection techniques was applied to monitor MPTP and its metabolites in rat striatal microdialysates in response to perfusions of 10 mM MPTP. In order to monitor as many as possible metabolites, the MS SIM scan mode was employed. The fully automated system was extensively used for determination of calibration curves, *in vitro* microdialysis probe recovery, and for *in vivo* experiments. All these experiments showed this system to be a powerful tool for real-time, highly specific and sensitive monitoring of targeted metabolites in biological systems.

Chapter Seven

Determination of Arachidonic Acid Metabolites in Rat Striatal Microdialysates by HPLC-MS/MS Utilizing Electron Capture Atmospheric Pressure Chemical Ionization.

A. Introduction

Chronic inflammation is becoming increasingly recognized as an important participant in numerous neurodegenerative diseases including Alzheimer's[227-229] and Parkinson's diseases.[230,231] Among the participants in the inflammatory process, the eicosanoids have received substantial attention. Eicosanoids originate from the enzymatic oxidation of arachidonic acid (AA) to produce proinflammatory prostaglandins, leukotrienes, thromboxanes and alcohols (Figure 7-1).[232-237] Accurate measurement of trace amounts of AA metabolites in brain may be an important step in understanding a role for these eicosanoids in neurodegenerative brain disorders. This is a considerable analytical challenge because of their low abundances (concentrations range from picomolar to nanomolar) in very complex biological backgrounds, and their isomeric properties (enantiomer, regioisomer and stereoisomer). Traditional methods of analysis for eicosanoids have employed HPLC coupled with UV[238-241], fluorescence[242-244] or ESI-MS[245-247] detection, GC-MS[248-250] and radioimmunoassay.[251-253] These methods suffer from inadequate detection limits, time-consuming sample preparation, inability to differentiate isomers, sample instability and cross reactivity. Recently, HPLC-MS/MS with electron capture atmospheric pressure chemical ionization (ECAPCI) has been demonstrated to be a promising

approach to analyze eicosanoids.[254,255] In the present study a modified form of this method was employed to analyze several eicosanoids in rat brain striatal microdialysates. Three eicosanoids – prostaglandin E_2 (PGE_2), prostaglandin D_2 (PGD_2), and prostaglandin $F_{2\alpha}$ ($PGF_{2\alpha}$) were successfully detected in microdialysate samples and both PGE_2, and PGF_{2a} were measured quantitatively and routinely. The recent use of arachidonic acid-d8 (AA-d8) as an internal standard has greatly increased confidence in the quantification process. By this analytical method, the LOD for PGE_2 and $PGF_{2\alpha}$ has been determined to be 0.1 nM, which is close to the LOD with radioimmunoassay, which is one of the most sensitive methods for eicosanoids analysis nowadays.

The difference between regular APCI and ECAPCI is that the analytes in ECAPCI undergo derivatization to tag them with an electron-capturing group such as the pentafluorobenzyl moiety before analysis. The pentafluorobenzyl derivatives undergo dissociative electron capture in the gas phase to generate negative ions through the loss of pentafluorobenzyl radicals. ECAPCI can provide an increase in sensitivity of 2 orders of magnitude when compared to regular APCI.[255] Figure 7-2 illustrates the whole ECAPCI scheme, where PGE_2 is the model compound.

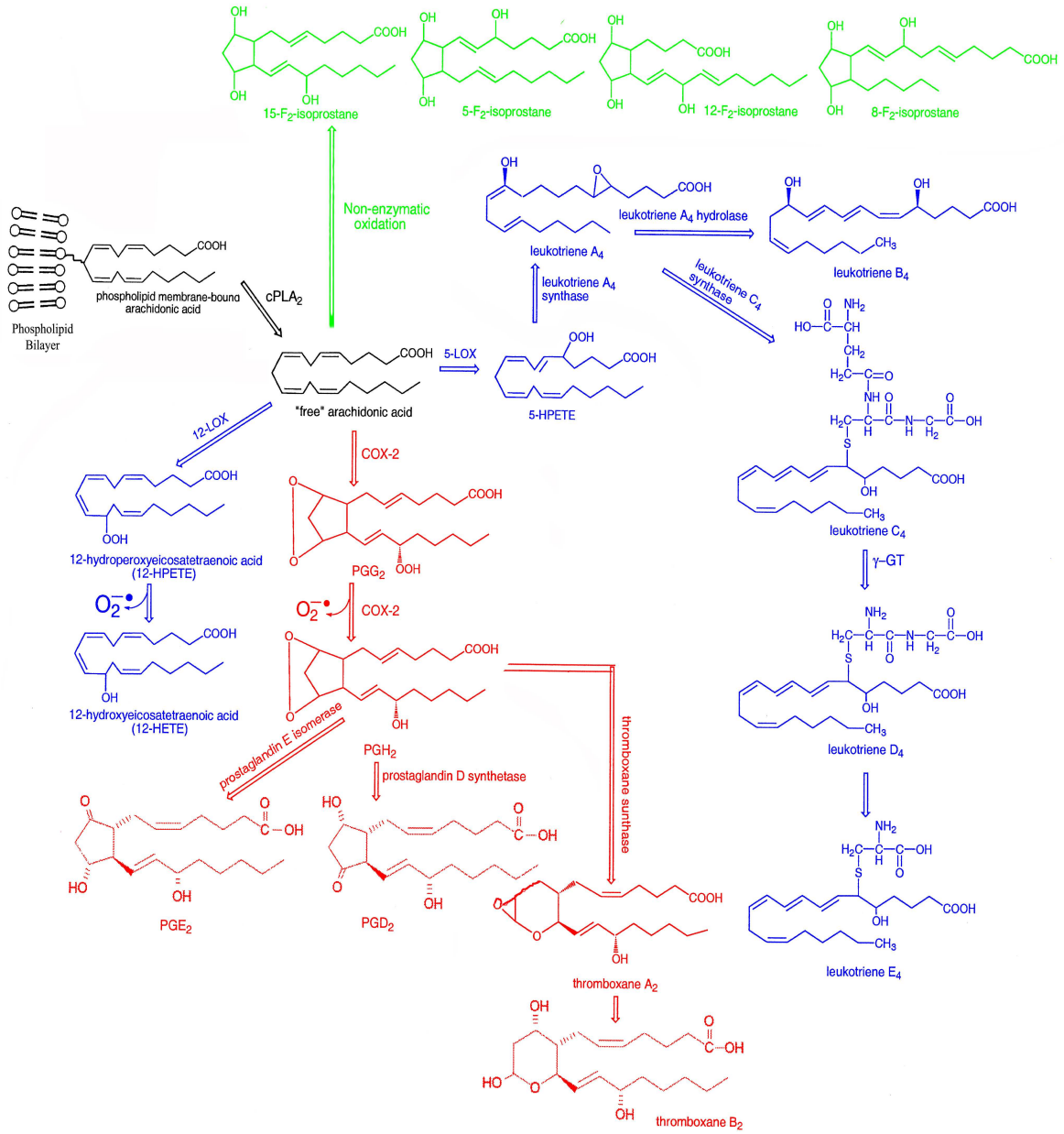

Figure 7- 1. Eicosanoid cascade and biological pathways: Cyclooxygenase pathway (red), lipoxygenase pathway (blue) and non-enzymatic pathway (green).

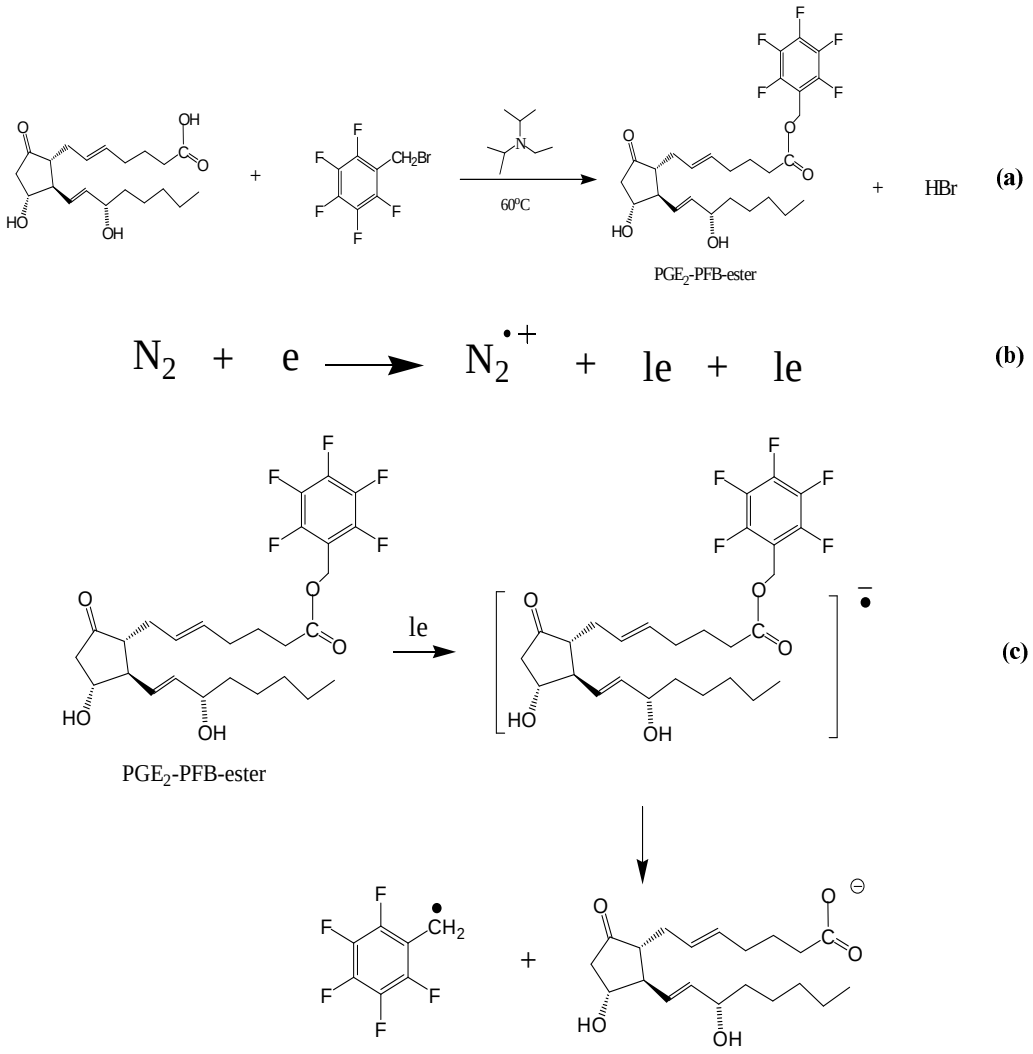

Figure 7- 2. Mechanism for ECAPCI analysis of PGE_2. (a) Esterfication reaction, introducing an electron capture tag (PFB moiety). (b) The production of low energy electron. (c) Electron capture dissociation.

B. Experimental

1. Reagents and Chemicals.

Most chemicals used were the same as in Chapters Two and Three. AA, deuterated AA (AA-d_8), PGE_2, PGD_2, and $PGF_{2\alpha}$ were purchased from Cayman Chemical, Inc. (Ann Arbor, MI). Butyl hydroxytoluene (BHT), diethyl ether, pentafluorobenzyl bromide (PFB) and diisopropylethylamine (DIPE) were obtained from Sigma-Aldrich. PFB was diluted in toluene (1 : 19; v/v). DIPE was also diluted in toluene (1 : 9; v/v). HPLC grade toluene, hexanes and isopropanol were purchased from Fisher Scientific.

2. Stock and Standard Solutions.

AA was provided as 100 μg/μL in ethanol solution. 10 μL of this solution was diluted in 990 μL of deoxygenated (He sparging) ethanol to obtain a 1 μg/μL solution. 100 μL of the latter solution was added to 900 μL deoxygenated ethanol to obtain a 100 ng/μL (~330 μM) solution which was stored below -20^{o}C.

PGE_2 and PGD_2 were provided as 1 mg solid samples contained in small glass vials with an open top septum cap. One mL of deoxygenated ethanol was added to each vial by syringe through the septum. The resulting solutions were shaken for several minutes to dissolve the solids to give a concentration of 1 μg/μL. 100 μL of such solutions was added to 900 μL of deoxygenated ethanol to obtain 100 ng/μL (~280 μM) solutions which were stored in a freezer at below -20^{o}C.

PGF_{2a} was provided as a100 ng/μL ethanol solution and stored below -20^{o}C.

100 μL of each of the above four 100 ng/μL solutions was added to 600 μL of deoxygenated ethanol to obtain the standard mixture solution which had a concentration of 10 ng/μL for each of the

analytes. This solution was stored at -20^{o}C or lower until needed.

AA-d_8 was provided as a100 ng/μL solution in ethanol. 10 μL of this solution was diluted in 990 μL of deoxygenated ethanol to obtain a 1 ng/μL solution. 20 μL of this solution was added to 980 μL of deoxygenated ethanol to obtain a 20 pg/μL solution which was stored at -20^{o}C or lower.

3. Equipment and Chromatographic Conditions

HPLC-APCI-MS/MS was performed with a Thermo Finnigan TSQ 7000 equipped with a Thermal Finnigan Surveyor® MS pump. A Thermo Hypersil® Silica (250 × 4.6 mm, 5 μm) normal-phase HPLC column from Thermo-Hypersil-Keystone (Bellefonte, PA) was used for all separations. The mobile phase was isocratic hexanes (90%, v/v) / isopropanol (10%, v/v), with flow rate at 1.2 mL/min. MS Conditions: APCI source in negative mode; vaporizer temperature, 450^{o}C; corona discharge needle, 10 μA; sheath and auxiliary gas pressures were 40 psi and 10 (arbitrary units), respectively. SRM with transitions of 351.2→ 271.2 (PGD_2/E_2), 353.2→309.2 ($PGF_{2\alpha}$), 303.3→259.3(AA) and 311.3→267.3 (AA-d_8) were monitored. Other conditions were the same as described in Chapter Two.

4. Sample Extraction and Derivatization.

Immediately after each microdialysate fraction was collected, 5 μL of the internal standard (AA-d_8, 20 pg/μL) was added and the microdialysate was extracted twice with 150 μL of diethyl ether. The organic extracts were combined and dried with a SpeedVAc (Thermo Savant®, Holbrook, NY).

Then, 100 µL of PFB (in toluene solution) and 100 µL of DIPE (in toluene solution) were added to each vial and the resulting solution placed in a heating block at 60 ^{o}C for 1 h. The product was allowed to cool and then evaporated to dryness on a SpeedVac at room temperature. Reconstitution was performed by added 100 µL MeOH to each vial. The resulting solutions were then ready for HPLC-ECAPCI-MS/MS analysis.

5. Selected Reaction Monitoring (SRM) Optimization.

SRM optimization was carried out in the same way as described in Chapter Four, except that 1 ng/µL of individual standard solutions were injected.

6. Calibration Curves

The mixture standard solution (10 ng/µL) was further diluted with deoxygenated ethanol and calculated amounts were spiked into 1mL of deoxygenated aCSF containing HCl (0.1 mM final concentration) and BHT (0.025 µg/µL final concentration). Standard curves were prepared for each analyte of interest over the concentration range 0.2 pg/µL to 1 ng/µL (*ca.* 0.6 nM to 3.0 µM). The sample treatment for calibration standards was the same as for microdialysate samples, *i.e.*, 105 µL standard mixture solution was spiked with 5 µL internal standard (AA-d_8, 20pg / µL), extracted and derivatized the same way as previously described. The calibration curve was plotted using the ratio of analyte peak area to that of the internal standard, AA-d_8.

7. Animals and Surgical Procedures

Animals and surgical procedures were the same as in Chapter Four.

8. *In Vivo* Microdialysis Sample Collection.

On the day of the experiment, the guide cannula was removed and replaced with a CMA 12® microdialysis probe with the tip 7.4 mm below dura. The probes were perfused with deoxygenated aCSF at 1.5 µL/min. Microdialysate was collected in a CMA 170® refrigerated fraction collector at 70 min intervals. Each vial initially contained 1.0 M HCl (1/10 final volume of microdialysate) and 1.0 µg/uL BHT (2.5% final volume) to insure eicosanoid stability. For each *in vivo* experiment a reagent blank was prepared. Thus, 105 µL aCSF was treated by the exact same procedure used with microdialysate samples.

9. Calculations and Statistics

Data calculations and statistics was the same as described in Chapter Four.

C. Results and Discussion

1. CID Optimization for AA, PGE_2, PGD_2, and $PGF_{2\alpha}$.

Daughter ion information and CID optimization were achieved by CID energy-step-increase experiments. The data processing technique for CID breakdown curve establishment was described in Chapter Four.

Figures 7-2 to 7-9 present spectra and CID breakdown curves for all four analytes. The optimized SRM conditions are summarized in Table 7-1.

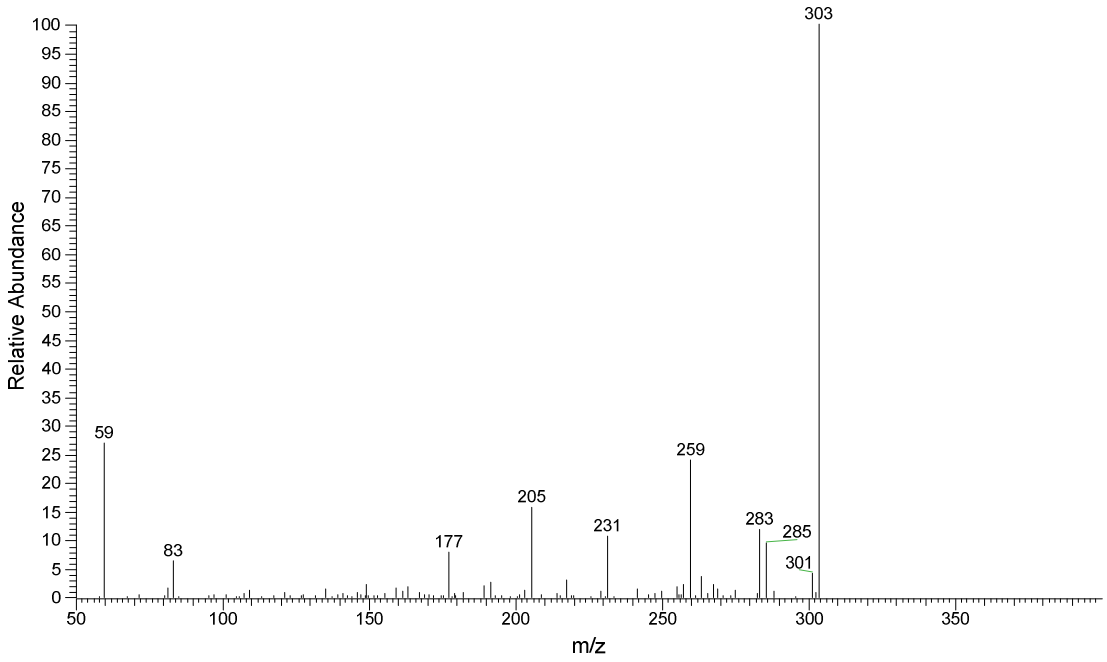

Figure 7- 3. MS/MS spectrum for AA

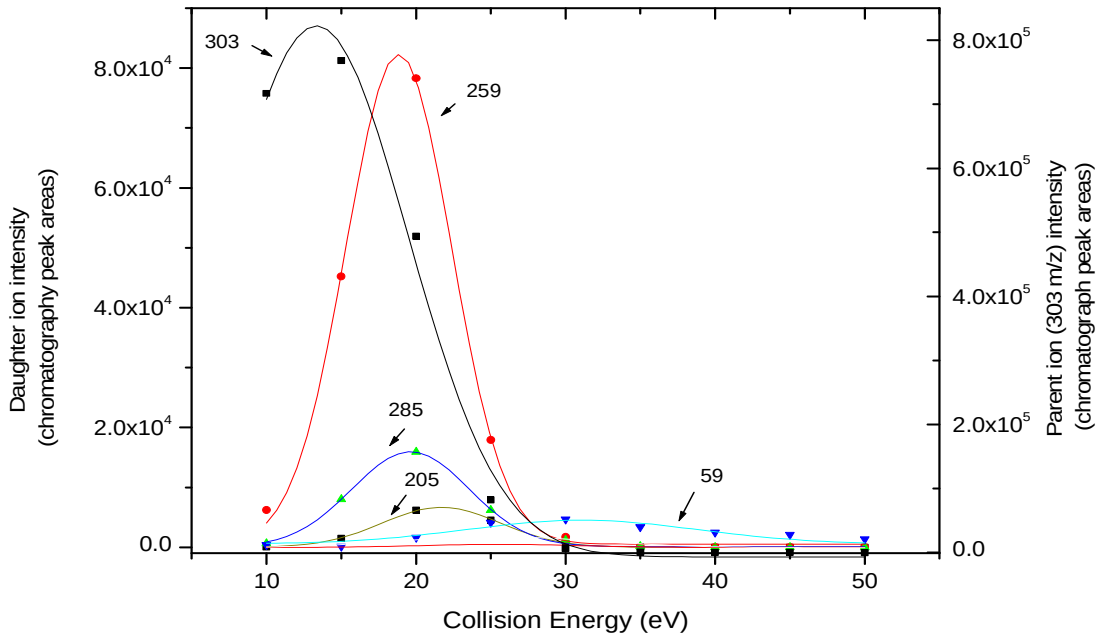

Figure 7- 4. CID breakdown curves for AA

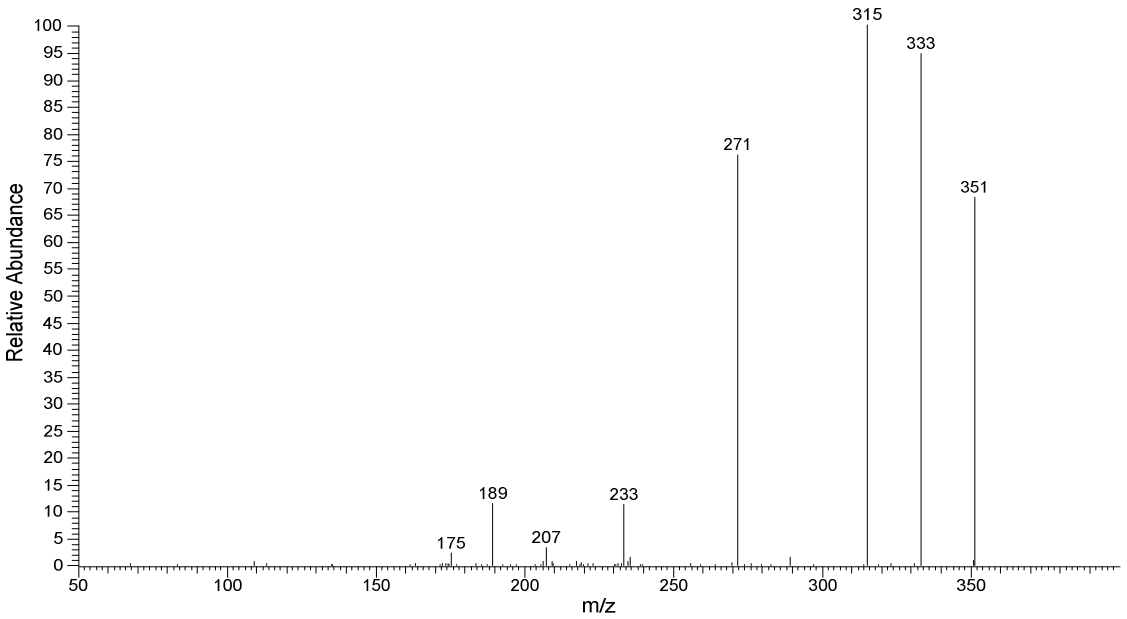

Figure 7- 5. MS/MS spectrum for PGE_2.

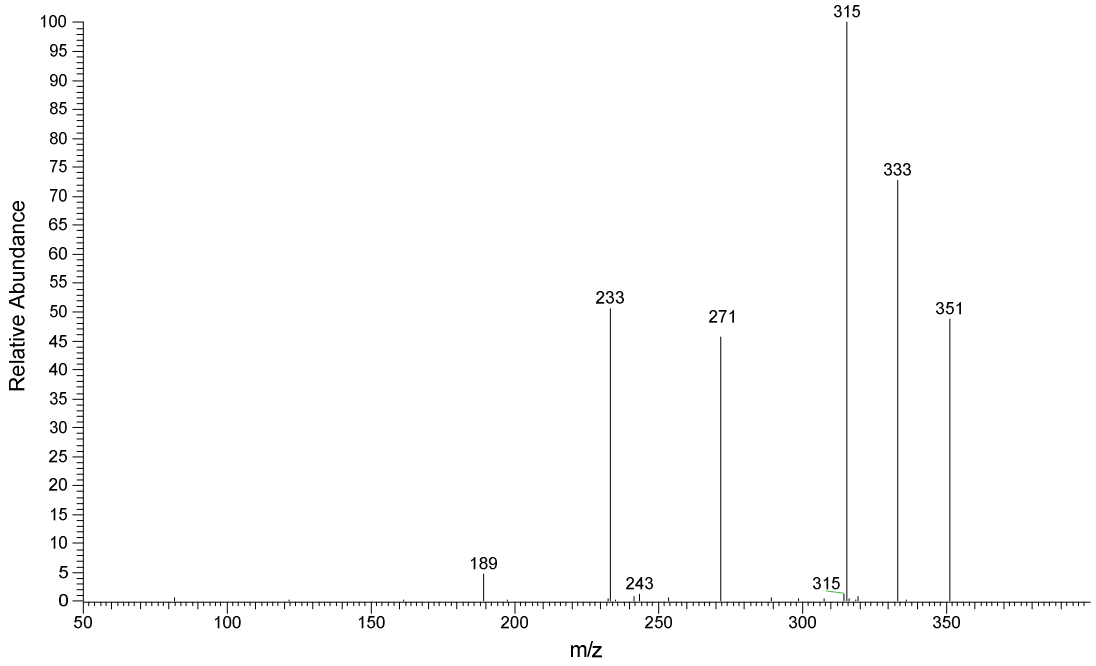

Figure 7- 6. MS/MS spectrum for PGD_2.

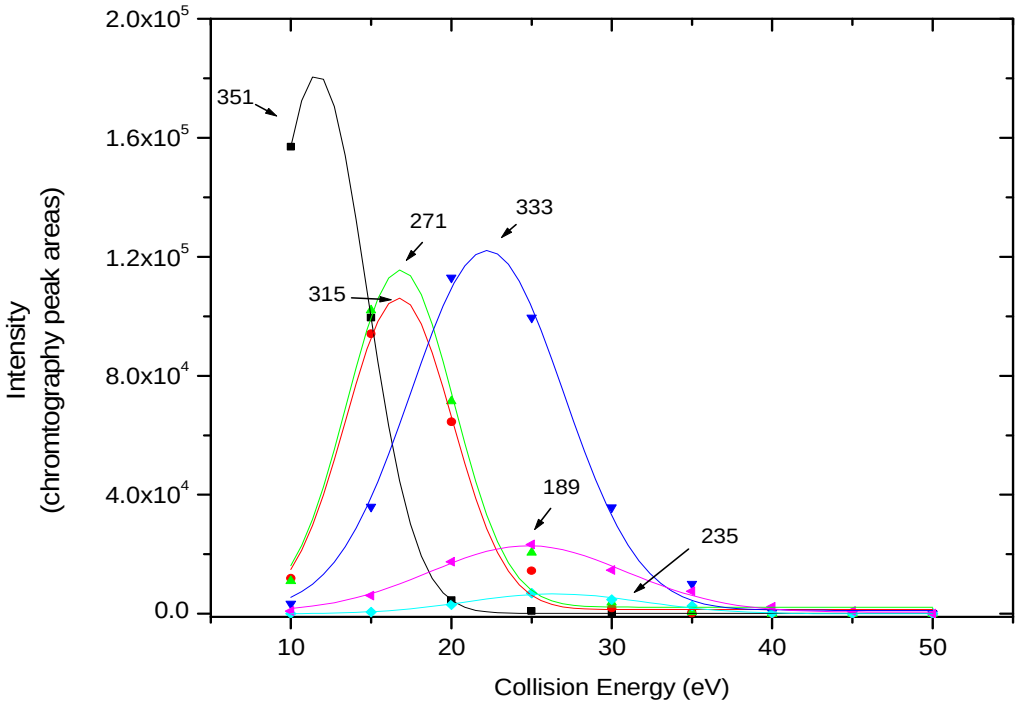

Figure 7- 7. CID breakdown curves for PGE_2/PGD_2

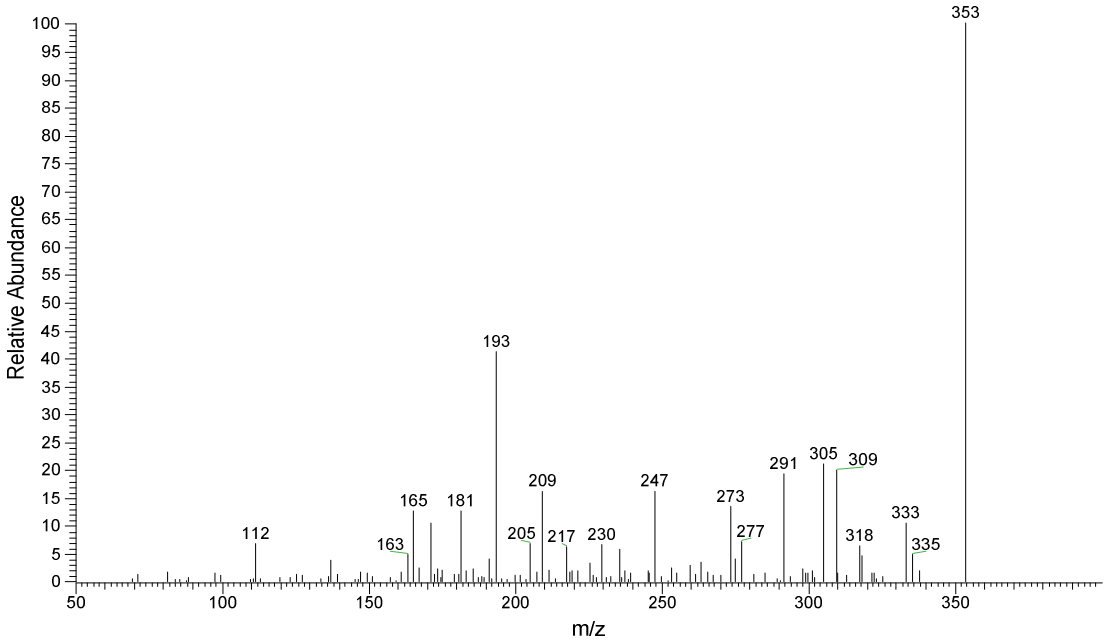

Figure 7- 8. MS/MS spectrum for $PGF_{2\alpha}$.

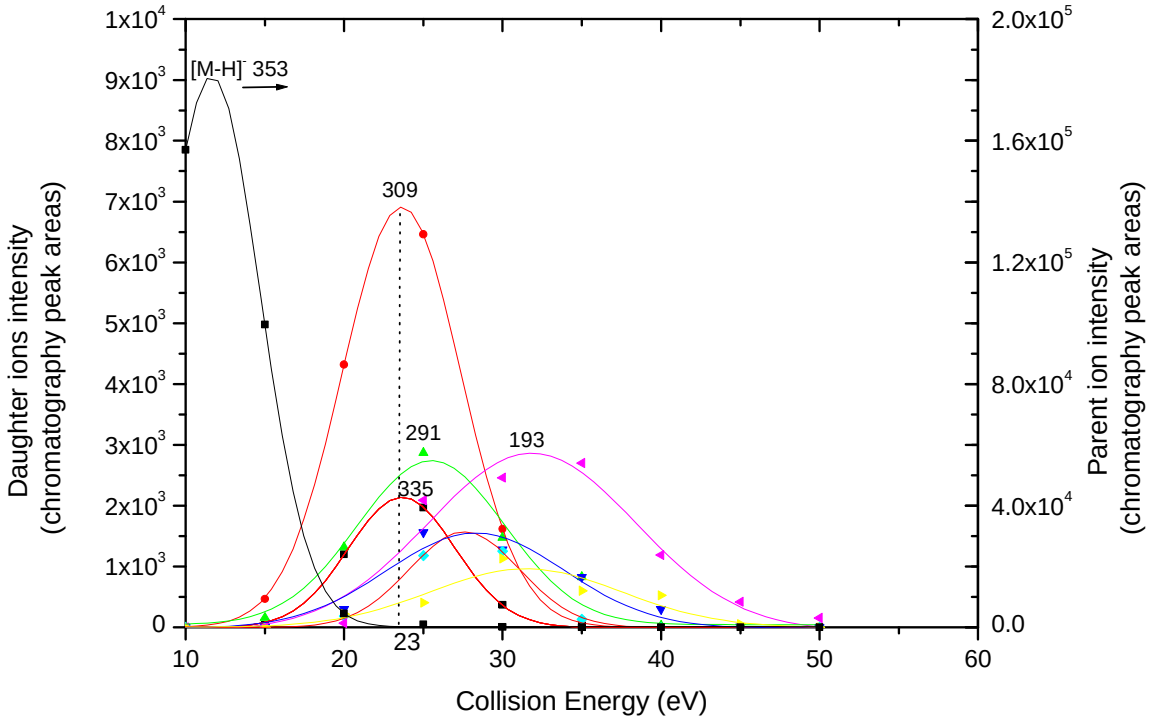

Figure 7- 9. CID breakdown curve for $PGF_{2\alpha}$.

Substance	SRM optimized conditions
AA	303 → 259 @ 18 eV
PGE_2	351 →271 @ 16 eV
PGD_2	351 →271 @ 16 eV
$PGF_{2\alpha}$	353 →309 @ 23 eV

Table 7- 1. SRM optimized conditions.

PGE_2, PGD_2 are enantiomers and therefore are not distinguishable by MS analysis *i.e.*, they both have the same parent ion and daughter ion patterns. However, they could be separated by normal phase HPLC chromatography utilized in this project. As shown in Figure 7-10.

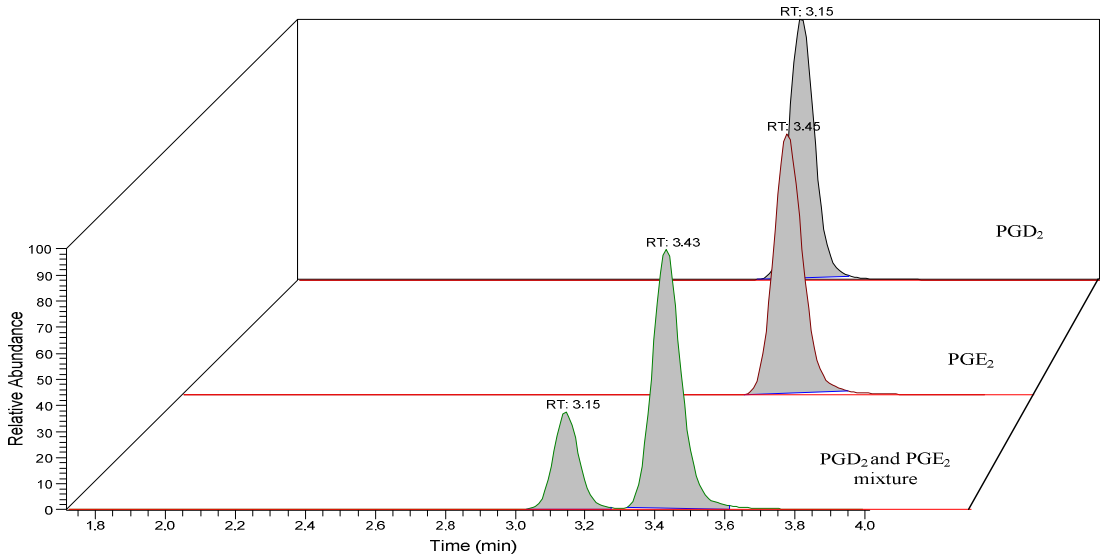

Figure 7- 10. Chromatograms for PGE_2/PGD_2 standards.

Figure 7-10 shows the results of three experiments: PGD_2 standard, PGE_2 standard , and PGE_2/PGD_2 mixture (both at the same concentration). For every experiment, reaction 351 →271 @ 16 eV was monitored. The retention time for PGD_2 was 3.15 min and for PGE_2 was 3.45 min and, therefore, a baseline separation was achieved.

2. Standard Curves and Sensitivity (Limits of Detection).

Analyte	Equation	Correlation coefficient	Liner range (nM)	LOD (nM)
AA	y = –1.905 + 1.124 · x	0.9998	0.6–1500	0.1
PGE_2	y = –0.167 + 0.833 · x	0.9990	0.6–1500	0.1
PGD_2	y = –0.710 + 0.908 · x	0.9997	1.2–1500	0.5
$PGF_{2\alpha}$	y = –0.577 + 1.882 · x	0.9998	1.2–2000	0.2

Table 7- 2. Calibration parameters, limit of detection (LOD) and linear dynamic range for all analytes

3. *In Vivo* Experiments.

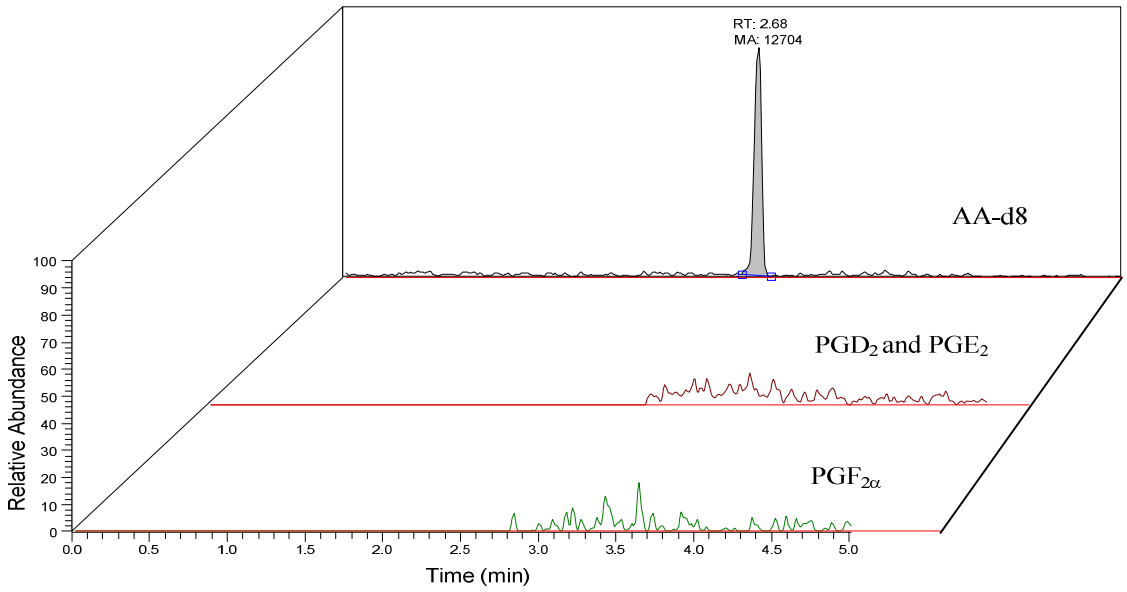

Figure 7- 11. Typical data of reagent blank, AA-d8 was internal standard.

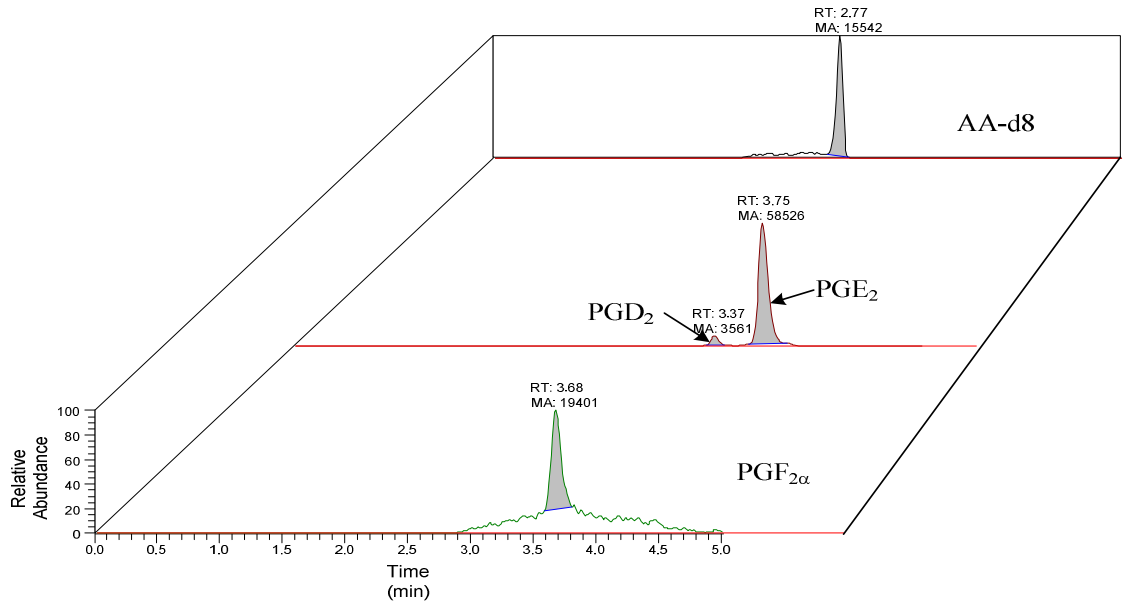

Figure 7- 12. Typical data from *in vivo* experiments: insertion of the microdialysis probe evoked a rise in extracellular (microdialysate) PGE_2, PGD_2, and $PGF_{2\alpha}$ levels.

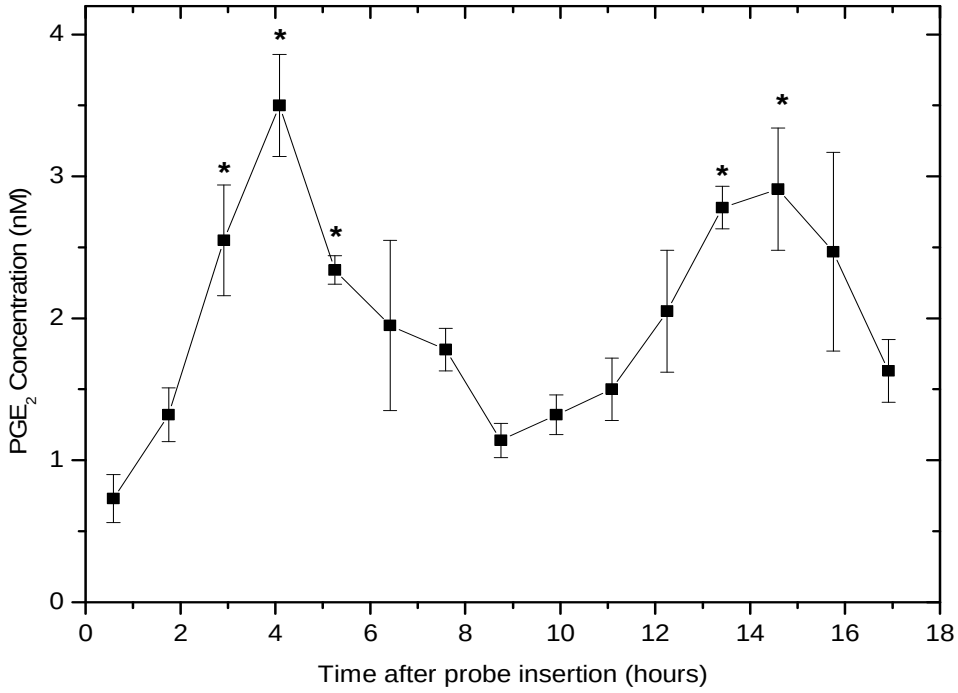

Figure 7- 13. Time-dependent effects of microdialysis probe insertion into rat striatum on microdialysate levels of PGE_2. Data are mean ± SEM (n = 3). * p < 0.05.

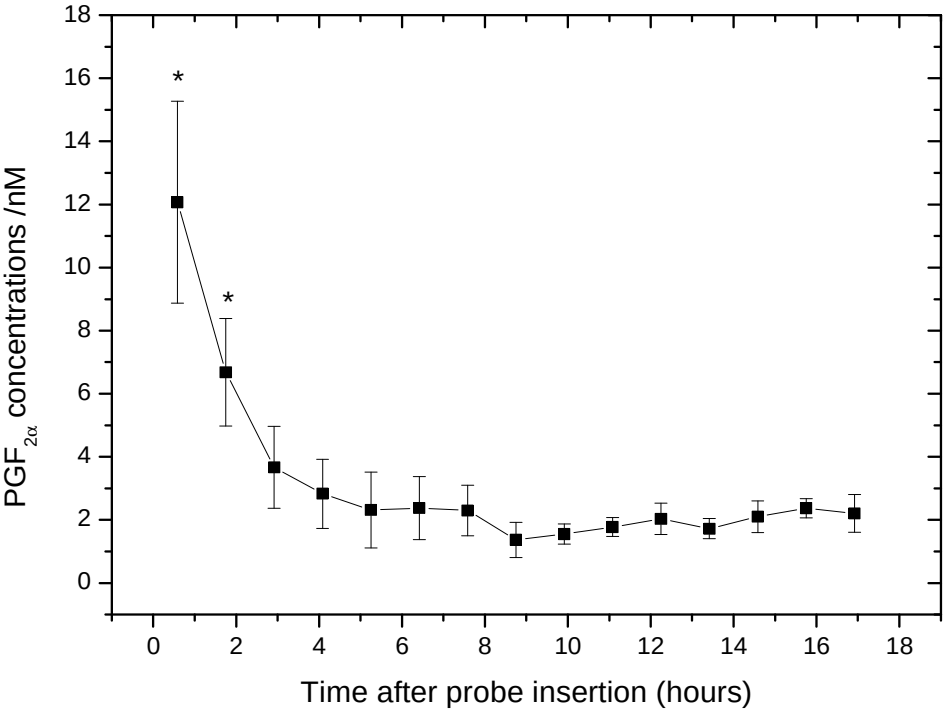

Figure 7- 14. Time-dependent effects of microdialysis probe insertion into rat striatum on microdialysate levels of $PGF_{2\alpha}$. Data are mean ± SEM (n = 3). * p < 0.05.

PGD_2 was detected only in the first sample after probe insertion. The concentration of PGD_2 measured was 1.2 ± 0.3 nM (mean ± S.E.M., n=3). The insertion of the microdialysis probe caused $PGF_{2\alpha}$ to significantly increase immediately. Subsequently, it slowly decreased to basal level in 2h. The probe insertion also caused PGE_2 levels to increase. However, this increase was much slower than for $PGF_{2\alpha}$ and required 4 h to reach the peak value of 3.5 nM PGE_2. PGE_2 then slowly declined to basal level (9-h). Interestingly, extracellular concentrations of PGE_2 increased again showing a second peak value of 3 nM after approximately 15 h after which it declined slowly back to basal level

It has previously been reported that insertion of the microdialysis probe evokes a rise in extracellular levels of ecosanoids.[256,257] However, such studies did not employ HPLC-MS.

D. Conclusions

A highly sensitivity and specific HPLC-ECAPCI-MS/MS method has been developed and applied to the analysis of basal levels of several eicosanoids in rat striatal microdialystates. However, this analytical method was impaired by its low sample throughput and time-consuming sample preparation. Nonetheless, as an instrumental analysis technique, HPLC-ECAPCI-MS/MS proved to be capable of *in vivo* monitoring metabolites in very low abundance.

Chapter Eight

Summary and Future Directions

"If you cannot see it, it doesn't exist!" – an unidentified scientist.

This dissertation research was dedicated (except Chapter 7) in developing an automated HPLC-MS method to monitor a number of important neurochemicals (metabolites) in rat brain striatum which might be of relevance to an understanding of the parthenogenesis of PD. Table 8-1 summarizes all the compounds targeted in this dissertation research.

Analyte	LOD	Basal dialysate levels ± SEM (n=3)	Maximum dialysate levels* ± SEM (n=3)
DA	0.5 nM	6.4 ± 0.7 nM	1.4 ± 0.6 μM
EPI	0.5 nM	/	/
NE	1.0 nM	0.8 ±0.2 nM	13.3 ± 3.0 nM
5-HT	0.5 nM	4.3 ± 2.1 nM	77.2 ± 22.5 nM
3-MT	1.0 nM	3.5 ± 0.4 nM	217.0 ± 37.3 nM
GSH	0.1 μM	0.6 ± 0.1 μM	3.7 ± 0.4 μM
CySH	1.0 μM	6.2 ± 0.4 μM	67.2 ± 3.5 μM
MPTP	1.0 nM	/	36.8 ± 5.0 μM
MPP^+	0.5 nM	/	482.4 ± 55.6 nM
$MPDP^+$	/	/	76 ± 12**
AA	0.1 nM	/	/
PGE_2	0.1 nM	0.7 ± 0.2 nM	3.5 ± 0.4 nM
PGD_2	0.5 nM	/	1.2 ± 0.3 nM
$PGF_{2\alpha}$	0.2 nM	2.0 ± 0.2 nM	12.0 ± 2.5 nM

Table 8- 1. Targeted analytes and their detection limits.

***The maximum level was caused by probe insertion for AA, PGE_2, PGD_2 and $PGF_{2\alpha}$; for other analytes it was caused by drug perfusion. **chromatograph peak area /10^6**

In experiments, selected reactions monitoring (SRM) was applied to all analytes except MPTP, MPP^+ $MPDP^+$, where selected ion monitoring (SIM) was applied. AA, PGE_2, PGD_2 and $PGF_{2\alpha}$ analysis were not performed by the fully automated system.

Before employing MS-based techniques, routine detection techniques employed in this field were electrochemical or UV-vis, which were also the major analytical methods employed in our lab. For these techniques, people have to "guess" from the LC chromatography data – what did the chromatography peak represent? If it has a similar retention time to the standard, then…it might be the same compound. In HPLC-MS, MS and MS/MS spectra data enable us to "see" the analyte. If the data displays the same molecular mass, the same fragmentation pattern (daughter ions) and the same retention time as the standard, it most likely is the same compound as the standard.

The fully automated system developed in the research and described in the dissertation is an essential tool for both method development and *in vivo* measurements.

Thus, analyte calibration, SPE breakthrough curves, pre-column derivatization (if necessary), *in vitro* experiments (microdialysis probe recovery studies) and *in vivo* experiments were all carried out in a largely labor-free, precise, expeditious and fully automated way. Figure 8-1 describes all experiments required to fulfill a project. The green blocks in the graph represent the experimental procedures that can be approached by the fully automated system.

Typically, all required experiments, including *in vivo* experiments employing multiple ($n \geq 3$) animals would only take 2-3 weeks to accomplish.

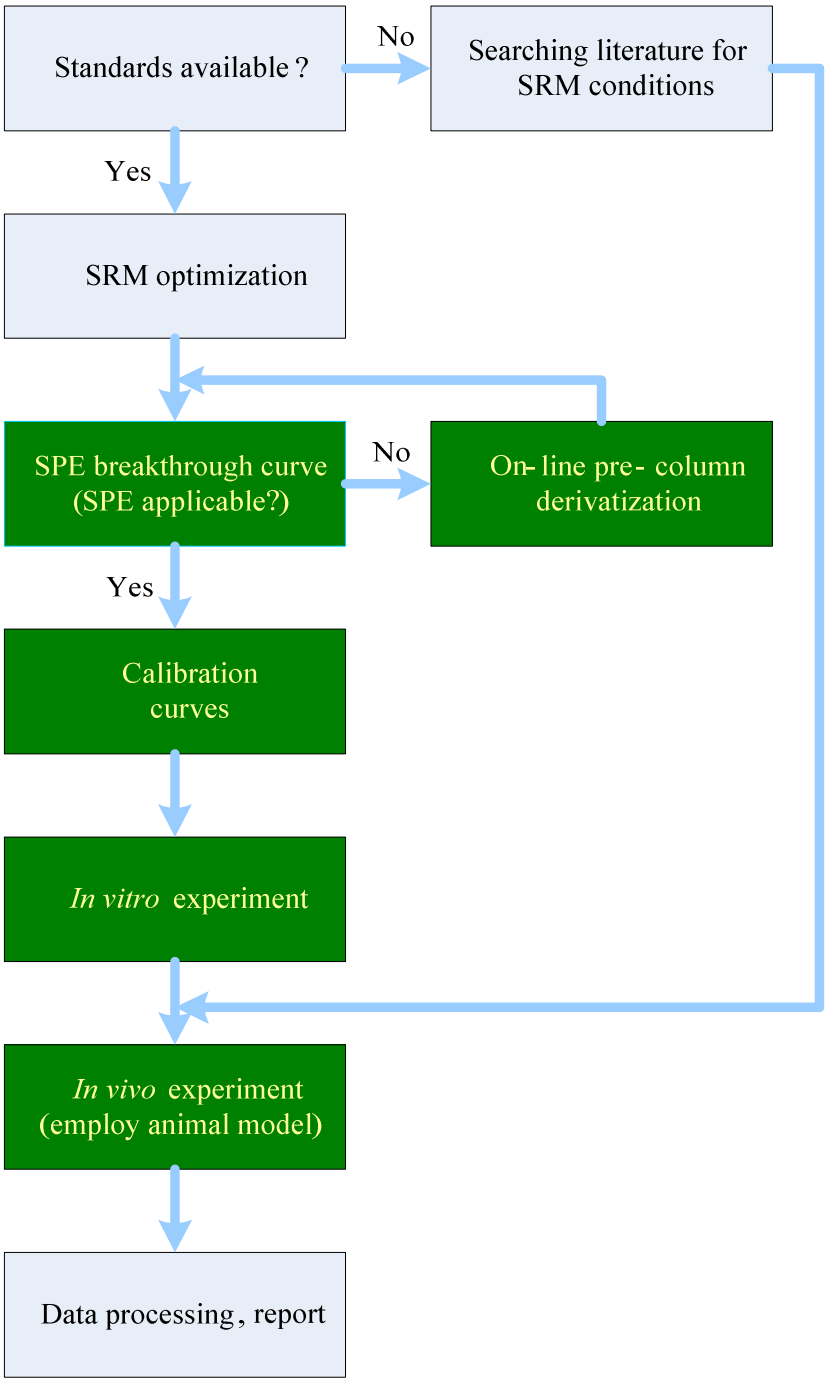

Figure 8- 1. General procedures for an *in vivo* project utilizing the fully automated system.

The future directions of HPLC-MS techniques in PD studies is hard to predict for a number of reasons: 1) the application of HPLC-MS in this area has just started and still in its infancy; 2)

HPLC-MS technology is growing extremely rapidly; and, 3) The establishment of human metabolome, which doesn't have a clear time schedule yet, could have profound impact on HPLC-MS applications in this field.

Currently, the main obstacles for MS-based applications are the complexity and expense of mass spectrometers; the difficulties associated with their use; and the lower reliability of mass spectrometers compared to other analytical instruments, such as chromatographs. The next generation of mass spectrometers are focused on solving these problems.[258-260] In addition, they will have unprecedented sensitivity, resolution and dynamic range – thanks for the exponential development of electronic technology and the urgent demand of life science.

Literature Cited

1. White, R.; Caskey, C. T., The human as an experimental system in molecular genetics. *Science* **1988,** 240, (4858), 1483-8.

2. Williams, M., Systems and integrative biology as alternative guises for pharmacology: prime time for an iPharm concept? *Biochem Pharmacol* **2005,** 70, (12), 1707-16.

3. Wood-Kaczmar, A.; Gandhi, S.; Wood, N. W., Understanding the molecular causes of Parkinson's disease. *Trends Mol Med* **2006,** 12, (11), 521-8.

4. Parkinson, J., An essay on the shaking palsy. 1817. *J Neuropsychiatry Clin Neurosci* **2002,** 14, (2), 223-36; discussion 222.

5. Samii, A.; Nutt, J. G.; Ransom, B. R., Parkinson's disease. *Lancet* **2004,** 363, (9423), 1783-93.

6. Carlsson, A., Thirty years of dopamine research. *Adv Neurol* **1993,** 60, 1-10.

7. Carlsson, A., Treatment of Parkinson's with L-DOPA. The early discovery phase, and a comment on current problems. *J Neural Transm* **2002,** 109, (5-6), 777-87.

8. Molloy, S. A.; Rowan, E. N.; O'Brien, J. T.; McKeith, I. G.; Wesnes, K.; Burn, D. J., Effect of levodopa on cognitive function in Parkinson's disease with and without dementia and dementia with Lewy bodies. *J Neurol Neurosurg Psychiatry* **2006,** 77, (12), 1323-8.

9. Bennett, J. P., Free radicals, oxidative stress and the origin of Parkinson's disease. *J Neurol Sci* **1999,** 170, (2), 75-6.

10. Broussolle, E.; Thobois, S., [Genetic and environmental factors of Parkinson's disease]. *Rev Neurol (Paris)* **2002,** 158, (122), 11-23.

11. Fong, C. S.; Wu, R. M.; Shieh, J. C.; Chao, Y. T.; Fu, Y. P.; Kuao, C. L.; Cheng, C. W., Pesticide exposure on southwestern Taiwanese with MnSOD and NQO1 polymorphisms is associated with increased risk of Parkinson's disease. *Clin Chim Acta* **2007,** 378, (1-2), 136-41.

12. Groen, J. L.; Kawarai, T.; Toulina, A.; Rivoiro, C.; Salehi-Rad, S.; Sato, C.; Morgan, A.;

Liang, Y.; Postuma, R. B.; St George-Hyslop, P.; Lang, A. E.; Rogaeva, E., Genetic association study of PINK1 coding polymorphisms in Parkinson's disease. *Neurosci Lett* **2004,** 372, (3), 226-9.

13. Lavedan, C.; Buchholtz, S.; Nussbaum, R. L.; Albin, R. L.; Polymeropoulos, M. H., A mutation in the human neurofilament M gene in Parkinson's disease that suggests a role for the cytoskeleton in neuronal degeneration. *Neurosci Lett* **2002,** 322, (1), 57-61.

14. Nicholl, D. J.; Bennett, P.; Hiller, L.; Bonifati, V.; Vanacore, N.; Fabbrini, G.; Marconi, R.; Colosimo, C.; Lamberti, P.; Stocchi, F.; Bonuccelli, U.; Vieregge, P.; Ramsden, D. B.; Meco, G.; Williams, A. C., A study of five candidate genes in Parkinson's disease and related neurodegenerative disorders. European Study Group on Atypical Parkinsonism. *Neurology* **1999,** 53, (7), 1415-21.

15. Polymeropoulos, M. H.; Lavedan, C.; Leroy, E.; Ide, S. E.; Dehejia, A.; Dutra, A.; Pike, B.; Root, H.; Rubenstein, J.; Boyer, R.; Stenroos, E. S.; Chandrasekharappa, S.; Athanassiadou, A.; Papapetropoulos, T.; Johnson, W. G.; Lazzarini, A. M.; Duvoisin, R. C.; Di Iorio, G.; Golbe, L. I.; Nussbaum, R. L., Mutation in the alpha-synuclein gene identified in families with Parkinson's disease. *Science* **1997,** 276, (5321), 2045-7.

16. Warner, T. T.; Schapira, A. H., The role of the alpha-synuclein gene mutation in patients with sporadic Parkinson's disease in the United Kingdom. *J Neurol Neurosurg Psychiatry* **1998,** 65, (3), 378-9.

17. Sian, J.; Gerlach, M.; Youdim, M. B.; Riederer, P., Parkinson's disease: a major hypokinetic basal ganglia disorder. *J Neural Transm* **1999,** 106, (5-6), 443-76.

18. Kish, S. J.; Shannak, K.; Hornykiewicz, O., Uneven pattern of dopamine loss in the striatum of patients with idiopathic Parkinson's disease. Pathophysiologic and clinical implications. *N Engl J Med* **1988,** 318, (14), 876-80.

19. Gerlach, M.; Riederer, P., Animal models of Parkinson's disease: an empirical comparison with the phenomenology of the disease in man. *J Neural Transm* **1996,** 103, (8-9), 987-1041.

20. Kelly, P. J.; Gillingham, F. J., The long-term results of stereotaxic surgery and L-dopa therapy in patients with Parkinson's disease. A 10-year follow-up study. *J Neurosurg* **1980,** 53, (3), 332-7.

21. Obeso, J. A.; Rodriguez-Oroz, M. C.; Rodriguez, M.; Macias, R.; Alvarez, L.; Guridi, J.; Vitek, J.; DeLong, M. R., Pathophysiologic basis of surgery for Parkinson's disease.

Neurology **2000,** 55, (12 Suppl 6), S7-12.

22. Defer, G. L.; Geny, C.; Ricolfi, F.; Fenelon, G.; Monfort, J. C.; Remy, P.; Villafane, G.; Jeny, R.; Samson, Y.; Keravel, Y.; Gaston, A.; Degos, J. D.; Peschanski, M.; Cesaro, P.; Nguyen, J. P., Long-term outcome of unilaterally transplanted parkinsonian patients. I. Clinical approach. *Brain* **1996,** 119 (Pt 1), 41-50.

23. Levy, Y. S.; Stroomza, M.; Melamed, E.; Offen, D., Embryonic and adult stem cells as a source for cell therapy in Parkinson's disease. *J Mol Neurosci* **2004,** 24, (3), 353-86.

24. Minguez-Castellanos, A.; Escamilla-Sevilla, F., [Cell therapy and other neuroregenerative strategies in Parkinson's disease (II)]. *Rev Neurol* **2005,** 41, (11), 684-93.

25. Martin, W. R.; Perlmutter, J. S., Assessment of fetal tissue transplantation in Parkinson's disease: does PET play a role? *Neurology* **1994,** 44, (10), 1777-80.

26. Ito, Y.; Fujita, M.; Shimada, S.; Watanabe, Y.; Okada, T.; Kusuoka, H.; Tohyama, M.; Nishimura, T., Comparison between the decrease of dopamine transporter and that of L-DOPA uptake for detection of early to advanced stage of Parkinson's disease in animal models. *Synapse* **1999,** 31, (3), 178-85.

27. Langston, J. W.; Ballard, P.; Tetrud, J. W.; Irwin, I., Chronic Parkinsonism in humans due to a product of meperidine-analog synthesis. *Science* **1983,** 219, (4587), 979-80.

28. Gerlach, M.; Riederer, P.; Przuntek, H.; Youdim, M. B., MPTP mechanisms of neurotoxicity and their implications for Parkinson's disease. *Eur J Pharmacol* **1991,** 208, (4), 273-86.

29. Tipton, K. F.; Singer, T. P., Advances in our understanding of the mechanisms of the neurotoxicity of MPTP and related compounds. *J Neurochem* **1993,** 61, (4), 1191-206.

30. Riachi, N. J.; Behmand, R. A.; Harik, S. I., Correlation of MPTP neurotoxicity in vivo with oxidation of MPTP by the brain and blood-brain barrier in vitro in five rat strains. *Brain Res* **1991,** 555, (1), 19-24.

31. Melamed, E.; Youdim, M. B.; Rosenthal, J.; Spanier, I.; Uzzan, A.; Globus, M., In vivo effect of MPTP on monoamine oxidase activity in mouse striatum. *Brain Res* **1985,** 359, (1-2), 360-3.

32. Giovanni, A.; Sieber, B. A.; Heikkila, R. E.; Sonsalla, P. K., Studies on species sensitivity to

the dopaminergic neurotoxin 1-methyl-4-phenyl-1,2,3,6-tetrahydropyridine. Part 1: Systemic administration. *J Pharmacol Exp Ther* **1994,** 270, (3), 1000-7.

33. Rollema, H.; Damsma, G.; Horn, A. S.; De Vries, J. B.; Westerink, B. H., Brain dialysis in conscious rats reveals an instantaneous massive release of striatal dopamine in response to MPP+. *Eur J Pharmacol* **1986,** 126, (3), 345-6.

34. Current concepts in molecular mechanisms of MPTP-induced toxicity. *Life Sci* **1987,** 40, (8), 697-754.

35. Di Monte, D. A.; Wu, E. Y.; Irwin, I.; Delanney, L. E.; Langston, J. W., Biotransformation of 1-methyl-4-phenyl-1,2,3,6-tetrahydropyridine in primary cultures of mouse astrocytes. *J Pharmacol Exp Ther* **1991,** 258, (2), 594-600.

36. Markey, S. P.; Johannessen, J. N.; Chiueh, C. C.; Burns, R. S.; Herkenham, M. A., Intraneuronal generation of a pyridinium metabolite may cause drug-induced parkinsonism. *Nature* **1984,** 311, (5985), 464-7.

37. Selkoe, D. J.; Schenk, D., Alzheimer's disease: molecular understanding predicts amyloid-based therapeutics. *Annu Rev Pharmacol Toxicol* **2003,** 43, 545-84.

38. Crameri, R.; Schulz-Knappe, P.; Zucht, H. D., The future of post-genomic biology at the proteomic level: an outlook. *Comb Chem High Throughput Screen* **2005,** 8, (8), 807-10.

39. Schwartz, K.; Mercadier, J. J., Molecular and cellular biology of heart failure. *Curr Opin Cardiol* **1996,** 11, (3), 227-36.

40. van der Greef, J.; Stroobant, P.; van der Heijden, R., The role of analytical sciences in medical systems biology. *Curr Opin Chem Biol* **2004,** 8, (5), 559-65.

41. Selkoe, D. J., Alzheimer's disease: genes, proteins, and therapy. *Physiol Rev* **2001,** 81, (2), 741-66.

42. Miklos, G. L.; Maleszka, R., Integrating molecular medicine with functional proteomics: realities and expectations. *Proteomics* **2001,** 1, (1), 30-41.

43. Horellou, P.; Mallet, J., Gene therapy for Parkinson's disease. *Mol Neurobiol* **1997,** 15, (2), 241-56.

44. Hollywood, K.; Brison, D. R.; Goodacre, R., Metabolomics: current technologies and future trends. *Proteomics* **2006,** 6, (17), 4716-23.

45. Kitano, H., Systems biology: a brief overview. *Science* **2002,** 295, (5560), 1662-4.

46. Jalanko, A.; Tyynela, J.; Peltonen, L., From genes to systems: new global strategies for the characterization of NCL biology. *Biochim Biophys Acta* **2006,** 1762, (10), 934-44.

47. Nachtomy, O.; Shavit, A.; Yakhini, Z., Gene expression and the concept of the phenotype. *Stud Hist Philos Biol Biomed Sci* **2007,** 38, (1), 238-54.

48. Huber, L. A., Is proteomics heading in the wrong direction? *Nat Rev Mol Cell Biol* **2003,** 4, (1), 74-80.

49. Weckwerth, W., Metabolomics in systems biology. *Annu Rev Plant Biol* **2003,** 54, 669-89.

50. Kell, D. B., Metabolomics and systems biology: making sense of the soup. *Curr Opin Microbiol* **2004,** 7, (3), 296-307.

51. Singh, O. V., Proteomics and metabolomics: the molecular make-up of toxic aromatic pollutant bioremediation. *Proteomics* **2006,** 6, (20), 5481-92.

52. Fan, T. W.; Lane, A. N.; Higashi, R. M., The promise of metabolomics in cancer molecular therapeutics. *Curr Opin Mol Ther* **2004,** 6, (6), 584-92.

53. Viant, M. R.; Lyeth, B. G.; Miller, M. G.; Berman, R. F., An NMR metabolomic investigation of early metabolic disturbances following traumatic brain injury in a mammalian model. *NMR Biomed* **2005,** 18, (8), 507-16.

54. Chen, H.; Pan, Z.; Talaty, N.; Raftery, D.; Cooks, R. G., Combining desorption electrospray ionization mass spectrometry and nuclear magnetic resonance for differential metabolomics without sample preparation. *Rapid Commun Mass Spectrom* **2006,** 20, (10), 1577-84.

55. Glinski, M.; Weckwerth, W., The role of mass spectrometry in plant systems biology. *Mass Spectrom Rev* **2006,** 25, (2), 173-214.

56. Bollard, M. E.; Stanley, E. G.; Lindon, J. C.; Nicholson, J. K.; Holmes, E., NMR-based metabonomic approaches for evaluating physiological influences on biofluid composition. *NMR Biomed* **2005,** 18, (3), 143-62.

57. Mashego, M. R.; Rumbold, K.; De Mey, M.; Vandamme, E.; Soetaert, W.; Heijnen, J. J., Microbial metabolomics: past, present and future methodologies. *Biotechnol Lett* **2007,** 29, (1), 1-16.

58. Sasano, R.; Hamada, T.; Kurano, M.; Furuno, M., On-line coupling of solid-phase extraction to gas chromatography with fast solvent vaporization and concentration in an open injector liner. Analysis of pesticides in aqueous samples. *J Chromatogr A* **2000,** 896, (1-2), 41-9.

59. Gullberg, J.; Jonsson, P.; Nordstrom, A.; Sjostrom, M.; Moritz, T., Design of experiments: an efficient strategy to identify factors influencing extraction and derivatization of Arabidopsis thaliana samples in metabolomic studies with gas chromatography/mass spectrometry. *Anal Biochem* **2004,** 331, (2), 283-95.

60. Styczynski, M. P.; Moxley, J. F.; Tong, L. V.; Walther, J. L.; Jensen, K. L.; Stephanopoulos, G. N., Systematic identification of conserved metabolites in GC/MS data for metabolomics and biomarker discovery. *Anal Chem* **2007,** 79, (3), 966-73.

61. Li, S. L.; Chan, S. W.; Li, P.; Lin, G.; Zhou, G. H.; Ren, Y. J.; Chiu, F. C., Pre-column derivatization and gas chromatographic determination of alkaloids in bulbs of Fritillaria. *J Chromatogr A* **1999,** 859, (2), 183-92.

62. Chan, E. C.; Yap, S. L.; Lau, A. J.; Leow, P. C.; Toh, D. F.; Koh, H. L., Ultra-performance liquid chromatography/time-of-flight mass spectrometry based metabolomics of raw and steamed Panax notoginseng. *Rapid Commun Mass Spectrom* **2007,** 21, (4), 519-28.

63. Nordstrom, A.; O'Maille, G.; Qin, C.; Siuzdak, G., Nonlinear data alignment for UPLC-MS and HPLC-MS based metabolomics: quantitative analysis of endogenous and exogenous metabolites in human serum. *Anal Chem* **2006,** 78, (10), 3289-95.

64. Bottcher, C.; Roepenack-Lahaye, E. V.; Willscher, E.; Scheel, D.; Clemens, S., Evaluation of matrix effects in metabolite profiling based on capillary liquid chromatography electrospray ionization quadrupole time-of-flight mass spectrometry. *Anal Chem* **2007,** 79, (4), 1507-13.

65. Tolstikov, V. V.; Lommen, A.; Nakanishi, K.; Tanaka, N.; Fiehn, O., Monolithic silica-based capillary reversed-phase liquid chromatography/electrospray mass spectrometry for plant metabolomics. *Anal Chem* **2003,** 75, (23), 6737-40.

66. Wagner, S.; Scholz, K.; Donegan, M.; Burton, L.; Wingate, J.; Volkel, W., Metabonomics and biomarker discovery: LC-MS metabolic profiling and constant neutral loss scanning combined with multivariate data analysis for mercapturic acid analysis. *Anal Chem* **2006,** 78,

(4), 1296-305.

67. Prokai, L.; Kim, H. S.; Zharikova, A.; Roboz, J.; Ma, L.; Deng, L.; Simonsick, W. J., Jr., Electrospray ionization mass spectrometric and liquid chromatographic-mass spectrometric studies on the metabolism of synthetic dynorphin A peptides in brain tissue in vitro and in vivo. *J Chromatogr A* **1998,** 800, (1), 59-68.

68. Ando, S.; Tanaka, Y., Mass spectrometric studies on brain metabolism, using stable isotopes. *Mass Spectrom Rev* **2005,** 24, (6), 865-86.

69. Robertson, M., Biology in the 1980s, plus or minus a decade. *Nature* **1980,** 285, (5764), 358-9.

70. Bergstrom, S. K.; Goiny, M.; Danielsson, R.; Ungerstedt, U.; Andersson, M.; Markides, K. E., Screening of microdialysates taken before and after induced liver damage; on-line solid phase extraction-electrospray ionization-mass spectrometry. *J Chromatogr A* **2006,** 1120, (1-2), 21-6.

71. Meyerson, B. A.; Linderoth, B.; Karlsson, H.; Ungerstedt, U., Microdialysis in the human brain: extracellular measurements in the thalamus of parkinsonian patients. *Life Sci* **1990,** 46, (4), 301-8.

72. Bourne, J. A., Intracerebral microdialysis: 30 years as a tool for the neuroscientist. *Clin Exp Pharmacol Physiol* **2003,** 30, (1-2), 16-24.

73. Bungay, P. M.; Morrison, P. F.; Dedrick, R. L., Steady-state theory for quantitative microdialysis of solutes and water in vivo and in vitro. *Life Sci* **1990,** 46, (2), 105-19.

74. de Lange, E. C.; de Boer, A. G.; Breimer, D. D., Methodological issues in microdialysis sampling for pharmacokinetic studies. *Adv Drug Deliv Rev* **2000,** 45, (2-3), 125-48.

75. Hamani, C.; Luer, M. S.; Dujovny, M., Microdialysis in the human brain: review of its applications. *Neurol Res* **1997,** 19, (3), 281-8.

76. Johnston, A. J.; Gupta, A. K., Advanced monitoring in the neurology intensive care unit: microdialysis. *Curr Opin Crit Care* **2002,** 8, (2), 121-7.

77. Kanthan, R.; Shuaib, A.; Goplen, G.; Miyashita, H., A new method of in-vivo microdialysis of the human brain. *J Neurosci Methods* **1995,** 60, (1-2), 151-5.

78. O'Connell, M. T.; Tison, F.; Quinn, N. P.; Patsalos, P. N., Clinical drug monitoring by microdialysis: application to levodopa therapy in Parkinson's disease. *Br J Clin Pharmacol* **1996,** 42, (6), 765-9.

79. Peerdeman, S. M.; van Tulder, M. W.; Vandertop, W. P., Cerebral microdialysis as a monitoring method in subarachnoid hemorrhage patients, and correlation with clinical events--a systematic review. *J Neurol* **2003,** 250, (7), 797-805.

80. Siddiqui, M. M.; Shuaib, A., Intracerebral microdialysis and its clinical application: a review. *Methods* **2001,** 23, (1), 83-94.

81. Stahl, M.; Bouw, R.; Jackson, A.; Pay, V., Human microdialysis. *Curr Pharm Biotechnol* **2002,** 3, (2), 165-78.

82. Bengtsson, J.; Jansson, B.; Hammarlund-Udenaes, M., On-line desalting and determination of morphine, morphine-3-glucuronide and morphine-6-glucuronide in microdialysis and plasma samples using column switching and liquid chromatography/tandem mass spectrometry. *Rapid Commun Mass Spectrom* **2005,** 19, (15), 2116-22.

83. Jiang, Y.; Hofstadler, S. A., A highly efficient and automated method of purifying and desalting PCR products for analysis by electrospray ionization mass spectrometry. *Anal Biochem* **2003,** 316, (1), 50-7.

84. Visser, N. F.; van Harmelen, M.; Lingeman, H.; Irth, H., On-line SPE-CE for the determination of insulin derivatives in biological fluids. *J Pharm Biomed Anal* **2003,** 33, (3), 451-62.

85. Sweeney, A. P.; Shalliker, R. A., Development of a two-dimensional liquid chromatography system with trapping and sample enrichment capabilities. *J Chromatogr A* **2002,** 968, (1-2), 41-52.

86. Souverain, S.; Rudaz, S.; Veuthey, J. L., Matrix effect in LC-ESI-MS and LC-APCI-MS with off-line and on-line extraction procedures. *J Chromatogr A* **2004,** 1058, (1-2), 61-6.

87. Brinkman, U. A., On-line sample treatment for or via column liquid chromatography. *J Chromatogr A* **1994,** 665, (2), 217-31.

88. de Castro, A.; Fernandez, M. D.; Laloup, M.; Samyn, N.; De Boeck, G.; Wood, M.; Maes, V.; Lopez-Rivadulla, M., High-throughput on-line solid-phase extraction-liquid chromatography-tandem mass spectrometry method for the simultaneous analysis of 14

antidepressants and their metabolites in plasma. *J Chromatogr A* **2007**.

89. Flanagan, R. J.; Harvey, E. J.; Spencer, E. P., HPLC of basic drugs on microparticulate strong cation-exchange materials - a review. *Forensic Sci Int* **2001,** 121, (1-2), 97-102.

90. Garcia-Villar, N.; Saurina, J.; Hernandez-Cassou, S., Determination of histamine in wines with an on-line pre-column flow derivatization system coupled to high performance liquid chromatography. *Analyst* **2005,** 130, (9), 1286-90.

91. Bobeldijk, I.; Broess, K.; Speksnijder, P.; van Leerdam, T., Determination of the herbicide amitrole in water with pre-column derivatization, liquid chromatography and tandem mass spectrometry. *J Chromatogr A* **2001,** 938, (1-2), 15-22.

92. Chaimbault, P.; Petritis, K.; Elfakir, C.; Dreux, M., Determination of 20 underivatized proteinic amino acids by ion-pairing chromatography and pneumatically assisted electrospray mass spectrometry. *J Chromatogr A* **1999,** 855, (1), 191-202.

93. De Schutter, J. A.; De Moerloose, P., Reversed-phase ion-pair liquid chromatography of some quaternary ammonium drugs. *J Pharm Biomed Anal* **1988,** 6, (6-8), 879-85.

94. Gao, S.; Bhoopathy, S.; Zhang, Z. P.; Wright, D. S.; Jenkins, R.; Karnes, H. T., Evaluation of volatile ion-pair reagents for the liquid chromatography-mass spectrometry analysis of polar compounds and its application to the determination of methadone in human plasma. *J Pharm Biomed Anal* **2006,** 40, (3), 679-88.

95. Garcia, M. C., The effect of the mobile phase additives on sensitivity in the analysis of peptides and proteins by high-performance liquid chromatography-electrospray mass spectrometry. *J Chromatogr B Analyt Technol Biomed Life Sci* **2005,** 825, (2), 111-23.

96. Goldade, D. A.; Primus, T. M.; Johnston, J. J.; Zapien, D. C., Reversed-Phase Ion-Pair High-Performance Liquid Chromatographic Quantitation of Difethialone Residues in Whole-Body Rodents with Solid-Phase Extraction Cleanup. *J Agric Food Chem* **1998,** 46, (2), 504-508.

97. Neubecker, T. A.; Coombs, M. A.; Quijano, M.; O'Neill, T. P.; Cruze, C. A.; Dobson, R. L., Rapid and selective method for norepinephrine in rat urine using reversed-phase ion-pair high-performance liquid chromatography-tandem mass spectrometry. *J Chromatogr B Biomed Sci Appl* **1998,** 718, (2), 225-33.

98. Odink, J.; Sandman, H.; Schreurs, W. H., Determination of free and total catecholamines and

salsolinol in urine by ion-pair reversed-phase liquid chromatography with electrochemical detection after a one-step sample clean-up. *J Chromatogr* **1986,** 377, 145-54.

99. Carson, M. C., Ion-pair solid-phase extraction. *J Chromatogr A* **2000,** 885, (1-2), 343-50.

100. Castro, R.; Moyano, E.; Galceran, M. T., On-line ion-pair solid-phase extraction-liquid chromatography-mass spectrometry for the analysis of quaternary ammonium herbicides. *J Chromatogr A* **2000,** 869, (1-2), 441-9.

101. Jones, C. W.; Chmel, H., Solid-phase ion-pair extraction and liquid chromatography of mezlocillin in serum. *Clin Chem* **1988,** 34, (10), 2155-6.

102. Rodriguez, I.; Lee, H. K.; Li, S. F., Ion-pair solid-phase extraction of biogenic amines before micellar electrokinetic chromatography with laser-induced fluorescence detection of their fluorescein thiocarbamyl derivatives. *Electrophoresis* **1999,** 20, (9), 1862-8.

103. Saradhi, U. V.; Prabhakar, S.; Reddy, T. J.; Vairamani, M., Ion-pair solid-phase extraction and gas chromatography-mass spectrometric determination of acidic hydrolysis products of chemical warfare agents from aqueous samples. *J Chromatogr A* **2006,** 1129, (1), 9-13.

104. Ye, X.; Kuklenyik, Z.; Needham, L. L.; Calafat, A. M., Automated on-line column-switching HPLC-MS/MS method with peak focusing for the determination of nine environmental phenols in urine. *Anal Chem* **2005,** 77, (16), 5407-13.

105. Pocurull, E.; Aguilar, C.; Alonso, M. C.; Barcelo, D.; Borrull, F.; Marce, R. M., On-line solid-phase extraction-ion-pair liquid chromatography-electrospray mass spectrometry for the trace determination of naphthalene monosulphonates in water. *J Chromatogr A* **1999,** 854, (1-2), 187-95.

106. Schutze, D.; Boss, B.; Schmid, J., Liquid chromatographic-tandem mass spectrometric method for the analysis of a neurokinin-1 antagonist and its metabolite using automated solid-phase sample preparation and automated data handling and reporting. *J Chromatogr B Biomed Sci Appl* **2000,** 748, (1), 55-64.

107. Wang, P. G.; Zhang, J.; Gage, E. M.; Schmidt, J. M.; Rodila, R. C.; Ji, Q. C.; El-Shourbagy, T. A., A high-throughput liquid chromatography/tandem mass spectrometry method for simultaneous quantification of a hydrophobic drug candidate and its hydrophilic metabolite in human urine with a fully automated liquid/liquid extraction. *Rapid Commun Mass Spectrom* **2006,** 20, (22), 3456-64.

108. Ciriacks, C. M.; Bowser, M. T., Measuring the effect of glutamate receptor agonists on extracellular D-serine concentrations in the rat striatum using online microdialysis-capillary electrophoresis. *Neurosci Lett* **2006,** 393, (2-3), 200-5.

109. O'Brien, K. B.; Bowser, M. T., Measuring D-serine efflux from mouse cortical brain slices using online microdialysis-capillary electrophoresis. *Electrophoresis* **2006,** 27, (10), 1949-56.

110. O'Brien, K. B.; Esguerra, M.; Miller, R. F.; Bowser, M. T., Monitoring neurotransmitter release from isolated retinas using online microdialysis-capillary electrophoresis. *Anal Chem* **2004,** 76, (17), 5069-74.

111. Takada, Y.; Yoshida, M.; Sakairi, M.; Koizumi, H., Detection of gamma-aminobutyric acid in a living rat brain using in vivo microdialysis-capillary electrophoresis/mass spectrometry. *Rapid Commun Mass Spectrom* **1995,** 9, (10), 895-6.

112. Chang, Y. L.; Chou, M. H.; Lin, M. F.; Chen, C. F.; Tsai, T. H., Determination and pharmacokinetic study of unbound cefepime in rat bile by liquid chromatography with on-line microdialysis. *J Chromatogr A* **2001,** 914, (1-2), 77-82.

113. Tsai, T. H.; Kao, H. Y.; Chen, C. F., Measurement and pharmacokinetic analysis of unbound cephaloridine in rat blood by on-line microdialysis and microbore liquid chromatography. *Biomed Chromatogr* **2001,** 15, (2), 79-82.

114. Mathy, F. X.; Vroman, B.; Ntivunwa, D.; De Winne, A. J.; Verbeeck, R. K.; Preat, V., On-line determination of fluconazole in blood and dermal rat microdialysates by microbore high-performance liquid chromatography. *J Chromatogr B Analyt Technol Biomed Life Sci* **2003,** 787, (2), 323-31.

115. Chen, A.; Lunte, C. E., Microdialysis sampling coupled on-line to fast microbore liquid chromatography. *J Chromatogr A* **1995,** 691, (1-2), 29-35.

116. Lin, C. H.; Wu, H. L.; Huang, Y. L., Microdialysis sampling coupled to on-line high-performance liquid chromatography for determination of arbutin in whitening cosmetics. *J Chromatogr B Analyt Technol Biomed Life Sci* **2005,** 829, (1-2), 149-52.

117. Zhang, W.; Cao, X.; Xie, Y.; Ai, S.; Jin, L.; Jin, J., Simultaneous determination of the monoamine neurotransmitters and glucose in rat brain by microdialysis sampling coupled with liquid chromatography-dual electrochemical detector. *J Chromatogr B Analyt Technol Biomed Life Sci* **2003,** 785, (2), 327-36.

118. Tseng, W. C.; Yang, M. H.; Chen, T. P.; Huang, Y. L., Automated, continuous, and dynamic speciation of urinary arsenic in the bladder of living organisms using microdialysis sampling coupled on-line with high performance liquid chromatography and hydride generation atomic absorption spectrometry. *Analyst* **2002,** 127, (4), 560-4.

119. Tseng, W. C.; Sun, Y. C.; Lee, C. F.; Yang, M. H.; Huang, Y. L., Continuous in vivo monitoring of blood diffusible calcium using on-line microdialysis sampling coupled with flame atomic absorption spectrometry. *Anal Sci* **2005,** 21, (3), 225-9.

120. Kehr, J., Determination of glutamate and aspartate in microdialysis samples by reversed-phase column liquid chromatography with fluorescence and electrochemical detection. *J Chromatogr B Biomed Sci Appl* **1998,** 708, (1-2), 27-38.

121. Tsai, T. H.; Cheng, F. C.; Hung, L. C.; Chen, C. F., Measurement of hydroxyl radical in rat blood vessel by microbore liquid chromatography and electrochemical detection: an on-line microdialysis study. *J Chromatogr B Biomed Sci Appl* **1999,** 734, (2), 277-83.

122. Kehr, J.; Dechent, P.; Kato, T.; Ogren, S. O., Simultaneous determination of acetylcholine, choline and physostigmine in microdialysis samples from rat hippocampus by microbore liquid chromatography/electrochemistry on peroxidase redox polymer coated electrodes. *J Neurosci Methods* **1998,** 83, (2), 143-50.

123. Osborne, P. G.; Niwa, O.; Kato, T.; Yamamoto, K., On-line, continuous measurement of extracellular striatal glucose using microdialysis sampling and electrochemical detection. *J Neurosci Methods* **1997,** 77, (2), 143-50.

124. Chaurasia, C. S.; Chen, C. E.; Ashby, C. R., Jr., In vivo on-line HPLC-microdialysis: simultaneous detection of monoamines and their metabolites in awake freely-moving rats. *J Pharm Biomed Anal* **1999,** 19, (3-4), 413-22.

125. Cheng, F. C.; Tsai, T. H.; Wu, Y. S.; Kuo, J. S.; Chen, C. F., Pharmacokinetic and pharmacodynamic analyses of trazodone in rat striatum by in vivo microdialysis. *J Pharm Biomed Anal* **1999,** 19, (3-4), 293-300.

126. Tsunoda, M.; Mitsuhashi, K.; Masuda, M.; Imai, K., Simultaneous determination of 3,4-dihydroxyphenylacetic acid and homovanillic acid using high performance liquid chromatography-fluorescence detection and application to rat kidney microdialysate. *Anal Biochem* **2002,** 307, (1), 153-8.

127. Zhou, S. Y.; Zuo, H.; Stobaugh, J. F.; Lunte, C. E.; Lunte, S. M., Continuous in vivo

monitoring of amino acid neurotransmitters by microdialysis sampling with on-line derivatization and capillary electrophoresis separation. *Anal Chem* **1995,** 67, (3), 594-9.

128. Yang, C. S.; Tsai, P. J.; Chen, W. Y.; Kuo, J. S., On-line, continuous and automatic monitoring of extracellular malondialdehyde concentration in anesthetized rat brain cortex. *J Chromatogr B Biomed Sci Appl* **2001,** 752, (1), 33-8.

129. Bowser, M. T.; Kennedy, R. T., In vivo monitoring of amine neurotransmitters using microdialysis with on-line capillary electrophoresis. *Electrophoresis* **2001,** 22, (17), 3668-76.

130. Robert, F.; Bert, L.; Parrot, S.; Denoroy, L.; Stoppini, L.; Renaud, B., Coupling on-line brain microdialysis, precolumn derivatization and capillary electrophoresis for routine minute sampling of O-phosphoethanolamine and excitatory amino acids. *J Chromatogr A* **1998,** 817, (1-2), 195-203.

131. Nanjo, Y.; Yano, T.; Hayashi, R.; Yao, T., Optically specific detection of D- and L-lactic acids by a flow-injection dual biosensor system with on-line microdialysis sampling. *Anal Sci* **2006,** 22, (8), 1135-8.

132. Palmisano, F.; Quinto, M.; Rizzi, R.; Zambonin, P. G., Flow injection analysis of L-lactate in milk and yoghurt by on-line microdialysis and amperometric detection at a disposable biosensor. *Analyst* **2001,** 126, (6), 866-70.

133. Li, B.; Zhang, Z.; Jin, Y., Plant tissue-based chemiluminescence flow biosensor for determination of unbound dopamine in rabbit blood with on-line microdialysis sampling. *Biosens Bioelectron* **2002,** 17, (6-7), 585-9.

134. Palmisano, F.; Centonze, D.; Quinto, M.; Zambonin, P. G., A microdialysis fibre based sampler for flow injection analysis: determination of L-lactate in biofluids by an electrochemically synthesised bilayer membrane based biosensor. *Biosens Bioelectron* **1996,** 11, (4), 419-25.

135. Kunnecke, B.; Kustermann, E.; Seelig, J., Simultaneous in vivo monitoring of hepatic glucose and glucose-6-phosphate by (13)C-NMR spectroscopy. *Magn Reson Med* **2000,** 44, (4), 556-62.

136. Shi, G.; Yamamoto, K.; Zhou, T.; Xu, F.; Kato, T.; Ji-ye, J.; Jin, L., On-line biosensors for simultaneous determination of glucose, choline, and glutamate integrated with a microseparation system. *Electrophoresis* **2003,** 24, (18), 3266-72.

137. Zhang, M.; Mao, L., Enzyme-based amperometric biosensors for continuous and on-line monitoring of cerebral extracellular microdialysate. *Front Biosci* **2005,** 10, 345-52.

138. Lai, L.; Lin, L. C.; Lin, J. H.; Tsai, T. H., Pharmacokinetic study of free mangiferin in rats by microdialysis coupled with microbore high-performance liquid chromatography and tandem mass spectrometry. *J Chromatogr A* **2003,** 987, (1-2), 367-74.

139. Canarelli, S.; Fisch, I.; Freitag, R., On-line microdialysis of proteins with high-salt buffers for direct coupling of electrospray ionization mass spectrometry and liquid chromatography. *J Chromatogr A* **2002,** 948, (1-2), 139-49.

140. Inchauspe, G.; Delrieu, P.; Dupin, P.; Laurent, M.; Samain, D., Mechanism of selectivity in ion-pair high-performance liquid chromatography of aminoglycoside antibiotics using perfluorinated pairing ions. *J Chromatogr* **1987,** 404, (1), 53-66.

141. Kontur, P.; Dawson, R.; Monjan, A., Manipulation of mobile phase parameters for the HPLC separation of endogenous monoamines in rat brain tissue. *J Neurosci Methods* **1984,** 11, (1), 5-18.

142. Krokhin, O. V., Sequence-specific retention calculator. Algorithm for peptide retention prediction in ion-pair RP-HPLC: application to 300- and 100-A pore size C18 sorbents. *Anal Chem* **2006,** 78, (22), 7785-95.

143. Vul'fson, A. N.; Iakimov, S. A., [High performance liquid chromatography of nucleotides. Major methods and their development]. *Bioorg Khim* **1983,** 9, (3), 365-90.

144. Yamamoto, R.; Seki, M.; Ouchi, K.; Koyano, S.; Nakazawa, S.; Nagatani, Y.; Sato, H., [A rapid determination of allantoin by high-performance liquid chromatography using tris(hydroxymethyl)aminomethane-HCl buffer as a mobile phase]. *Yakugaku Zasshi* **1998,** 118, (8), 310-6.

145. Reemtsma, T., Analysis of sulfophthalimide and some of its derivatives by liquid chromatography-electrospray ionization tandem mass spectrometry. *J Chromatogr A* **2001,** 919, (2), 289-97.

146. Yoshida, T., Peptide separation by Hydrophilic-Interaction Chromatography: a review. *J Biochem Biophys Methods* **2004,** 60, (3), 265-80.

147. Castro, R.; Moyano, E.; Galceran, M. T., Ion-pair liquid chromatography--atmospheric pressure ionization mass spectrometry for the determination of quaternary ammonium

herbicides. *J Chromatogr A* **1999,** 830, (1), 145-54.

148. Castro, R.; Moyano, E.; Galceran, M. T., Determination of quaternary ammonium pesticides by liquid chromatography-electrospray tandem mass spectrometry. *J Chromatogr A* **2001,** 914, (1-2), 111-21.

149. Dass, C.; Mahalakshmi, P.; Grandberry, D., Manipulation of ion-pairing reagents for reversed-phase high-performance liquid chromatographic separation of phosphorylated opioid peptides from their non-phosphorylated analogues. *J Chromatogr A* **1994,** 678, (2), 249-57.

150. Pearson, J. D.; McCroskey, M. C., Perfluorinated acid alternatives to trifluoroacetic acid for reversed-phase high-performance liquid chromatography. *J Chromatogr A* **1996,** 746, (2), 277-81.

151. Petritis, K.; Brussaux, S.; Guenu, S.; Elfakire, C.; Dreux, M., Ion-pair reversed-phase liquid chromatography-electrospray mass spectrometry for the analysis of underivatized small peptides. *J Chromatogr A* **2002,** 957, (2), 173-85.

152. Piraud, M.; Vianey-Saban, C.; Petritis, K.; Elfakir, C.; Steghens, J. P.; Bouchu, D., Ion-pairing reversed-phase liquid chromatography/electrospray ionization mass spectrometric analysis of 76 underivatized amino acids of biological interest: a new tool for the diagnosis of inherited disorders of amino acid metabolism. *Rapid Commun Mass Spectrom* **2005,** 19, (12), 1587-602.

153. Piraud, M.; Vianey-Saban, C.; Petritis, K.; Elfakir, C.; Steghens, J. P.; Morla, A.; Bouchu, D., ESI-MS/MS analysis of underivatised amino acids: a new tool for the diagnosis of inherited disorders of amino acid metabolism. Fragmentation study of 79 molecules of biological interest in positive and negative ionisation mode. *Rapid Commun Mass Spectrom* **2003,** 17, (12), 1297-311.

154. Steffenrud, S.; Salari, H., Reversed-phase ion-interaction chromatography of leukotrienes, lipoxins and related compounds. *J Chromatogr* **1988,** 427, (1), 1-7.

155. Keevil, B. G.; Lockhart, S. J.; Cooper, D. P., Determination of tobramycin in serum using liquid chromatography-tandem mass spectrometry and comparison with a fluorescence polarisation assay. *J Chromatogr B Analyt Technol Biomed Life Sci* **2003,** 794, (2), 329-35.

156. Yoshimura, Y.; Ohnishi, K.; Hamamura, M.; Oda, T.; Sohda, T., Automated high-performance liquid chromatographic determination of hydroxylysylpyridinoline and

lysylpyridinoline in urine using a column-switching method. *J Chromatogr* **1993,** 613, (1), 43-9.

157. Zhang, K.; Tang, H., Analysis of core histones by liquid chromatography-mass spectrometry and peptide mapping. *J Chromatogr B Analyt Technol Biomed Life Sci* **2003,** 783, (1), 173-9.

158. Garcia, M. C.; Hogenboom, A. C.; Zappey, H.; Irth, H., Effect of the mobile phase composition on the separation and detection of intact proteins by reversed-phase liquid chromatography-electrospray mass spectrometry. *J Chromatogr A* **2002,** 957, (2), 187-99.

159. Shou, W. Z.; Naidong, W., Simple means to alleviate sensitivity loss by trifluoroacetic acid (TFA) mobile phases in the hydrophilic interaction chromatography-electrospray tandem mass spectrometric (HILIC-ESI/MS/MS) bioanalysis of basic compounds. *J Chromatogr B Analyt Technol Biomed Life Sci* **2005,** 825, (2), 186-92.

160. Kiridena, W.; Poole, C. F.; Koziol, W. W., Effect of solvent strength and temperature on retention for a polar-endcapped, octadecylsiloxane-bonded silica stationary phase with methanol-water mobile phases. *J Chromatogr A* **2004,** 1060, (1-2), 177-85.

161. Layne, J., Characterization and comparison of the chromatographic performance of conventional, polar-embedded, and polar-endcapped reversed-phase liquid chromatography stationary phases. *J Chromatogr A* **2002,** 957, (2), 149-64.

162. Contin, M.; Balboni, M.; Callegati, E.; Candela, C.; Albani, F.; Riva, R.; Baruzzi, A., Simultaneous liquid chromatographic determination of lamotrigine, oxcarbazepine monohydroxy derivative and felbamate in plasma of patients with epilepsy. *J Chromatogr B Analyt Technol Biomed Life Sci* **2005,** 828, (1-2), 113-7.

163. Khan, S.; Ahmad, A.; Ahmad, I., A sensitive and rapid liquid chromatography tandem mass spectrometry method for quantitative determination of 7-ethyl-10-hydroxycamptothecin (SN-38) in human plasma containing liposome-based SN-38 (LE-SN38). *Biomed Chromatogr* **2003,** 17, (8), 493-9.

164. Schmidt, R.; Coste, O.; Geisslinger, G., LC-MS/MS-analysis of prostaglandin E2 and D2 in microdialysis samples of rats. *J Chromatogr B Analyt Technol Biomed Life Sci* **2005,** 826, (1-2), 188-97.

165. Smythies, J.; De Iuliis, A.; Zanatta, L.; Galzigna, L., The biochemical basis of Parkinson's disease: the role of catecholamine o-quinones: a review-discussion. *Neurotox Res* **2002,** 4, (1), 77-81.

166. Goldstein, D. S.; Lenders, J. W.; Kaler, S. G.; Eisenhofer, G., Catecholamine phenotyping: clues to the diagnosis, treatment, and pathophysiology of neurogenetic disorders. *J Neurochem* **1996,** 67, (5), 1781-90.

167. Schatzberg, A. F.; Orsulak, P. J.; Rosenbaum, A. H.; Kruger, E. R.; Schildkraut, J. J.; Cole, J. O., Catecholamine measures for diagnosis and treatment of patients with depressive disorders. *J Clin Psychiatry* **1980,** 41, (12 Pt 2), 35-9.

168. Schildkraut, J. J., The catecholamine hypothesis of affective disorders: a review of supporting evidence. *Am J Psychiatry* **1965,** 122, (5), 509-22.

169. Schildkraut, J. J., The catecholamine hypothesis of affective disorders: a review of supporting evidence. 1965. *J Neuropsychiatry Clin Neurosci* **1995,** 7, (4), 524-33; discussion 523-4.

170. Foster, S. B.; Wrona, M. Z.; Han, J.; Dryhurst, G., The parkinsonian neurotoxin 1-methyl-4-phenylpyridinium (MPP(+)) mediates release of l-3,4-dihydroxyphenylalanine (l-DOPA) and inhibition of l-DOPA decarboxylase in the rat striatum: a microdialysis study. *Chem Res Toxicol* **2003,** 16, (10), 1372-84.

171. Rollema, H.; Alexander, G. M.; Grothusen, J. R.; Matos, F. F.; Castagnoli, N., Jr., Comparison of the effects of intracerebrally administered MPP+ (1-methyl-4-phenylpyridinium) in three species: microdialysis of dopamine and metabolites in mouse, rat and monkey striatum. *Neurosci Lett* **1989,** 106, (3), 275-81.

172. Asanuma, M.; Miyazaki, I.; Ogawa, N., Dopamine- or L-DOPA-induced neurotoxicity: the role of dopamine quinone formation and tyrosinase in a model of Parkinson's disease. *Neurotox Res* **2003,** 5, (3), 165-76.

173. Halliwell, B. G., J, *Free Radicals in Biology and Medicine*. Oxford Univrsity Press: Oxford, N.Y., 1999.

174. Tabatabaie, T.; Goyal, R. N.; Blank, C. L.; Dryhurst, G., Further insights into the molecular mechanisms of action of the serotonergic neurotoxin 5,7-dihydroxytryptamine. *J Med Chem* **1993,** 36, (2), 229-36.

175. Baranyi, M.; Milusheva, E.; Vizi, E. S.; Sperlagh, B., Chromatographic analysis of dopamine metabolism in a Parkinsonian model. *J Chromatogr A* **2006,** 1120, (1-2), 13-20.

176. Patel, V.; Borysenko, M.; Kumar, M. S., Effect of delta 9-THC on brain and plasma

catecholamine levels as measured by HPLC. *Brain Res Bull* **1985,** 14, (1), 85-90.

177. Strobel, G.; Weicker, H., Catecholamine sulfates as internal standards in HPLC determinations of sulfoconjugated catecholamines in plasma and urine. *Clin Chem* **1991,** 37, (2), 196-9.

178. Stewart, J.; Rajabi, H., Estradiol derived from testosterone in prenatal life affects the development of catecholamine systems in the frontal cortex in the male rat. *Brain Res* **1994,** 646, (1), 157-60.

179. Todorov, L. D.; Mihaylova-Todorova, S.; Craviso, G. L.; Bjur, R. A.; Westfall, D. P., Evidence for the differential release of the cotransmitters ATP and noradrenaline from sympathetic nerves of the guinea-pig vas deferens. *J Physiol* **1996,** 496 (Pt 3), 731-48.

180. de Jong, J.; Point, A. J.; Tjaden, U. R.; Beeksma, S.; Kraak, J. C., Determination of catecholamines in urine (and plasma) by liquid chromatography after on-line sample pretreatment on small alumina or dihydroxyborylsilica columns. *J Chromatogr* **1987,** 414, (2), 285-300.

181. Nohta, H.; Mitsui, A.; Umegae, Y.; Ohkura, Y., Determination of free and total catecholamines in human urine by HPLC with fluorescence detection. *Biomed Chromatogr* **1987,** 2, (1), 9-12.

182. Tsunoda, M.; Nagayama, M.; Funatsu, T.; Hosoda, S.; Imai, K., Catecholamine analysis with microcolumn LC-peroxyoxalate chemiluminescence reaction detection. *Clin Chim Acta* **2006,** 366, (1-2), 168-73.

183. Chan, S. A.; Smith, C., Physiological stimuli evoke two forms of endocytosis in bovine chromaffin cells. *J Physiol* **2001,** 537, (Pt 3), 871-85.

184. Hasegawa, T.; Wada, K.; Hiyama, E.; Masujima, T., Pretreatment and one-shot separating analysis of whole catecholamine metabolites in plasma by using LC/MS. *Anal Bioanal Chem* **2006,** 385, (5), 814-20.

185. Magera, M. J.; Stoor, A. L.; Helgeson, J. K.; Matern, D.; Rinaldo, P., Determination of homovanillic acid in urine by stable isotope dilution and electrospray tandem mass spectrometry. *Clin Chim Acta* **2001,** 306, (1-2), 35-41.

186. Bergquist, J.; Silberring, J., Identification of catecholamines in the immune system by electrospray ionization mass spectrometry. *Rapid Commun Mass Spectrom* **1998,** 12, (11),

683-8.

187. Chen, S.; Li, Q.; Carvey, P. M.; Li, K., Analysis of 9-fluorenylmethyloxycarbonyl derivatives of catecholamines by high performance liquid chromatography, liquid chromatography/mass spectrometry and tandem mass spectrometry. *Rapid Commun Mass Spectrom* **1999,** 13, (18), 1869-77.

188. Miles, L. A.; Andronicos, N. M.; Baik, N.; Parmer, R. J., Cell-surface actin binds plasminogen and modulates neurotransmitter release from catecholaminergic cells. *J Neurosci* **2006,** 26, (50), 13017-24.

189. Vuorensola, K.; Siren, H.; Karjalainen, U., Determination of dopamine and methoxycatecholamines in patient urine by liquid chromatography with electrochemical detection and by capillary electrophoresis coupled with spectrophotometry and mass spectrometry. *J Chromatogr B Analyt Technol Biomed Life Sci* **2003,** 788, (2), 277-89.

190. Foster, S. B. Neurochemical and Immunohistochemical Effects Induced by the 1-Methyl-4-Phenylpyridinium Animal Model of Parkinson's Disease: An In Vivo Microdialysis Investigation in Freely-Moving Rats. The University of Oklahoma, Norman, 2003.

191. Butcher, S. P.; Fairbrother, I. S.; Kelly, J. S.; Arbuthnott, G. W., Amphetamine-induced dopamine release in the rat striatum: an in vivo microdialysis study. *J Neurochem* **1988,** 50, (2), 346-55.

192. Droge, W., Cysteine and glutathione in catabolic conditions and immunological dysfunction. *Curr Opin Clin Nutr Metab Care* **1999,** 2, (3), 227-33.

193. Pastore, A.; Federici, G.; Bertini, E.; Piemonte, F., Analysis of glutathione: implication in redox and detoxification. *Clin Chim Acta* **2003,** 333, (1), 19-39.

194. Potesil, D.; Petrlova, J.; Adam, V.; Vacek, J.; Klejdus, B.; Zehnalek, J.; Trnkova, L.; Havel, L.; Kizek, R., Simultaneous femtomole determination of cysteine, reduced and oxidized glutathione, and phytochelatin in maize (Zea mays L.) kernels using high-performance liquid chromatography with electrochemical detection. *J Chromatogr A* **2005,** 1084, (1-2), 134-44.

195. Copper, C. L.; Collins, G. E., Separation of thiol and cyanide hydrolysis products of chemical warfare agents by capillary electrophoresis. *Electrophoresis* **2004,** 25, (6), 897-902.

196. Carlucci, F.; Tabucchi, A.; Biagioli, B.; Sani, G.; Lisi, G.; Maccherini, M.; Rosi, F.; Marinello,

E., Capillary electrophoresis in the evaluation of ischemic injury: simultaneous determination of purine compounds and glutathione. *Electrophoresis* **2000,** 21, (8), 1552-7.

197. Davey, M. W.; Bauw, G.; Van Montagu, M., Simultaneous high-performance capillary electrophoresis analysis of the reduced and oxidised forms of ascorbate and glutathione. *J Chromatogr B Biomed Sci Appl* **1997,** 697, (1-2), 269-76.

198. Hoque, M. E.; Arnett, S. D.; Lunte, C. E., On-column preconcentration of glutathione and glutathione disulfide using pH-mediated base stacking for the analysis of microdialysis samples by capillary electrophoresis. *J Chromatogr B Analyt Technol Biomed Life Sci* **2005,** 827, (1), 51-7.

199. Mendoza, J.; Soto, P.; Ahumada, I.; Garrido, T., Determination of oxidized and reduced glutathione, by capillary zone electrophoresis, in Brassica juncea plants treated with copper and cadmium. *Electrophoresis* **2004,** 25, (6), 890-6.

200. Camera, E.; Picardo, M., Analytical methods to investigate glutathione and related compounds in biological and pathological processes. *J Chromatogr B Analyt Technol Biomed Life Sci* **2002,** 781, (1-2), 181-206.

201. Michelet, F.; Gueguen, R.; Leroy, P.; Wellman, M.; Nicolas, A.; Siest, G., Blood and plasma glutathione measured in healthy subjects by HPLC: relation to sex, aging, biological variables, and life habits. *Clin Chem* **1995,** 41, (10), 1509-17.

202. Paroni, R.; De Vecchi, E.; Cighetti, G.; Arcelloni, C.; Fermo, I.; Grossi, A.; Bonini, P., HPLC with o-phthalaldehyde precolumn derivatization to measure total, oxidized, and protein-bound glutathione in blood, plasma, and tissue. *Clin Chem* **1995,** 41, (3), 448-54.

203. Raggi, M. A.; Mandrioli, R.; Casamenti, G.; Musiani, D.; Marini, M., HPLC determination of glutathione and other thiols in human mononuclear blood cells. *Biomed Chromatogr* **1998,** 12, (5), 262-6.

204. Sian, J.; Dexter, D. T.; Cohen, G.; Jenner, P. G.; Marsden, C. D., Comparison of HPLC and enzymatic recycling assays for the measurement of oxidized glutathione in rat brain. *J Pharm Pharmacol* **1997,** 49, (3), 332-5.

205. Rabenstein, D. L.; Saetre, R., Mercury-based electrochemical detector of liquid chromatography for the detection of glutathione and other sulfur-containing compounds. *Anal Chem* **1977,** 49, (7), 1036-9.

206. Richie, J. P., Jr.; Lang, C. A., The determination of glutathione, cyst(e)ine, and other thiols and disulfides in biological samples using high-performance liquid chromatography with dual electrochemical detection. *Anal Biochem* **1987,** 163, (1), 9-15.

207. Han, J.; Cheng, F. C.; Yang, Z.; Dryhurst, G., Inhibitors of mitochondrial respiration, iron (II), and hydroxyl radical evoke release and extracellular hydrolysis of glutathione in rat striatum and substantia nigra: potential implications to Parkinson's disease. *J Neurochem* **1999,** 73, (4), 1683-95.

208. Mansoor, M. A.; Svardal, A. M.; Ueland, P. M., Determination of the in vivo redox status of cysteine, cysteinylglycine, homocysteine, and glutathione in human plasma. *Anal Biochem* **1992,** 200, (2), 218-29.

209. Camera, E.; Rinaldi, M.; Briganti, S.; Picardo, M.; Fanali, S., Simultaneous determination of reduced and oxidized glutathione in peripheral blood mononuclear cells by liquid chromatography-electrospray mass spectrometry. *J Chromatogr B Biomed Sci Appl* **2001,** 757, (1), 69-78.

210. Norris, R. L.; Eaglesham, G. K.; Shaw, G. R.; Smith, M. J.; Chiswell, R. K.; Seawright, A. A.; Moore, M. R., A sensitive and specific assay for glutathione with potential application to glutathione disulphide, using high-performance liquid chromatography-tandem mass spectrometry. *J Chromatogr B Biomed Sci Appl* **2001,** 762, (1), 17-23.

211. Petritis, K.; Elfakir, C.; Dreux, M., A comparative study of commercial liquid chromatographic detectors for the analysis of underivatized amino acids. *J Chromatogr A* **2002,** 961, (1), 9-21.

212. Cohen, G.; Mytilineou, C., Studies on the mechanism of action of 1-methyl-4-phenyl-1,2,3,6-tetrahydropyridine (MPTP). *Life Sci* **1985,** 36, (3), 237-42.

213. Heikkila, R. E.; Nicklas, W. J.; Duvoisin, R. C., Studies on the mechanism of the dopaminergic neurotoxicity of 1-methyl-4-phenyl-1,2,3,6-tetrahydropyridine. *Adv Neurol* **1987,** 45, 149-52.

214. Zuddas, A.; Corsini, G. U.; Schinelli, S.; Barker, J. L.; Kopin, I. J.; di Porzio, U., Acetaldehyde directly enhances MPP+ neurotoxicity and delays its elimination from the striatum. *Brain Res* **1989,** 501, (1), 11-22.

215. Irwin, I.; DeLanney, L. E.; Di Monte, D.; Langston, J. W., The biodisposition of MPP+ in mouse brain. *Neurosci Lett* **1989,** 101, (1), 83-8.

216. Smith, M. T.; Ekstrom, G.; Sandy, M. S.; Di Monte, D., Studies on the mechanism of 1-methyl-4-phenyl-1,2,3,6-tetrahydropyridine cytotoxicity in isolated hepatocytes. *Life Sci* **1987,** 40, (8), 741-8.

217. Nicklas, W. J.; Youngster, S. K.; Kindt, M. V.; Heikkila, R. E., MPTP, MPP+ and mitochondrial function. *Life Sci* **1987,** 40, (8), 721-9.

218. Walker, M. J.; Jenner, P.; Marsden, C. D., A redox reaction between MPP+ and MPDP+ to produce superoxide radicals does not impair mitochondrial function. *Biochem Pharmacol* **1991,** 42, (4), 913-9.

219. Peterson, L. A.; Caldera, P. S.; Trevor, A.; Chiba, K.; Castagnoli, N., Jr., Studies on the 1-methyl-4-phenyl-2,3-dihydropyridinium species 2,3-MPDP+, the monoamine oxidase catalyzed oxidation product of the nigrostriatal toxin 1-methyl-4-phenyl-1,2,3,6-tetrahydropyridine (MPTP). *J Med Chem* **1985,** 28, (10), 1432-6.

220. Ohya, Y.; Naoi, M.; Ochi, N.; Mizutani, N.; Watanabe, K.; Nagatsu, T., Uptake of N-methyl-4-phenyl-1,2,3,6-tetrahydropyridine (MPTP) and the N-methyl-4-phenylpyridinium ion (MPP+) into fetal mouse brain through the placenta. *Neurosci Lett* **1989,** 105, (1-2), 221-6.

221. Desole, M. S.; Esposito, G.; Enrico, P.; Miele, M.; Fresu, L.; De Natale, G.; Miele, E.; Grella, G., Effects of ageing on 1-methyl-4-phenyl-1,2,3,6-tetrahydropyridine (MPTP) neurotoxic effects on striatum and brainstem in the rat. *Neurosci Lett* **1993,** 159, (1-2), 143-6.

222. Schmidt, N.; Ferger, B., Neuroprotective effects of (+/-)-kavain in the MPTP mouse model of Parkinson's disease. *Synapse* **2001,** 40, (1), 47-54.

223. Goodwin, B. L.; Kite, G. C., Environmental MPTP as a factor in the aetiology of Parkinson's disease? *J Neural Transm* **1998,** 105, (10-12), 1265-9.

224. Irwin, I.; Ricaurte, G. A.; DeLanney, L. E.; Langston, J. W., The sensitivity of nigrostriatal dopamine neurons to MPP+ does not increase with age. *Neurosci Lett* **1988,** 87, (1-2), 51-6.

225. Kajita, M.; Niwa, T.; Fujisaki, M.; Ueki, M.; Niimura, K.; Sato, M.; Egami, K.; Naoi, M.; Yoshida, M.; Nagatsu, T., Detection of 1-phenyl-N-methyl-1,2,3,4-tetrahydroisoquinoline and 1-phenyl-1,2,3,4-tetrahydroisoquinoline in human brain by gas chromatography-tandem mass spectrometry. *J Chromatogr B Biomed Appl* **1995,** 669, (2), 345-51.

226. Farina, A.; Gostoli, G.; Bossu, E.; Montinaro, A.; Lestingi, C.; Lecce, R., LC-MS

determination of MPTP at sub-ppm level in pethidine hydrochloride. *J Pharm Biomed Anal* **2005,** 37, (5), 1089-93.

227. Bazan, N. G.; Palacios-Pelaez, R.; Lukiw, W. J., Hypoxia signaling to genes: significance in Alzheimer's disease. *Mol Neurobiol* **2002,** 26, (2-3), 283-98.

228. Lebeau, A.; Terro, F.; Rostene, W.; Pelaprat, D., Blockade of 12-lipoxygenase expression protects cortical neurons from apoptosis induced by beta-amyloid peptide. *Cell Death Differ* **2004,** 11, (8), 875-84.

229. Sun, G. Y.; Xu, J.; Jensen, M. D.; Simonyi, A., Phospholipase A2 in the central nervous system: implications for neurodegenerative diseases. *J Lipid Res* **2004,** 45, (2), 205-13.

230. Klivenyi, P.; Beal, M. F.; Ferrante, R. J.; Andreassen, O. A.; Wermer, M.; Chin, M. R.; Bonventre, J. V., Mice deficient in group IV cytosolic phospholipase A2 are resistant to MPTP neurotoxicity. *J Neurochem* **1998,** 71, (6), 2634-7.

231. Youdim, K. A.; Martin, A.; Joseph, J. A., Essential fatty acids and the brain: possible health implications. *Int J Dev Neurosci* **2000,** 18, (4-5), 383-99.

232. Balazy, M., Eicosanomics: targeted lipidomics of eicosanoids in biological systems. *Prostaglandins Other Lipid Mediat* **2004,** 73, (3-4), 173-80.

233. Dempsey, R. J.; Roy, M. W.; Meyer, K.; Cowen, D. E.; Tai, H. H., Development of cyclooxygenase and lipoxygenase metabolites of arachidonic acid after transient cerebral ischemia. *J Neurosurg* **1986,** 64, (1), 118-24.

234. Hsu, C. Y.; Liu, T. H.; Xu, J.; Hogan, E. L.; Chao, J.; Sun, G.; Tai, H. H.; Beckman, J. S.; Freeman, B. A., Arachidonic acid and its metabolites in cerebral ischemia. *Ann N Y Acad Sci* **1989,** 559, 282-95.

235. Wolfe, L. S.; Pappius, H. M.; Pokrupa, R.; Hakim, A., Involvement of arachidonic acid metabolites in experimental brain injury. Identification of lipoxygenase products in brain. Clinical studies on prostacyclin infusion in acute cerebral ischemia. *Adv Prostaglandin Thromboxane Leukot Res* **1985,** 15, 585-8.

236. Janssen-Timmen, U.; Tomic, I.; Specht, E.; Beilecke, U.; Habenicht, A. J., The arachidonic acid cascade, eicosanoids, and signal transduction. *Ann N Y Acad Sci* **1994,** 733, 325-34.

237. Shimizu, T.; Wolfe, L. S., Arachidonic acid cascade and signal transduction. *J Neurochem* **1990,** 55, (1), 1-15.

238. Fitzpatrick, F. A.; Murphy, R. C., Cytochrome P-450 metabolism of arachidonic acid: formation and biological actions of "epoxygenase"-derived eicosanoids. *Pharmacol Rev* **1988,** 40, (4), 229-41.

239. Powell, W. S.; Wang, L.; Khanapure, S. P.; Manna, S.; Rokach, J., High-pressure liquid chromatography of oxo-eicosanoids derived from arachidonic acid. *Anal Biochem* **1997,** 247, (1), 17-24.

240. Eberhard, J.; Jepsen, S.; Albers, H. K.; Acil, Y., Quantitation of arachidonic acid metabolites in small tissue biopsies by reversed-phase high-performance liquid chromatography. *Anal Biochem* **2000,** 280, (2), 258-63.

241. McManus, M.; Serhan, C.; Jackson, P.; Strange, K., Ketoconazole blocks organic osmolyte efflux independently of its effect on arachidonic acid conversion. *Am J Physiol* **1994,** 267, (1 Pt 1), C266-71.

242. Yue, H.; Strauss, K. I.; Borenstein, M. R.; Barbe, M. F.; Rossi, L. J.; Jansen, S. A., Determination of bioactive eicosanoids in brain tissue by a sensitive reversed-phase liquid chromatographic method with fluorescence detection. *J Chromatogr B Analyt Technol Biomed Life Sci* **2004,** 803, (2), 267-77.

243. Demin, P.; Reynaud, D.; Pace-Asciak, C. R., Extractive derivatization of the 12-lipoxygenase products, hepoxilins, and related compounds into fluorescent anthryl esters for their complete high-performance liquid chromatography profiling in biological systems. *Anal Biochem* **1995,** 226, (2), 252-5.

244. Watkins, W. D.; Peterson, M. B., Fluorescent/ultraviolet absorbing ester derivative formation and analysis of eicosanoids by high-pressure liquid chromatography. *Anal Biochem* **1982,** 125, (1), 30-40.

245. Yang, P.; Felix, E.; Madden, T.; Fischer, S. M.; Newman, R. A., Quantitative high-performance liquid chromatography/electrospray ionization tandem mass spectrometric analysis of 2- and 3-series prostaglandins in cultured tumor cells. *Anal Biochem* **2002,** 308, (1), 168-77.

246. Kempen, E. C.; Yang, P.; Felix, E.; Madden, T.; Newman, R. A., Simultaneous quantification of arachidonic acid metabolites in cultured tumor cells using high-performance liquid

chromatography/electrospray ionization tandem mass spectrometry. *Anal Biochem* **2001,** 297, (2), 183-90.

247. Reynaud, D.; Sun, A.; Demin, P.; Pac-Asciak, C. R., Improved high-performance liquid chromatographic method for the combined analysis of phospholipase, lipoxygenase and cyclooxygenase activities. *J Chromatogr B Biomed Sci Appl* **2001,** 762, (2), 175-80.

248. Grundmann, J. U.; Wiswedel, I.; Hirsch, D.; Gollnick, H. P., Detection of monohydroxyeicosatetraenoic acids and F2-isoprostanes in microdialysis samples of human UV-irradiated skin by gas chromatography-mass spectrometry. *Skin Pharmacol Physiol* **2004,** 17, (1), 37-41.

249. Blair, I. A., Measurement of eicosanoids by gas chromatography and mass spectrometry. *Br Med Bull* **1983,** 39, (3), 223-6.

250. Candelario-Jalil, E.; Gonzalez-Falcon, A.; Garcia-Cabrera, M.; Alvarez, D.; Al-Dalain, S.; Martinez, G.; Leon, O. S.; Springer, J. E., Assessment of the relative contribution of COX-1 and COX-2 isoforms to ischemia-induced oxidative damage and neurodegeneration following transient global cerebral ischemia. *J Neurochem* **2003,** 86, (3), 545-55.

251. Hofer, G.; Bieglmayer, C.; Kopp, B.; Janisch, H., Measurement of eicosanoids in menstrual fluid by the combined use of high pressure chromatography and radioimmunoassay. *Prostaglandins* **1993,** 45, (5), 413-26.

252. Salmon, J. A., Measurement of eicosanoids by bioassay and radioimmunoassay. *Br Med Bull* **1983,** 39, (3), 227-31.

253. Stevens, M. K.; Yaksh, T. L., Time course of release in vivo of PGE2, PGF2 alpha, 6-keto-PGF1 alpha, and TxB2 into the brain extracellular space after 15 min of complete global ischemia in the presence and absence of cyclooxygenase inhibition. *J Cereb Blood Flow Metab* **1988,** 8, (6), 790-8.

254. Lee, S. H.; Williams, M. V.; DuBois, R. N.; Blair, I. A., Targeted lipidomics using electron capture atmospheric pressure chemical ionization mass spectrometry. *Rapid Commun Mass Spectrom* **2003,** 17, (19), 2168-76.

255. Singh, G.; Gutierrez, A.; Xu, K.; Blair, I. A., Liquid chromatography/electron capture atmospheric pressure chemical ionization/mass spectrometry: analysis of pentafluorobenzyl derivatives of biomolecules and drugs in the attomole range. *Anal Chem* **2000,** 72, (14), 3007-13.

256. Patel, P. M.; Drummond, J. C.; Sano, T.; Cole, D. J.; Kalkman, C. J.; Yaksh, T. L., Effect of ibuprofen on regional eicosanoid production and neuronal injury after forebrain ischemia in rats. *Brain Res* **1993,** 614, (1-2), 315-24.

257. Huttemeier, P. C.; Kamiyama, Y.; Su, M.; Watkins, W. D.; Benveniste, H., Microdialysis measurements of PGD2, TXB2 and 6-KETO-PGF1 alpha in rat CA1 hippocampus during transient cerebral ischemia. *Prostaglandins* **1993,** 45, (2), 177-87.

258. Hu, Q.; Noll, R. J.; Li, H.; Makarov, A.; Hardman, M.; Graham Cooks, R., The Orbitrap: a new mass spectrometer. *J Mass Spectrom* **2005,** 40, (4), 430-43.

259. Jebanathirajah, J. A.; Pittman, J. L.; Thomson, B. A.; Budnik, B. A.; Kaur, P.; Rape, M.; Kirschner, M.; Costello, C. E.; O'Connor, P. B., Characterization of a new qQq-FTICR mass spectrometer for post-translational modification analysis and top-down tandem mass spectrometry of whole proteins. *J Am Soc Mass Spectrom* **2005,** 16, (12), 1985-99.

260. O'Connor P, B.; Pittman, J. L.; Thomson, B. A.; Budnik, B. A.; Cournoyer, J. C.; Jebanathirajah, J.; Lin, C.; Moyer, S.; Zhao, C., A new hybrid electrospray Fourier transform mass spectrometer: design and performance characteristics. *Rapid Commun Mass Spectrom* **2006,** 20, (2), 259-66.